BEHAVIOUR OF AXIALLY LOADED SHORT RECTANGULAR COLUMNS STRENGTHENED WITH CFRP COMPOSITE WRAPPING

TECHNICAL REPORT
BY

Omar Chaallal, Ph.D., P.E.
Mohsen Shahawy, Ph.D.,
P.E. Adnan Al-Saad, P.E.

FDOT
Structures Research Center
2007 E. Paul Dirac Drive
Tallahassee, FL 32310

August 2000

.

LIST OF TABLES

LIST OF FIGURES

ABSTRACT

This study presents results of a comprehensive experimental investigation on the behavior of axially loaded short rectangular columns strengthened with CFRP wrap. An extended literature review is provided discussing the existing confinement models developed for FRP confined concrete columns. Six series, a total of 90 specimens, of uniaxial compression tests are conducted on rectangular short columns. The behavior of the specimens is investigated in the axial and transverse directions. The parameters considered in this study are : (a) concrete strength (targeted strengths 3 ksi and 6 ksi), aspect ratio (a/b = 0.5, 0.65 and 1.0) and number of CFRP layers (0, 1, 2, 3 and 4).

The findings of this research can be summarized as follows

The confinement provided by the CFRP improves both the load-carrying capacity and the ductility of the column. This method of structural rehabilitation was shown to be applicable to prismatic sections. (

2) The gain in compressive strength increased with the number of layers. The maximum gain was achieved by columns with a/b = 0.65 for $f_{c.}$ = 3 ksi and a/b = 0.5 for 6 ksi. The maximum gain achieved was respectively 86% and 31 %, with respect to control specimen.

The gain in performance (strength and ductility) due to wrapping was greater for 3 ksi concrete wrapped columns, than for corresponding 6 ksi concrete columns, with respect to control. The maximum gain achieved for 3 ksi concrete wrapped columns was 86% compared to only 31 % for the 6 ksi columns.

(4) Generally, as f_c increased the axial strain substantially decreased and the transverse strain slightly decreased.

(5.) Given the number of CFRP layers, the initial axial stiffness, characterized by the slope of the elastic range, was greater for 3 ksi specimens, in comparison to 6 ksi specimens. This may be due to the contribution of the axial stiffness of CFRP composite wrap, which is more effective for less stiff concrete.

(6) Given the number of CFRP layers, the transverse initial elastic stiffness (slope of the curve in the elastic domain) was similar for both 3 ksi and 6 ksi concretes.

(7) Generally, volume expansion up to failure was greater for 3 ksi than 6 ksi specimens. Also, the bulk modulus achieved by 3 ksi concrete specimens was generally higher than that achieved by 6 ksi concrete specimens. This was probably due to the CFRP wrap, which may have contributed more to 3 ksi concrete than to 6 ksi concrete specimens in the axial direction (axial stiffness).

(8) The rate of dilation prior to cracking was very close to 0.2 for both concretes. Generally, given the number of CFRP layers, the peak of lateral expansion of 3 ksi confined specimens was higher than that of 6 ksi counterparts. It also occurred at a higher axial strain.

(9) The stiffness of the applied FRPC jacket is the key parameter in the design of external jacket retrofits. The jacket must be sufficiently stiff to develop appropriate confining forces at relatively low column axial strain levels. Furthermore, a stiff jacket will better control the dilation of the cross-section, resulting in larger axial strain capacities.

(10) Testing of square and rectangular confined columns shows that confinement can improve their ductility, but to a lesser degree than for cylinders.

CHAPTER 1
INTRODUCTION

This chapter introduces the report. It states the problem and poses the objectives of the study. It also presents the outline of the present report.

1.1 Problem Statement

In North America, many of reinforced concrete bridges are deteriorating due to problems related to environment, increase in quantity and permissible weight of load bearing trucks and under design of older structures. Bridge columns and piers are not an exception.

In recent years, considerable attention has been focused on the use of FRP (Fiber Reinforced Plastic) for structural rehabilitation and strengthening. However, most of research work carried out so far, dealt with standard 6" x 12" cylinders and an analytical model derived from experimental data on such cylinders retrofitted with different layers of CFRP wraps has been achieved by the FDOT Structures Research Center in Tallahassee, Florida. Very limited research data has been reported dealing with rectangular columns retrofitted with composite wrapping. No thorough research has been achieved taking into account all the influencing parameters, such as concrete strength, the aspect ratio of the rectangular specimens, and the number of wrap layers.

1.2 Research Objectives

This project is intended to examine several aspects in the use of fiber reinforced plastic (FRP) laminates for strengthening rectangular short columns subjected to axial compression.

The objectives of this study are as follows:

1. Carry out a comprehensive study state-of-the art review on the axial behavior of short columns confined with external jacketing.
2. Design and carry out an experimental study on the axial behavior of rectangular short columns confined with externally bonded CFRP laminates.
3. Investigate the axial behavior of carbon-wrapped rectangular short concrete columns and compare it to concrete cylinders.

1.3 Report Outline

This report consists of three parts:

- *Part 1: Review of literature, is* presented in chapter 2. The latter provides a review of the relevant literature, and presents the different relevant models used for FRP confined columns under axial loading.
- *Part II: Test program and procedure, is* contained in chapter 3. The latter describes the specimens, the materials, as well as the instrumentation used and presents the testing procedure and the experimental program.
- *Part HL Presentation and analysis of the results, is* covered by chapter 4 (Presentation of the results), and chapter 5 (Analysis of the results).

Chapter 6 summarizes the conclusions and discusses various recommendations.

PART I
REVIEW OF LITERATURE

CHAPTER 2

REVIEW OF LITERATURE AND MODELS

This chapter will focus on the literature review of recent research findings, in particular, those related to concrete columns confined by FRP jacket and subjected to axial loading.

2.1 Research on Circular Short Columns

FRP composites have been used for confinement of concrete since the early 1980's, although using commercially available plastic pipes (PVC) filled with concrete was already suggested in the late 1970's (Kurt 1978).

Fardis and Khalili (1981) conducted uniaxial compression tests on 3" x 6" and 4" x 8" concrete cylinders wrapped with different types of CFRP fabrics and reported enhanced strength and ductility due to confinement. They later proposed an analytical hyperbolic model for the compressive strength of confined concrete.

In an attempt to make the confinement model proposed by Ahmed and Shah (1982), usable for concrete confined by FRP spirals, Ahmed et al., (1991) carried out axial compression tests on 33 - 4" x 8" concrete cylinders confined with GFRP spirals and proposed an expression for the peak stress and peak strain of confined concrete.

Saadatmanesh et al. (1994) conducted a parametric analytical study on the behavior of circular and rectangular columns strengthened with external composite procured E-glass or carbon thin straps. They used the confinement model of Mander et al. (1988). Four parameters were considered: the concrete strength, the FRP strap thickness, the strap spacing, and the material of the straps.

Nanni and Bradford (1995) investigated the behavior of 6" x 12" concrete cylinders confined by three types of fiber-wraps: pretensioned braided aramid cables, procured hybrid glass-aramid shells, and glass filament-winding. For the first series, they tested 16 specimens with variable diameter and spacing of the cables. Four specimens were tested in the second series, and 15 in the third series. The cylinders of the third series were made with a central rod, which was then placed on a filament-winding machine, and wrapped with 1, 2, 4, or 8 plies of E-glass fibers and vinylester resin (or polyester for some of the specimens). The strength of concrete core was reported as: 5.2, 6.6 and 5.3 ksi for the three series, respectively. They concluded that the stress-strain response of FRP-encased concrete, in general, could be modeled by a simple bilinear curve with a bend-over point at the peak stress of unconfined concrete, which corresponds to a strain of 0.003. They, however, did not develop a confinement model. Test results were also compared with the confinement models by Mander et al. (1988) and Fardis and Khalili (1982), both of which grossly underestimated the ultimate strain of encased concrete, but compared reasonably well for strength of confined concrete.

Mirmiran and Shahawy (1995) proposed a concrete-filled FRP tube (CFFT), in which the tube acts as a form-work for the encased concrete, hoop and longitudinal reinforcement, and corrosion-resistant casing for the concrete. The CFFT was proposed for bridge columns as well as for pile splicing. The Florida Department of Transportation (FDOT) sponsored a series of projects in order to investigate the behavior of the proposed CFFT. Several parameters were considered in these studies, e.g. the type of loading, the cross-section, the bond, and the length effect.

Kargahi (1995) investigated the strength of CFFT under uniaxial compression. A total of 12 cylindrical specimens were tested, 9 CFFTs and three 6" x 12" plain concrete cylinders. Filament-wound E-glass/polyester tubes were used, with a winding angle of ± 75º with respect to the longitudinal axis of the tube. Three different tube thicknesses were included, namely, 0.074", 0.13" and 0.237". An enhancement in the concrete strength, in the order of 2.5 to 3.5 times the unconfined strength, was reported. The author also performed a series of split-cylinder tests, in order to investigate the improvement of the tensile strength of the FRP-confined concrete. It was concluded that the FRP tube improves the behavior of the concrete section in tension by containing the cracked

concrete rather than confining it. A parametric study was also performed on the effect of ply thickness, winding angle, and the composite action on confined strength of the column. The analysis was based on the confinement model of Mander et al. (1988). It was concluded that the thickness of the tube increases the pure axial strength. The presence of full composite action does not significantly improve the axial capacity of the column but rather the flexural capacity. Moreover, an increase in the fiber winding angle will decrease the pure axial strength. The pure flexural capacity is maximum at a winding angle of ± 45º.

Scherer (1996) extended the study by Kargahi and investigated the shape of the stress-strain curve and also the dilatancy properties of the same type of tubes under the same type of loading. He further studied the cost optimization of the proposed composite structure.

The bond effect was investigated by Mastrapa (1997). He tested thirty-two 6"A2' composite cylinders, half of which were wrapped in 1, 3, 5, or 7 layers of S-glass fabric, while for the other half concrete of the same batch was poured in tubes made of the same S-glass fabric and with the same number of layers. Tests were done in two series. In Series 1, multi-layer jackets were made layer-by-layer with a splice of about 17% of the perimeter of the cylinders, while in Series 2, the jacket was made of a continuous wrap of the fabric with an overlap of about 32% of the perimeter of the cylinder. The average unconfined strength of concrete for specimens of Series 1 was 5.4 ksi.The hoop strength and modulus of the FRP jacket were 85 ksi and 2,984 ksi, respectively. It was concluded that the effect of construction bond on axially loaded confined concrete is not significant.

El Echary (1997) evaluated the effects of length-to-diameter (L/D) and diameter-to-thickness (D/t) ratios on the behavior of the CFFT. A total of 24 circular CFFTs (Dine, = 5.7l') with three different tube thicknesses (6, 10, and 14 layers) and four different lengths (12", 18", 24" and 30") were tested. No buckling was observed during the tests. The analysis of the test results indicated that the maximum eccentricity was within 10-12% of the section width. The reduction in strength was not significant. It was concluded that up to a ratio L/D of 5: 1, slenderness effects are negligible.

Bavarian et al. (1996) investigated the effects of externally wrapping concrete cylinders with composite materials. Three sizes of cylinder: 3" x 6", 4" x 8", and 6" x 12"; two types of composite material: S-glass and Kevlar-29, were considered. It was found that the ultimate stress and strain respectively doubled and tripled when using 4 layers of S-glass and 4 layers of Kevlar-29.

Monti and Spoelstra (1997) proposed a confinement model for circular columns wrapped with fiber-reinforced plastics. The procedure is basically the same as the model by Ahmad and Shah (1982). For a certain axial strain ϵ_{ci} a value f_{ri} is assumed. The axial stress f_{ci} is then calculated using the confinement model of Mander et al. (1988) as an active confinement model. The lateral strain ϵ_r is then calculated using the expression developed by Pantazopoulou (1995). Knowing f_r and the constitutive relationship of the jacket, a new value of f_r is calculated and compared with the previous value. The procedure is repeated until f_r converges to a stable value.

Miyauchi and al. (1997) performed uniaxial compression tests on concrete columns reinforced with carbon fiber sheet (CFS) to estimate the strengthening effects. They took into account the compressive strength of the concrete (30 and 50 MPa), the number of layers of CFS (1, 2 and 3 layers) and the dimensions of the column (ϕ 10 x 20cm and ϕ15 x 30cm). Test results show that: (a) the compressive strength of the concrete strengthened with CFS is enhanced in proportion to the number of layers of CFS, but not the compressive strength of the plain concrete and the dimensions of the specimens; (b) the axial strain at maximum stress of the concrete strengthened with CFS exponentially extends with the number of layers of CFS and is influenced by the compressive strength of plain concrete. Based on these results, a stress-strain relationship, consisting of a parabola and a straight line tangent to the parabola, for the strengthened concrete is proposed and used to perform a time history response analysis for existing bridge piers strengthened with CFS and subjected to earthquake motion. The analytical results show that existing piers strengthened with 2 layers of CFS would be able to withstand an earthquake equal in intensity to the Southern Hyogo Prefecture Earthquake.

Watanabe et al. (1997) investigated experimentally and analytically the confinement effect of FRP sheets on the strength and ductility of concrete cylinders subjected to a uniaxial compression. Plain concrete cylinder specimens with dimensions of ϕ 100 x 200mm retrofitted with FRP sheets were tested under a uniaxial compression. Variables selected for the test and analysis include the type and the number of FRP sheets. Carbon fiber reinforced plastic (CFRP), high stiffness carbon fiber reinforced plastic (HCFRP) and aramid fiber reinforced plastic (AFRP) were used and the number of FRP sheet layers varied from 1 to 4. The analytical procedure used considered a nonlinear 3-Dimensional FEM, which implements Endochronic theory. Comparison of test results with those obtained by the analytical study showed good agreements and the following conclusions were drawn: • A nonlinear 3-dimensonal finite element procedure, which implemented the Endochronic theory proposed by Bazant, can be applicable to predict responses of concrete cylinders under a uniaxial compression.

- The proposed FE analysis procedure can simulate the confinement effect of FRP sheets on the strength and ductility of concrete cylinders under a uniaxial compression.
- If FRP sheets are used to improve the strength and the ductility of concrete cylinder, then the relationship between the Young's modulus and the confinement effect of FRP sheets need to be clarified.
- Compressive strength of concrete cylinders retrofitted with the sheets linearly increased with an increase in the number of plies.

Kono et al. (1998) investigated the confining effects of CFRP. They conducted compressive tests on twenty seven 100 x 200mm concrete cylinders of different mix proportion with different amount of confining (one layer, two layers and three layers) to measure the stress-strain relations. The results showed that the increase in the compressive strength and strain at maximum stress of the cylinder specimens confined by the CFRP sheet vary linearly with the increasing of the amount and the tensile strength of CFRP sheet. They suggested the following equations for concretes between 30 and 40 MPa and CFRP with tensile strength between 1280 and 3820 MPa and modulus of elasticity between 220 and 235 GPa.

$$I_s = 0.0286\, C_f + 1.0 \qquad (2.4)$$

$$I_c = 0.140\, C_f + 1.0 \qquad (2.5)$$

where C_f is a confinement index equal to the product of CFRP volume ratio $_{pf}$ and the tensile strength of the CFRP (in MPa), $I_s = f_{cc}/f'_c$ and $I_e = \epsilon_{cc}/\epsilon_c$.

Kanatharana and Lu (1998) studied the behavior of FRP-reinforced concrete columns under uniaxial compression. Two types of FRP tubes were used in this study; namely the filament-wound FRP (FFRP) and the pultruded FRP (PFRP) tubes. The FFRP has continuous glass fibers winding at 53º and 127º from its circumference, whereas the PFRP has continuous fibers running along its axis. Based on the results obtained from FRP tube tests, 3 configurations of FRP incorporated concrete were selected: Type A configuration simulating a situation similar to a concrete-filled steel tube; Type B configuration simulating a condition similar to an ordinary spiral reinforced concrete column; Type C configuration combining type A and B type configurations. The experimental results showed that significant increases in concrete ductility and FRP strength occurred in all the FFRP specimens but not in the PFRP specimens. Detailed examination revealed that the inclined orientations of the glass fibers provide the FFRP with a circumferential strength necessary for confining concrete, which in turn restrains the FFRP from local instability, and enables strength and ductility gains in the FFRP specimens.

Harmon et al. (1998) investigated the behavior and the failure modes of confined concrete subjected to cyclic axial loading. Composite tubes, 51 mm in diameter and 102 mm long, were fabricated by filament winding, then filled with concrete. The resulting confined cylinders were loaded in uniaxial compression for up to 10,000 cycles. Variables included amplitude, range, fiber type (carbon and glass) and fiber to concrete volume ratio (0, 2, 4 and 6%). The authors reached the following conclusions:

- Cyclic loading increased axial, radial and volume strains for a given range and amplitude. Monotonic loading following cyclic loading rejoined the monotonic stress-strain relationship unless failure occurs first. Cyclic loading at a given amplitude is equivalent to preloading to a higher load which depends on the amplitude, range and number of cycles, followed by unloading to the given amplitude.
- Failure occurred when the circumferential strain in the wrap exceeded the strain capacity of the fiber. The critical threshold can be crossed either by monotonic loading or by cycling loading. Under cyclic loading, the load at failure may be much lower than under monotonic loading. Some evidence suggested that the critical strain threshold may be reduced due to cyclic loading.
- Radial strain tended to stabilize with increasing number of cycles for high wrap stiffness.
- Void compaction increased with load level and decreased with concrete strength and wrap stiffness. Shear slip and void compaction were closely related.
- A reasonable cyclic model for failure and stress-strain behavior can be constructed from a monotonic model and models for the increase in radial strain, the increase in void compaction and the reduction in the critical threshold level with number of cycles.

2.2 Research on rectangular short columns

Pico (1997) tested a total of nine 6" x6" x 12" square concrete-filled FRP tubes under axial compression, in order to study the effect of the CFFT cross section. No bond was provided between the concrete core and the FRP tube. A marginal increase in strength was observed independent of the jacket thickness. The over-riding parameter in controlling the confinement was shown to be the product of the corner radius and the confining pressure.

Picher et al. (1996) examined the effect of the orientation of the confining fibers on the behavior of concrete cylinders wrapped with CFRP composite material. They also evaluated the application of the method to short columns having rectangular and square sections. Twenty-seven short columns in total were wrapped with CFRP material with different fiber orientations, as follows: fifteen 152 x 304 nun - cylinders, eight 152 x 152 x 500 mm square and four 152 x 203 x 500 mm (a x b x h) rectangular prisms. The following observations were reached:

- Confining the cylinders with CFRP greatly improved ductility and compression strength.
- The method can be efficiently applied to prismatic sections, provided the corners are rounded off prior to application of CFRP composite material. The compression capacity enhancement can reach 20% for square sections.
- The variation of wrapping orientation demonstrated that although axial stiffness decreases with an increase of the angle of orientation, ductility remained constant.
- No improvement in failure mode by varying orientations of the confinement was observed.

Restrepol and DeVino (1996) proposed analytical expressions based on Mander's model for the determination of the capacity of axially loaded reinforced concrete columns which are confined by a combination of steel hoops and composite jackets externally applied on the perimeter of the columns. The paper develops equations that can be used to determine the axial compressive load carrying capacity of reinforced concrete rectangular columns, with externally bonded FRP. The equations take into account the confinement effect due to both steel and FRP jacket.

Hosotani et al. (1997) studied the confinement effect of concrete cylinders by carbon fiber sheets (CFS) for seismic strengthening. They conducted a series of compressive loading test on 600 x 200mm concrete cylinders (10 circular and 12 square) to investigate the stress-strain relation under confinement by CFS. The parameters considered in the tests were the shape of the specimen, the content and the type of CFS (normal and high elastic modulus). Three series of specimens were considered: (a) N-series (cylinders without confinement), (b) S-series (cylinders confined by the CFS with normal elastic modulus - 230GPa), and (c) H-series (cylinders confined by the CFS with high elastic modulus - 392MPa). All the specimens were loaded in axial direction under the displacement control with a loading rate of 0.2 mm/min. The following conclusions were dawn from the test results:

1. At a carbon ratio in the range of 0.05 to 0.15%, the peak axial stress of concrete, f_c, and the axial strain of concrete corresponding to the peak stress, e_c, do not increase as the carbon fiber ratio increases, and are almost independent of the cross sectional shape of specimens.

However, the deteriorating rate of the axial concrete stress after the peak stress decreases and the axial strain of concrete at rupture of the CFS increases as the carbon fiber ratio increases.

2. At a carbon ratio greater than about 1 %, the axial stress of concrete continues to increase with a change of gradient at an axial concrete strain of 3,000 to 3,500" until failure of CFS.

3. The circumferential strain of the CFS at the peak axial stress of concrete ϵ_{cfs}, is 1,100 to 2,500ge for a carbon fiber ratio of 0.056 to 0.16%, while the circumferential strain of the CFS where the gradient changes from the initial value to the second gradient, ϵ_{cft} is 1,800 to 1,900με for a carbon fiber ratio of 1.336%; thus, ϵ_{cfs} is quite close to ϵ_{cft}.

Kataoka and al. (1997) studied the ductility improvement of RC columns wrapped with continuous fiber sheets. In order to investigate the restoring strength characteristics of RC columns wrapped by sheets empirically and to propose an evaluation method of structural performance of RC columns wrapped with sheets, Kataoka et al. conducted an experimental program consisting of 3 series of tests:

(a) The objective of the first series was to evaluate the shear strengthening effect of sheets. A total of 15 RC 300 x 300mm square columns with 1100mm clear span length were tested under anti-symmetrical moment condition with constant axial force (cyclic loading controlled by deflection angle). The main parameters selected for this test were the amount of sheets, the type of sheets and the amount of hoops. Four (4) specimens were conventional RC columns (without wrapping sheets), 10 specimens were sheet-RC columns (wrapped by sheets), and one column was wrapped with sheets after shear failure had occurred, without repair of shear cracks.

(b) The objective of the second series of test was to evaluate the post yielding ductility of RC members wrapped with sheets. A total of 9 RC 300x300mm square columns with clear span length of 900mm were tested. The load was applied similarly to the first series. The main parameters selected for the test were the amount of sheets and the amount of hoops. One specimen was standard column (with 0.13% shear reinforcement ratio and without wrapping sheets), 2 specimens were

conventional RC columns (without wrapping sheets), and 6 specimens were sheet-RC columns (wrapped by sheets).

(c) The objective of the third series of test was to investigate the axial compressive behavior of columns wrapped with sheets, empirically. A total of 10 specimens were tested. The dimensions of the columns were the same as those of the second series. The main parameters selected for the test were the amount of sheets and the amount of hoops. One specimen was standard, one was conventional RC column, and 8 were sheet-RC columns. In this last series, two types of tests were carried out : one was normal monotonic axial compression test and the other was axial compression test to investigate the axial compression capacity of the columns which had already failed under lateral loading in the second series.

From the test results over the three series of test, the following conclusions were achieved: (i) the sheet-wrapping method can enhance the seismic behavior, the capacity as well as the ductility, of existing RC columns; (ii) structural performance of RC columns wrapped with sheets can generally be evaluated using the effective shear reinforcement ratio $\Sigma p_w \epsilon_{cfs} \sigma = p_w + (f\sigma_u / \sigma_{wy}) fp_w$, where: p_w = shear reinforcement ratio of hoops, fp_w = shear reinforcement ratio of sheets, σ_{wy} = yield strength of hoops $f\sigma_u$ = tensile strength of sheets.

Harries et al. (1998) presented the results of an extensive experimental investigation on the axial behavior of reinforced concrete columns retrofit with FRPC jackets. Initially, 152 x 610 mm plain concrete cylinders and 152 x 152 x 610 mm square concrete prisms having FRPC jackets were tested under monotonically increasing concentric axial compression. These tests were aimed at addressing some of the issues raised in previous studies.

Following these tests, 8 full-scale, 508mm diameter circular and 457mm square reinforced concrete columns confined with external FRPC jackets were tested under monotonically increasing concentric axial compression. Reinforcing details of the columns were typical of those designed prior to 1971. In these tests, 3 different FRPC materials were used: (a) A stitched multi-directional

E-Glass fabric with 50% of the fibers oriented at 0° with respect to the circumferential direction of the column and 25% of the fibers oriented at each of ± 45°; (b) A women unidirectional E-Glass fabric oriented in the circumferential direction of the column; and (c) A unidirectional carbon fiber tow sheet oriented in the circumferential direction of the column. The results of this study showed that external FRPC jackets retrofits increase axial force capacity and axial deformation capacity and suggested that practical retrofit measures will provide confinement equivalent to that provided by closely spaced, well detailed, conventional transverse reinforcement. The stiffness of the applied FRPC jacket was found to be the key parameter in the design of external jacket retrofits. The results of this study suggested that there was no significant scale effect where jackets with similar confinement capacity were provided.

2.3 Available models for FRP wrapped columns under uniaxial loading

Table 2.1 summarizes the confinement models for FRP wrapped circular columns. No model was specifically developed and reported for rectangular columns.

Authors	Models	Comments
Fardis and Khalili (1981)	$f_c = \frac{E_c \varepsilon_c}{1 + \varepsilon_c \left[\frac{E_c}{f'} - \frac{1}{\varepsilon_{cc}} \right]}$ (2.6) $\varepsilon_{cc} = 0.002 + 0.001 \frac{E_j t_j}{D f'_c}$ (2.7)	E_j, t_j modulus of elasticity and thickness of FRP jacket. E_c = initial tangent modulus of concrete.
Ahmad et al. (1991)	$f'_{cc} = f'_c \left(1 + \frac{k}{4^{nSsp}} \right)$ (2.8) $\varepsilon_{cc} = \varepsilon_{co} \left[1 + \frac{k}{4^{nSsp}} \right]$ (2.9)	k and n are functions of f'$_c$ S_{sp} = spacing of FRP spirals.
Monti and Spoe Istra (1997)	$\varepsilon_r = 0.5 \beta \frac{E_c - E_{\sec}}{E_{\sec}}$ (2.10) $\varepsilon_{\sec} = f_c / \varepsilon_c$ $\beta = -\frac{V_p^3 v_c}{3}$ $v_c = 3.22 \frac{w_o - 03064 \alpha_x}{1 + 3.22 w_o}$ $\alpha_x = \frac{1.031 w_o}{0.194 + w_o}$	Basically the same as the model by Ahmad and Shah (1982) V_p = volume fraction of paste in concrete v_c = natural capillary porosity of paste w_o = water-cement ratio α_x = degree of hydration
Samaan, Mirmiran and Shahawy (1998)	(a) Model for axial strains (see Fig. 3.2) $f_c = \frac{(E_1 - E_2)\varepsilon_c}{\left[1 + \left(\frac{(E_1 - E_2)\varepsilon_c}{f_o} \right)^n \right]^{\frac{1}{n}}} + E_2 \varepsilon_c$ (2.11) $f'_{cu} = f'_c + 3.38 f_r^{0.7}$ (2.12)	• See definitions of f_c, E_l, E_2, ϵ_c f_o, f'$_{cu}$ in Fig. 3.2. • f_j, E_j and t_j = tensile strength, modulus of elasticity and thickness of FRP wrap.

Authors	Models	Comments
	$f_r = \frac{2 f_j t_j}{D}$ (2.13)	• D = diameter of column
	$E_1 = 47.586\sqrt{1{,}000 f'_c}$ (2.14)	• n = curve shape parameter (n = 1.5 for circular).
	$E_2 = 52.4111 f'^{\,0.2}_c + 1.3456 \frac{E_j t_j}{D}$ (2.15)	• E 1 and E2 in ksi
	$f_o = 0.872 f'_c + 0.371 f_r + 0.908$ (2.16)	
	$\varepsilon_{cu} = \frac{f'_{cu} - f_o}{E_2}$ (2.17)	
	(b) Model for lateral strains (see Fig. 3.3)	• r denotes lateral (radial) direction
	$f_c = \frac{(E_{1r} - E_{2r})\varepsilon_r}{\left[1 + \left(\frac{(E_{1r} - E_{2r})\varepsilon_r}{f_{or}}\right)^{nr}\right]^{\frac{1}{nr}}} + E_{2r}\varepsilon_r$ (2.18)	• v = Poisson's ratio • μ = dilation rate • ϵ_{ru} = ultimate radial strain
	$E_{1r} = \frac{E_1}{V}$ (2.19)	
	$\mu = \frac{d\varepsilon_r}{d\varepsilon_c}$ (2.20)	
	$\mu = -0.187 Ln\left(\frac{2E_j t_j}{f'_c D}\right) + 0.881$ (2.21)	
	$E_{2r} = \frac{E_2}{\mu_u}$ (2.22)	
	$n_r = \frac{n}{\mu_n}$ (2.23)	
	$f_{or} = 0.636 f'_c + 0.233 f_r + 0.661$ (2.24)	
	$\varepsilon_{ru} = \frac{f'_{cu} - f_{or}}{E_{2r}}$ (2.25)	

2.4 Results from Previous Investigation on Small-Scale Specimens

A number of researchers have conducted fundamental tests examining the axial stress-strain behavior of plain concrete with FRP materials. Most of the research to date has involved testing standard 150 mm (6 in.) diameter cylinders having various FRP material jackets. A summary of findings of such investigations is given below in Table 2.2.

Table 2.2 Summary of experimental Studies on Wrapped Concrete Specimens

Researchers	Size (mm)	Confinement	f_{cc}/f_{c}'	ϵ_{cc}
Demers et al.	150 dia. x 300	3-12 plies aramid	1.0-1.65	0.018
(1996)	150 x 150 x 150	tape	1.14-1.25	0.003
Hannon and Slattery (1992)	51 dia. x 102	1, 2 ,3 and 7 plies CFRP'	1.33-5.87	0.010 - 0.035
Howie and Karbhari (1994)	150 dia. x 300	1, 2, 3 and 4 plies CFRP	1.16-2.32	Not reported
		CFRP having Various orientations	1.02-1.77	
Karbhari and Eckel (1993, 1995)	150 dia. x 300	2 plies GFRP2	1.22-1.28	0.020
		2 plies CFRP	1.26-1.32	0.008
		2 plies Aramid	1.01-1.06	0.005
Karchari and Eckel (1995)	150 dia. x 300	2 and 4 plies GFRP	1.47-1.94	0.005
		1 ply CFRP	1.85	0.006
Labossiere et al. (1992)	150 dia. x 300	1 and 3 plies GFRP	1.00-1.50	0.010 - 0.020
		1 ply CFRP	1.25	0.015
Nanni et al. (1995)	150 dia. x 300	Braided Aramid tape	1.13-1.75	0.005 - 0.013
Rochette and Labossiere (1996)	150 x 150 x 150	4 and 5 plies CFRP different corner radii	1.4-1.8	0.020
Soudki and Green (1996)	150 dia. x 300	1 and 2 plies CFRP	1.15-1.28	0.006 - 0.008

[1] CFRP- Carbon Fiber Reinforced Polmer

[2] GFRP- Glass Reinforced Polmer

As the use of FRP materials for the retrofit of concrete structures is a relatively recent development, the existing experimental investigations involve widely varying parameters and are often difficult to correlate. In most cases, the specimen size used is 152 mm (6 in.) round or square. No rectangular specimens of different aspect ratios were tested.

It can be seen in Table 2.2 that the axial concrete strength relative to the unconfined concrete; compressive strength f,,', consistently increases when confined by FRP jackets. Axial strains, E_c, exhibited and the peak axial stresses, f_c, exhibit greater variability due to the differences in FRP strain capacities and stiffnesses. Axial deformation capacity of confined concrete does, however, increase; over that of unconfined concrete (typically) reported as an axial strain of 0.002. The following, sections summarize some key conclusions of some of the investigations reported and relevant to the; present project.

Demers et al. (1996) investigated the behavior of both circular and square specimens confined with varying amounts of FRP materials. A notable difference between the behaviors of circular and square specimens is reported. Circular specimens engage a uniform confining pressure around their entire circumference and thus confinement of the entire cross section is provided. Square specimens, however, engage high confining pressures at their corners but little pressure on their flat sides. As such, the entire cross section is not effectively confined resulting in a lower increase in strength. This shape effect can be reduced by rounding the corners of a square member. Demers et al. (1996) and Rochette and Labossiere (1996) report the effects of varying corner radii. Rochette and Labossiere reported that changing the corner radius from 25 mm (1 in.) to 38 mm (1.5 in.) on a 152 mm (6 in.) square element increased the axial force capacity between 6 and 16 percent, Varying the corner radii had little effect on the ultimate axial strain.

Harmon and Slattery (1992) confirmed the generally bi-linear nature of heavily confined concrete cylinders in addition to demonstrating that cyclic axial loads have little effect on the backbone monotonic response.

Demers (1994) conducted the only study, that the authors are aware of, investigating the axial behavior of reinforced concrete columns having FRP jackets. Demers tested sixteen 300 mrr[(11.8 in.) diameter by 1200 mm (47.2 in.) tall reinforced concrete tied columns having longitudinal steel ratios ranging from 0.7% to 3.6% and transverse steel ratios ranging from 0.17% to 1.07%, Each column was jacketed with a carbon fiber jacket designed to provide a confining pressure of 5MPa (727 psi). On average, Demers noted a 17% increase in axial load carrying capacity and a 300% increase in axial strain capacity over the unjacketed response. A key observation made by Demers was that the jacket ruptured at strains between 0.005 and 0.01, although tensile tests of the composite material indicate a rupture strain of 0.015.

2.5 Analysis and Summary of Previous Research

FRP jackets are usually applied to the exterior of existing concrete columns Often, no initial stresses are introduced in the jacket. As such, FRPC jackets provide passive confinement that is, confining pressure us engaged as a result of the lateral dilation of the axially loaded column. The linear-elastic behavior to rupture of FRPC materials results in an increasing level of confinement through out the load history. This method of providing confinement has a number of implications for the design of column rehabilitation measures.

Axial versus transverse strain relationships for unconfined concrete typically assume a constant value of the dilation ratio, defined as the ratio of transverse to axial strains, equal to Poisson's ratio for concrete (usually between 0.15 and 0.20) through an axial stress of about $0.7f_c'$. Between $0.7f_{,,}'$ and f_c', the dilation ratio increases rapidly from its initial value to about 0.50 (Chen, 1982). The post peak behavior of unconfined concrete is characterized by unstable dilation as the dilation ratio increases beyond 0.50.

Axial versus transverse strain relationships for confined concrete, on the other hand, exhibit relatively controlled transverse dilation beyond the unconfined concrete compressive strength f_c', and up to the confined concrete compressive strength, f_c, As the level of confinement increases, the dilation ratio at $f_{c,}$: is reduced. Additionally, because FRP materials are linear-elastic up to failure,

dilation ratios greater than 0.50 can be stable. The amount of post-peak dilation exhibited is inversely proportional to the stiffness of the FRP jacket.

Jacket Stiffness must be sufficient to develop the required confining pressures at relatively low transverse strains. Initially, as loading begins, no confinement is provided. At low load levels confined concrete behavior will not differ from that of unconfined concrete. As the load level increases, transverse dilation of the concrete first takes up any slack in the jacket and then engages confining pressure by generating hoop strains in the jacket. If the jacket is flexible, very small confining stresses will be generated resulting in small increases in concrete strength and deformation capacity and a stress-response similar to that of unconfined concrete. In such a case, significant confining pressures may not be achieved until large post-peak dilations have occurred, resulting in a second peak on the axial stress-strain response.

A stiff jacket is therefore desirable. However, care must be taken to ensure that the jacket has sufficient deformation capacity so as not to rupture prematurely, resulting in a brittle axial response. Is has been noted (Demers et al. 1996; Harmon et al. 1998, Labossiere et al. 1992) that very stiff jackets result in an essentially bilinear axial stress-strain response with failure corresponding to rupture of the jacket. In such heavily confined cases, the dilation ratio of the concrete at initiation of the jacket rupture is typically less than 0.50.

Column Geometry also significantly effects the level of confinement. Whereas all of the section is fully confined in a circular column, considerable dilation of the section is required before the flat sides of a jacket are able to provide confinement to a square or rectangular column. Due to the relatively small strain capacity of FRP materials, the jacket will typically rupture at its corners before significant confinement can be afforded by the sides of the jacket. The resulting stress-strain response of a square member has an ascending branch, an abrupt decrease in load carrying ability, followed by a slow increase as more confinement is engaged due to dilation of the cross-section.

An effective confinement ratio based on the shape of the section, x_s , is defined as the ratio of the area of concrete which may be considered confined to the gross cross-sectional area (Rastrepol and DeVino, 1996)

$$k_s = \frac{I - \left(\frac{(b-2r)^2 + (d-2r^2)}{3db} \right)}{I - r} \tag{2.26}$$

where

b and d = width and depth of cross section;

r = radius of corner; and,

p = longitudinal reinforcement ratio of section

For a square column, this ratio may be as low as 0.33, although when one considers the beneficial effects of providi corner radii, this value is around 0.50 for square columns having typical sectional dimensions. An effective confinement ratio of 0.50 for square and rectangular columns (having aspect ratios less than 1.5) is implied by recen proposed FRP jacket design recommendations (Seible et al. 1997). The results from the present investigation demonstrate the importance of this issue.

PART II

TESTING PROGRAM AND PROCEDURE

CHAPTER 3
EXPERIMENTAL PROGRAM

This chapter presents the experimental program and the parameters of the study. It also gives details of the specimens, the material used, the instrumentation as well as the testing procedures.

3.1 Parameters of the study

3.1.1 Geometry of specimen

In order to cover a wide range of cross-sectional dimension ratios the length (12"), the cross-sectional area (28.3 in ^{2}) and the corner radius (I") of the specimens were kept constant and equal to ASTM cylindrical specimens. However, three aspects ratio (a/b) were considered.

Specimen dimension	Aspect Ratio (a/b)
5^1/4" x 5 '/4" x 12"	*1.0*
4^1/4" x 6 '/2" x 12"	*0.654*
3^3/4" *x7'/z"x 12"*	0.50

3.1.2 Concrete Strength

Two (2) concrete strengths are considered for the study:

(a) $f'_c = 3000\ psi$

(b) $f'_c = 6000\ psi$

3.1.3 Number of CFRP Layers

Five (5) numbers of CFRP layers are considered as follows

Number of Specimens	Number of CFRP Layers
3	0
3	1
3	2
3	3
3	4

3.1.4 Repeatability

Three (3) specimens of each parameter are considered for reasonable repeatability as shown in the above table.

This results into 90 specimens as follows

- For fc = 3000 psi

  15 Specimens @ 5.25" x 5.25" x 12"
  15 Specimens @ 4.25" x 6.50" x 12"
  15 Specimens @ 3.75" x 7.50" x 12"

- For fc = 6000 psi

  15 Specimens @ 5.25" x 5.25" x 12"
  15 Specimens @ 4.25" x 6.50" x 12"
  15 Specimens @ 3.75" x 7.50" x 12"

3.2 Materials

Two ordinary commercial concretes were delivered by the same supplier with specified compression strengths of 3000 psi (21 MPa) and 6000 psi (42 MPa), thereby simulating a poor concrete and a moderately high-strength concrete respectively. The specimens were cast in specially manufactured aluminum mould with rounded corners (see Fig. 3.1). The concrete mix designs used are presented in Table 3.1. The strengths achieved by control specimens are presented in Table 3.2. No additive was used in any of the concrete mix.

In the specimens receiving carbon lamination, the required layers of the standard CFRP system are applied. The standard system consists of a bi-directional weave with an average of 6.7 yarns per inch in each direction and per layer. Adhesive used for this project is an Aerospace-grade Amine based epoxy. Details of the material properties of CFRP and adhesive are presented in Table 3.3. Regardless of the number of CFRP layers, the entire jacket was made of one continuous sheet of fabric that was cut to the proper length and width. An additional 2" of overlap splice was provided. All specimens were capped with sulfur mortar using a specially made stands (see Fig. 3.2).

3.2 Instrumentation

All specimens were instrumented using surface strain gages in the longitudinal, and in the transverse direction, glued either on a concrete surface or on CFRP outer layer. The surface gages were attached to the jacket after sanding and cleaning the contact surface of the specimen. A schematic view of the location gages is presented in Fig. 3.3 and the view of typical specimens ready for testing is presented in Fig. 3.4. During the test, the applied load as well as the displacements of the specimens were monitored throughout the test. A view of test apparatus and setup is presented in Fig. 3.5.

3.3 Testing Procedure and Program

For each of the concrete, three series (i.e. six series in total, see Table 3.4) of tests are performed in this study. Each series is made of short columns without CFRP jacket as control specimens and columns retrofitted with CFRP jacket. In all specimens, the corners were rounded

with a corner radius equal to 1" (25 mm) to improve their behavior and to avoid premature failure of CFRP material due to shearing at sharp corners. The three series correspond to the following; aspect ratios (a/b) as follows : Series 1 with a/b = 1.0, Series 2 with a/b = 0.65, and Series 3 with (a/b) = 0.5, respectively. All specimens were tested using a 550-kip MTS compression machine and an automatic data acquisition system. Specimens were tested to failure under a monotonically increased concentric load and a displacement control mode with a constant rate of 0.22 in. per minute.

The test program of the different series is presented in Table 3.4. Note that the specimens were labeled as follows

SC -XLY-A/B

where : X, Y, and Z are all numeric values. SC stands
for "Short Column" project.
XLY stands for "X" number of carbon "L" ayers with a concrete strength of "Y" ksi. A/B stands for aspect ratio (a/b).

	3000 psi concrete	*6000 psi concrete*
Water	*313 lbs (142 kg)*	*313 lbs (142 kg)*
Cement	*4601bs (209 kg)*	*763 lbs (346 kg)*
Coarse aggregate	*1772 lbs (804 kg)*	*1772 lbs (804 kg)*
Fine aggregate	*1660 lbs (754 kg)*	*1408 lbs (639 kg)*
W/C Ratio	*0.68*	*0.41*

(1) ¾" Maximum aggregate size, river rock

Table 3.1 - Concrete Mix Designs (per cubic yard)

	3000 psi concrete	*6000 psi concrete*
Water	*313 lbs (142 kg)*	*313 lbs (142 kg)*
Cement	*4601bs (209 kg)*	*763 lbs (346 kg)*
Coarse aggregate	*1772 lbs (804 kg)*	*1772 lbs (804 kg)*
Fine aggregate	*1660 lbs (754 kg)*	*1408 lbs (639 kg)*
W/C Ratio	*0.68*	*0.41*

(1) ¾" Maximum aggregate size, river rock

Table 3.2 - Concrete Compressive Strength of Control Specimens, ksi (MPa)

Series	*Test No.*	*Max Load*	*Strength*	*Average*
(a) 3000psi concrete	*1*			
5.25" x 5.25"	*2*			
(A = 26.70 in.)	*3*			
2	*1*	*96*	*3.59* (24.75)	
4.25" x 6.5"	*2*	*101*	*3.77* (26.00)	*3.66* (25.23)
(A = 26.76 in.)	*3*	*97*	*3.62* (24.96)	
3	*1*	*97*	*3.56* (24.54)	
3.75" x 7,5"	*2*	*93*	*3.41* (23.51)	*3.35* (23.10)
(A = 27.26 in²)	*3*	*84*	*3.08* (21.24)	
		Overall Average		*3.50* (24.13)
(b) *6000 psi concrete*				
4	*1*	*215*	*8.05* (55.50)	
5.75" x 5.75"	*2*	*203*	*7.60* (52.24)	*7.60* (52.40)
	3	*191*	*7.15* (49.30)	
5	*1*	*218*	*8.15* (56.20)	
4.25" x 6.5"	*2*	*226*	*8.44* (58.20)	*8.43* (58.12)
(A = 26.76 in)	*3*	*233*	*8.71* (60.05)	
6	*1*	*190*	*6.97* (48.06)	
3.75" x *7.5"*	*2*	*188*	*6.90* (47.57)	*6.76* (46.60)
(A = 27.26 in)	*3*	*175*	*6.42* (42.26)	
		Overall Average		*7.60* (52.40)

Note *(1)* * = inaccurate results;
(2) A = net area with due account of round comer.

Table 3.3 - Material Properties of Carbon Wraps

Description	Manufacturer's data(')	FDOT's suggested values for Dry Composites(2)
Tensile Strength	530 ksi (3.65 GPa)	124 ksi (0.85 GPa)
Tensile Modulus of Elasticity	33500 ksi (231 GPa)	10,000 ksi (68.9 GPa)
Ultimate Tensile Elongation	1.4%	1.2%
Filament Diameter	7 μm	7 μm
Filaments/yarn	12000	12000
Thickness of layer		0.02 in. (0.5)

(1) Reported for the carbon fabric only (11 yarns/inch, 70 x 10^{-5} in'/yarns)
(2) Apparent values based on 6.7 yarns/in. in average and 0.02 in. thickness/layer.

Series	Specimen No.	Number of CFRP layers	Number of specimens
(a) 3000 psi Concrete			**45**
1	SC-OL3-1.0	0	3
	SC-1L3-1.0	1	3
	SC-2L3-1.0	2	3
	SC-3L3-1.0	3	3
	SC-41-3-1.0	4	3
2	SC-OL3-0.7	0	3
	SC-1 L3-0.7	1	3
	SC-21-3-0.7	2	3
	SC-31,3-0.7	3	3
	SC-4L3-0.7	4	3
3	SC-01-3-0.5	0	3
	SC-11,3-0.5	1	3
	SC-2L3-0.5	2	3
	SC-3L3-0.5	3	3
	SC-41,3-0.5	4	3
(b) **6000 psi Concrete**			**45**
4	SC-OL6-1.0	0	3
	SC-1L6-1.0	1	3
	SC-2L6-1.0	2	3
	SC-3L6-1.0	3	3
	SC-31,6-1.0	4	3
5	SC-OL6-0.7	0	3
	SC-1L6-0.7	1	3
	SC-2L6-0.7	2	3
	SC-3L6-0.7	3	3
	SC-41-6-0.7	4	3
6	SC-OL6-0.5	0	3
	SC-11-6-0.5	1	3
	SC-2L6-0.5	2	3
	SC-3L6-0.5	3	3
	SC-4L6-0.5	4	3

CHAPTER 4

PRESENTATION OF THE RESULTS

This chapter presents the experimental results of all the series mainly in terms of load or moment versus mid-span deflections, secondary moments and strain distribution.

4.1 Overall Observed Behavior

Typical failure of specimens from the six series is presented in Fig. 4.1 to 4.3. Failure of carbon-wrapped specimens was typically marked by fiber fracture at or near the corners of the! specimens. No delamination was observed at the splice. Once the jacket was removed, it became, clear that shear cones were formed at the top and bottom of some specimens (see Fig. 4.4). Failures was generally sudden. Unlike the glass-wrapped concrete core. However, popping noises were; heard during various stages of loading. The sounds were attributed to the micro-cracking of concrete and shifting of aggregates.

The control, unjacketed specimens behaved very much as expected. Axial strains at peak: stress of about 0.002 were observed and a dilation ratio of 0.50 at the peak stress was exhibited, At an axial stress near the maximum unconfined strength f'_c the axial and radial strains begin to increase rapidly. Even though the curves indicate an increase of ductile behavior, failure of confined concrete prisms occurs without much apparent warning. Failure is usually caused by a sudden breakage of the composite wrap due to the fragile behavior of CFRP. When the confinement fails, the concrete core is unable to withstand the load which produces a stress over f'_c. Breakage of the confinement thus triggers a sudden failure mechanism.

After failure, confined concrete is found to be disintegrated in about one third of the total volume of the cylinder. Experimental observations suggest that the micro-cracking occurs in a

more diffuse manner than in unconfined concrete. Despite all measurements, it is almost impossible to identify precisely the location of the initial failure in the confining laminate and to follow the progression of damages.

4.2 Test Results for 3 ksi Concrete

The maximum experimental values obtained from tests for 3 ksi concrete are summarized in Table 4.1. The table gives the maximum axial load, and the maximum axial deflection. It also gives the maximum axial stress and the maximum axial and transverse strains. The initial modulus of elasticity of concrete and the Poisson's ratio based on the average axial and transverse train are, also provided in Table 4.1. Some of the experimental values were not reported in the table due to malfunction of some of the instruments during testing. As expected, it is observed that the maximum axial stress and the maximum axial strain increase as the number of layers increase.

4.2.1 Series One: 5.25" x 5.25" specimens

The modes of failure of specimens of series 1 are shown in Fig. 4.1 for different CFRP layers. The results of specimens of series 1 (i.e., 5.25" x 5.25" and f'_c = 3ksi) are presented in Figures 4.5 to 4.9 and Figures 4.10 to 4.14. Figures 4.5 to 4.9 show the curves presenting the axial load versus axial deflection. It is seen that the curves are essentially linear up to a load of 90 kips (corresponding to a stress approaching f'_c). Thereafter, the slope decreases and the specimens underwent deformations, the magnitude of which depends on the number of layers : the higher the number of layers, the higher the deformations. Figures 4.10 to 4.14 display the stress-strain response of the tested specimens. Each plot shows the axial stress versus axial strain and. transverse strain. Transverse strains are negative (tensile).

4.2.2 Series Two: 4.25" x 6.5" specimens

The modes of failures of specimens of Series 2 (i.e., 4.25" x 6.5" and f'_c = 3 ksi) are presented in Fig. 4.2 for different number of layers. The curves representing the axial load versus axial deflection are presented in Fig. 4.15 to 4.19, whereas those representing the stress-strain

response in Fig. 4.20 to 4.29. Here again each plot shows the axial stress versus axial and transverse strain.

4.2.3 Series Three: 3.75" x 7.5" specimens

The modes of failures of specimens of Series 3 (i.e., 3.75" x 7.5" and f'c = 3 ksi) were presented in Fig. 4.3 for different number of layers. The curves of axial load versus axial strain are displayed in Fig. 4.25 to 4.29 and the curves plotting the axial stress versus the axial strain and the axial stress versus transverse strain are presented in Fig. 4.30 to 4.34.

4.3 Test Results for 6 ksi Concrete

The maximum experimental values obtained from tests for 6 ksi concrete are summarized in Table 4.2. The table gives the maximum axial load, and the maximum axial deflection. It also gives the maximum axial stress and the maximum axial and transverse strains, as well as the modes of failures. The initial modulus of elasticity of concrete and the Poisson's ratio based on the average axial and transverse train are also provided in Table 4.2. Some of the experimental values were not reported in the table due to malfunction of some of the instruments during testing. As expected, it is observed that the maximum axial stress and the maximum axial strain increase as the number of layers increase

4.3.1 Series Four: 5.25" x 5.25" specimens

The modes of failure of specimens of series 4 are shown in Fig. 4.1 for different CFRI' layers. The results of specimens of series 4 (i.e., 5.25" x 5.25" and f'_c = 6 ksi) are presented in Figures 4.35 to 4.39 and Figures 4.40 to 4.44. Figures 4.35 to 4.39 show the curves presenting; the axial load versus axial deflection. It is seen that the curves are essentially linear up to a load of' 90 kips (corresponding to a stress approaching f'_c). Thereafter, the slope decreases and the: specimens underwent deformations, the magnitude of which depends on the number of layers : the: higher the number of layers, the higher the deformations. Figures 4.40 to 4.44 display the stressstrain response of the tested specimens. Each plot shows the axial stress versus axial strain and transverse strain. Transverse strains are negative (tensile).

4.3.2 Series Five: 4.75" x 6.5" specimens

The modes of failures of specimens of Series 5 (i.e., 4.75" x 6.5" and f'_c = 6 ksi) are presented in Fig. 4.2 for different number of layers. The curves representing the axial load versus axial deflection are presented in Fig. 4.45 to 4.49, whereas those representing the stress-strain response in Fig. 4.55 to 4.59. Here again each plot shows the axial stress versus axial and transverse strain.

4.3.3 Series Six: 3.75" x 7.5" specimens

The modes of failures of specimens of Series 6 (i.e., 3.75" x 7.5" and f'_c = 6 ksi) are presented in Fig. 4.3 for different number of layers. The curves of axial load versus axial strain are displayed in Fig. 4.55 to 4.59 and the curves plotting the axial stress versus the axial strain and the axial stress versus transverse strain are presented in Fig. 4.60 to 4.64.

Series	Specimen No.	Max. Axial Load (Kips)	Max. Axial Deflection (in.)	Section Area (in.')	Max. Axial Stress (ksi)	Max. Axial Microstrain	Max. Transverse Microstrain
1	SC-OL3-1.0	112	.140255	26.70	4.2	4200	5500
	SC-OL3-1.0	103	.135334	26.70	3.8	4959	6854
	SC-OL3-1.0	120	.185819	26.70	4.5	3566	9459
	SC-OL3-1.0	148	.161486	26.70	5.5	4029	6459
	SC-OL3-1.0	169	.192661	26.70	6.3	4197	7096
2	SC-OL3-0.7	101	.0981758	27.26	3.7	3080	1857
	SC-OL3-0.7	116	.0633876	27.26	4.2	4601	3466
	SC-OL3-0.7	136	.181475	27.26	5.0	4949	7353
	SC-OL3-0.7	160	.150762	27.26	5.9	4727	8712
	SC-OL3-0.7	188	.14957	27.26	6.9	4992	7487
3	SC-OL3-0.5	97	.0551614	26.76	3.6	2751	1376
	SC-OL3-0.5	113	.0886042	26.76	4.2	4276	3111
	SC-OL3-0.5	134	.0946393	26.76	5.0	4962	5534
	SC-OL3-0.5	153	.181168	26.76	5.7	5817	7210
	SC-OL3-0.5	170	.188548	26.76	6.3	5358	9616

Series	Specimen No.	Max. Axial Load (Kips)	Max. Axial Deflection (in.)	Section Area (in.')	Max. Axial Stress (ksi)	Max. Axial Microstrain	Max. Transverse Microstrain
1	SC-OL6-1.0	215	.122162	26.70	8.0	3064	1813
	SC-1L6-1.0	238	.108901	26.70	8.9	3360	2994
	SC-2L6-1.0	234	.0789173	26.70	8.8	3458	2836
	SC-3L6-1.0	258	.0904493	26.70	9.7	3963	1957
	SC-4L6-1.0	274	.106018	26.70	10.3	3637	4445
2	SC-OL6-0.7	233	.0747274	27.26	8.5	2664	819
	SC-1L6-0.7	247	.0952543	27.26	9.0	3094	3131
	SC-2L6-0.7	263	.109285	27.26	9.6	3713	2621
	SC-3L6-0.7	271	.0788404	27.26	9.9	4203	2157
	SC-4L6-0.7	297	.102827	27.26	10.9	3571	3016
3	SC-OL6-0.5	190	.0779948	26.76	7.1	1997	513
	SC-1L6-0.5	213	.151569	26.76	7.9	3140	918
	SC-2L6-0.5	228	.0751502	26.76	8.5	3468	1582
	SC-3L6-0.5	247	.083261	26.76	9.2	3473	2377
	SC-4L6-0.5	248	.082031	26.76	9.3	1989	3106

CHAPTER 5

ANALYSIS AND DISCUSSION

This chapter analyzes and discusses the experimental results in terms of the moment versus mid-span deflection, the stress-strain distribution and the enhancement of the axial load carrying capacity.

5.1 Overall Behavior

The maximum experimental values obtained form tests for all series were summarized in Table 4.1 for 3 ksi concrete specimens and Table 4.2 for 6 ksi concrete specimens. Tables 5.1 and 5.2 give a summary of results in terms of compressive axial stress for 3 ksi and 6 ksi concretes. From this table, it is seen that confinement by CFRP layers improved compressive strength. The gain in compressive strength increased as the number of layers increased. The maximum gain was achieved by specimens with alb = 0.65 and alb = 0.5 for 3 ksi and 6 ksi concretes, respectively, which is rather unexpected. The maximum gain achieved was respectively 86% and 31 %, with respect to control specimens.

For 3 ksi concrete, the observed increase in axial capacity ranged from -9 to 17 %, 19 to 39%, 31 to 58% and 50 to 86% for 1, 2, 3 and 4 layers, respectively. For 6 ksi concrete, this increase ranged from 6 to 11%, 10 to 20%, 16 to 30 and 28 to 31%. This increase in axial capacity achieved by 3 ksi wrapped columns with respect to control is substantially greater than that of corresponding 6 ksi concrete columns. The maximum gain achieved for 3 ksi concrete wrapped columns was 86 %, compared to only 31 % for the 6 ksi columns.

Square and rectangular confined short columns behave roughly like circular cylinders, although the increase of strength is not as important. Their stress-strain curves show an initial slope which follows the unconfined concrete slope up to an inflexion point, and then a plastic zone. The large ductility allows a high level of axial strain, and final failure corresponds to the breakage of the CFRP wrapping. Because of the stress concentration, wrapping failure occurs at or near a corner.

Il can be observed that the variation of the number of laps had little effect on the initial slope. However, the increase of layers moved the inflexion point to a higher stress level (see Fig. 4.10 to Fig. 4.14 for example).

In all cases, confinement improved column ductility. In all tests, the ultimate transverse: strain was two or three times the ultimate axial strain. This is a major difference with circular cylinders, for which radial strain was lower than axial strain. Generally, as f'c increased the axial strain substantially decreased, whereas the transverse strain slightly decreased.

It is clear from the axial stress-strain curves for the 6 ksi concrete square columns with one or two layers of CFRP, that the level of confinement provided was insufficient to significantly increase the axial force or deformation capacity of these columns (see Table 5.1). The slope of the: second branch of the stress-strain curves increased with the number of CFRP layers, whereas the first branch was generally not affected.

5.2 Stress-Strain Response

The stress-strain plots for the tested specimens are grouped together by the concrete strength and number of layers. Figures 5.1 to 5.3 show the average stress-strain diagrams for the 3 ksi specimens (Series 1 to 3) with zero to 4 layers of CFRP. Similarly, Figures 5.4 to 5.6 show the stress-strain diagrams for the 6 ksi specimens (Series 4 to 6). Each plot shows the axial stress versus axial and transverse strains. Transverse strains are positive (tensile). The first slope generally follows the modulus of elasticity of unconfined concrete, while the second slope depends on the number of

layers and the stiffness of the jacket. The transition zone between the two slopes is indicative of FRP jacket taking the role of dilation restraint for the concrete core.

For each thickness, three specimens with the same properties were tested, and the figure shows consistency of the results. The curves to the right represent the plots of axial stresses versus lateral strains, whereas the curves to the left show the plots of axial stresses versus axial strains. Recent studies by Picher, Rochette and Labossiere (1996), and Nanni and Bradford (1995) have shown a similar response for fiber-wrapped columns with glass, Kevlar and carbon fibers. By examining the stress-strain curves, the following observations are made.

1. The figure clearly shows that confinement with CFRP can significantly enhance concrete's performance, i.e., both strength and ductility. Confinement effectiveness for strength varies between two and three, depending on the jacket thickness. Confinement effectiveness is defined as the ratio of peak strength of confined concrete to that of unconfined concrete. Enhancement in ductility is more pronounced, as the ultimate strain of confined concrete is 10 to 15 times greater than that of plain (unconfined) concrete. Confinement effectiveness, however, is not a linear function of jacket thickness, as the difference between the 3 and 4 layers columns is not as much as that between the two and 3 layer columns.

2. Unlike steel-encased concrete, response of FRP-encased is bilinear with no descending branch. The bilinear trend is also confirmed by other investigators (Picher et al. 1996; Nanni and Bradford 1995). The response consists of three distinct regions. In the first region, behavior is similar to plain concrete, since the lateral expansion of the core is insignificant. With the increase in micro-cracks, a transition zone is entered in which the tube exerts a lateral pressure on the core to counteract the core's tendency for stiffness degradation. Finally, a third region is recognized in which the tube is fully activated, and the stiffness is generally stabilized around a constant rate. The response in this region is mainly dependent on the stiffness of the tube.

3. In the third region, response in the lateral direction is closer to a straight line than the response in the axial direction. This is due to excessive cracking of the concrete core which. is no longer a homogeneous material. Therefore, lateral expansion of the specimen is, directly dependent on the response of the jacket, which is linear-elastic. On the other hand, as the lateral cracks in the core expand, slight shifting and settling of the aggregates occur., whereby the specimen experiences mild softening in the axial direction. Ultimate failure is realized when the jacket can no longer carry any load. This occurs when the jacket fails in shear fracture mode.

5.3 Volumetric Strains

Average axial normalized stress versus change in volume curves are presented in Fig. 5.7 to 5.9 for f'_c = *3* ksi specimens, i.e. series 1 to 3 and similarly in Fig. 5.10 to 5.12 for f'_c = 6 ksi, i.e. for series 4 to 6. Note that volume reduction is negative in these figures. For each thickness, three specimens with the same properties were tested, and the figures show consistency of the results. In each plot, the horizontal axis represents the change in volume per unit volume of concrete core. This can be calculated as the sum of axial and lateral (radial) strains as below

$$\frac{\Delta V}{V} = \varepsilon_v = \varepsilon_1 + \varepsilon_2 + \varepsilon_3 \qquad (5.1)$$

where ϵ_v = volumetric strain, ϵ_1 = longitudinal strain, and ϵ_2 and ϵ_3 are transverse strains in the long and short sides of the rectangular column. Note that transverse strains are negative (tensile).

The response of plain concrete is similar to that observed by other researchers (Chen 1982). Initially, volume change is in the form of compaction and is almost linear up to the critical stress of around 0.9 f'_c. At this point, direction of volume change is reversed, resulting in a volumetric expansion, called dilatancy, near or at peak strength. The expansion becomes unstable at the crushing phase of concrete, that is beyond the peak strength. Tests by Kupter, Hilsdorf and Rusch (1969) and others (Cedolin et al. 1977; Gerstle et al. 1980) have shown that concrete behaves in the same manner under biaxial compression, although the critical stress and the volume reduction are

both increased with lateral pressure. Similar investigations by Ahmad and Shah (1982) and others have shown that volumetric strains of steel-encased concrete also become unstable after the steel casing yields.

As shown in the figures, initially, volume compaction occurs at a rate similar to the bulk modulus of the unconfined concrete. Owing to lateral pressure, however, the dilatancy phenomenon occurs at a higher stress and strain level than those of an unconfined concrete. Research on circular concrete columns confined with FRP jacket has shown that with an increase in the jacket thickness, the dilation phenomenon can be contained. In this case, the response would show a distinct point of maximum dilation where the second strain reversal occurs, and the dilatancy of concrete becomes contained. For example, for a confinement assured by a 14 layer FRP jacket the dilation was completely inhibited (Mirmiran and Shahawy,1997). The volumetric response beyond the point of maximum dilation whould show a linear trend that corresponds mainly to the hoop extension of the FRP column.

The dilation behavior obtained for circular columns described above (Mirmiran and Shahawy, 1997), in particular the strain reversal and containment of dilatancy, was not achieved in the present study. This may be attributed to two factors

(i) The number of jacket layers did not provide enough lateral stiffness relative to the axial stiffness of the short columns considered in this study.

(ii) This study considered rectangular columns, which may exhibit a dilatancy behavior different from that of circular columns. The dilatancy of rectangular columns is not documented.

5.4 Poisson's Ratio and Dilation Rate

It is well known that the Poisson's ratio for concrete v remains in the range of 0.15 to 0.22, until approximately 0.7f, at which stress the *apparent* (or secant) *Poisson's ratio* (or strain ratio $\epsilon_r/\ \epsilon_c$) begins to increase. At the unstable crushing phase (Richart et al. 1928), this ratio assumes values much higher than 0.5. Ottosen (1979) proposed an elliptical variation for the strain ratio ($v = \epsilon_r/\epsilon_c$) as a function of plasticity index $\beta\ {}^{=}f_c/\ f'_{cc}$, where f'_{cc} = confined strength of concrete, for $\beta > 0.8$. Another variation for Poisson's ratio has been suggested by Elwi and Murray (1979) as a third degree polynomial in the form of

$$v = v_o\left[1 + 1.3763\left(\frac{\varepsilon_c}{\varepsilon_{cr}}\right) - 5.36\left(\frac{\varepsilon_c}{\varepsilon_{cr}}\right)^2 + 8.586\left(\frac{\varepsilon_c}{\varepsilon_{cr}}\right)^3\right] \tag{5.2}$$

where E_c, = critical strain of concrete. At a strain ratio of about 0.75, the value of v exceeds 0.5, which indicates the start of dilatancy. A better representation of the dilation characteristics of concrete is the tangent Poisson's ratio or the rate of change of radial (lateral) strains with respect to axial strains (dE~dE,,), which is herein termed as the dilation rate, [L. For the polynomial model proposed by Elwi and Murray (1979), the tangent and secant Poisson's ratios will behave similarly, with a higher rate of change for the latter. The dilatation rate for this model can be written as

$$\mu = \frac{d\varepsilon_r}{d\varepsilon_c} = v_o\left[1 + 2.7526\left(\frac{\varepsilon_c}{\varepsilon_{cr}}\right) - 16.08\left(\frac{\varepsilon_c}{\varepsilon_{cr}}\right)^2 + 34.344\left(\frac{\varepsilon_c}{\varepsilon_{cr}}\right)^3\right] \tag{5.3}$$

where the dilation rate exceeds 0.5 at a strain ratio of 0.49. Figure 5.13 shows a typical plot dilation rate versus axial strain for one of the tested specimens with a 10-ply tube. The experimental dilation rate is calculated for every two consecutive readings as below

$$\mu = \frac{\Delta\varepsilon_r}{\Delta\varepsilon_r} = \frac{\varepsilon_{r\,new} - \varepsilon_{r\,old}}{\varepsilon_{c\,new} - \varepsilon_{c\,cold}} \tag{5 .4}$$

Note that the perturbations in the experimental dilation rate are due to the extensive number of reading per second, rather than the quality of experimental results. In fact, if the number of data points kept is reduced, less perturbation will be seen. The solid line in the figure represents the dilation rate as the moving average of μ_{exp}. Also, one should note that the trend shown in the experimental curve has been consistent in all tested specimens, and can be captured by a fractional equation in the following form:

$$\mu = \frac{\mu_o + ax + bx^2}{1 + ax + dx^2} \tag{5.5}$$

where μ_o = initial dilation rate, $x = \epsilon_c / \epsilon_{co}$, ϵ_{co} peak strain of unconfined concrete, and a, b, c and d are coefficients. The dilation curve shows three regions that generally correspond to those explained for the stress-strain response. First, the initial dilation rate (μ_o) is the same as the Poisson's ratio of unconfined concrete (v_o). As the microcracks develop, dilation rate tends to increase. The increase becomes more rapid at about 0.7 f_c. Approaching the ultimate strain of unconfined concrete, where concrete has lain itself entirely on to the jacket, the dilation rate reaches a peak value of μ_{max}. Once the jacket assumes full control of lateral expansion, dilation rate stabilizes and decreases to an asymptotic value of μ_u. A review of the properties of the dilation curve results in the following geometric constraints

$$\mu(x=0) = \mu_o, \frac{d\mu}{dx}(x=0) = 0$$

$$\mu(x=1) = \mu_{max}, \frac{d\mu}{dx}(x=1) = 0 \tag{5.6}$$

$$\mu(x \to \infty) = \mu_u, \frac{d\mu}{dx}(x \to \infty) = 0$$

]

Upon imposing the above geometric constraints on the dilation curve, the four constants in equation (5.3) can be related to the initial peak and ultimate dilation rates as follows:

$$a=\mu_o\, c$$
$$b=\mu_u d \qquad (5.7)$$
$$c=-2$$
$$d=\frac{\mu_{\max}-\mu_o}{\mu_{\max}-\mu_u}$$

The results obtained in this study are grouped together by the concrete strength and number of layers. Figures 5.14 to 5.16 show the average dilation curves for the 3 ksi specimens with 0-4 layers (i.e. Series 1 to 3), and Figures 5.17 to 5.19 show the average dilation curves for the 6 ksi: specimens with 0-4 layers (i.e. Series 4 to 6). Obviously, the curve corresponding to 0 layer and 3 ksi (Fig. 5.14) should be disregarded since the readings were not correct due to malfunction of surface gages. The dilation response of carbon-wrapped concrete rectangular columns appears to be generally unstable and different from that of circular columns, with, however, three distinct regions. The first region corresponds to micro-cracking of concrete and rapid increase of lateral expansion. The peak of lateral expansion coincides with the ultimate failure strain of unconfined concrete, signifying that concrete has lain itself completely onto the jacket. At that point, the jacket takes over and consistently reduces the lateral expansion rate, until it stabilizes it at a constant rate just before failure. It appears that generally thinner jackets have higher peak and ultimate dilation rates than do thicker jackets. Note that the perturbations of the experimental dilation are due to the fact that unlike circular columns, the transverse strains achieved by the rectangular specimens were very scatter. Figures 5.14 to 5.19 shows the dilation curves for various jacket thicknesses. As shown in the figures, the initial dilation rate μ_o only depends on the concrete core, whereas the peak and ultimate dilation rates depend on the stiffness of the jacket. As the thickness (or stiffness) of the jacket increases, μ_o and μ_u both decrease. However, the decrease in μ_{max} in more pronounced than the decrease in μ_u, This indicates that thicker jackets contain the dilation of the concrete core sooner than their thin counterparts.

It must be noted that, contrary to circular columns where the dilation curves were reported to be regular and consistent (see Fig. 5.13), this was not the case for the rectangular columns considered in this study. This is attributed to the shape of the rectangular section and to the fact that ϵ_2 and ϵ_3 were generally very scarce. However, the results obtained in this study featured a general tendency' which is similar to that observed for circular columns and described earlier.

5.5 Effect of Concrete Strength

This section presents the effect of concrete strength (3 ksi versus 6 ksi concrete) on the response of concrete short columns in terms of : (a) stress-strain response, (b) volumetric strain, and. (c) dilation rate. For convenience and clarity of presentation only those curves corresponding to 0, 2. and 4 CFRP layers are considered for comparison. For each CFRP thickness, three specimens with the same properties were tested and the curves present the average of the three tests.

(a) Stress-strain response

Figure 5.20 compares the average normalized stress-strain curves of 3 ksi concrete with the corresponding curves of 6 ksi concrete specimens. The curves to the left represent the plots of axial stresses versus axial strains, whereas the curves to the right show the plots of axial stresses versus lateral (transverse) strains. By examining these curves, the following observations can be made

- Generally, the gain in performance (strength and ductility) achieved by 3 ksi concrete is higher than that achieved by 6 ksi concrete.
- Given the number of CFRP layers, the initial axial stiffness, characterized by the slope of the elastic range, was greater for 3 ksi specimens, in comparison to 6 ksi specimens. This may be due to the contribution of the axial stiffness of CFRP composite wrap, which is more effective for less stiff concrete.

- Given the number of CFRP layers, the transverse initial elastic stiffness (slope of the curve in the elastic domain) was similar for both 3 ksi and 6 ksi concretes.

(b) Volumetric strain

Figure 5.21 compares the average normalized axial stress versus volumetric strain curves of 3 ksi specimens with those of 6 ksi specimens. As noted earlier, negative volumetric strain indicates a volume reduction. By examining these curves, the following observations can be made

- Generally, volume expansion up to failure was greater for 3 ksi than 6 ksi specimens.

- The bulk modulus achieved by 3 ksi concrete specimens was generally higher than that achieved by 6 ksi concrete specimens. This was probably due to the CFRP wrap, which may have contributed more to 3 ksi concrete than to 6 ksi concrete specimens in the axial direction (axial stiffness).

(c) Dilation rate

Figure 5.22 compares average dilation rate versus axial strain curves of 3 ksi concrete specimens with those of 6 ksi specimens. On the basis of theses curves, the following observations can be made

- The rate of dilation prior to cracking was very close to 0.2 for both concretes.

- Generally, given the number of CFRP layers, the peak of lateral expansion of 3 ksi confined specimens was higher than that of 6 ksi counterparts. It also occurred at a higher axial strain.

Table 5.1 Experimental Axial Load Capacity for 3 ksi Concrete Columns

3 ksi Concrete					
Ratio	f c no layer ksi	fcc 1 layer ksi	fcc 2 layers ksi	fcc 3 layers ksi	fcc 4 layers ksi
a/b = 1.0 alb = 0.65 a/b = 0.5	4.2 3.7 3.6	3.8(-9%) 4.2(+13%) 4.2(+17%)	5.0(+19%) 5.0(+35%) 5.0(+39%)	5.5(+31%) 5.9(+60%) 5.7(+58%)	6.3(+50%) 6.9(+86%) 6.3(+75%)

Table 5.2 Experimental Axial Load Capacity for 6 ksi Concrete Columns

6 ksi Concrete					
Ratio	f c no layer ksi	fcc 1 layer ksi	fcc 2 layers ksi	fcc 3 layers ksi	fcc 4 layers ksi
a/b = 1.0 a/b = 0.65 a/b = 0.5	8.0 8.5 7.1	8.9(+11%) 9.06(+6%) 7.9(+11%)	8.8(+10%) 9.6(+13%) 8.5(+20%)	9.7(+21%) 9.9(+16%) 9.2(+30%)	10.3(+29%) 10.9(+28%) 9.3(+31%)

CHAPTER 6

SUMMARY, CONCLUSIONS AND RECOMMENDATIONS

This chapter presents the conclusions reached in this study. It also provides some recommendations for further studies.

6.1 Summary

This study presents a comprehensive experimental investigation on the behavior of axially loaded short rectangular columns strengthened with CFRP wrap. An extended literature review was provided discussing the existing confinement models developed for FRP confined concrete columns. Six series, a total of 90 specimens, of uni-axial compression tests were conducted on rectangular short columns. The behavior of those specimens was investigated in the axial and transverse directions. The parameters considered in this study are: (a) concrete strength (targeted strengths 3 ksi and 6 ksi), aspect ratio (a/b = 0.5, 0.65 and 1.0) and number of CFRP layers (0, 1, 2, 3 and 4).

6.2 Conclusions

The results of an experimental investigation on the performance of reinforced concrete rectangular short columns strengthened with externally applied bi-directional carbon fiber reinforced plastic material were presented. The findings of this research can be summarized as follows:

(1) The confinement provided by the CFRP improves both the load-carrying capacity and the ductility of the column. This method of structural rehabilitation was shown to be applicable to prismatic sections.

(2) The gain in compressive strength increased with the number of layers. The maximum gain was achieved by columns with a/b = 0.65 for $f_{c.}$ = 3 ksi and a/b = 0.5 for 6 ksi. The maximum gain achieved was respectively 86% and 31 %, with respect to control specimen.

(3) The gain in performance (strength and ductility) due to wrapping was greater for 3 ksi concrete wrapped columns, than for corresponding 6 ksi concrete columns, with respect to control. The maximum gain achieved for 3 ksi concrete wrapped columns was 86% compared to only 31 % for the 6 ksi columns.

(4) Generally, as f'_c increased the axial strain substantially decreased and the transverse strain slightly decreased.

(5) Given the number of CFRP layers, the initial axial stiffness, characterized by the slope of the elastic range, was greater for 3 ksi specimens, in comparison to 6 ksi specimens. This may be due to the contribution of the axial stiffness of CFRP composite wrap, which is more effective for less stiff concrete.

(6) Given the number of CFRP layers, the transverse initial elastic stiffness (slope of the curve in the elastic domain) was similar for both 3 ksi and 6 ksi concretes.

(7) Generally, volume expansion up to failure was greater for 3 ksi than 6 ksi specimens. Also, the bulk modulus achieved by 3 ksi concrete specimens was generally higher than that achieved by 6 ksi concrete specimens. This was probably due to the CFRP wrap, which may have contributed more to 3 ksi concrete than to 6 ksi concrete specimens in the axial direction (axial stiffness).

(8) The rate of dilation prior to cracking was very close to 0.2 for both concretes. Generally, given the number of CFRP layers, the peak of lateral expansion of 3 ksi confined specimens was higher than that of 6 ksi counterparts. It also occurred at a higher axial strain.

(9) The stiffness of the applied FRPC jacket is the key parameter in the design of external jacket. retrofits. The jacket must be sufficiently stiff to develop appropriate confining forces at relatively low column axial strain levels. Furthermore, a stiff jacket will better control the dilation of the cross-section, resulting in larger axial strain capacities.

(10) Testing of square and rectangular confined columns shows that confinement can improve their ductility, but to a lesser degree than for cylinders.

6.3 Recommendations

The present study focused on the performance of short columns wrapped with CFRP jackets. The following recommendations can be formulated for further studies

i) The height of the specimens is most often only 305 mm (12 in.). Does the small aspect ratio (2: 1) introduce additional confining effects from the loading platens, particularly near the cylinder ends?

ii) Because of the small sections used and the fact that the FRP materials typically used are in fabric form, having a discrete thickness, the reinforcement ratio of the confinement is often very high. In some cases the volumetric confinement ratio is well above 5 percent. Such levels of confinement would be inappropriate and difficult to attain in full-scale applications. As such, reported increases in strength and deformation capacity are likely greater than that which may be expected in practical applications.

iii) In some studies there is no characterization of the FRP material - only the fiber material is characterized, rather than the fiber-resin matrix composite jacket material. As such, assessing normalized confinement ratios is not possible.

REFERENCES

Ahmad, S.H., and Shah, S.P. (1982a). *"Complete triaxial stress-strain curves for concrete",* Proceedings, ASCE, v. 108, ST4, 728-742.

Ahmad, S.H. and Shah, S.P. (1982b). *'Stress-strain curves of concrete confined by spiral reinforcement';* ACI Journal, 79(6), 484-490.

Ahmad, S.J., Khaloo, A.R. and Irshaid, A. (1991). *`Behavior of concrete spirally confined by fiberglass filaments':* Mag. of Concrete Research, 43 (156), 143-148.

Bavarian, B., Shively, R., Ehrgott, R., and DiJulio, R., (1996), *"External Support of Concrete, Structures Using Composite Materials, "* Proceedings of the First International Using Composites in Infrastructure, ICCI `96, H. Saadatmanesh and M. R. Ehsani, Editors, Tucson, Arizona, pp. 917-928.

Chen, W.F. (1982). *"Plasticity in Reinforced Concrete",* McGraw Hill, New York.

Cedolin, L., Crutzen, U.R.J. and Poli, S.D. (1977), *"Traxial stress-strain relationship for concrete",* J. Eng. Mech., 103, 423-439.

Demers, M., Hebert, D., Labossiere, P. and Neale, K.W. (1996). "The Strengthening of Structural Concrete with an Aramid Woven Fiber/Epoxy Resin Composite," *Proceedins of Advanced Composite Materials in Bridges and Structures II,* Montreal, August 1995, pp 435442.

Demers, M. (1994). "D6termlination des Parametres Influengant le Comportement des Colonnes en B6ton Confinees par une Enveloppe Mince en Composite D'Avant-Garde", M.A.Sc. Thesis, Universite de Sherbrooke, 98 pp.

El Echary, H. , (1997). *'Length effect on concrete-filled FRP tubes using acoustic emission"* . *MS* thesis, University of Central Florida, Orlando, FL.

Elwi, A.A., and Murray, D.W. (1979). "A *3D Hypoelastic Concrete Constitutive Relationship "*. J. Eng. Mech. 105, 623-641.

Fardis, M.N., and Khalili, H.H. (1982). *'FRP-encased concrete as a structural material'* . Mag. of Concrete Research., 34 (121), 191-201.

Fardis, M. N., and Khalili, H. H. (1981). *"Concrete encased in fiberglass-reinforced plastic".* ACI J., 78 (6), 440-446.

Gerstle, K.H. *et al.* (1980), *"Behavior of concrete under multiaxial stress states",* J. Eng. Mech. 106,1383-1403.

Harmon, T.G., Gould, P.L., Wang, E. and Ramakrishnan, S., (1998), *'Behavior of Confined Concrete Under Cyclic Loading,* "Proceedings of the Second International on Composites in Infrastructures, ICCI'98, H. Saadatmanesh and M.R. Ehsani, Editors, Tucson, Arizona, pp. 398-409.

Harmon, T.G. and Slattery, K.T. (1992). "Advanced Composite Confinement of Concrete", *Advanced Composite Materials in Bridges and Structures,* CSCE, pp 299-306.

Harries, K.A., Kestner, J., Pessiki, S., Sause, R., and Ricles, J., (1998), *"Axial Behavior of Reinforced Concrete Columns Retrofit with FRPC Jackets,"* Proceedings of the First International Using Composites in Infrastructure, ICCI '98, H. Saadatmanesh and M. R. Ehsani, Editors, Tucson, Arizona, pp. 411-425.

Hosotani, M., Kawashima, K. and Hoshikima, J., (1997), "A *study on Confinement Effect of Concrete Cylinders by Carbon Fiber Sheets,"* Non metallic (FRP) Reinforcement for Concrete Structures, Proceedings of the Third International Symposium, Vol. 1, Sapporo, Japan, pp, 209-216.

Howie, I. and Karbhari, V.M. (1994). "Effect of Materials Architecture on Strengthening; Efficiency of Composite Wraps for Deteriorating Columns in the North-East," *Infrastructure: New Materials and Methods of Repair - Proceedings of the Third Materials Engineering Conference,* San Diego, 1994, pp 199-206.

Kanatharana, J. and Lu, L.-W., (1998), *"Strength and Ductility of Concrete Columns Reinforced with FRP Tubes,"* Proceedings of the Second International on Composites in Infrastructure., ICCI '98, H. Saadatmanesh and M. R. Ehsani, Editors, Tucson, Arizona, pp. 370-384.

Kargahi, M., (1995), *"Fiber reinforced plastic (FRP) shell as external reinforcement for concrete! columns",* MS thesis, University of Central Florida, Orlando, FL.

Karbhari, V.M. and Eckel, D.A. (1995) "Effects of Short-Term Environmental Exposure on Axial Strengthening Capacity of Composite Jacketed Concrete," *Journal of Composites Technology and Research,* ASTM, Vol. 17, No. 2, pp 99-106.

Karbhari, V.M. and Eckel, D.A. (1993). "Strengthening of Concrete Column Stubs Through Resin Infused Composite Wraps, " *Journal of Thermoplastic Composite Materials, Vol.* 6, April 1993, pp 92-107.

Kataoka, T. et al. (1997), *"Ductility of Retrofitted RC Columns with Continuous Fiber Sheets,"* Non metallic (FRP) Reinforcement for Concrete Structures, Proceedings of the Third International Symposium, Vol. 1, Sapporo, Japan, pp.547-554.

Kono, S. Inazumi, M. and Kaku, T., *(1998), "Evaluation of Confining Effects of CRFP Sheets on Reinforced Concrete members,"* Proceedings of the Second International on Composites in Infrastructure, ICCI *'98, H.* Saadatmanesh and M. R. Ehsani, Editors, Tucson, Arizona, pp. *343-355.*

Kurt, C.E., *(1978).* "Concrete-filled structural plastic columns". J. Struct. Div., ASCE, 104(1), *55-63.*

Labossiere, P., Neale, K., Demers, M. and Picher, F. *(1992).* "Repair of Reinforced Concrete Columns with Advanced Composite Materials Confinement," *Advanced Composite Materials in Bridges and Structures,* CSCE.

Mander, J.B., Priestley, M.J.N., and Park, R., *(1988), `Theoretical Stress-Strain Model for Confined Concrete",* Journal of Structural Engineering, ASCE, Vol. 114, No. *8, pp. 1804-1826.*

Mastrapa, J. C., *(1997), "Effect of bonded and unbonded construction on confinement with fiber composites".* MS thesis, University of Central Florida, Orlando, FL.

Mirmiran, A., Kargahi, M., Samaan, M., and Shahawy, M.., *(1996), "Composite FRP- Concrete Column with Bi-Directional External Reinforcement,* "Proceedings of the First International Conference on Composites in Infrastructure, ICCI *'96, H.* Saadatmenash and M. R. Ehsani, Editors, Tucson, Arizona, pp. *903-916.*

Mirmiran, A., and Shahawy, M., *(1997),'Behavior of Concrete Columns Confined with Fiber Composites".* Journal of Structural Engineering, ASCE, Vol. *123, pp. 583-590.*

Miyaushi, K., Nishibayashi, S. and Inoue, S., (1997), *"Estimation of Strengthening Effects with Carbon Fiber Sheet for Concrete column,"* Non metallic (FRP) Reinforcement for Concrete Structures, Proceedings of the Third International Symposium, Vol. 1, Sapporo, Japan, pp.217-232.

Monti, G., and Spoelstra, M.R. (1997). *"Fiber-section analysis ofRCbridge piers retrofitted with FRP jackets ".* Proc. Structures Congress XV Building to Last, ASCE, Portland, OR., 884888.

Nanni, A., and Bradford, M.N. (1995). *"FRP jacketed concrete under uniaxial compression".* Constr. & Bldg. Mater., 9 (2), 115-124.

Ottosen, N.S., (1979). *"Constitutive Model for Short Time Loading of Concrete ".* J. Eng. Mech., 105, 127-141.

Pantazopoulou, S.J. (1995). *`Role of expansion on mechanical behavior of concrete ".* J. Struct. Engr., ASCE, 121 (12), 1795-1805.

Picher, F., Rochetter, P. and Labossiere, p. (1996), *"Confinement of Concrete Cylinders with CFRP,* "Proceedings of the First International Conference on Composites in Infrastructure, ICCI `96, Edited by Saadatmanesh and Ehsani, Tucson, Arizona, pp. 829-841.

Pico, O. (1997). *"Confinement effectiveness of square FRP tubes in hybrid columns ".* MS thesis, University of Central Florida, Orlando, FL.

Restrepol, III. I., and DeVino, B., (1996). *'Enhancement of the Axial Load Carrying Capacity of Reinforced Concrete Columns by Means of Fiberglass-Epoxy Jackets,* "Advanced Composite Materials in Bridges and Structures, Second International Conference, Canadian Society of Engineering, M.M. El-Badry, Editor, pp. 547-553.

Richard, R.M., and Abbott, B.J. (1975). "Versatile elastici-plastic stress-strain formula." J. *Engrg.,* Mech., ASCE, 101(4), 511-515.

Richart, F.E., Brantzag, A., and Brown, R.L. (1928). "A Study of the Failure of Concrete Under Combined Compressive Stresses". Engineering Experiment Station Bulletin No. 185, University of Illinois, Urbana, IL.

Rochette, P. and Labossiere, P. (1996). "A Plasticity Approach for Concrete Columns Confined with Composite Materials," *Proceedings of Advanced Composite Materials in Bridges and Structures II,* Montreal, August 1995, pp 359-366.

Saadatmanesh M., Ehsani, M. R., Limin Jin, (1996), *`Behavior of Concrete Retrofitted with Fiber Composite Straps Under Cyclic Loading'* . Fiber Composites Infrastructure. Proceedings of the First International Conference on Composites in Infrastructures, ICCI `96, H. Saadatmanesh and M.R. Ehsani, Editors, Tucson, Arizona, U.S.A., pp. 842-856.

Samaan, M., Mirmiran, A., and Shahawy, M., (1998), *"Modeling of Concrete Confined by Fiber Composites",* J. Strict. Engrg., ASCE (in Press).

Scherer, M. E. (1996). *`Design optimization and behavior of concrete-filled FRP tubes ".* MS thesis, University of Central Florida, Orlando, FL.

Seible, F. Preistley, N. Hegemier, G.A., and Innamorato, D. (1997). "Seismic Retrofit of RC Columns with Continuous Carbon Fiber Jackets", *Journal of Composites for Construction,* Vol. 1, No. 2, pp. 52-62.

Soudki, K.A. and Green, M.F. (1996). "Performance of CFRP Retrofitted Concrete Columns at Low Temperatures," *Proceedings ofAdvanced Composite Materials in Bridges and Structures* II, Montreal, August 1995, pp 427-434.

Watanabe, K., and al. (1997), *"Confinement Effect of FRP Sheet on Strength and Ductility oj' Concrete Cylinders Under Uniaxial Compression,"* Non metallic (FRP) Reinforcement for Concrete Structures, Proceedings of the Third International Symposium, Vol. 1, Sapporo, Japan, pp.233-238.

ACKNOWLEDGMENTS

The authors would like to acknowledge the assistance from the staff of the Structures Research Center and, in particular, Adnan Al-Saad, P.E. and Tom Beitelman, P.E. The conclusions and recommendations presented in this paper are those of the authors and not necessarily those of the Florida Department of Transportation.

Fig. 3.2 - View of Specially Made Stands for Capping the Specimens

Fig. 3.4 - View of Typical Specimen Ready for Testing

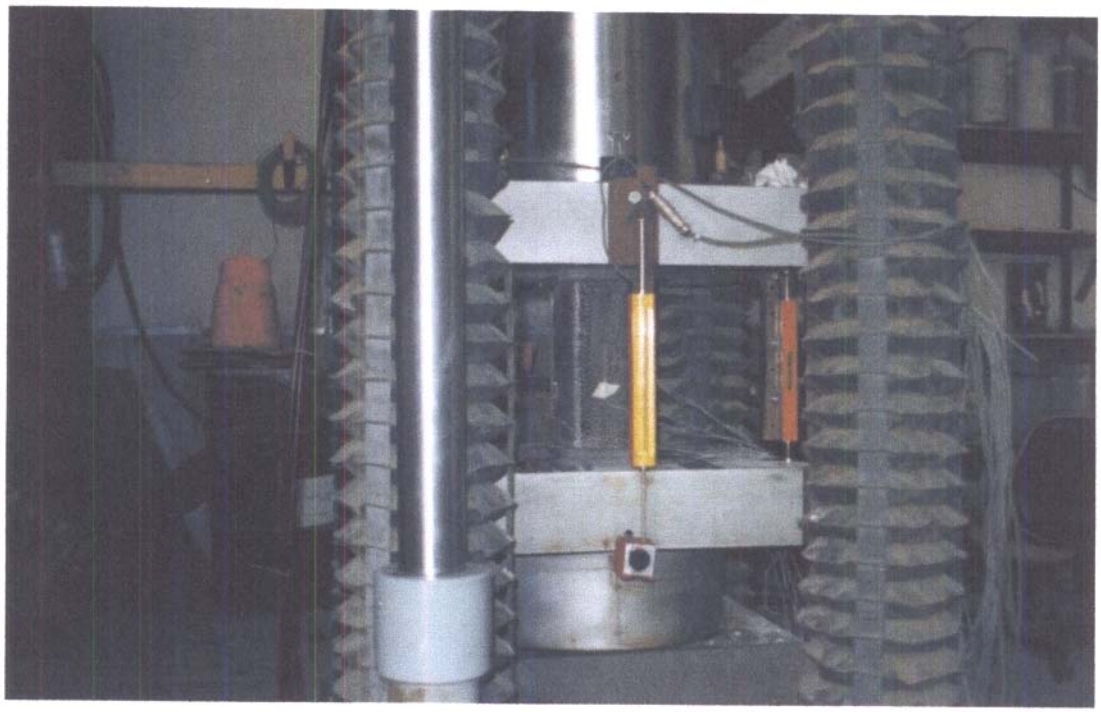

Fig. 3.5 - View of Test Apparatus and Set Up

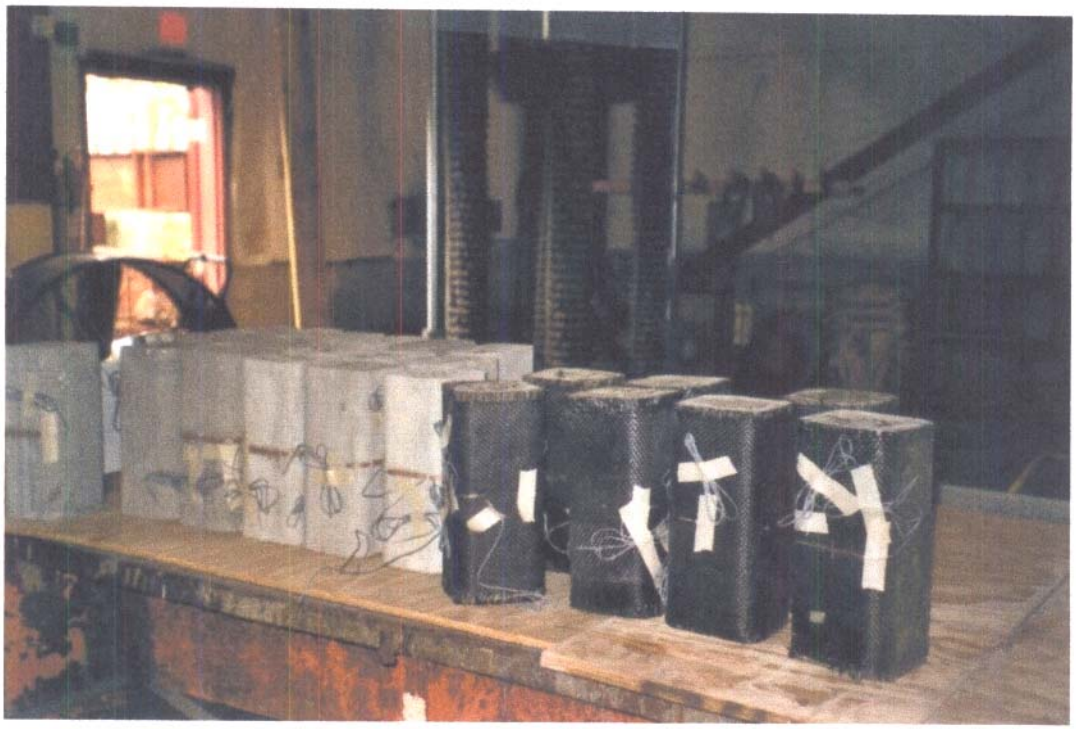

Fig. 3.6 - View of Specimens With Different Aspect Ratios

Fig. 4.1 a) - Typical Failure of Specimens (a/b=1), Series 1: 3 ksi Concrete

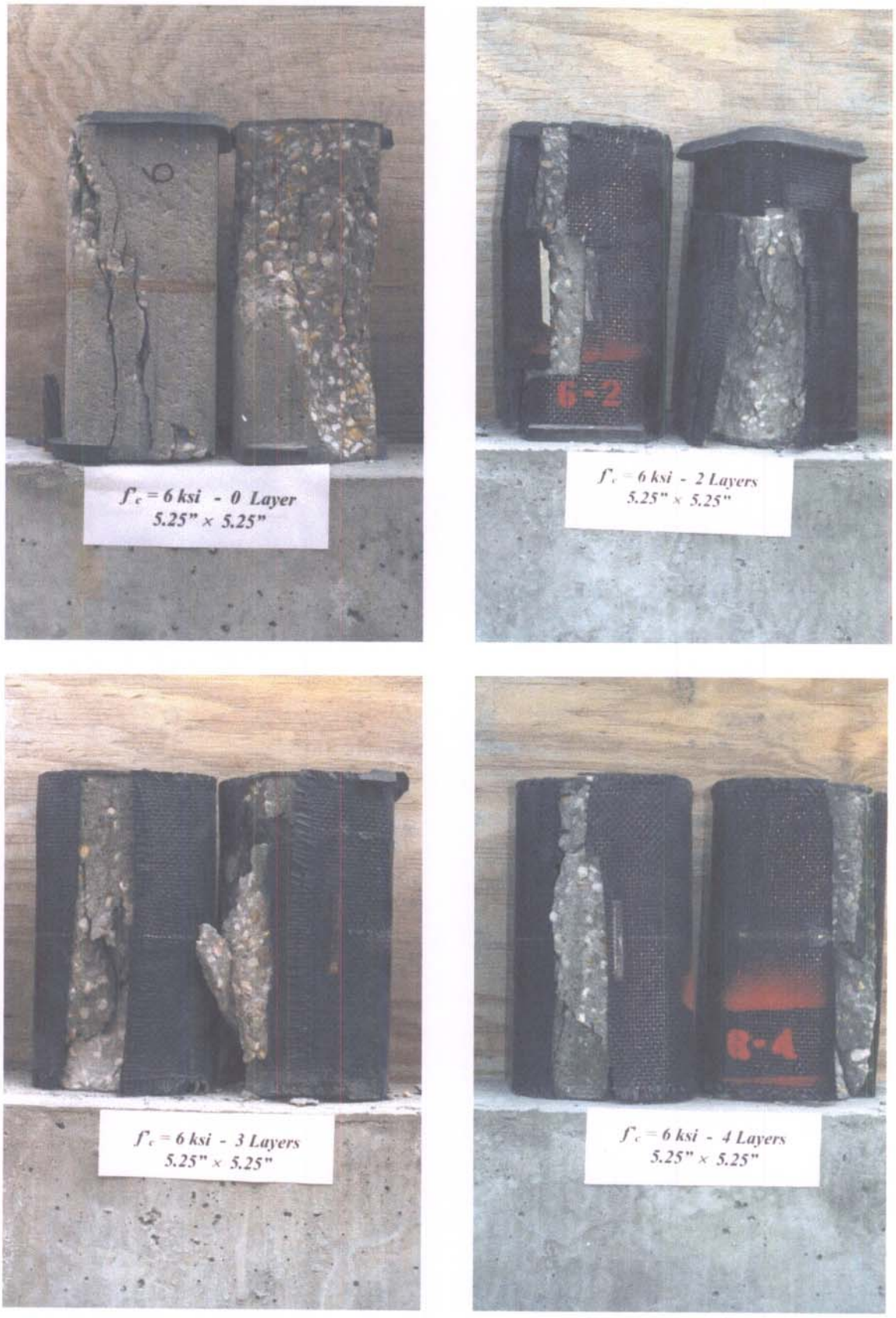

Fig. 4.1 b) - Typical Failure of Specimens (alb=1), Series 4: 6 ksi Concrete

Fig. 4.2 a) - Typical Failure of Specimens (alb=0.65), Series 2: 3 ksi Concrete

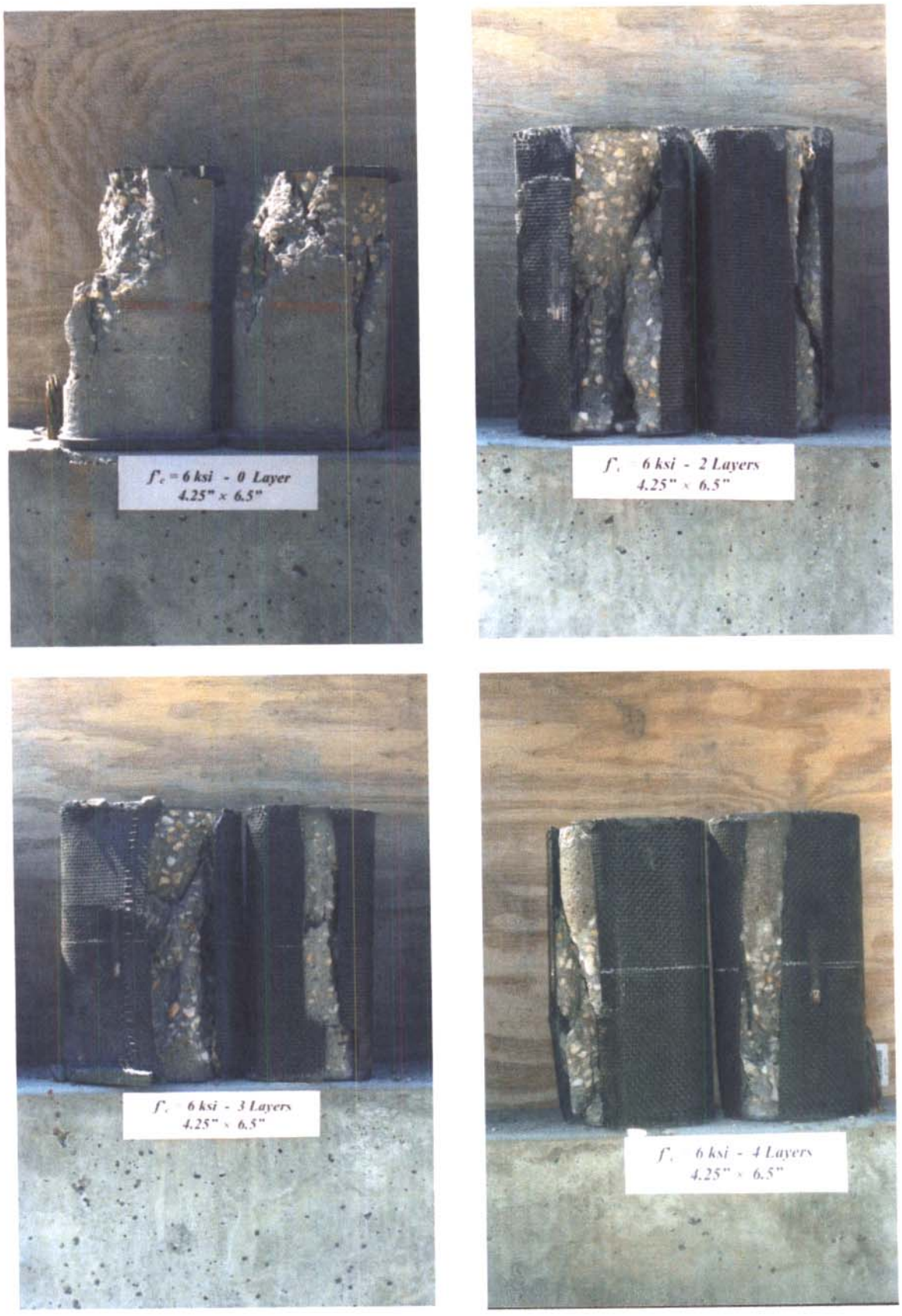

Fig. 4.2 b) - Typical Failure of Specimens (a/b=0.65), Series 5: 6 ksi Concrete

Fig. 4.3 a) - Typical Failure of Specimens (a/b=0.50), Series 3: 3 ksi Concrete

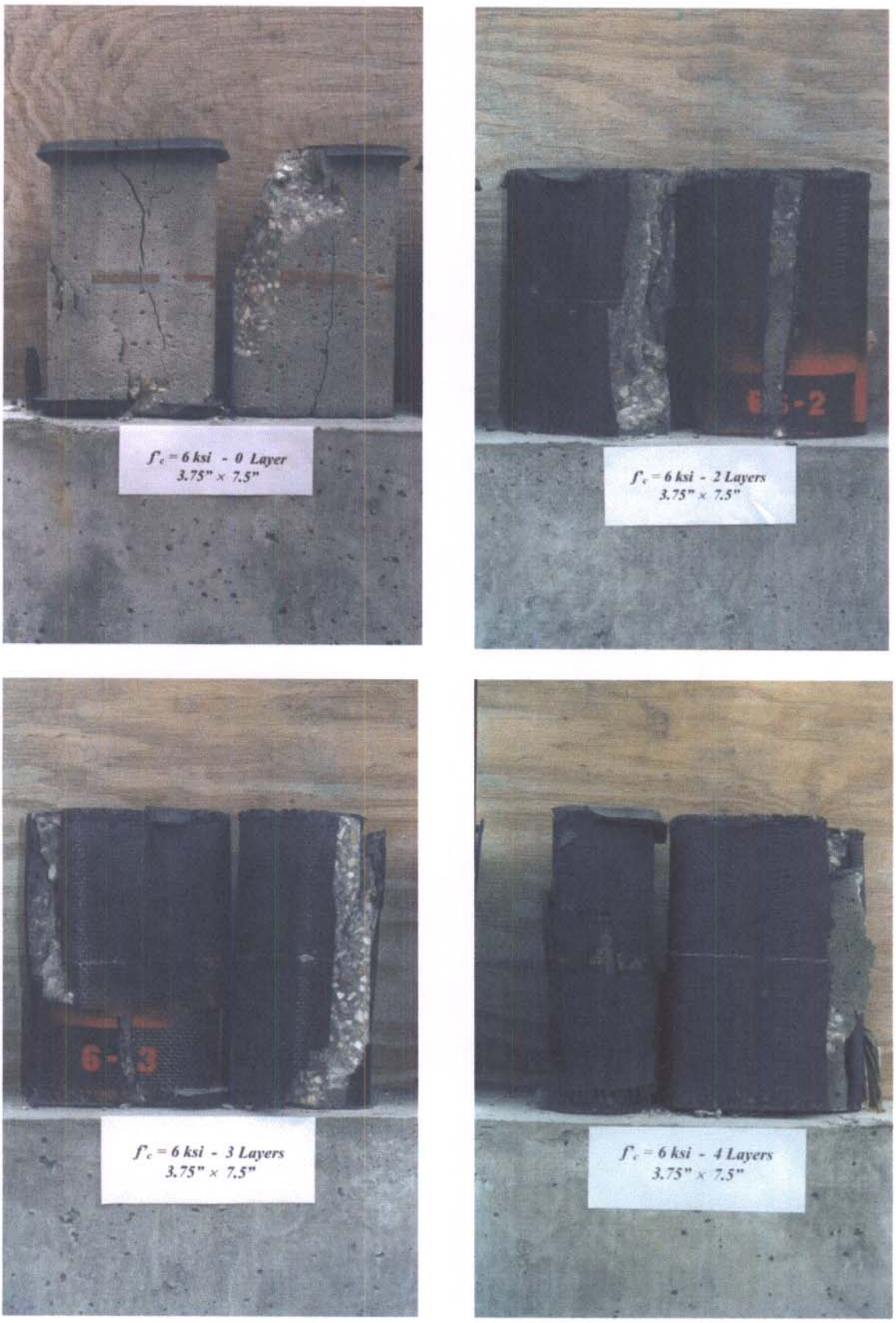

Fig. 4.3 b) - Typical Failure of Specimens (alb=0.50), Series 6: 6 ksi Concrete

Fig. 4.4 - Typical View of Inside Wrapped Specimen After Test

Fig. 4.5 Axial Force vs Axial Deflection Control
(Series 1: 5.25x5.25, fc'= 3 ksi)

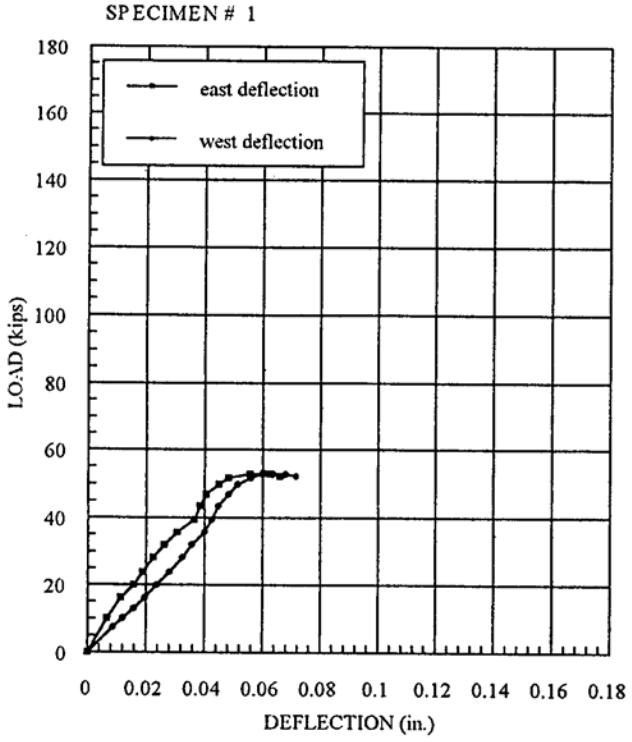

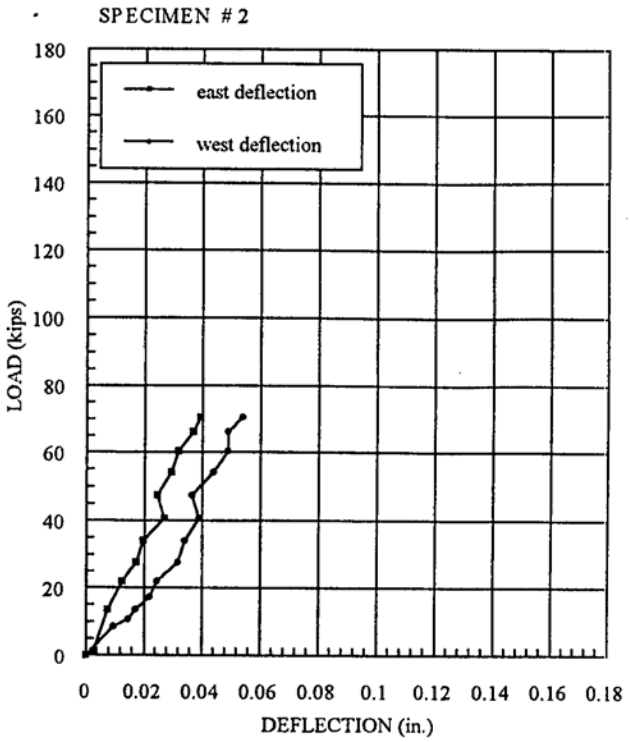

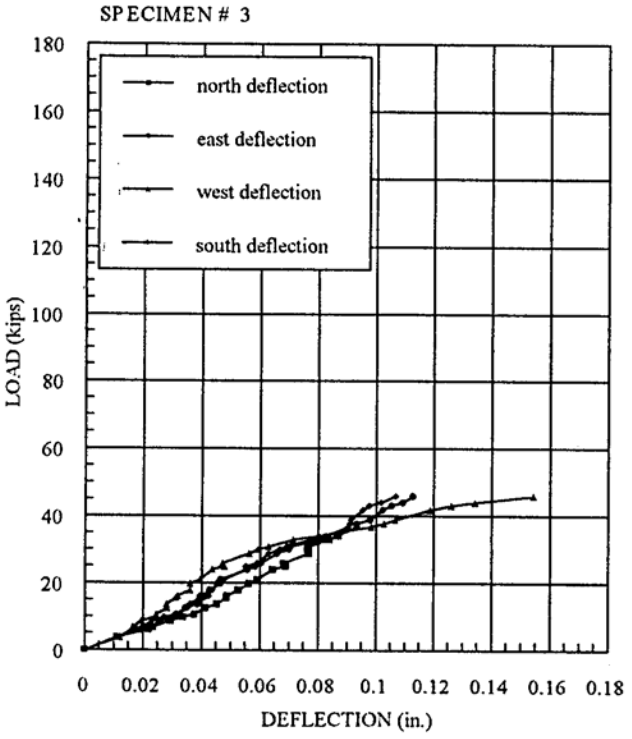

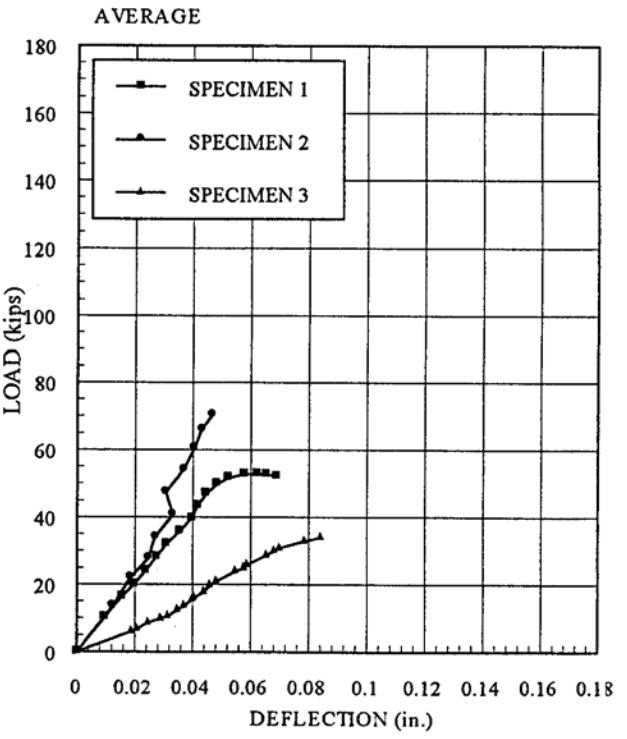

Fig. 4.6 Axial Force vs Axial Deflection One Layer
(Series 1: 5.25x5.25, fc'= 3 ksi)

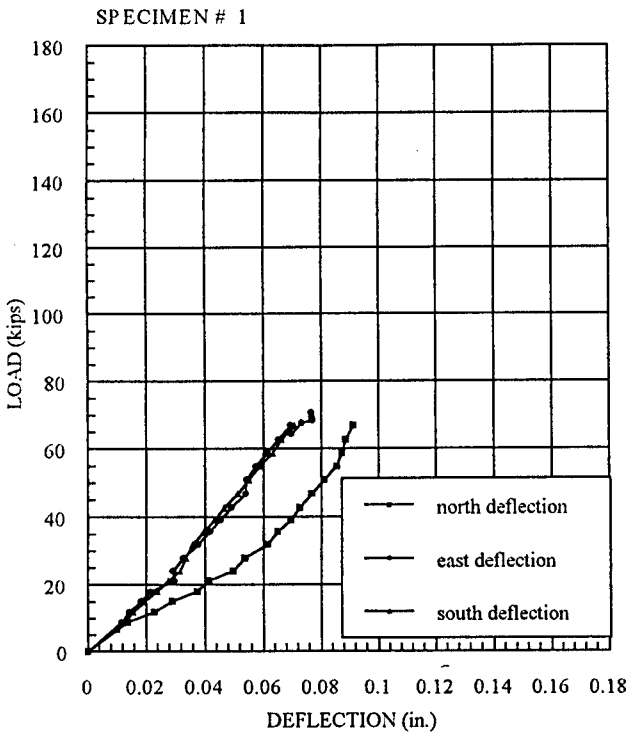

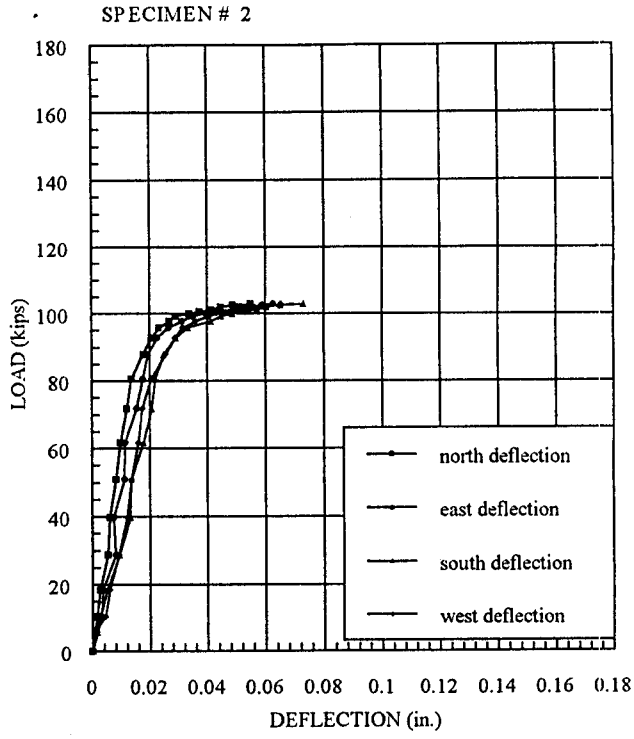

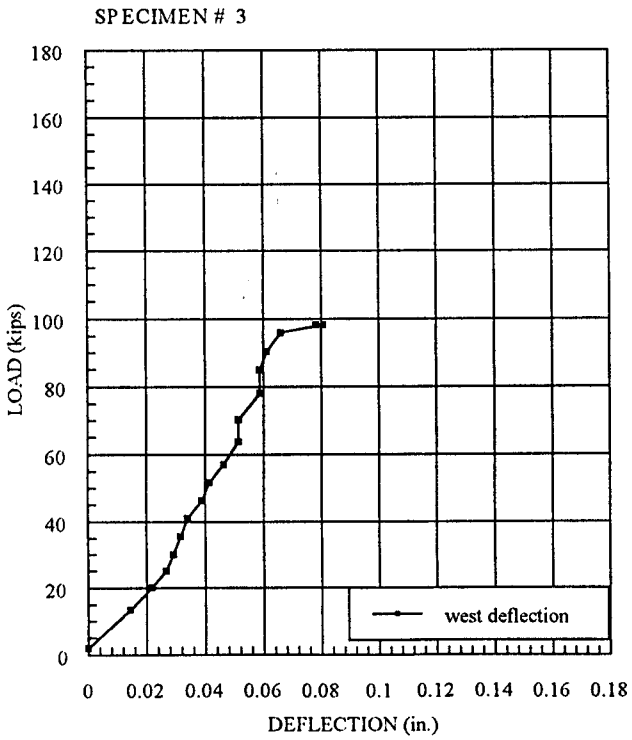

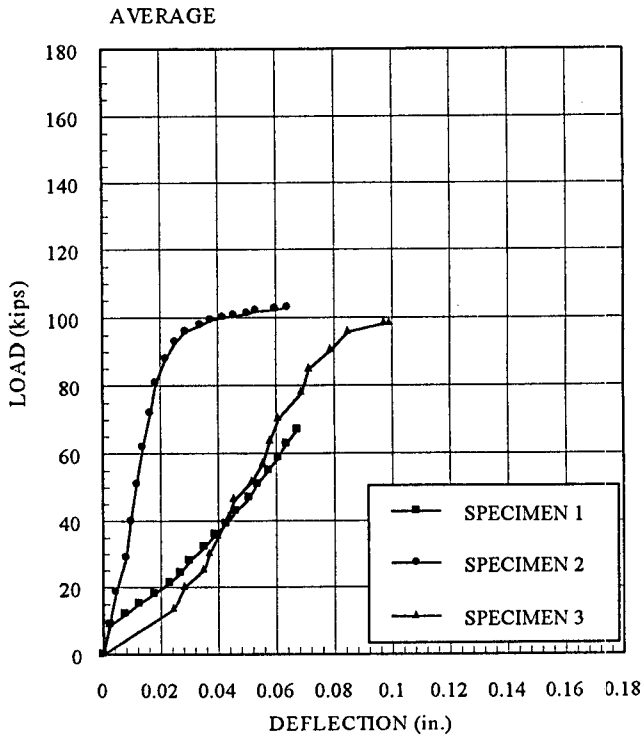

Fig. 4.7 Axial Force vs Axial Deflection Two Layer

(Series 1: 5.25x5.25, fc'= 3 ksi)

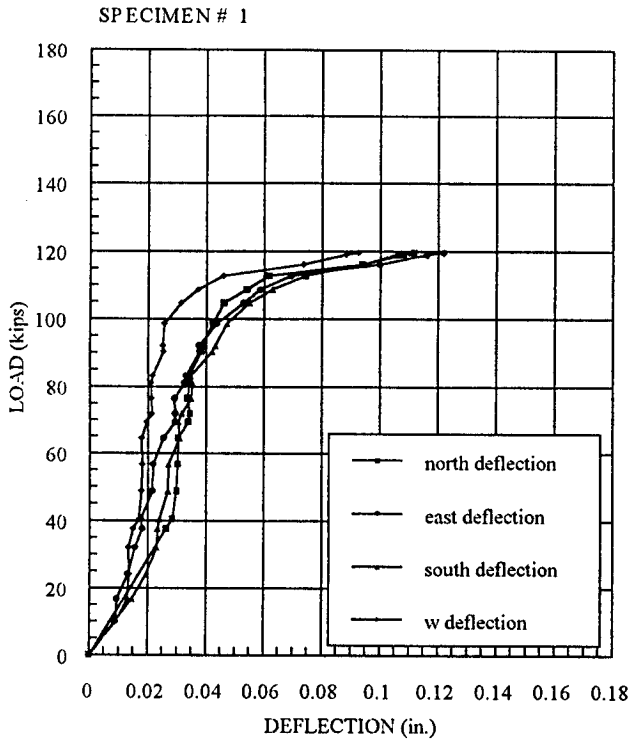

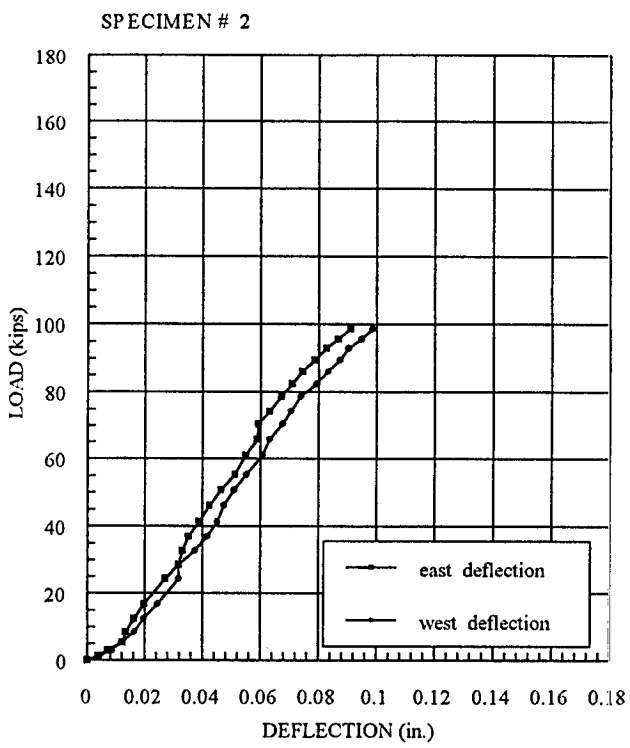

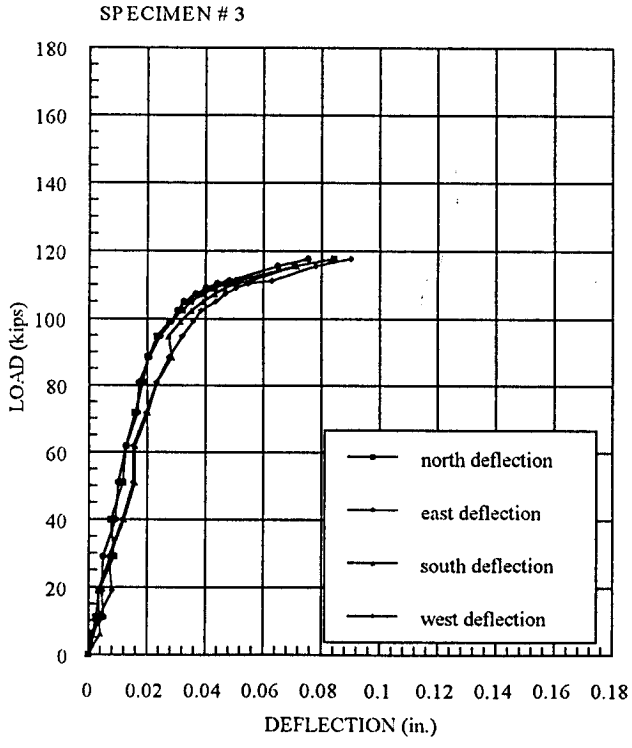

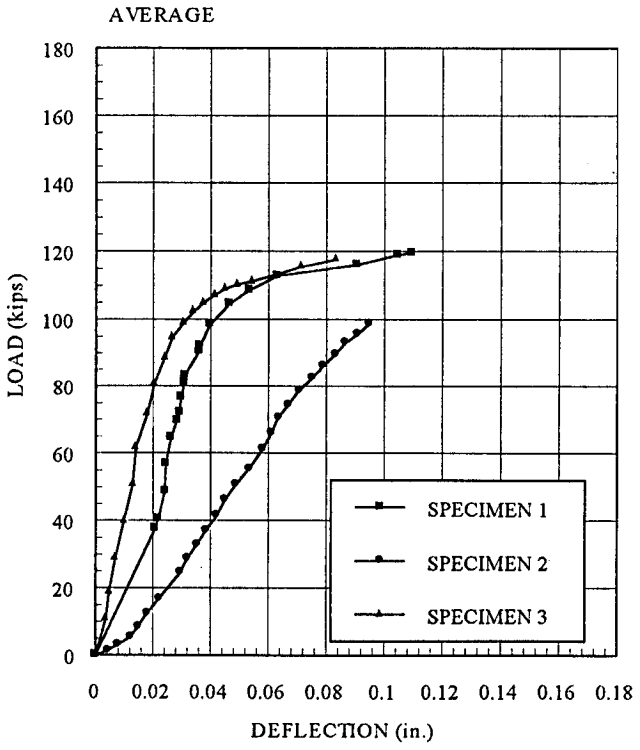

Fig. 4.8 Axial Force vs Axial Deflection Three Layer
(Series 1: 5.25x5.25, fc'= 3 ksi)

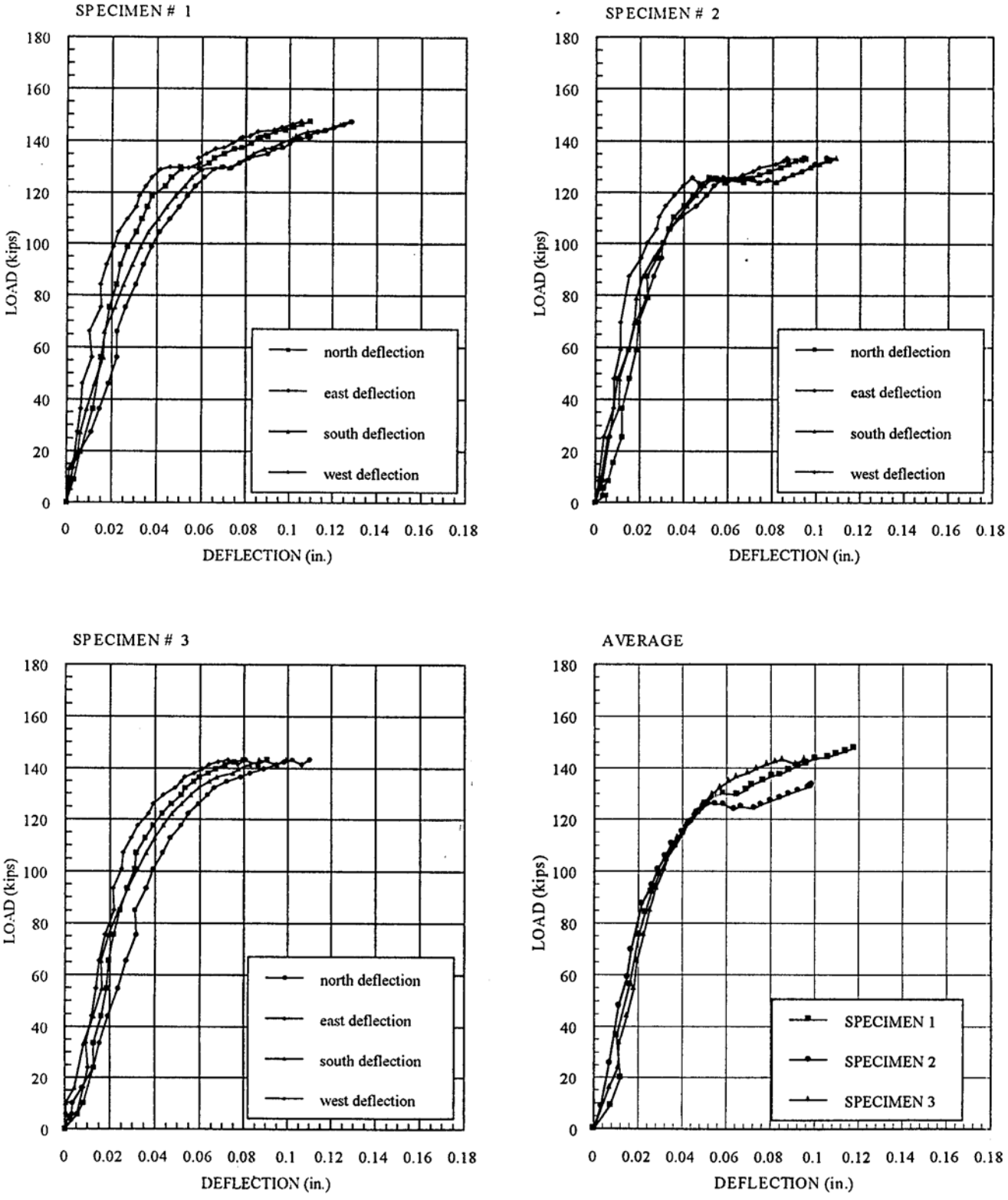

Fig. 4.9 Axial Force vs Axial Deflection Four Layer
(Series 1: 5.25x5.25, fc'= 3 ksi)

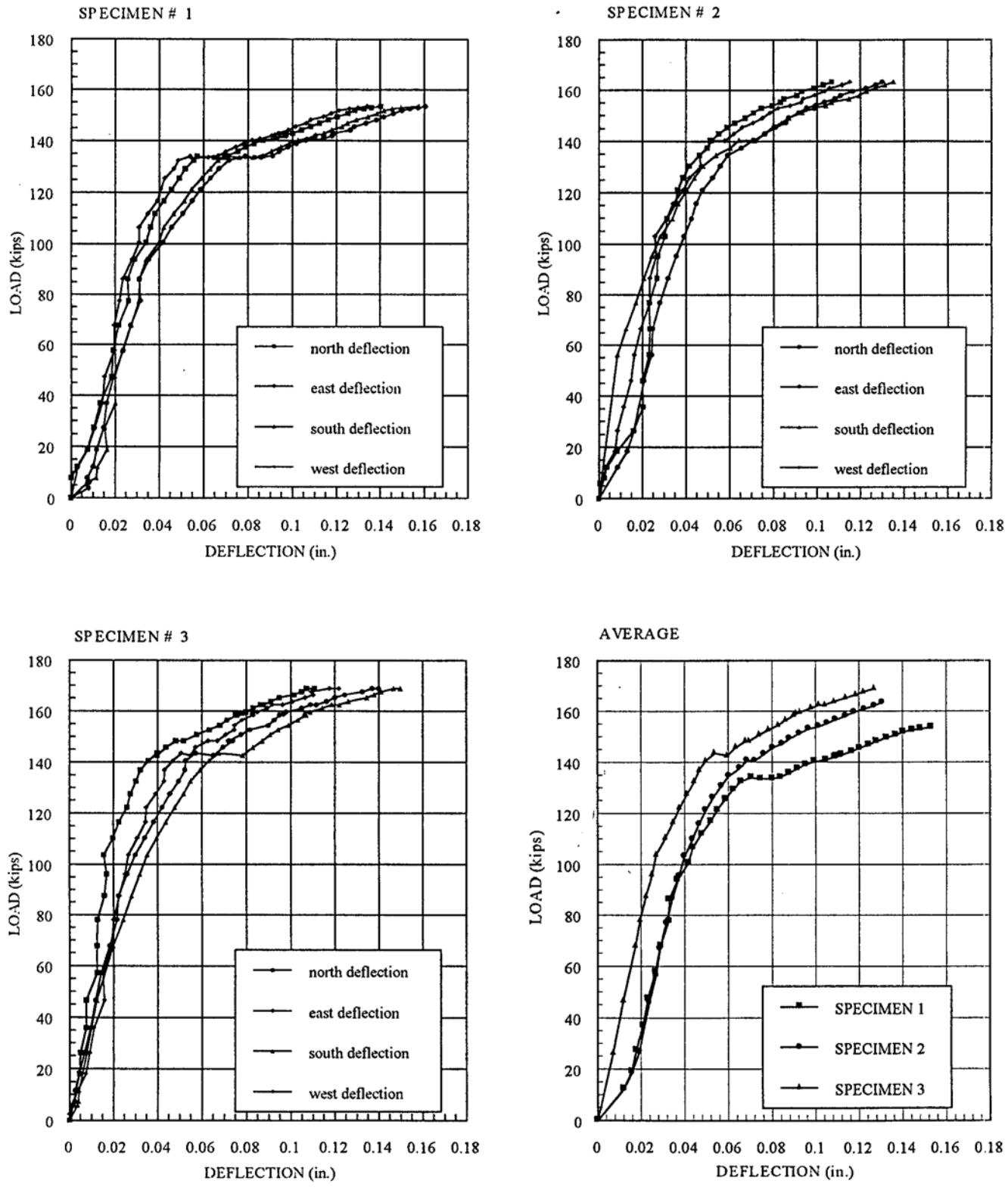

Fig. 4.10 Axial Stress vs Axial and Transverse Strain Control
(Series 1: 5.25x5.25, f'c = 3 ksi)

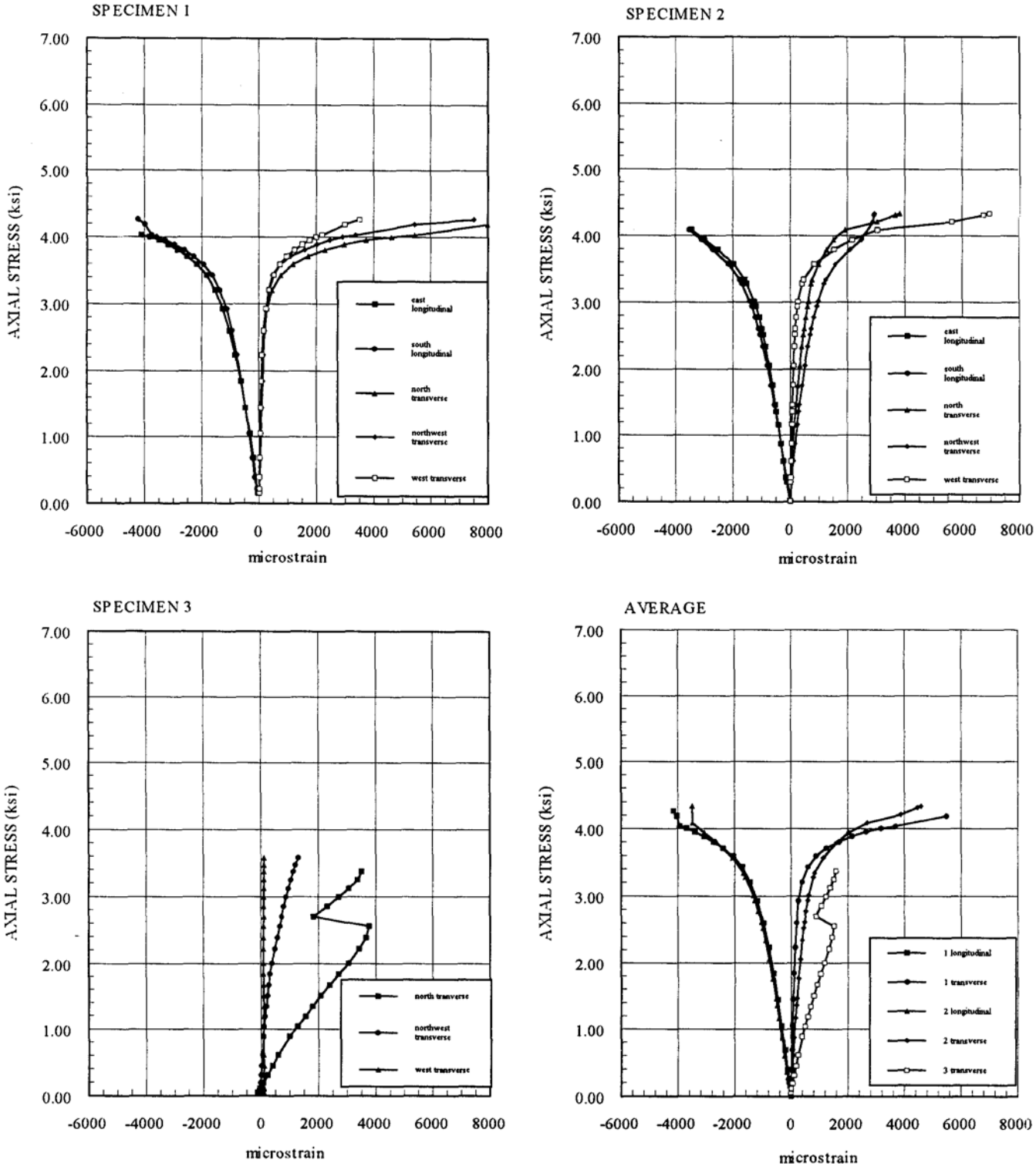

Fig. 4.11 Axial Stress vs Axial and Transverse Strain One Layer
(Series 1: 5.25x5.25, fc'= 3 ksi)

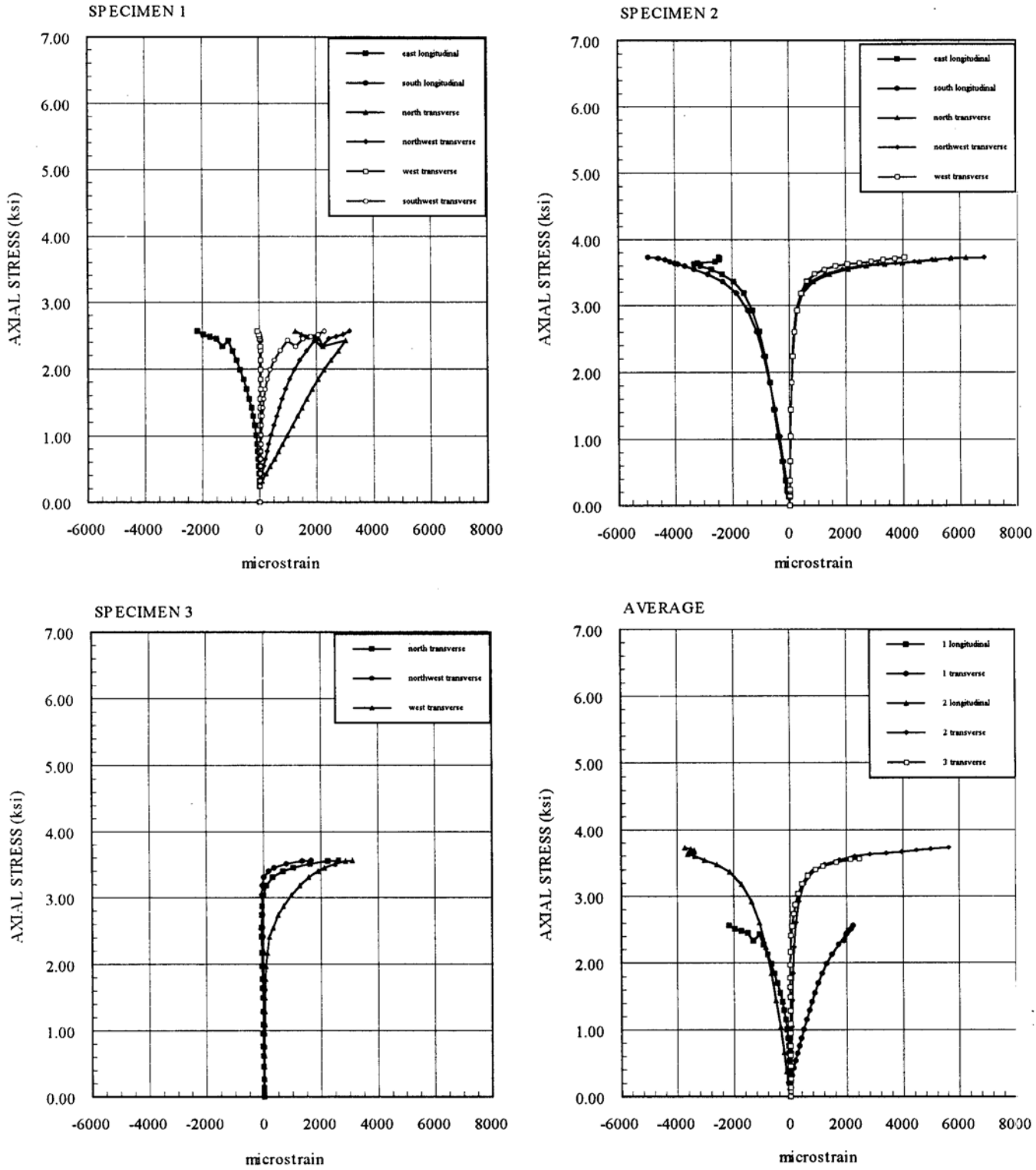

Fig. 4.12 Axial Stress vs Axial and Transverse Strain Two Layers (Series 1: 5.25x5.25, fc'= 3 ksi)

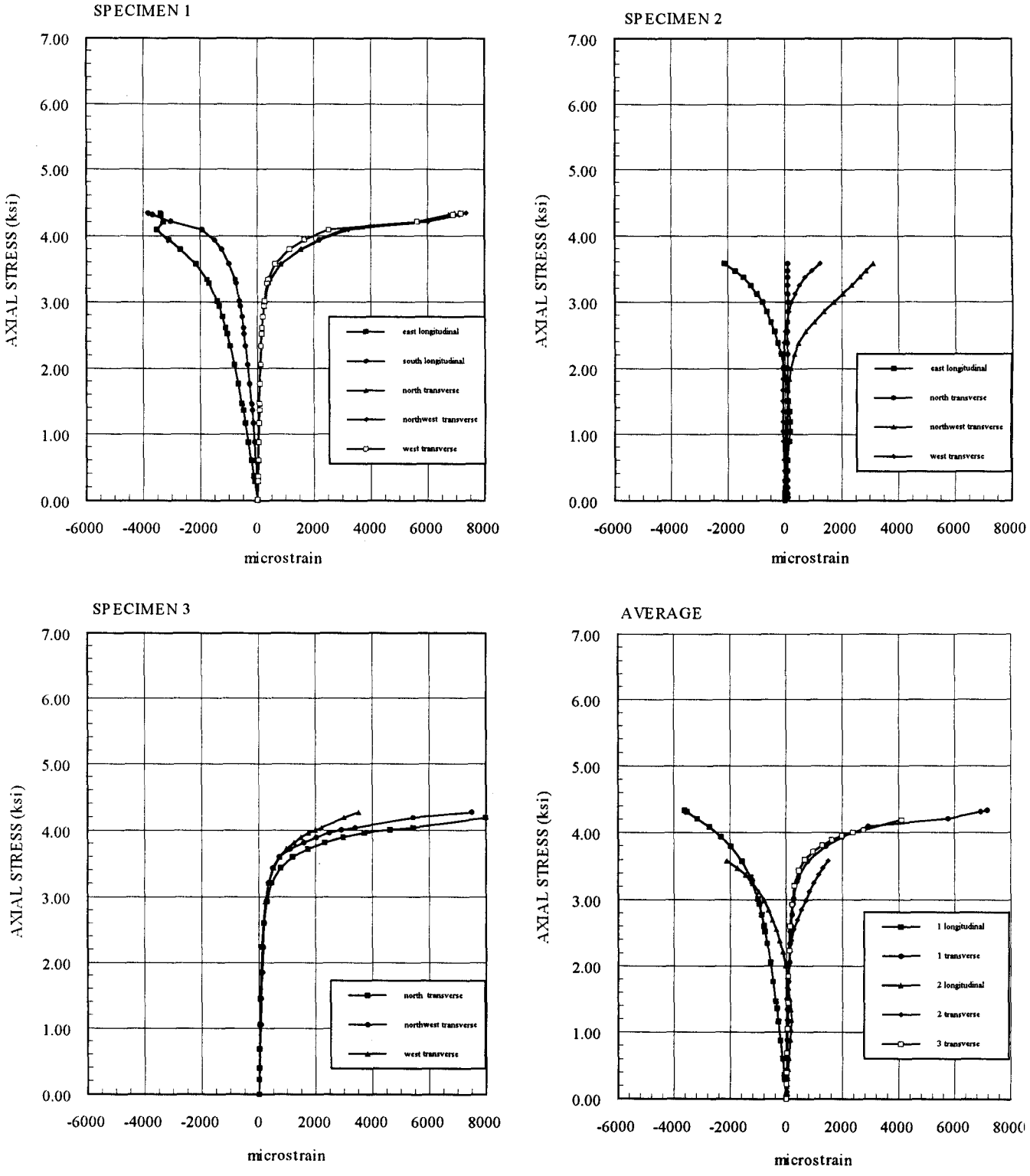

Fig. 4.13 Axial Stress vs Axial and Transverse Strain Three Layers
(Series 1: 5.25x5.25, fc'= 3 ksi)

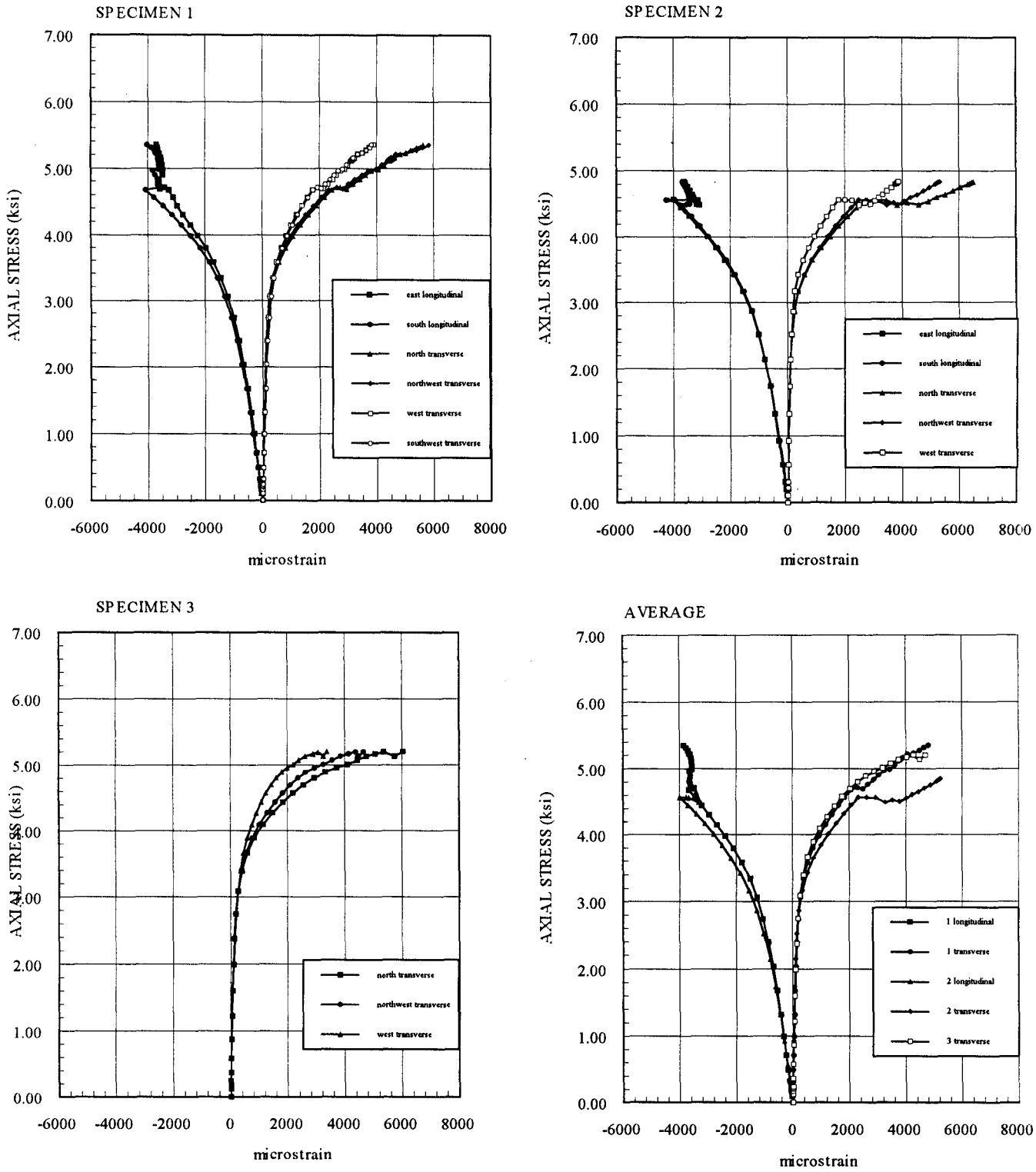

Fig. 4.14 Axial Stress vs Axial and Transverse Strain Four Layers (Series 1: 5.25x5.25, fc'= 3 ksi)

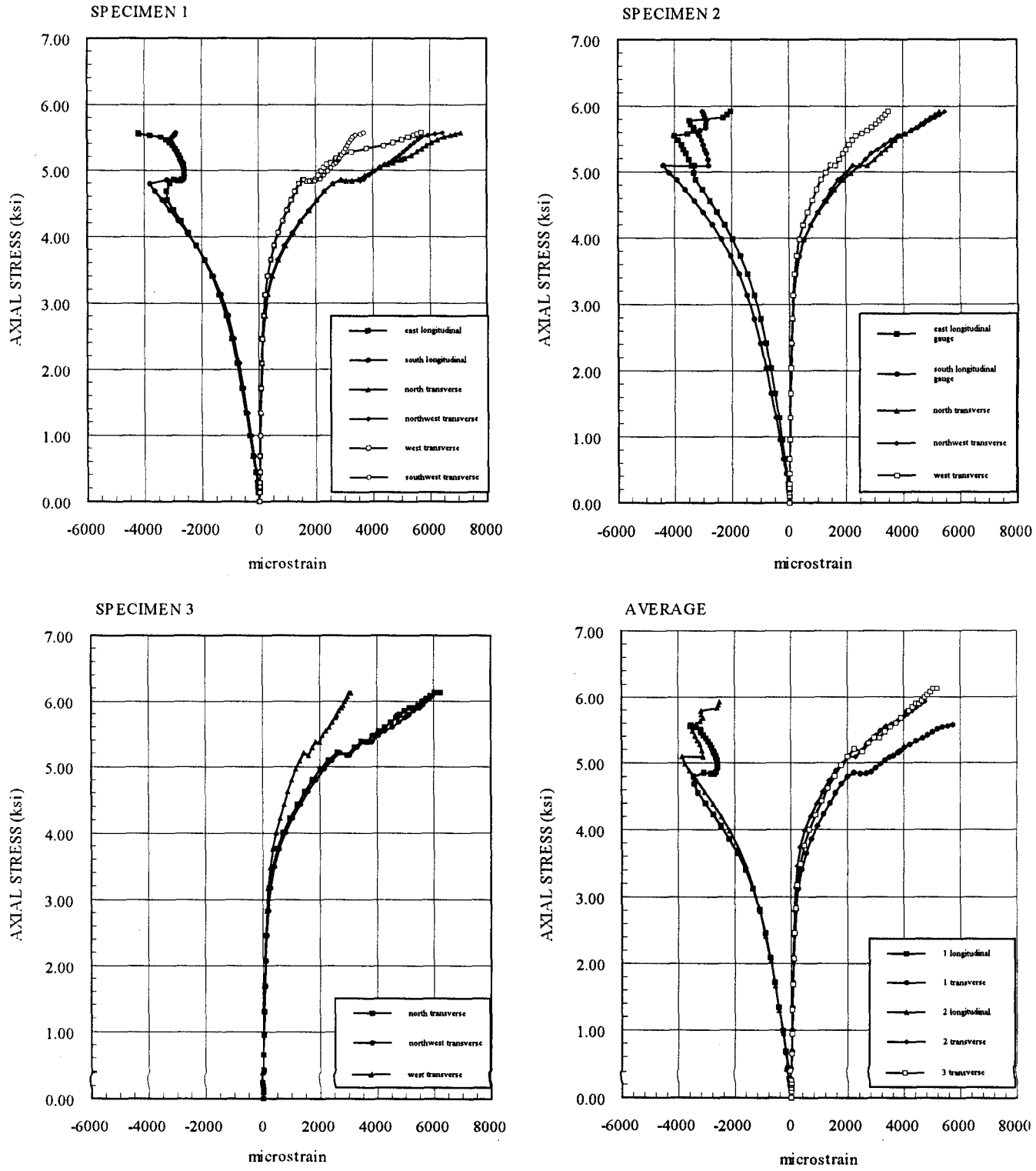

Fig. 4.15 Axial Force vs Axial Deflection Control
(Series 2: 4.25x6.5 , fc'= 3 ksi)

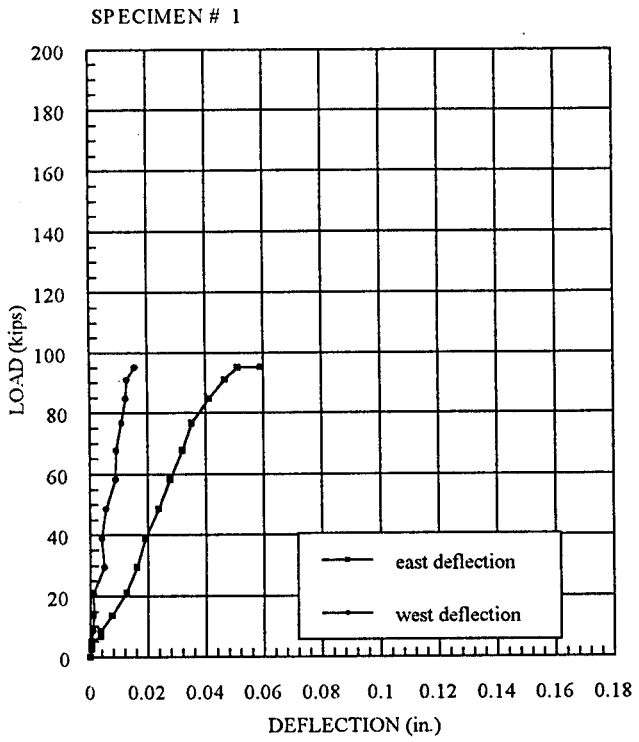

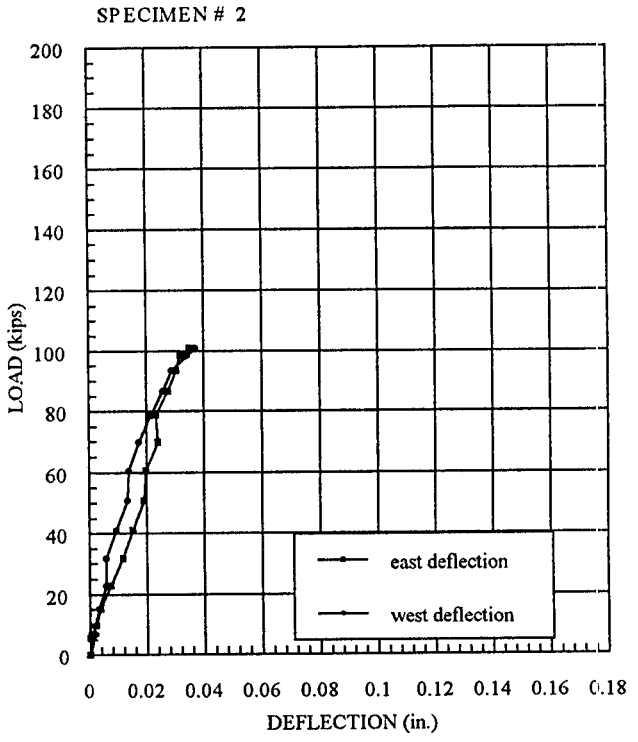

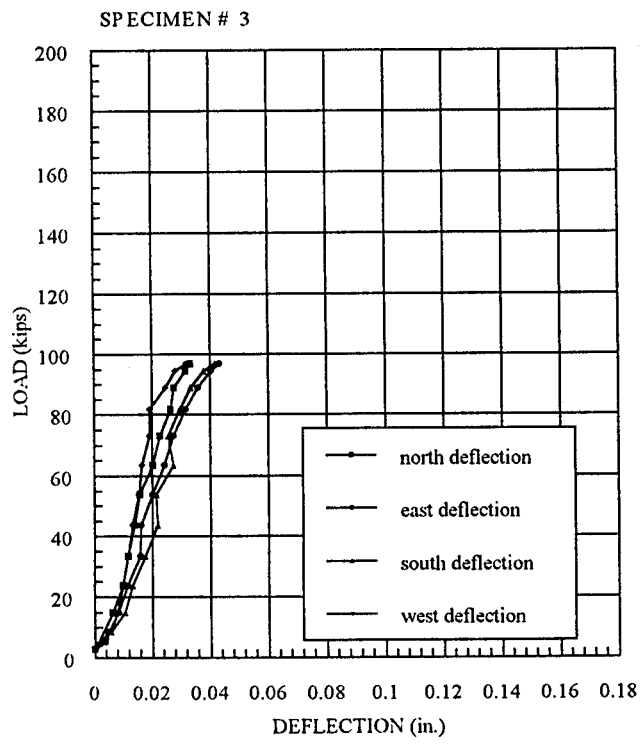

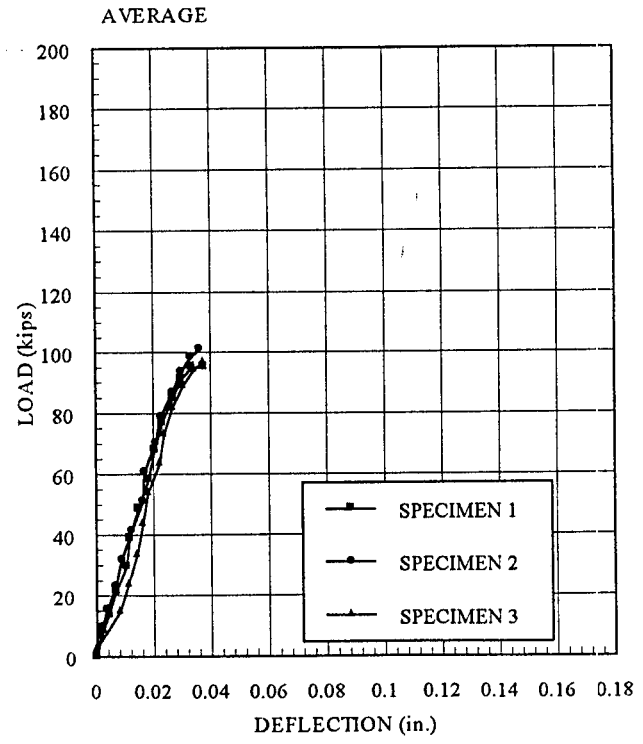

Fig. 4.16 Axial Force vs Axial Deflection One Layer
(Series 2: 4.25x6.5 , fc'= 3 ksi)

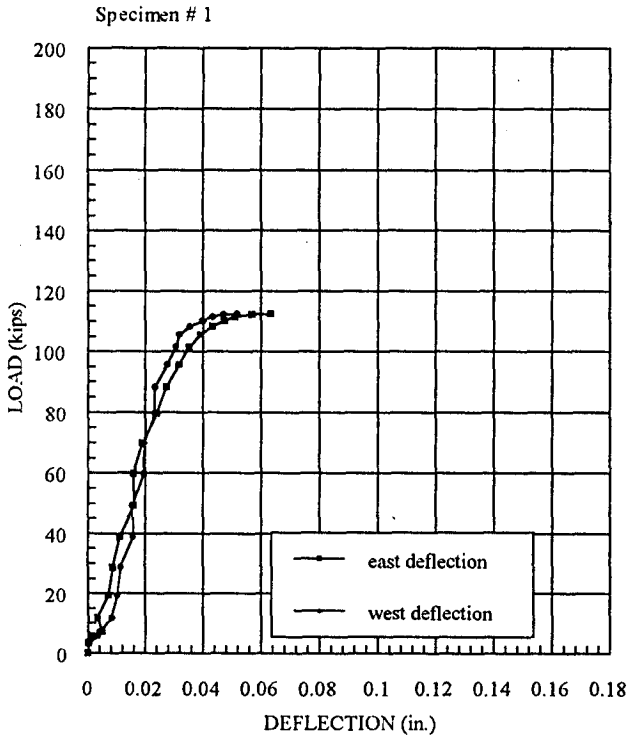

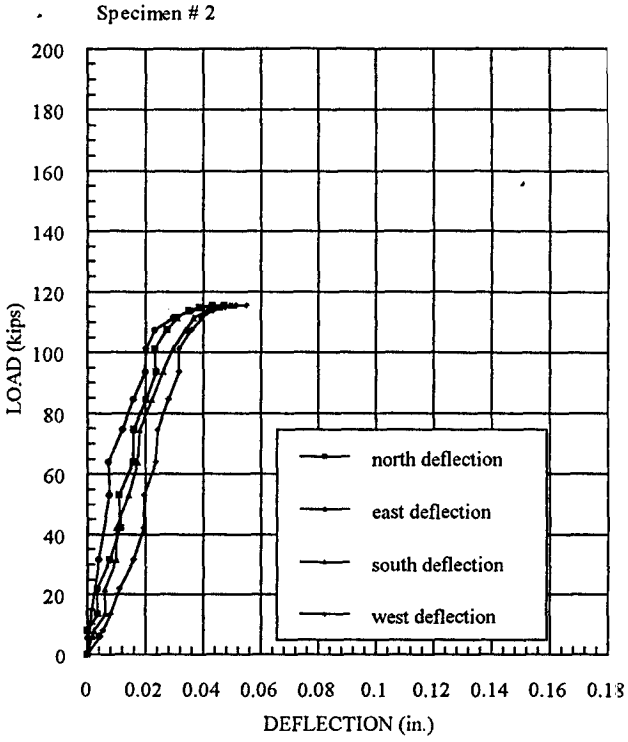

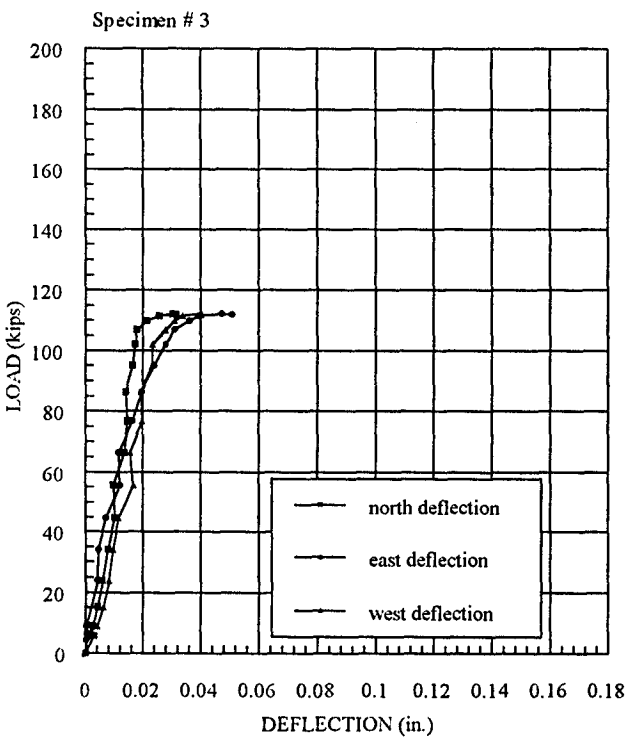

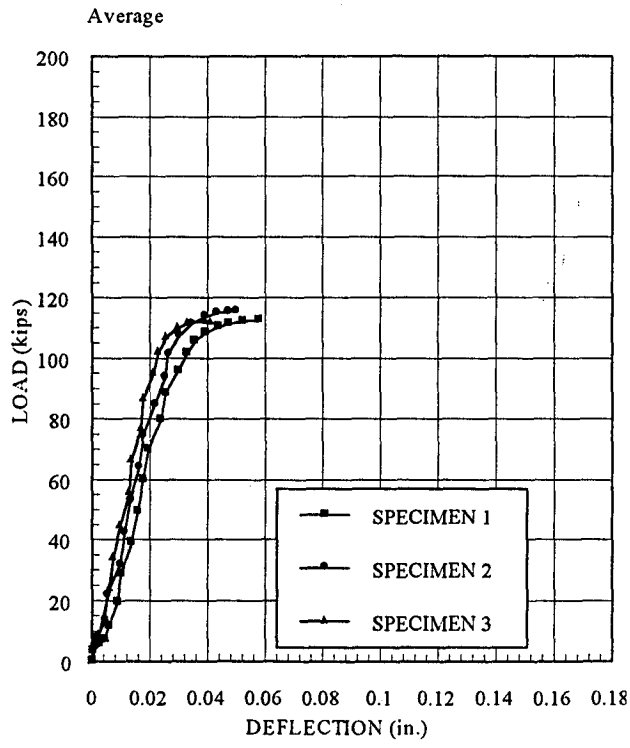

Fig. 4.17 Axial Force vs Axial Deflection Two Layer
(Series 2: 4.25x6.5 , fc'= 3 ksi)

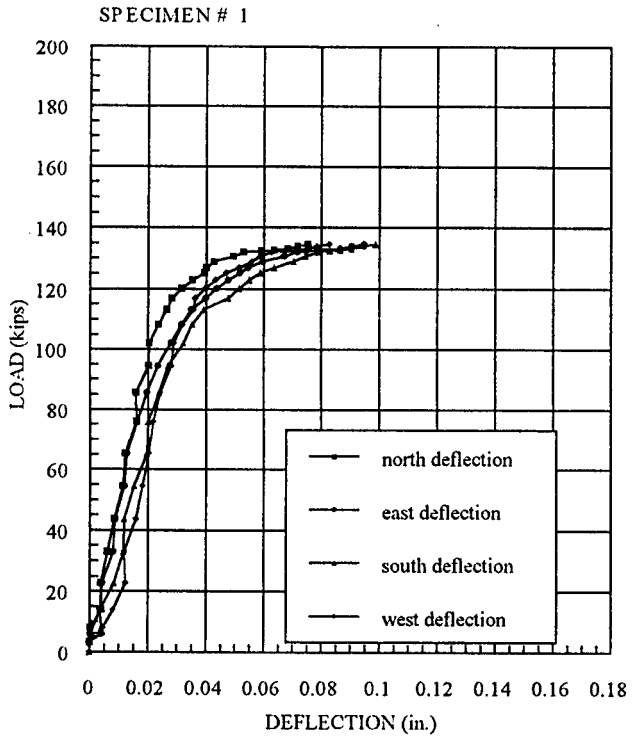

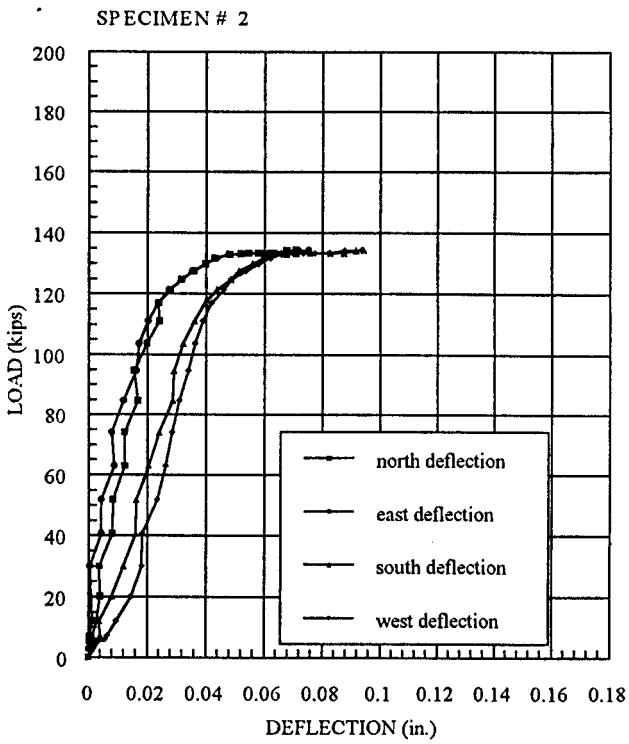

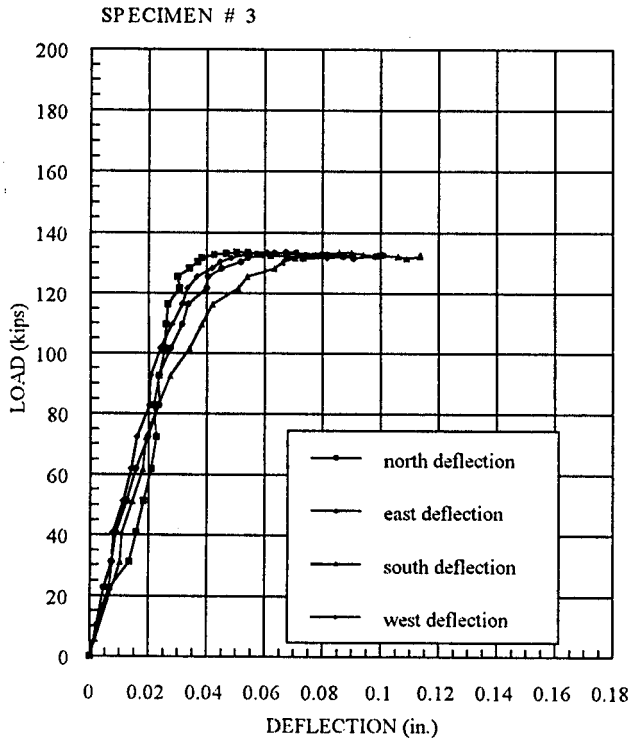

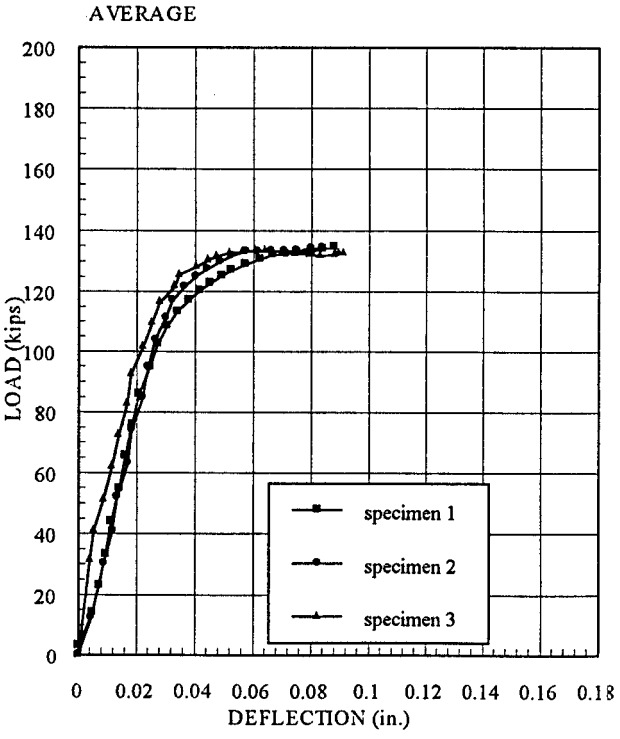

Fig. 4.18 Axial Force vs Axial Deflection Three Layer

(Series 2: 4.25x6.5 , fc'= 3 ksi)

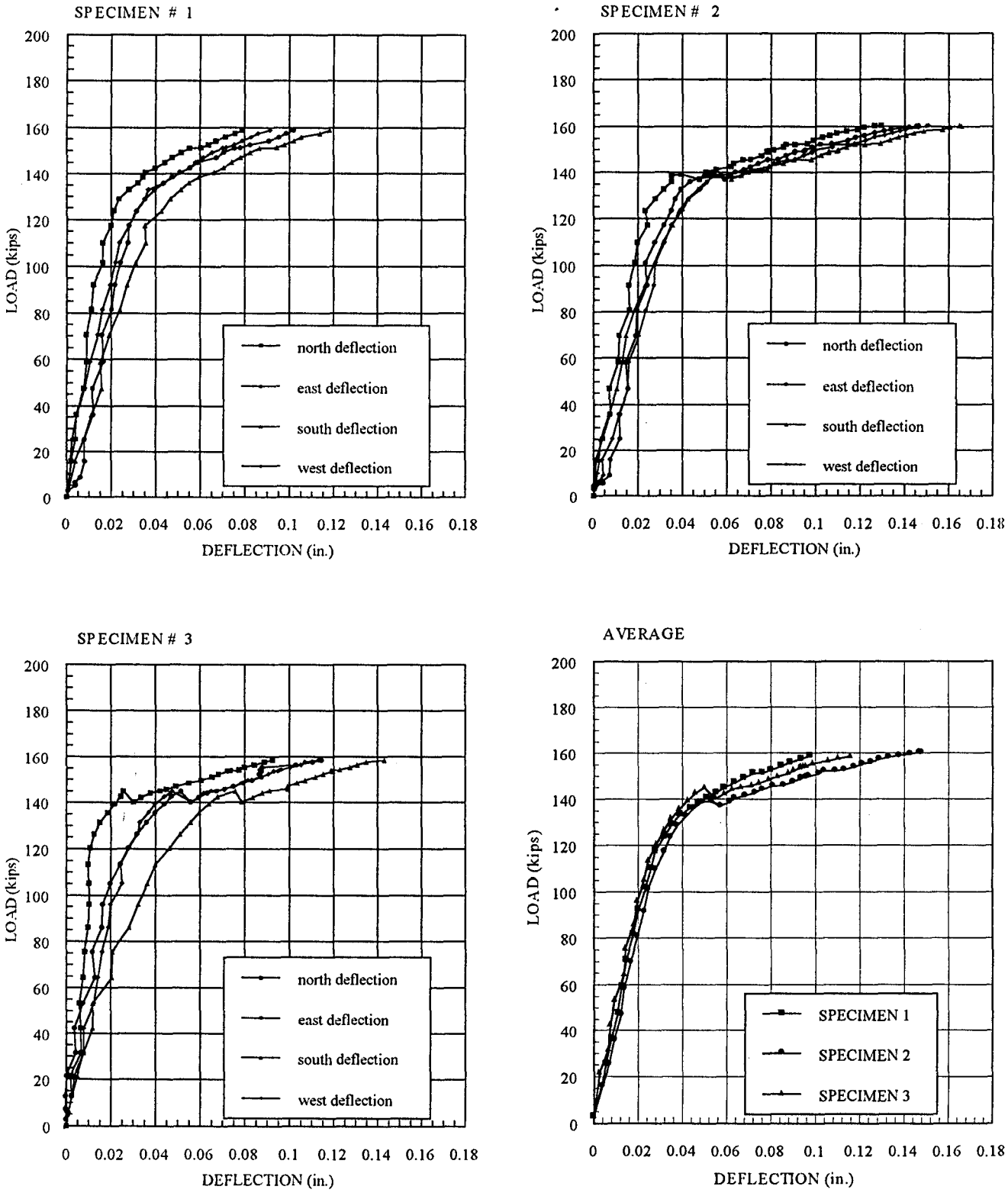

Fig. 4.19 Axial Force vs Axial Deflection Four Layer (Series 2: 4.25x6.5 , fc'= 3 ksi)

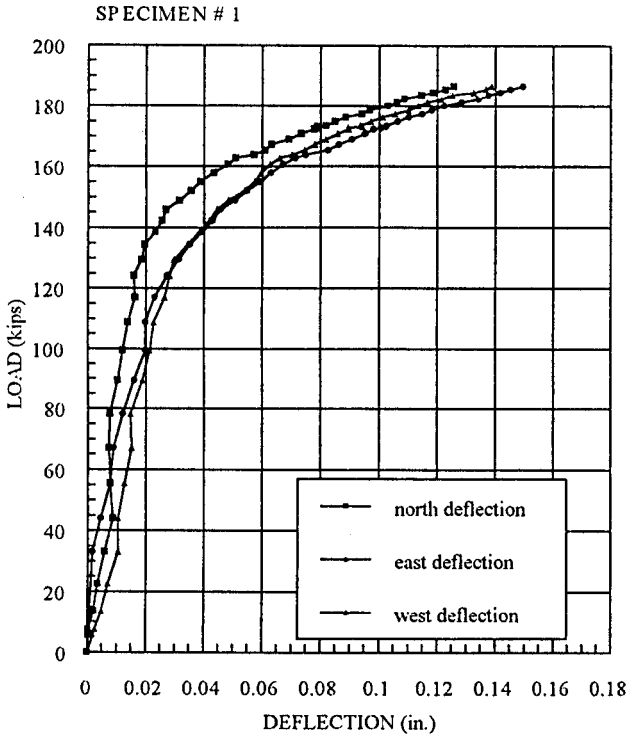

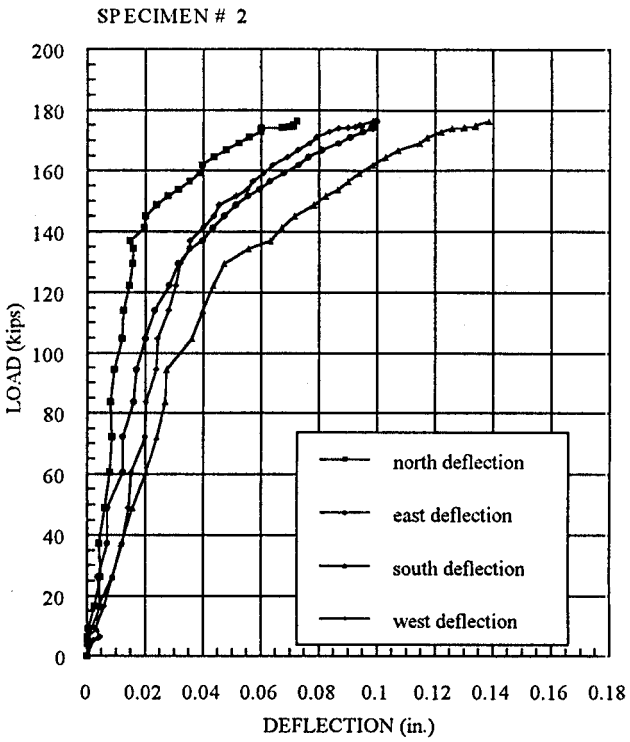

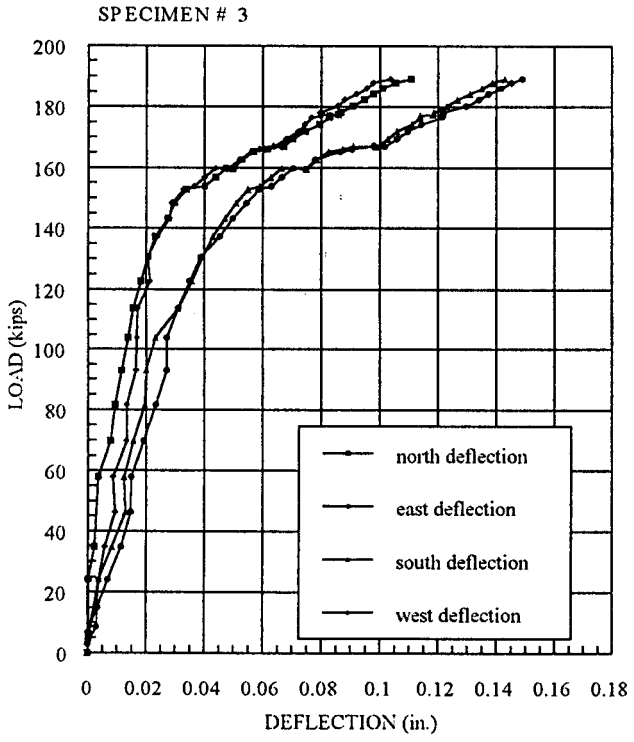

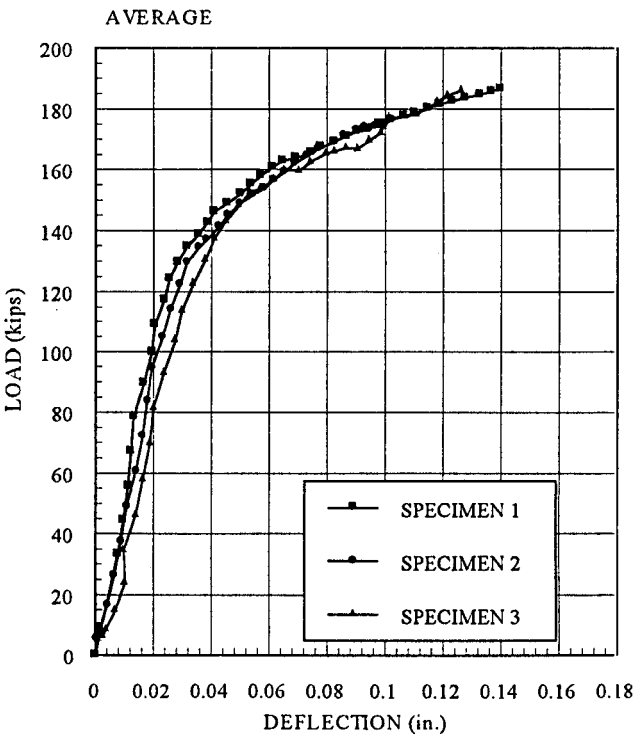

Fig. 4.20 Axial Stress vs Axial and Transverse Strain Control

(Series 2: 4.25x6.5 , fc'= 3 ksi)

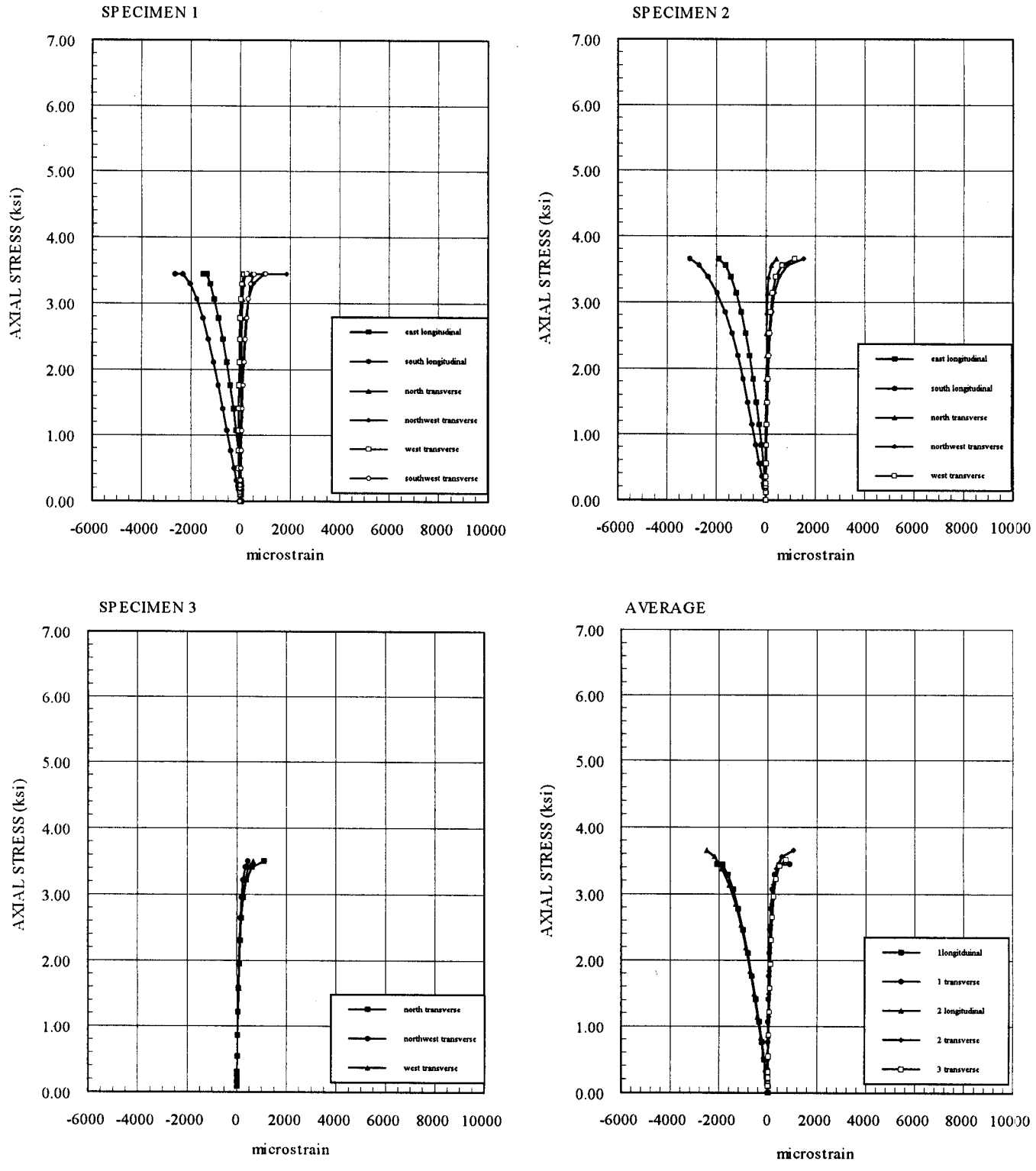

Fig. 4.21 Axial Stress vs Axial and Transverse Strain One Layer (Series 2: 4.25x6.5 , fc'= 3 ksi)

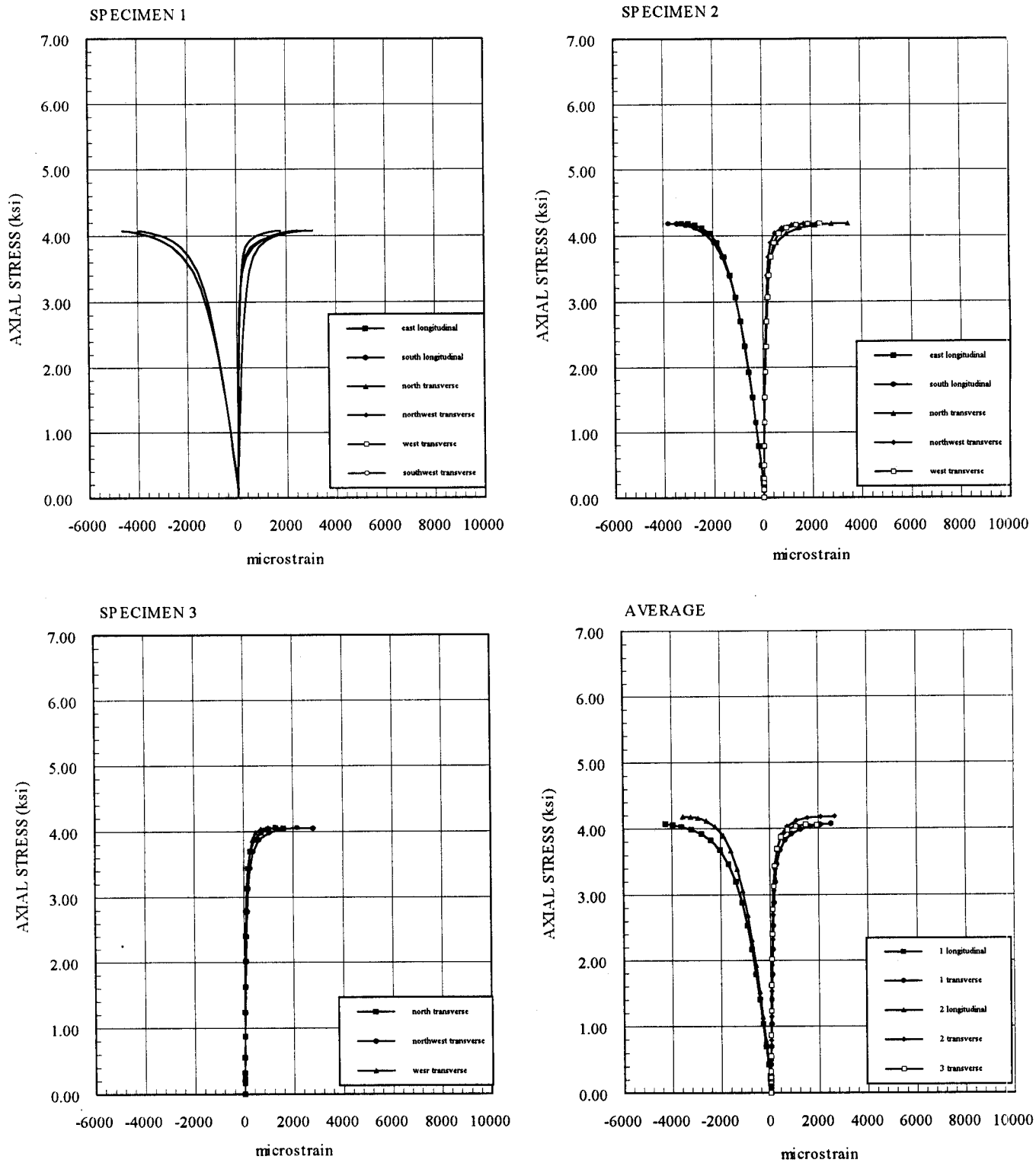

Fig. 4.22 Axial Stress vs Axial and Transverse Strain Two Layers
(Series 2: 4.25x6.5 , fc'= 3 ksi)

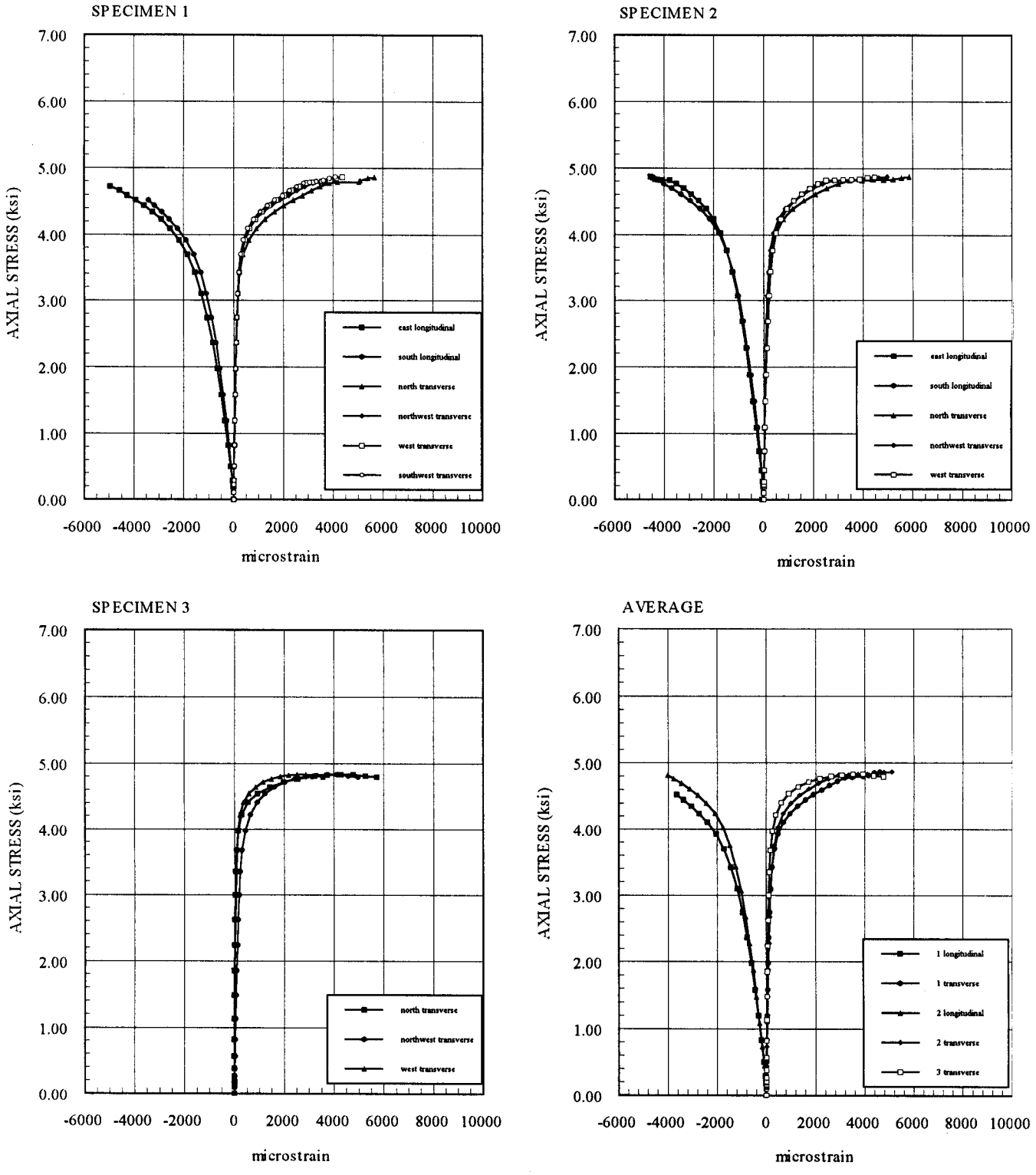

Fig. 4.23 Axial Stress vs Axial and Transverse Strain Three Layers

(Series 2: 4.25x6.5 , fc'= 3 ksi)

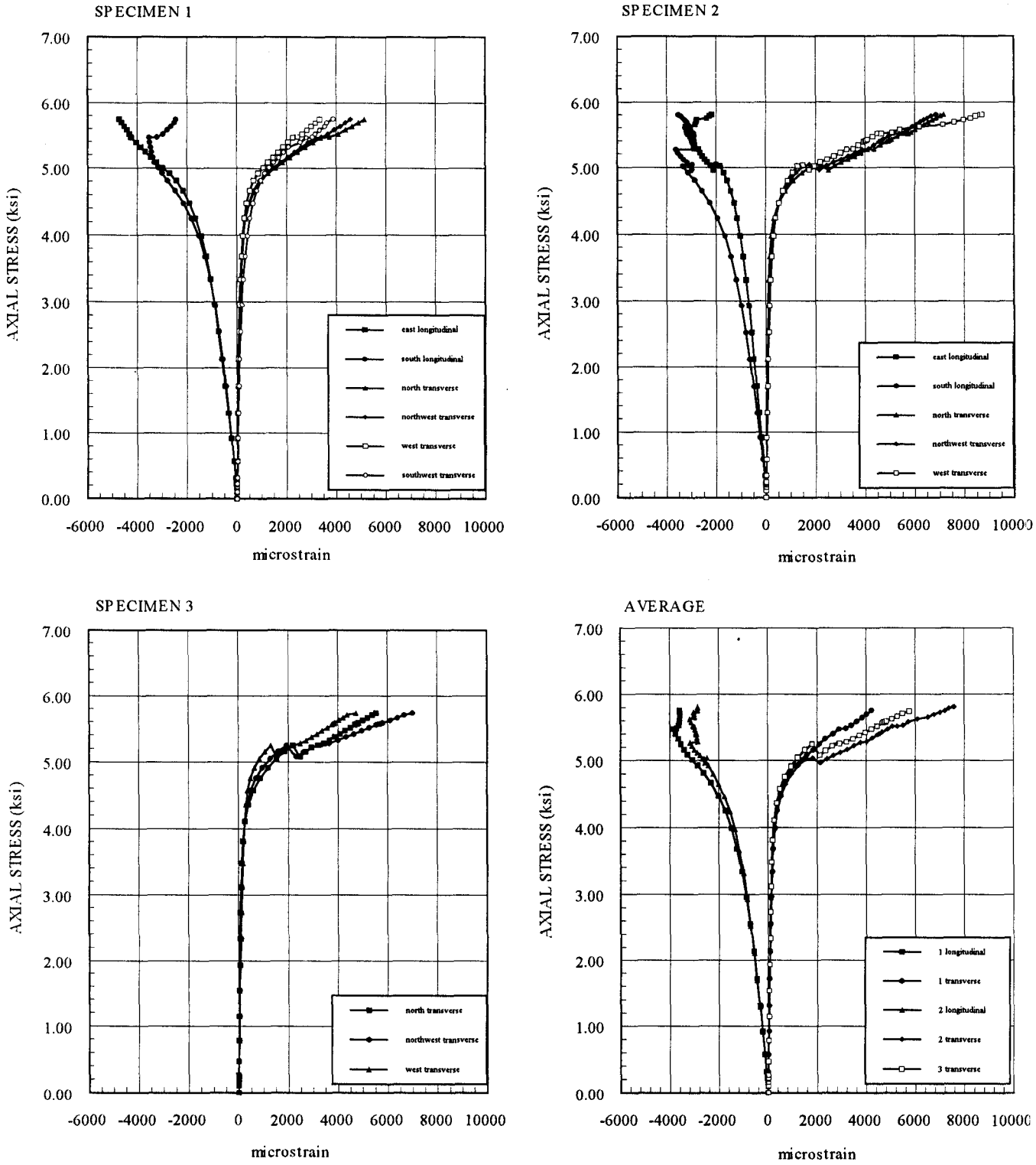

Fig. 4.24 Axial Stress vs Axial and Transverse Strain Four Layers

(Series 2: 4.25x6.5 , fc'= 3 ksi)

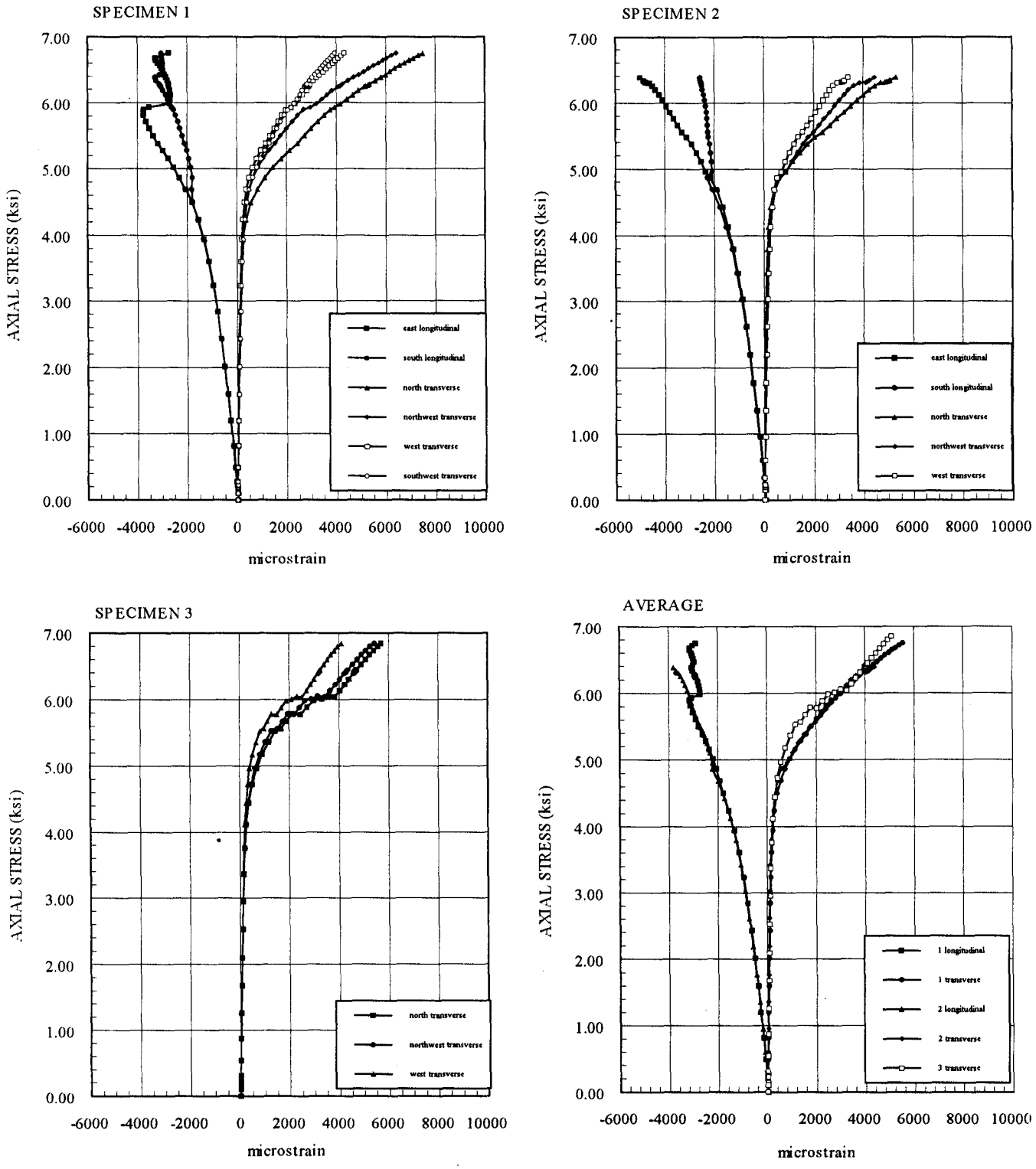

Fig. 4.25 Axial Force vs Axial Deflection Control
(Series 3: 3.75x7.5 , fc'= 3 ksi)

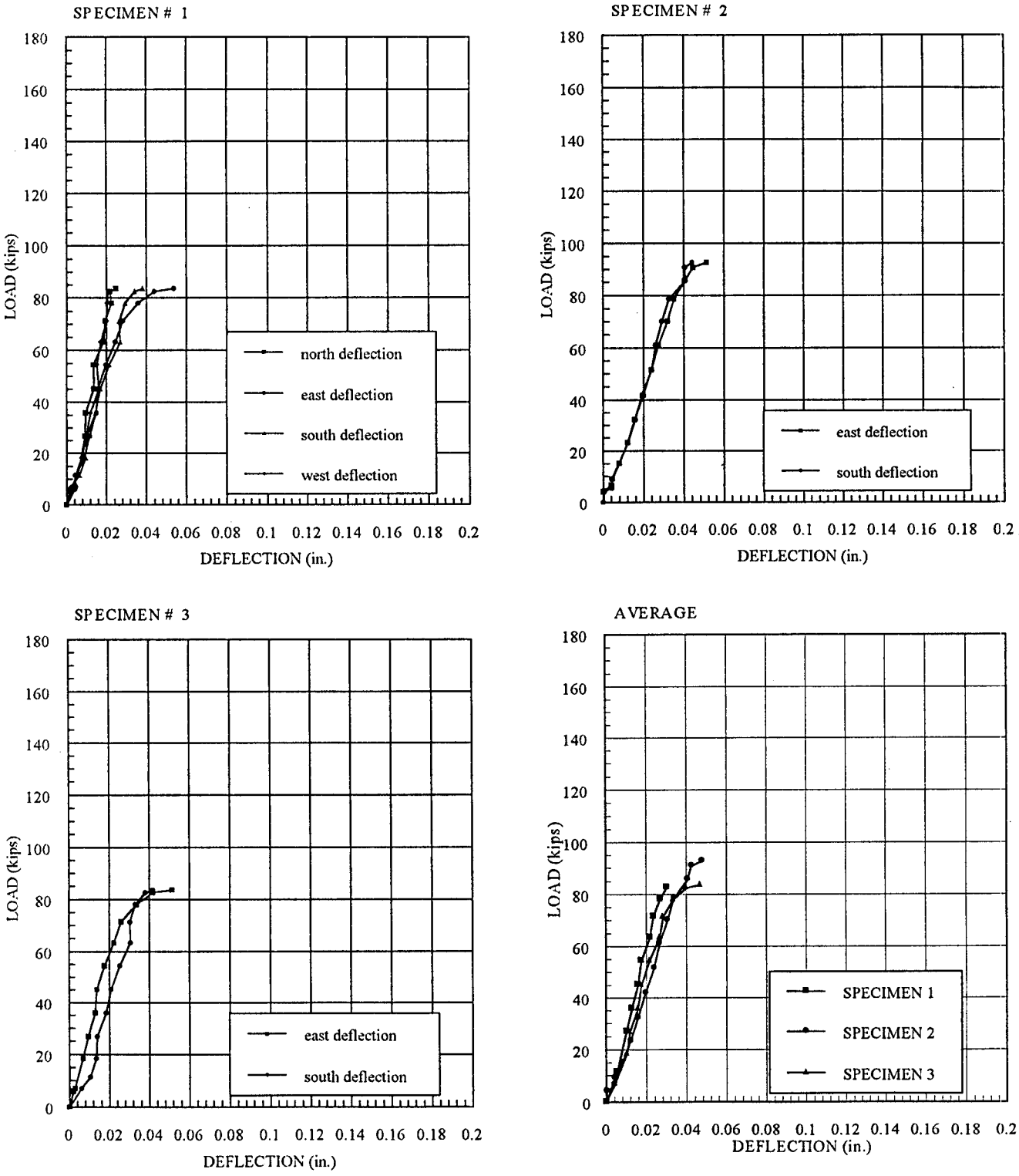

Fig. 4.26 Axial Force vs Axial Deflection One Layer
(Series 3: 3.75x7.5 , fc'= 3 ksi)

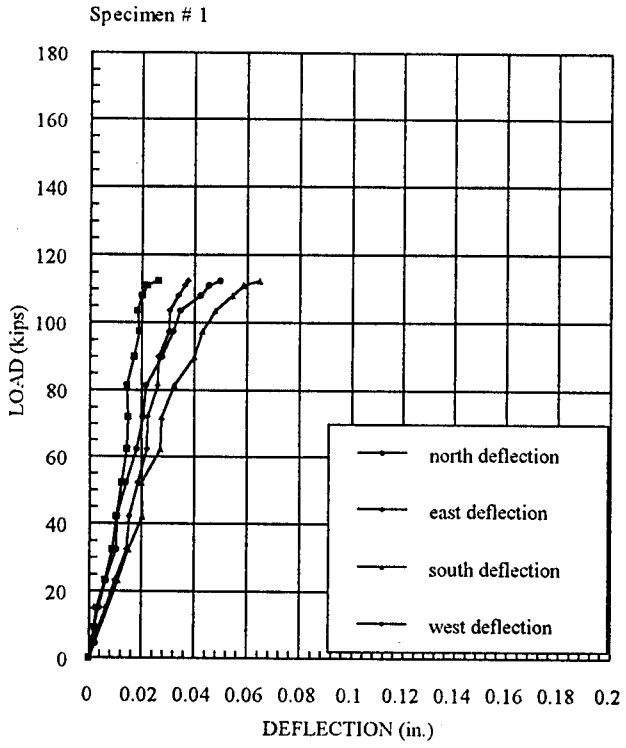

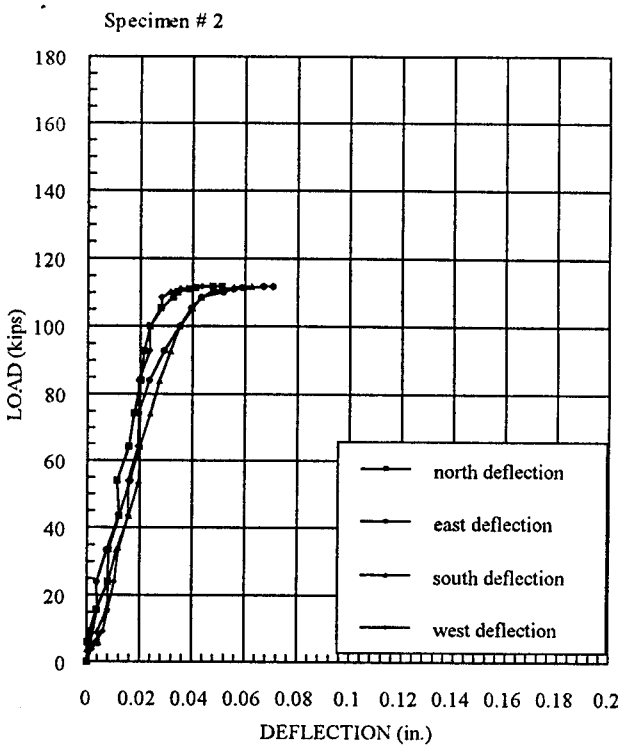

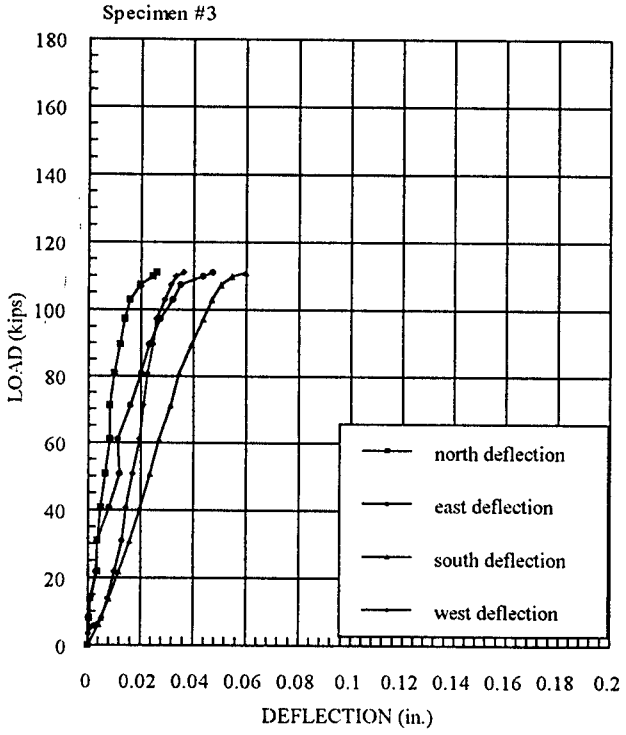

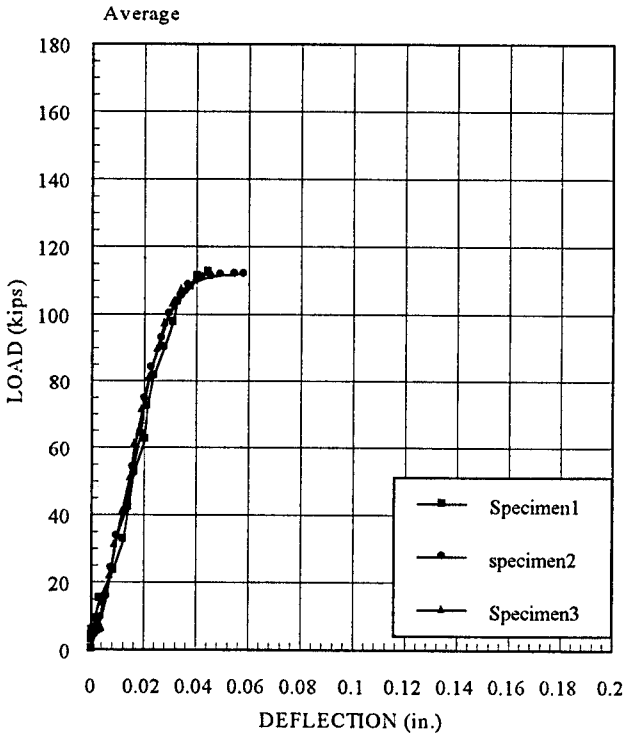

Fig. 4.34 Axial Stress vs Axial and Transverse Strain Four Layers

(Series 3: 5.25x5.25, fc'= 3 ksi)

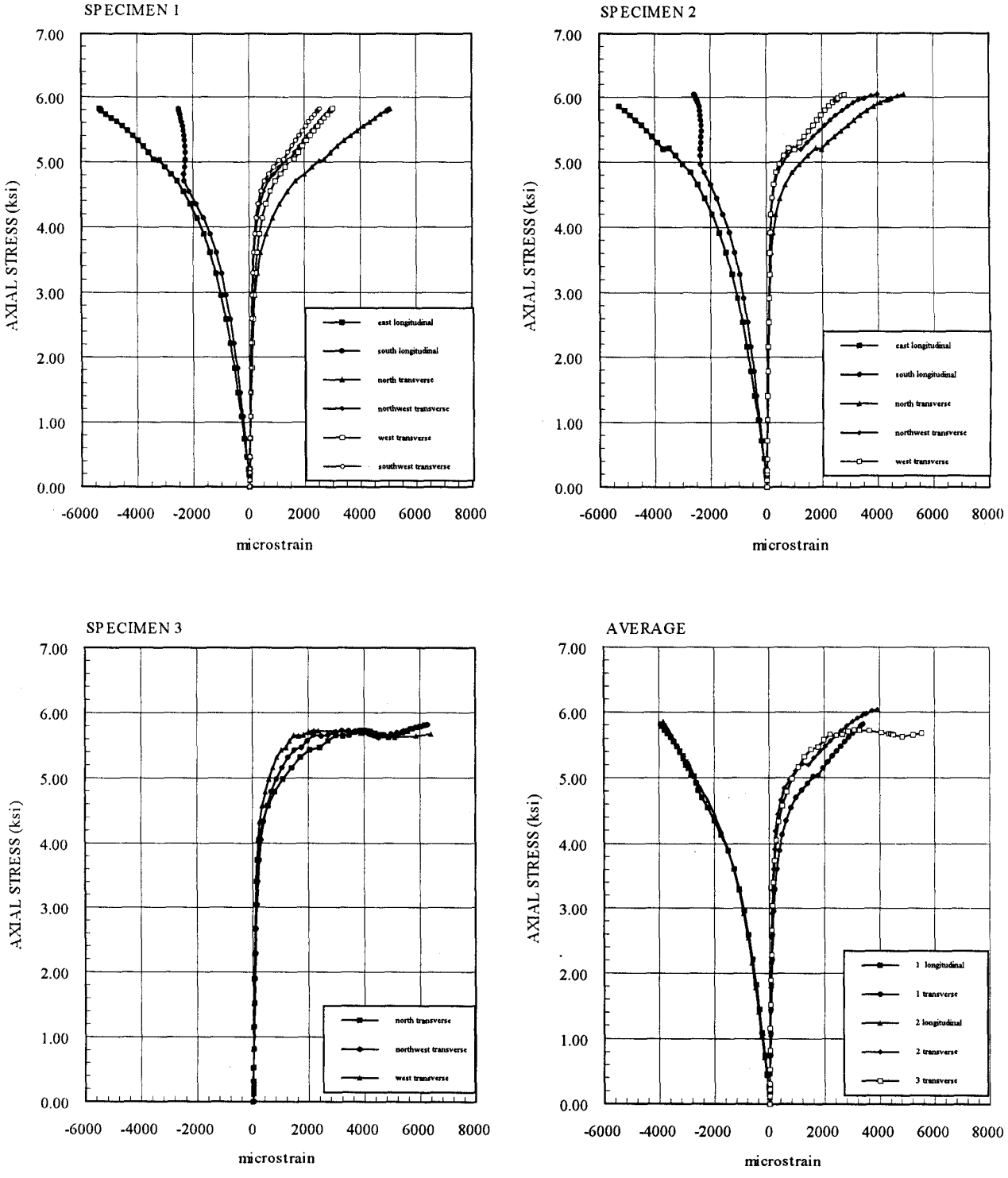

Fig. 4.28 Axial Force vs Axial Deflection Three Layers
(Series 3: 3.75x7.5 , fc'= 3 ksi)

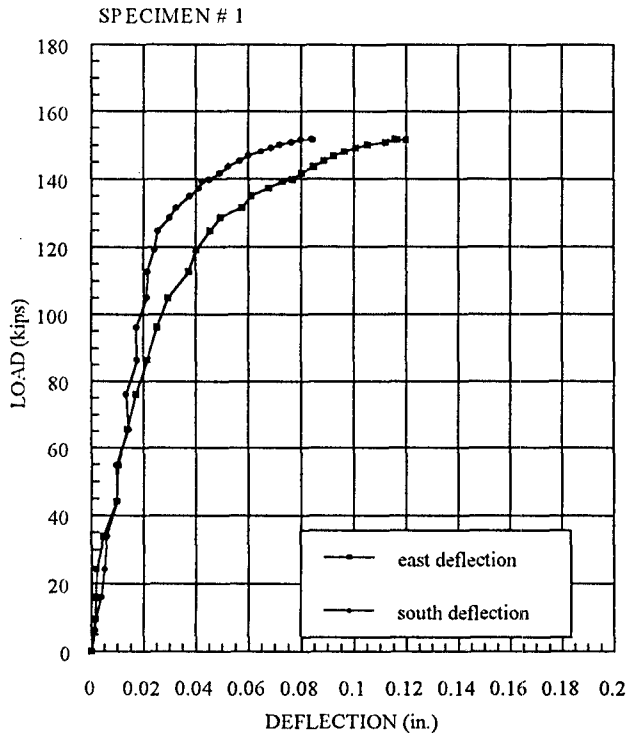

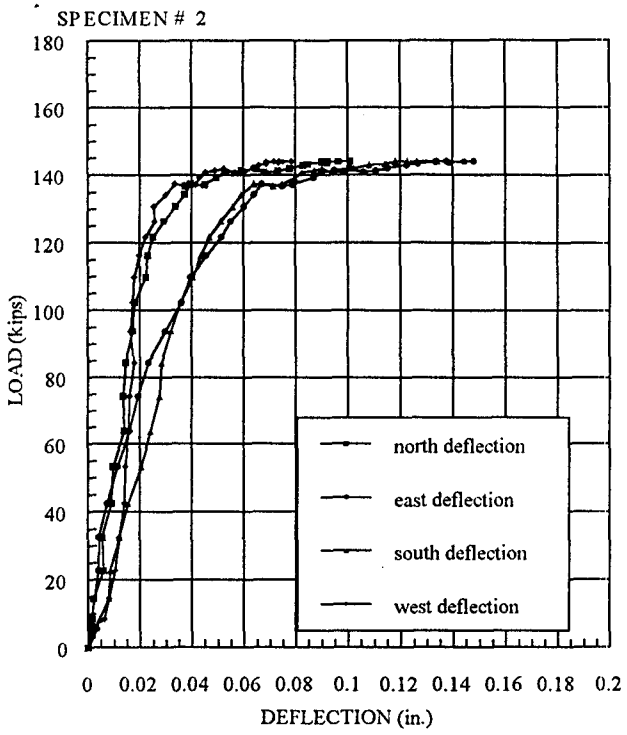

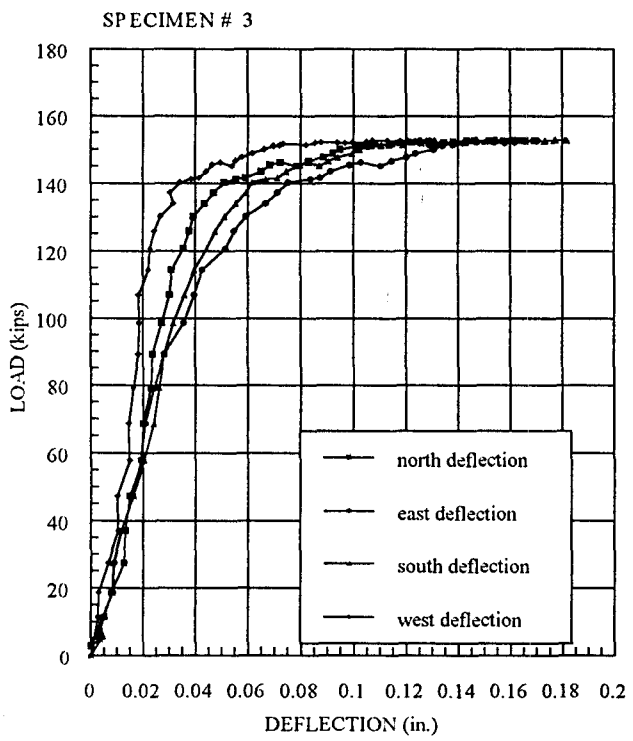

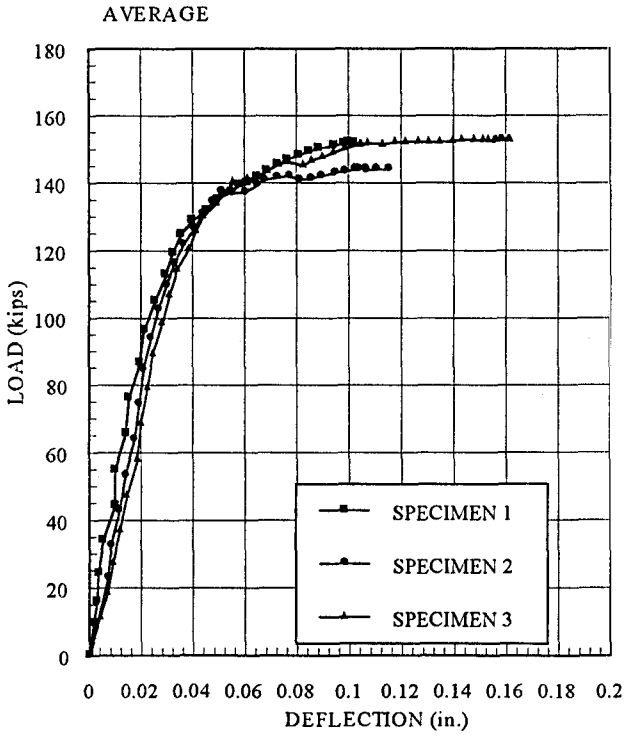

Fig. 4.29 Axial Force vs Axial Deflection Four Layer
(Series 3: 3.75x7.5 , fc'= 3 ksi)

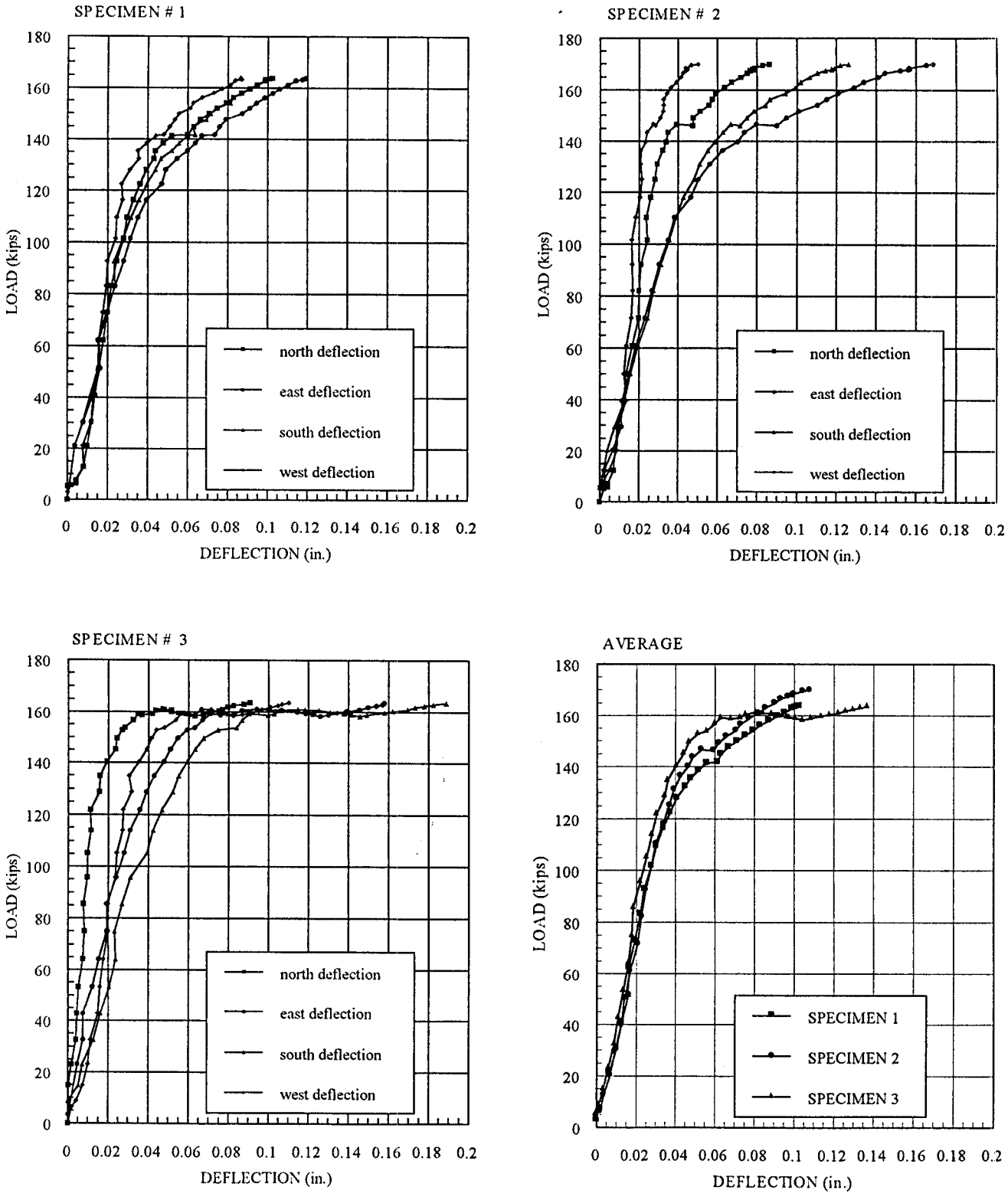

Fig. 4.30 Axial Stress vs Axial and Transverse Strain Control

(Series 3: 3.75x7.5 , fc'= 3 ksi)

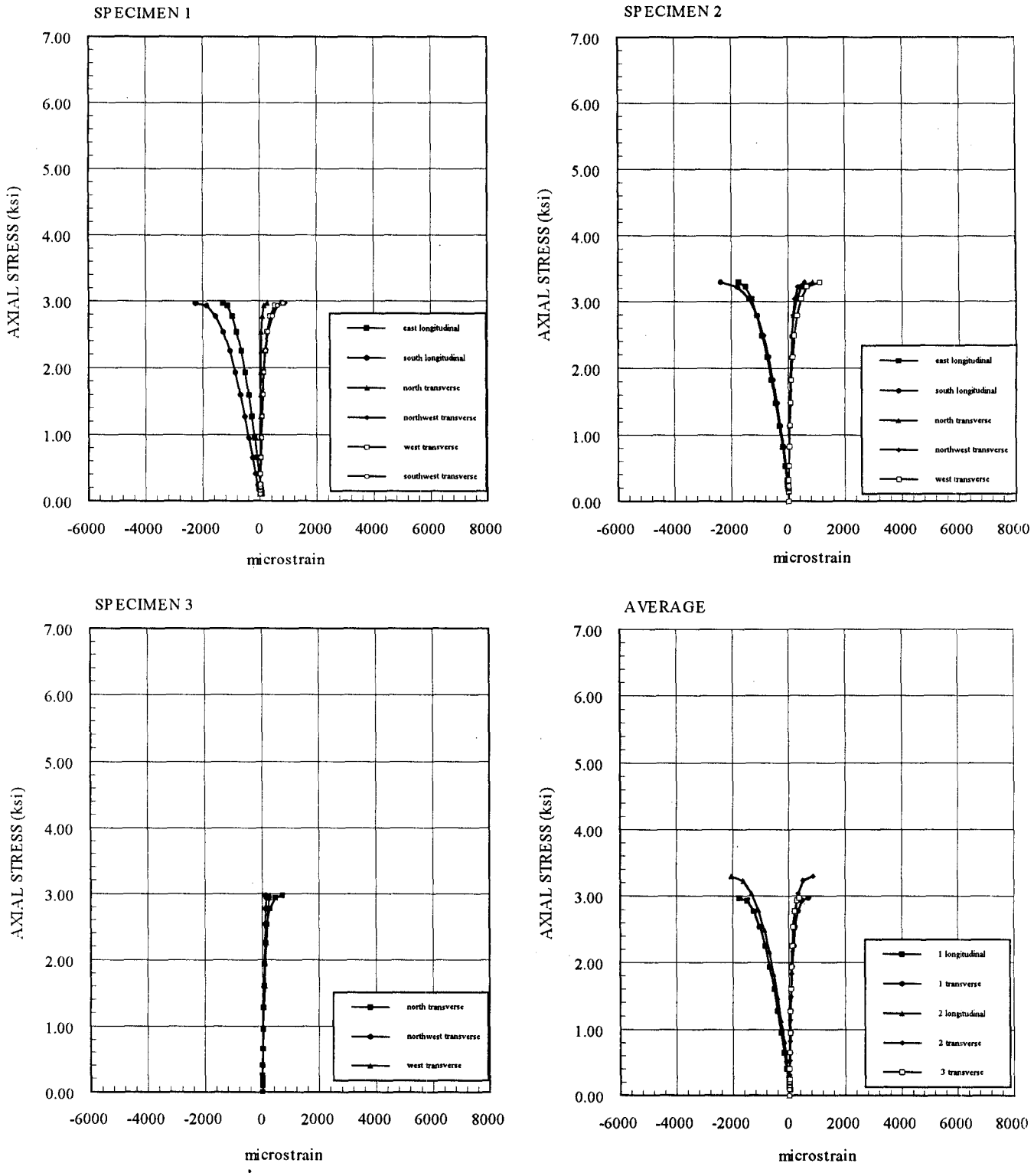

Fig. 4.31 Axial Stress vs Axial and Transverse Strain One Layer (Series 3: 3.75x7.5 , fc'= 3 ksi)

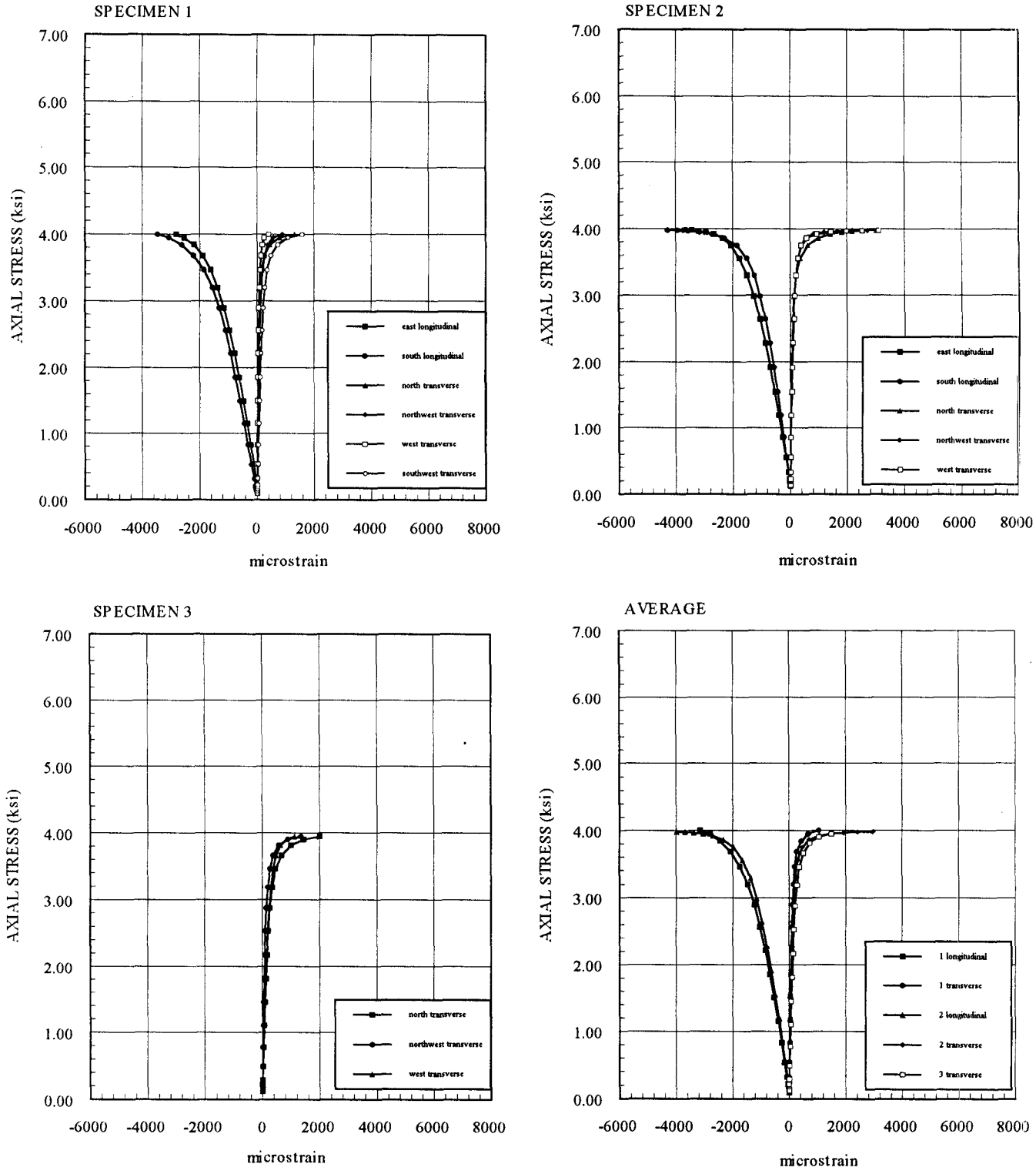

Fig. 4.32 Axial Stress vs Axial and Transverse Strain Two Layers

(Series 3: 3.75x7.5 , fc'= 3 ksi)

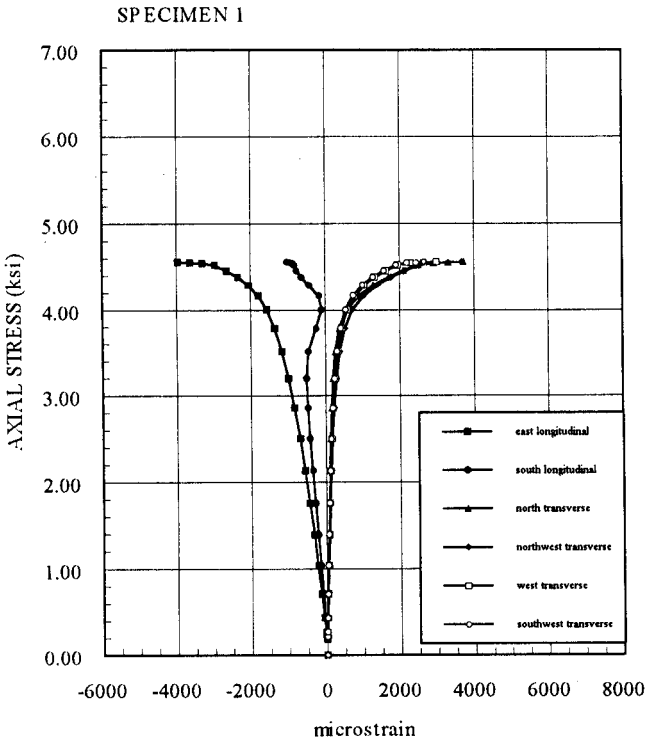

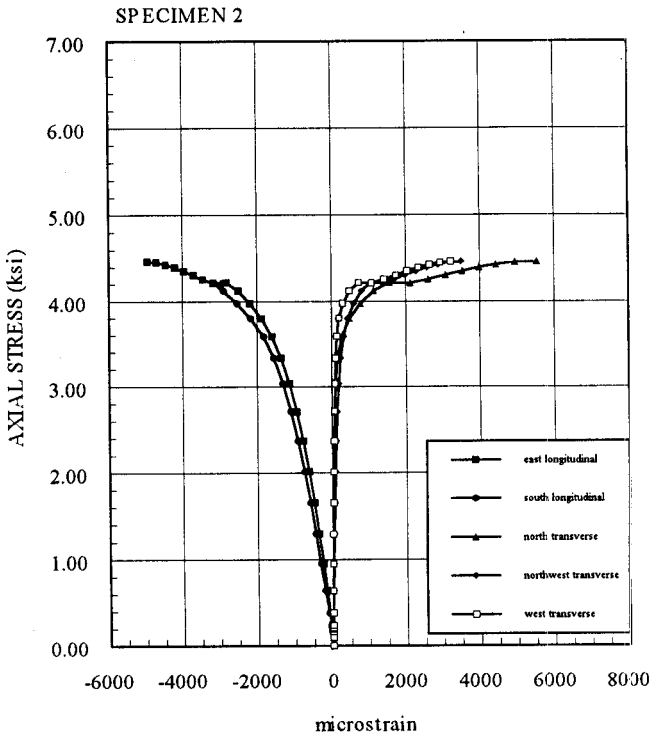

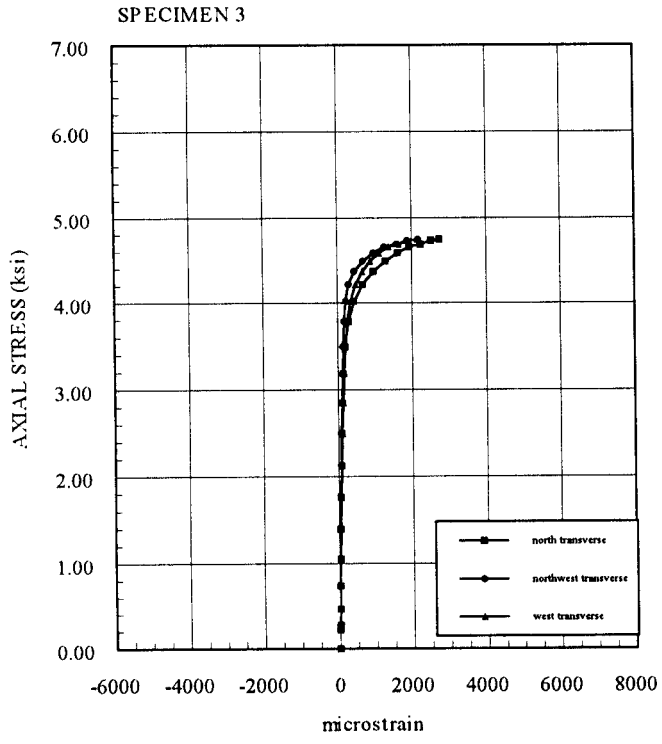

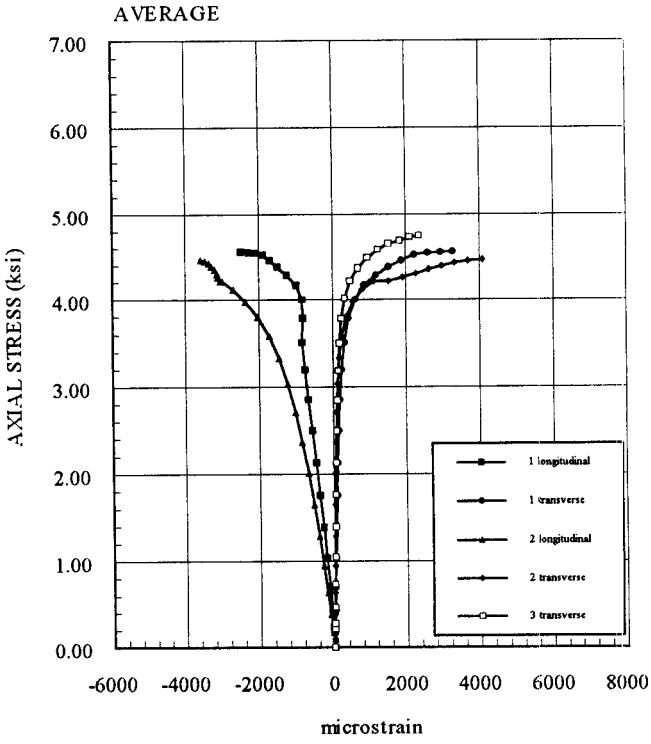

Fig. 4.33 Axial Stress vs Axial and Transverse Strain Three Layers (Series 3: 3.75x7.5 , fc'= 3 ksi)

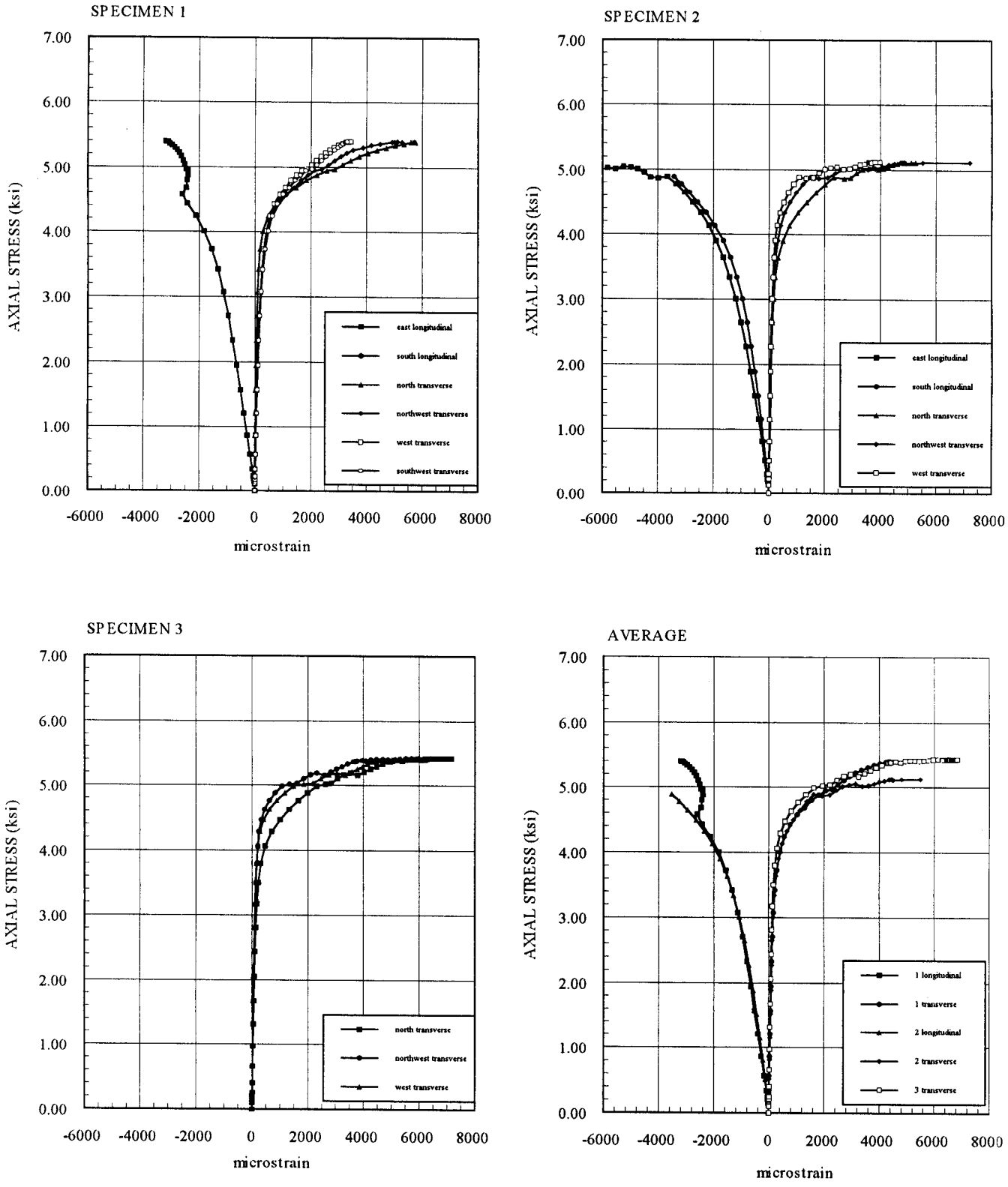

Fig. 4.34 Axial Stress vs Axial and Transverse Strain Four Layers (Series 3: 5.25x5.25, fc'= 3 ksi)

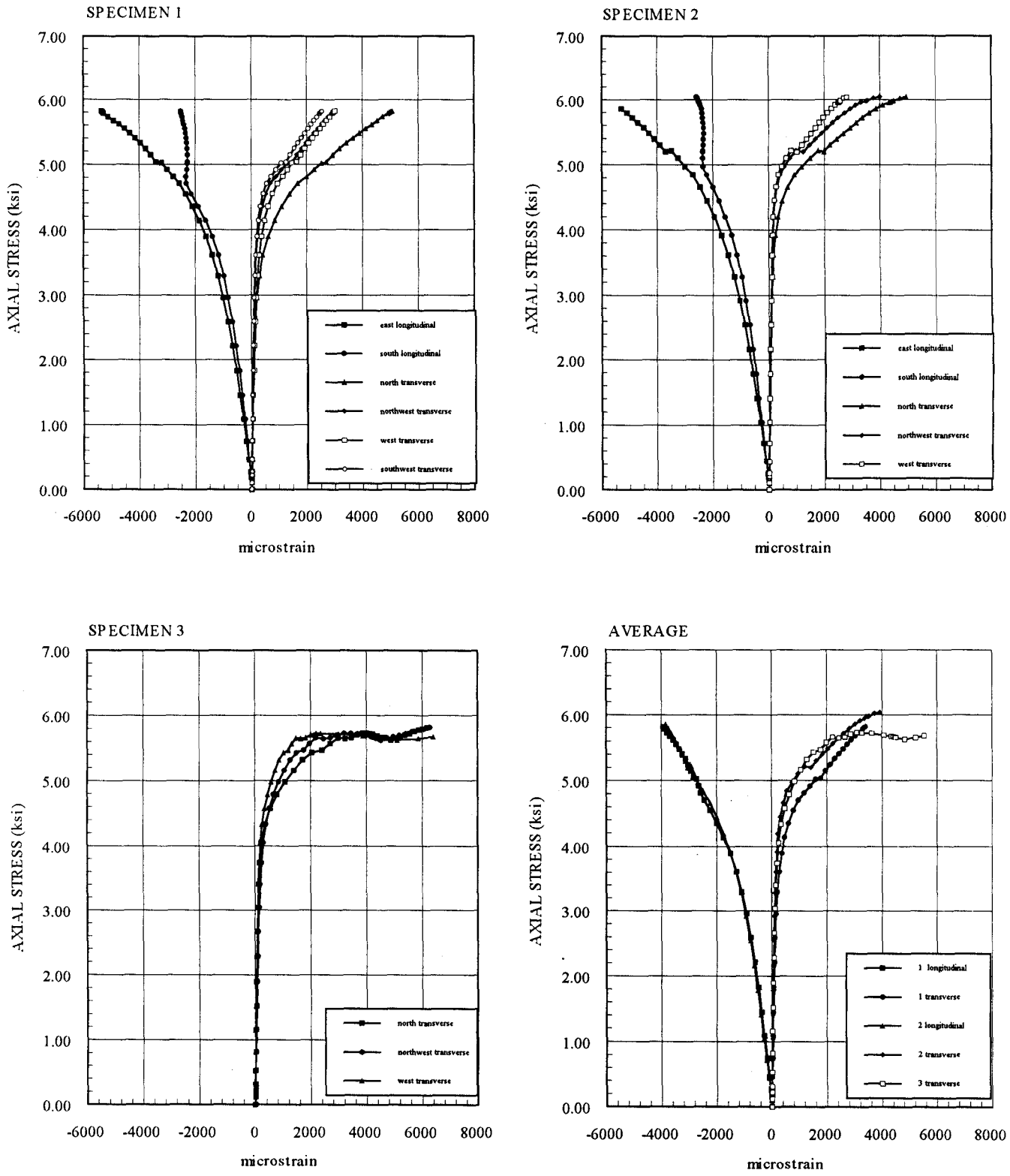

Fig. 4.35 Axial Force vs Axial Deflection Control
(Series 4: 5.25x5.25, fc'= 6 ksi)

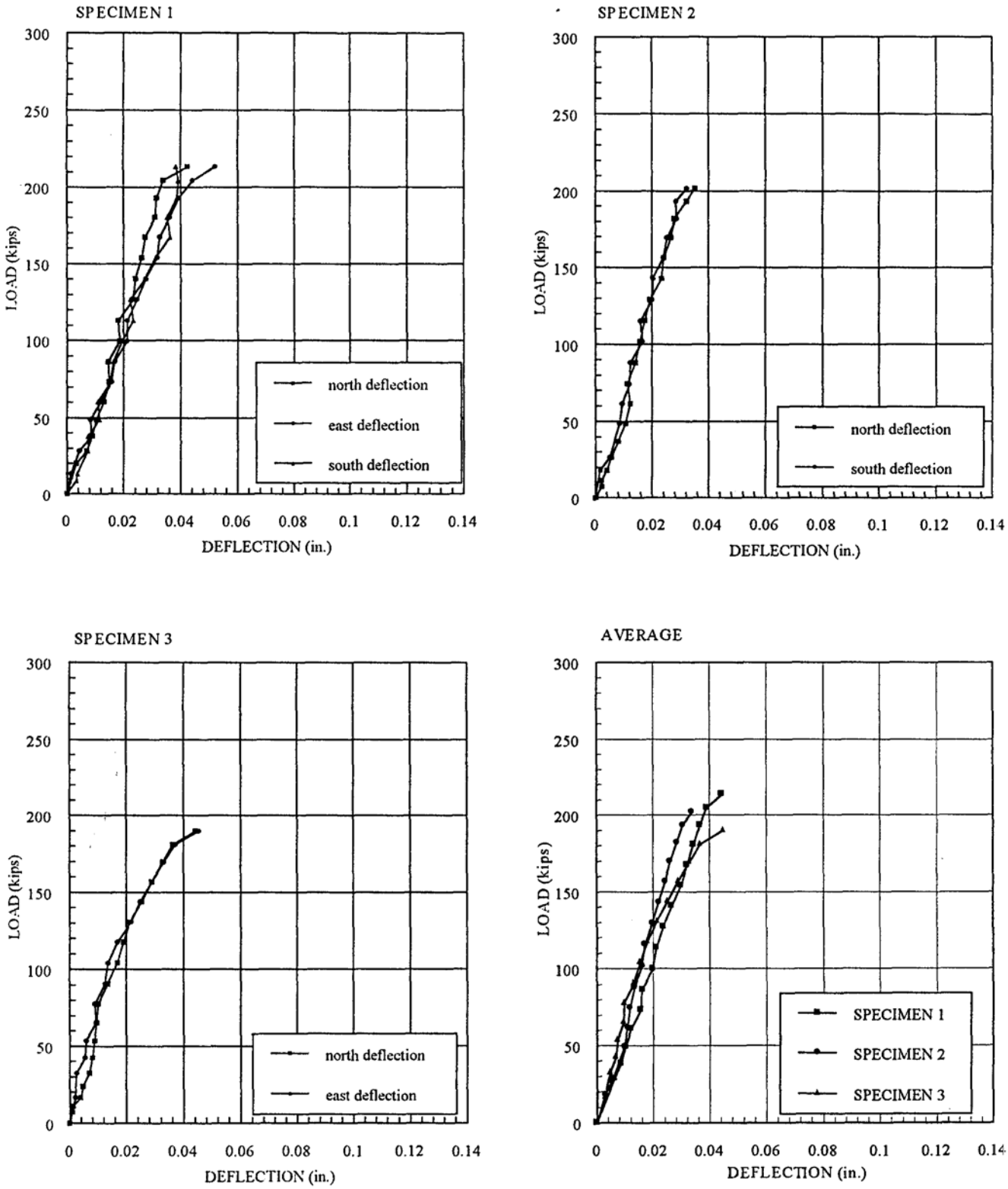

Fig. 4.36 Axial Force vs Axial Deflection One Layer

(Series 4: 5.25x5.25, fc'= 6 ksi)

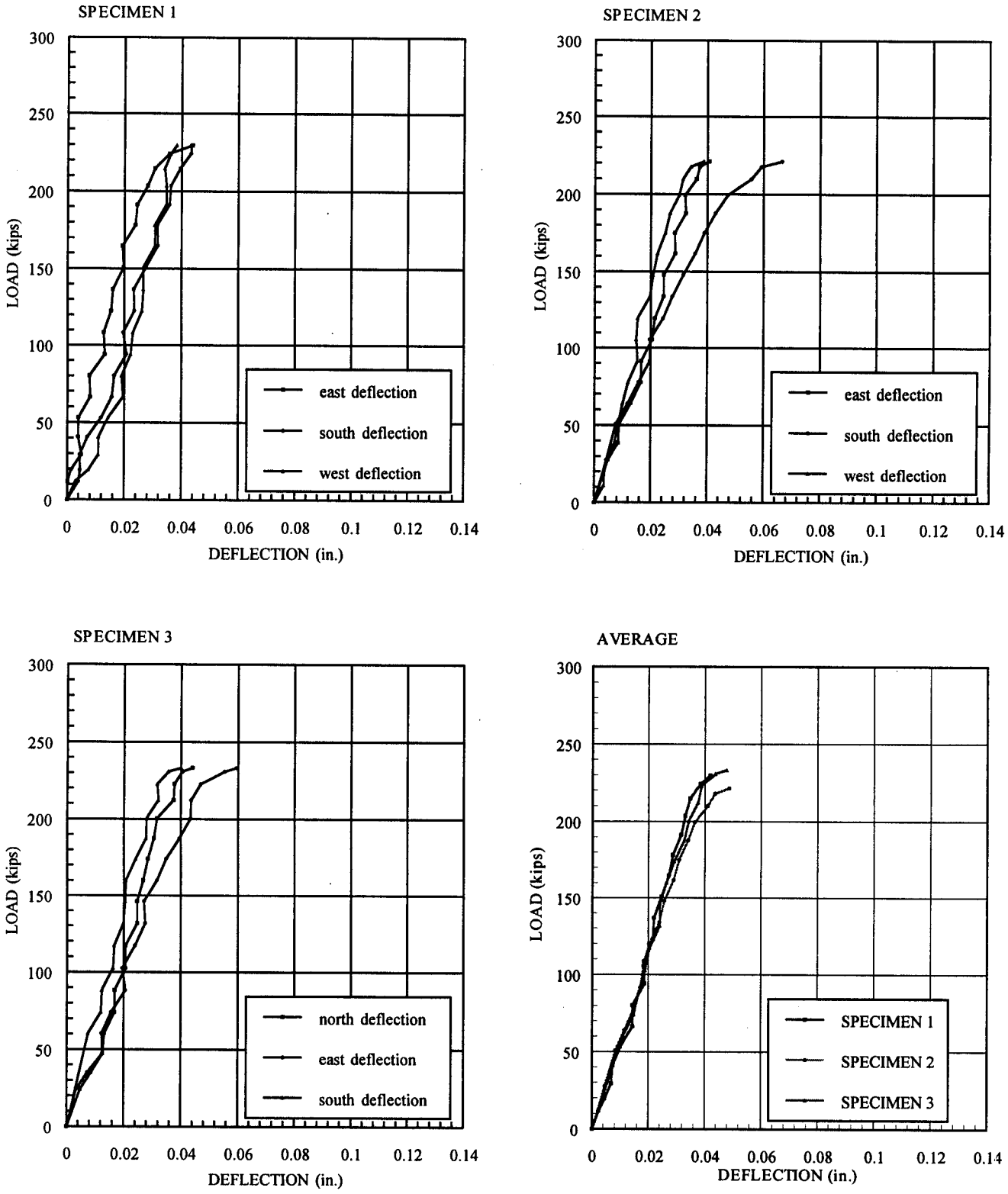

Fig. 4.37 Axial Force vs Axial Deflection Two Layers
(Series 4: 5.25x5.25, fc'= 6 ksi)

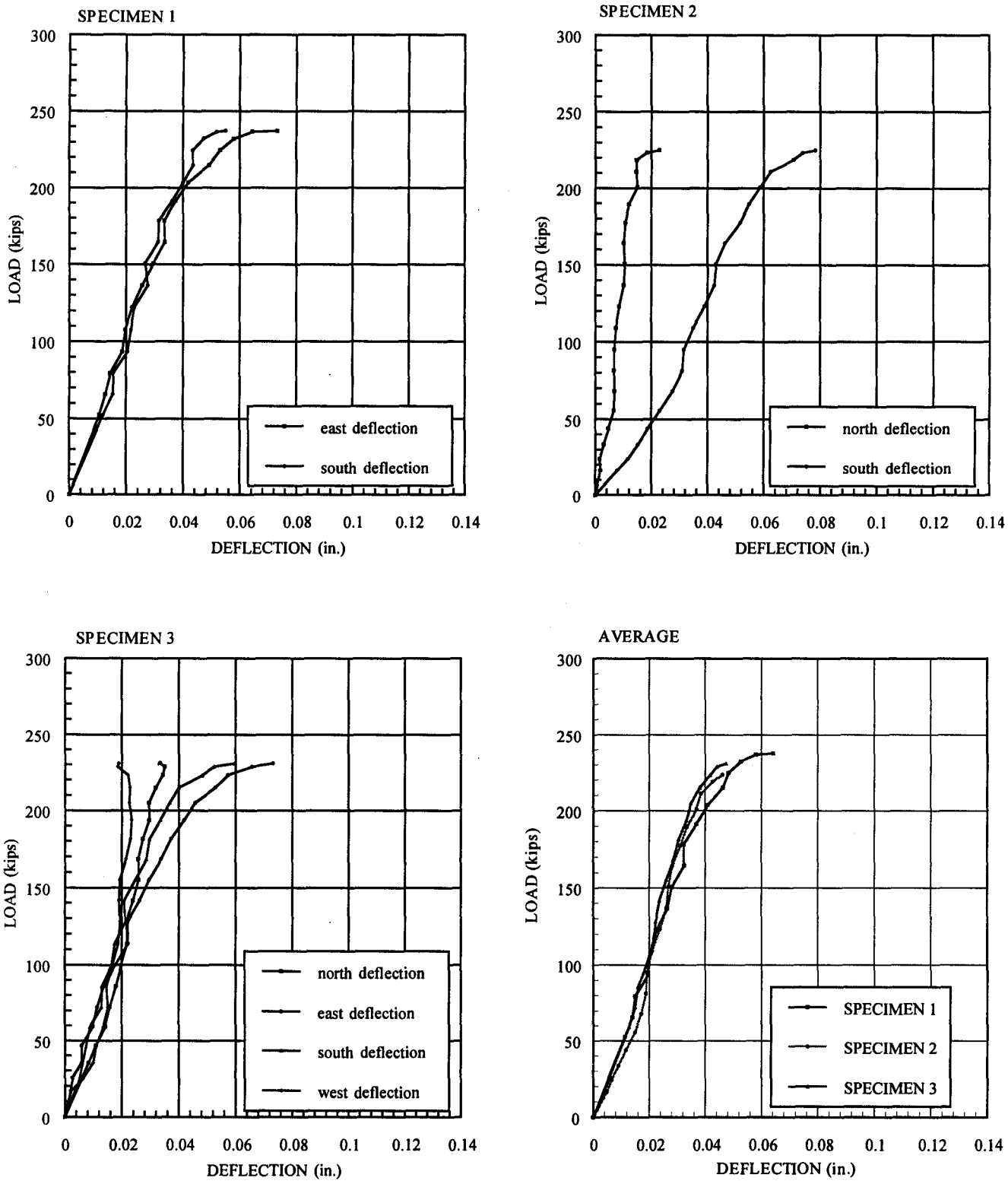

Fig. 4.38 Axial Force vs Axial Deflection Three Layers (Series 4: 5.25x5.25, fc'= 6 ksi)

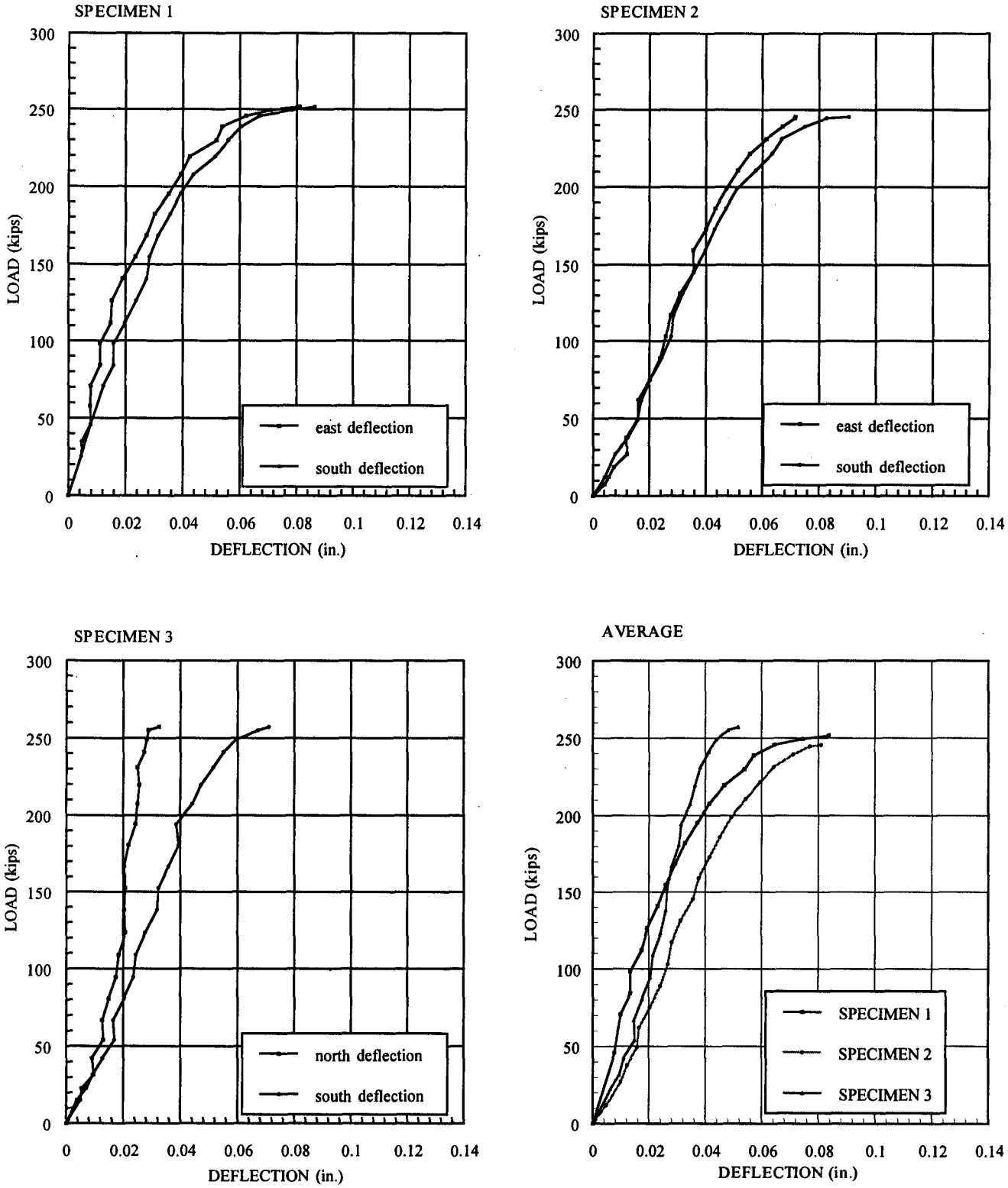

Fig. 4.39 Axial Force vs Axial Deflection Four Layers
(Series 4: 5.25x5.25, fc'= 6 ksi)

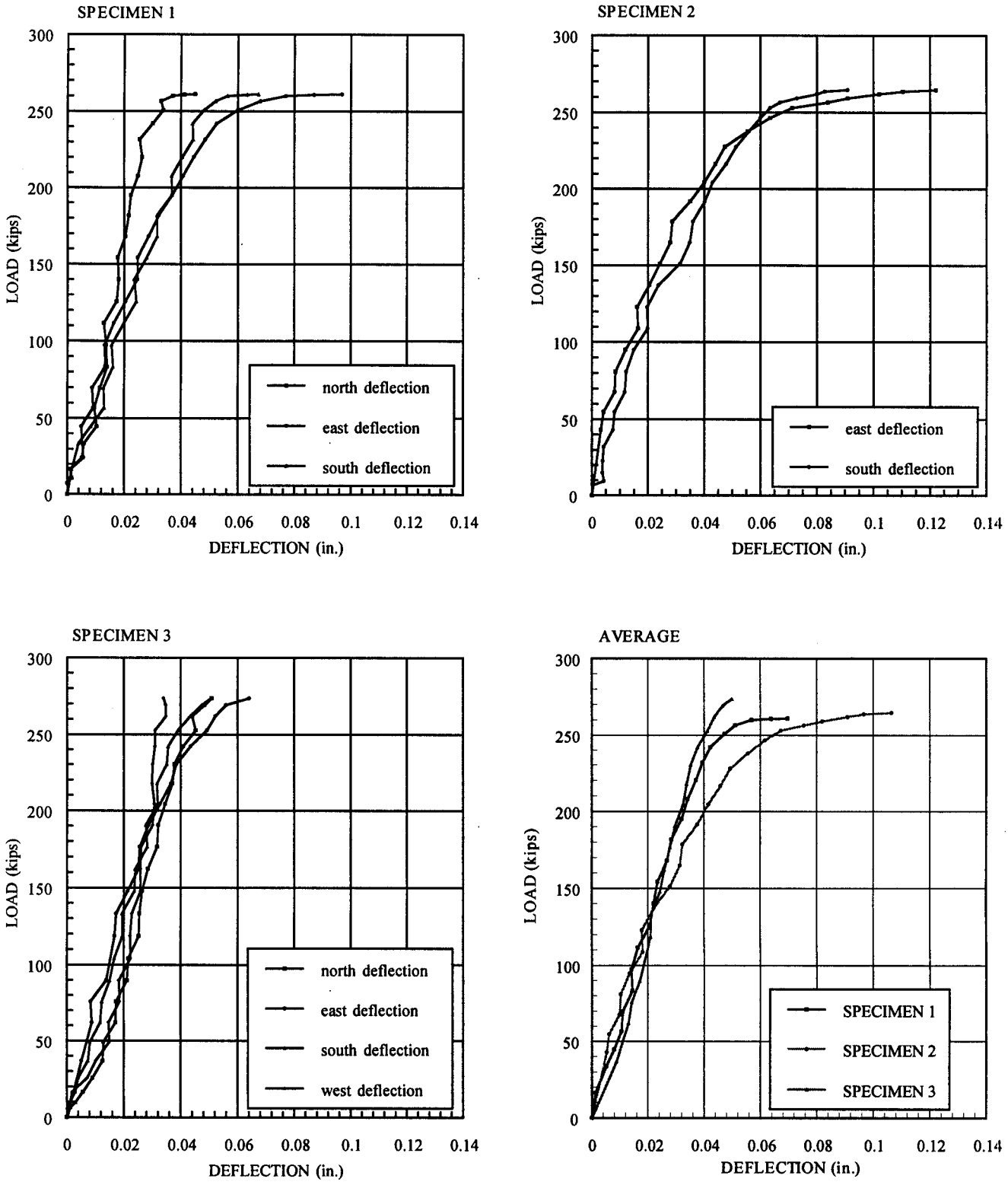

Fig. 4.40 Axial Stress vs Axial and Transverse Strain Control

(Series 4: 5.25x5.25, fc'= 6 ksi)

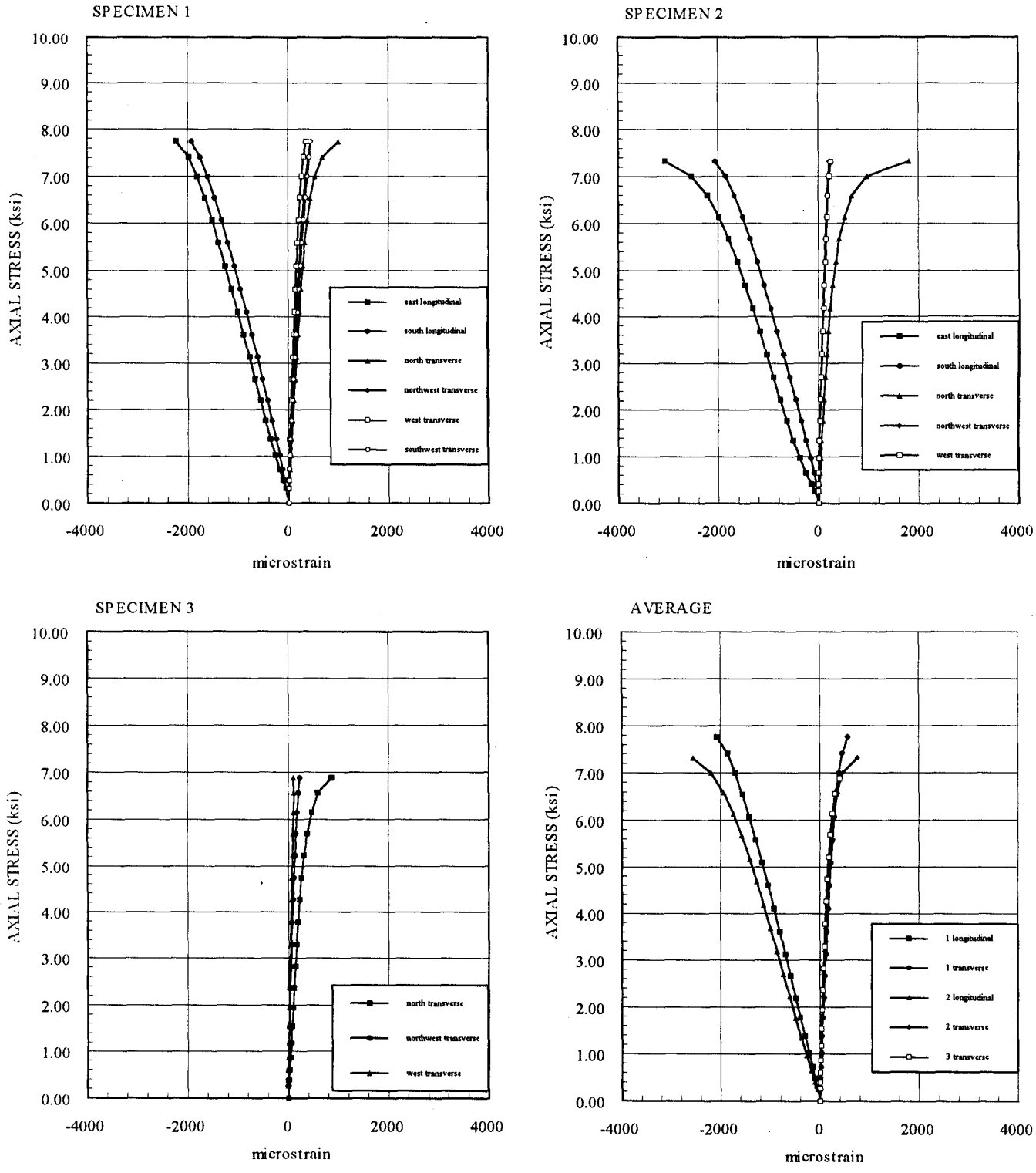

Fig. 4.41 Axial Stress vs Axial and Transverse Strain One Layer
(Series 4: 5.25x5.25, fc'= 6 ksi)

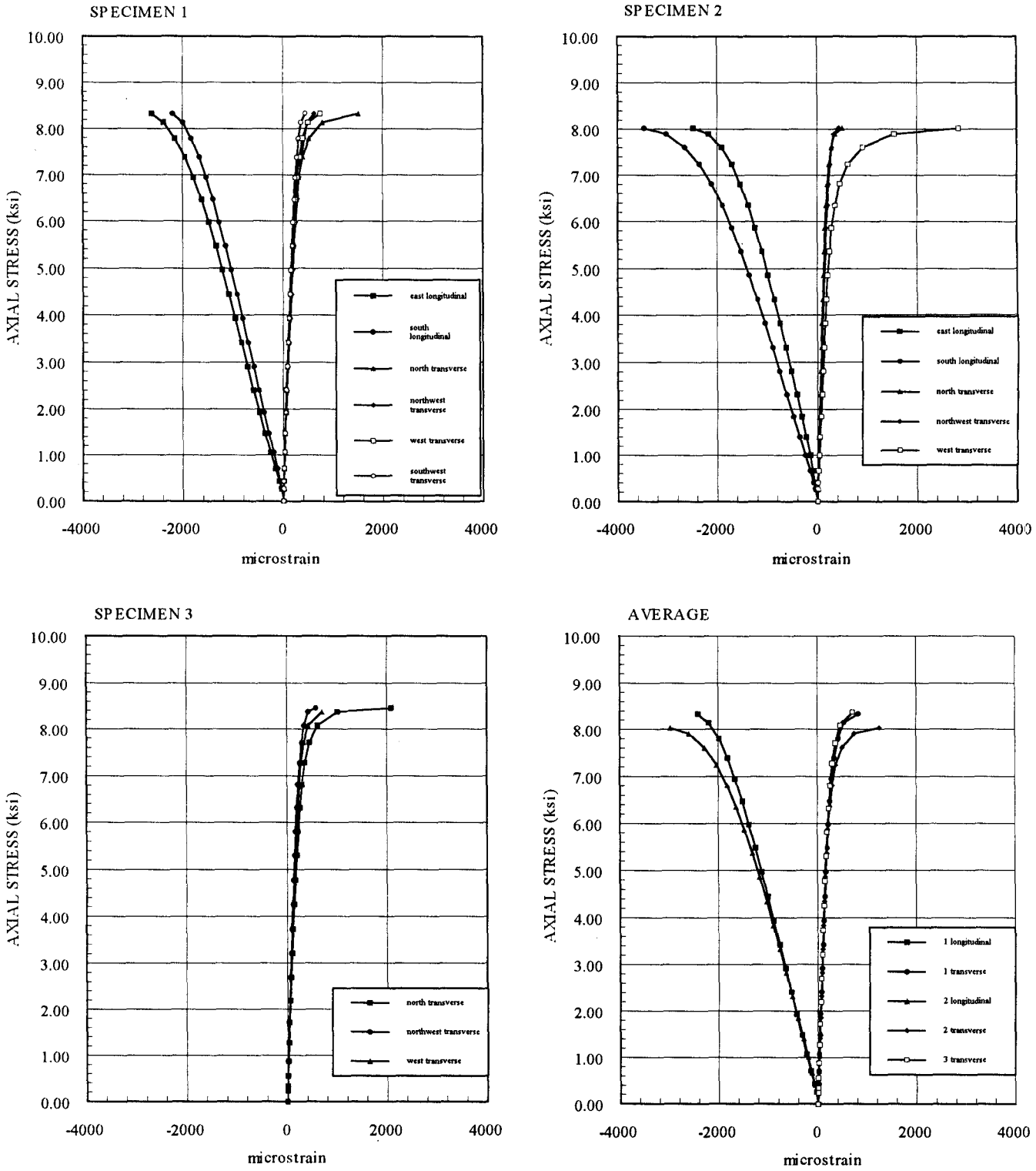

Fig.4.42 Axial Stress vs Axial and Transverse Strain Two Layers

(Series 4: 5.25x5.25, fc'= 6 ksi)

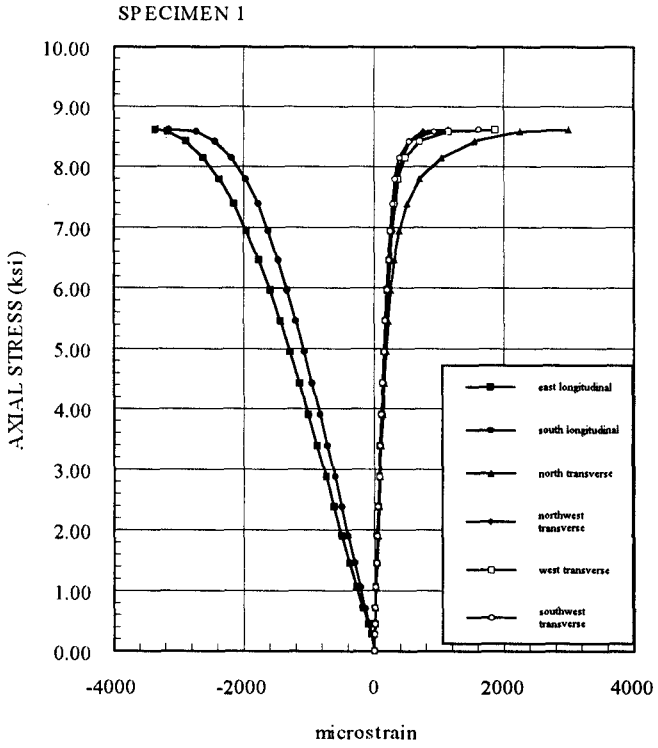

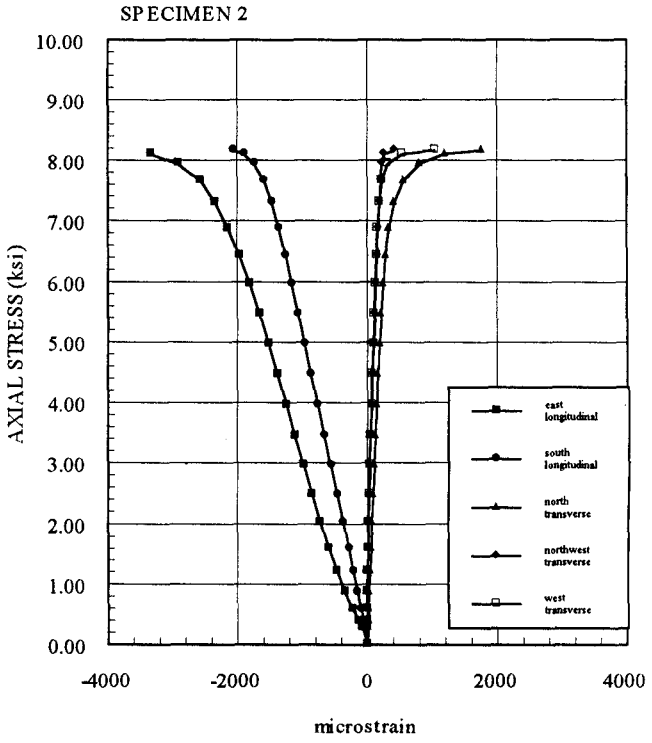

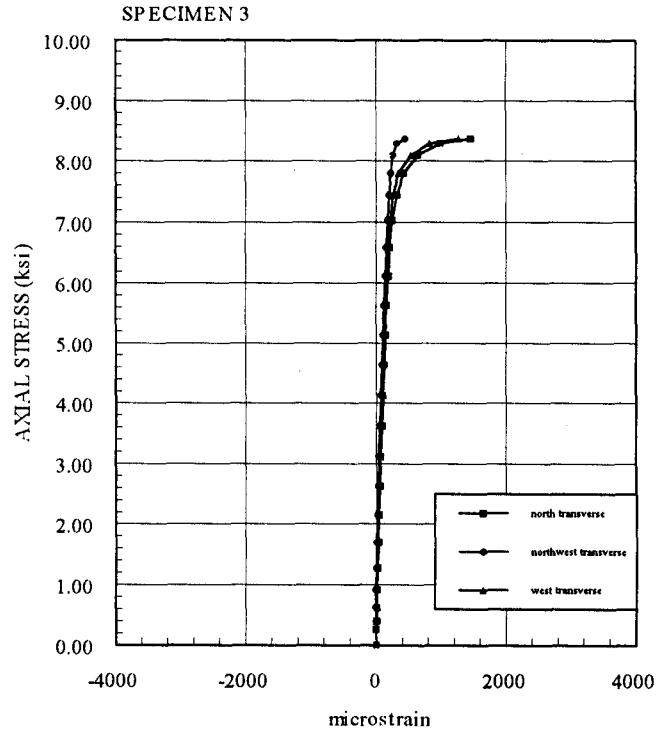

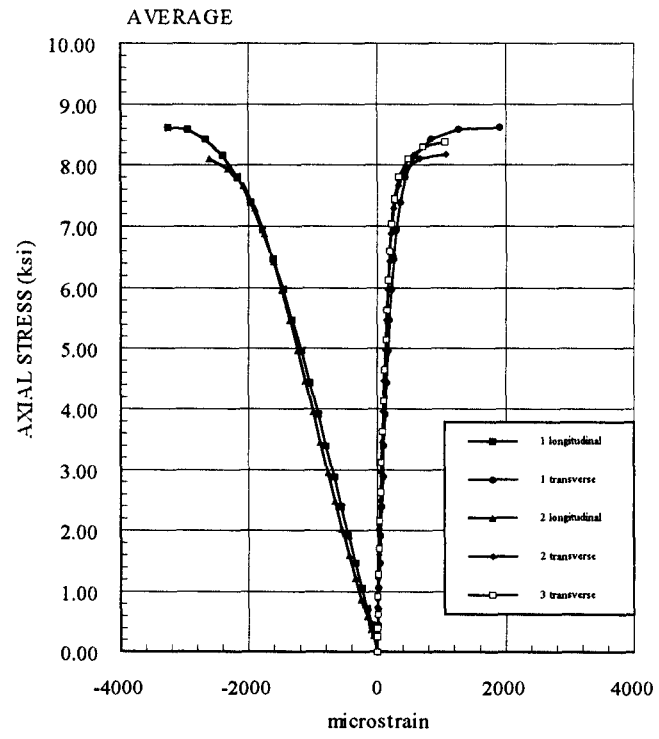

Fig. 4.43 Axial Stress vs Axial and Transverse Strain Three Layers (Series 4: 5.25x5.25, fc'= 6 ksi)

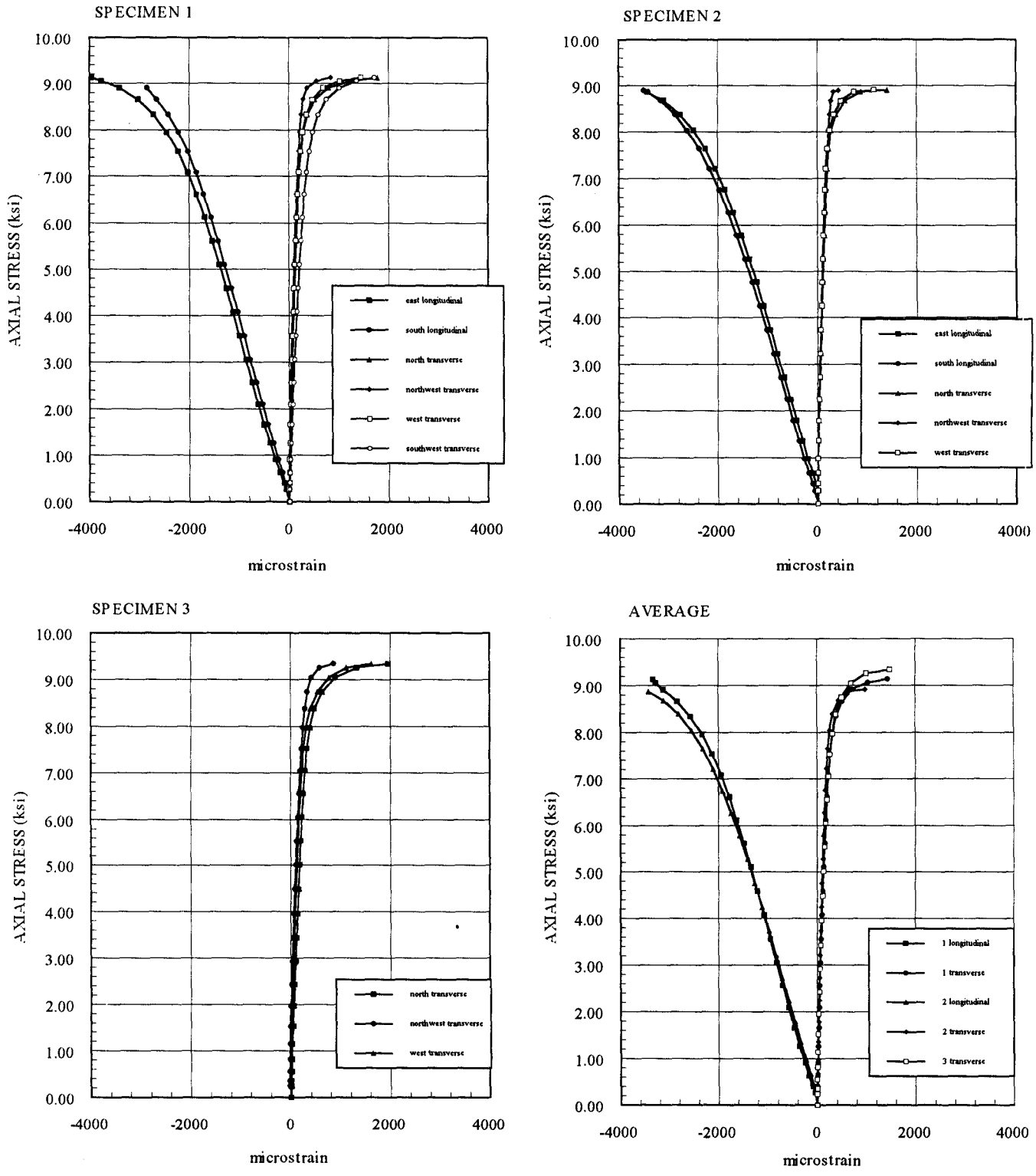

Fig. 4.44 Axial Stress vs Axial and Transverse Strain Four Layers
(Series 4: 5.25x5.25, fc'= 6 ksi)

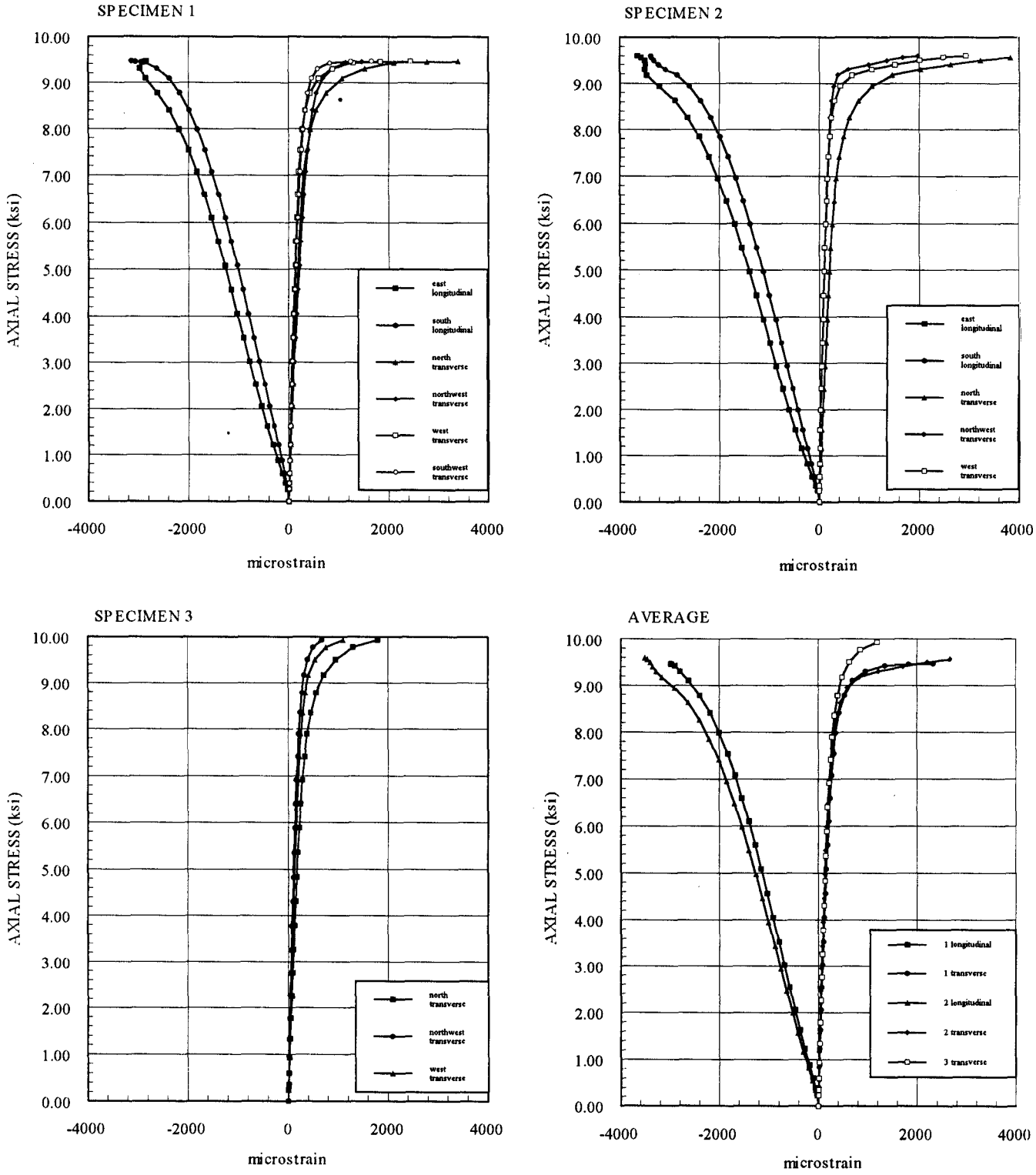

Fig. 4.45 Axial Force vs Axial Deflection Control
(Series 5: 4.25x6.5 , fc'= 6 ksi)

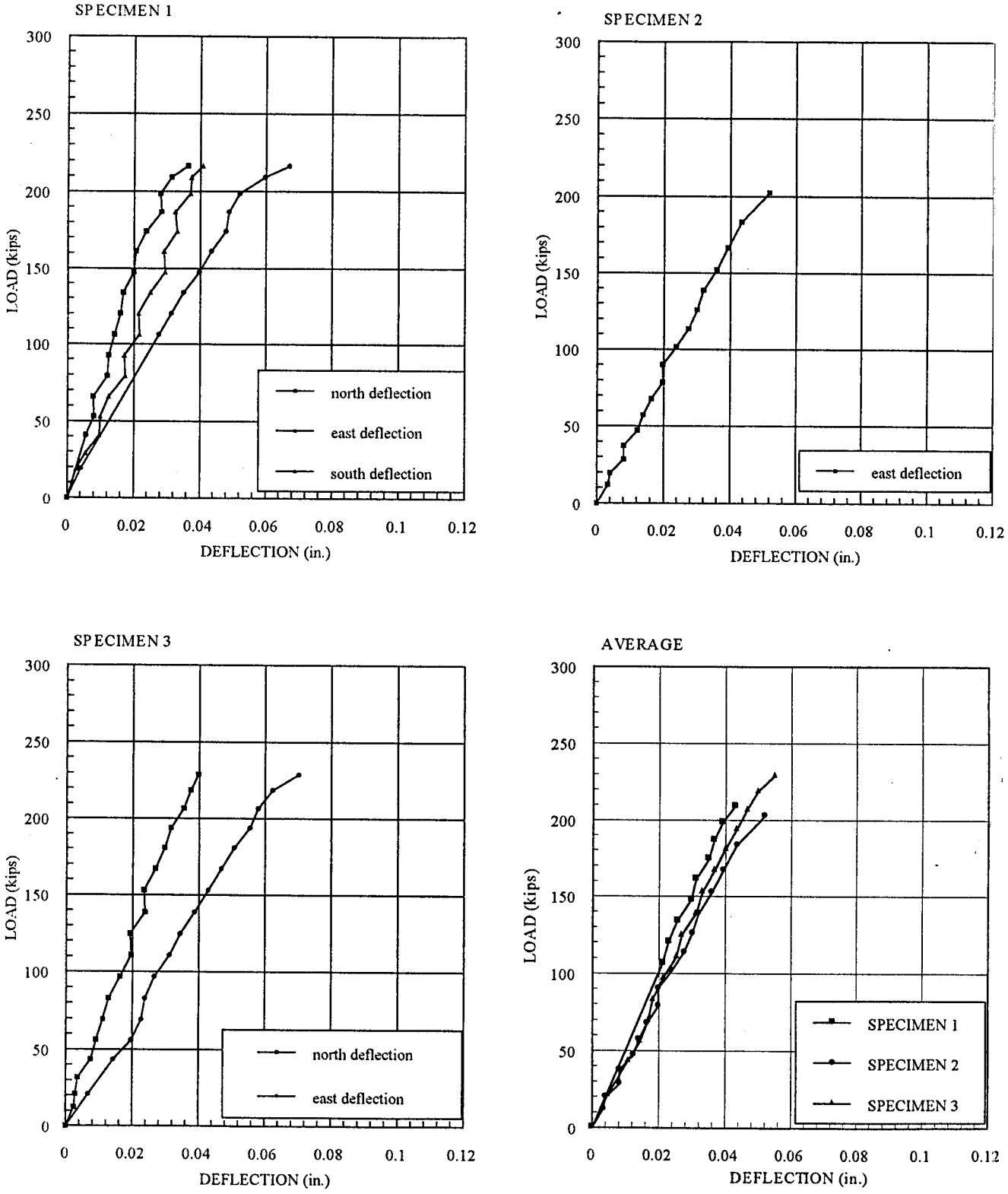

Fig. 4.46 Axial Force vs Axial Deflection One Layer
(Series 5: 4.25x6.5 , fc'= 6 ksi)

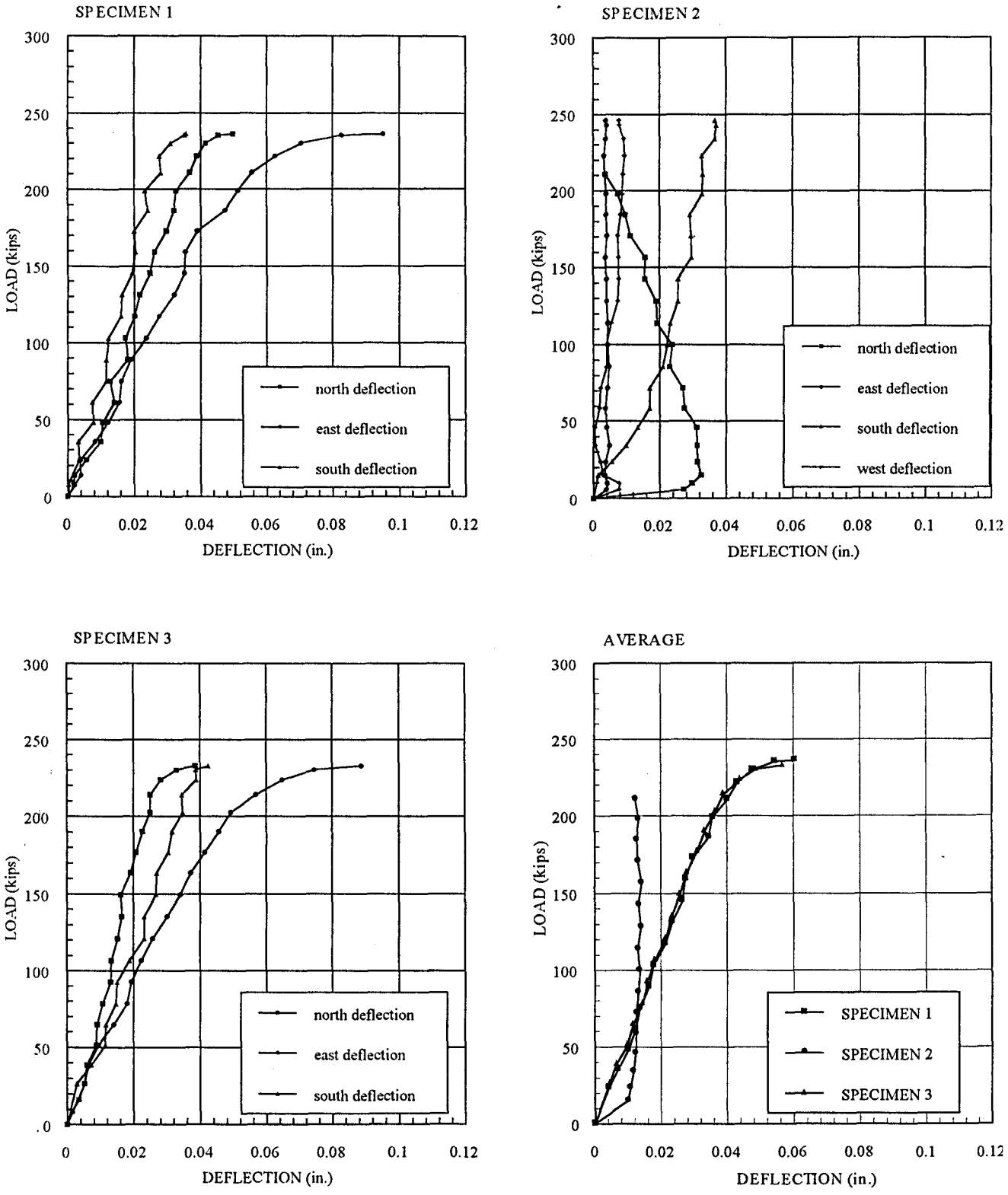

Fig. 4.47 Axial Force vs Axial Deflection Two Layer
(Series 5: 4.25x6.5 , fc'= 6 ksi)

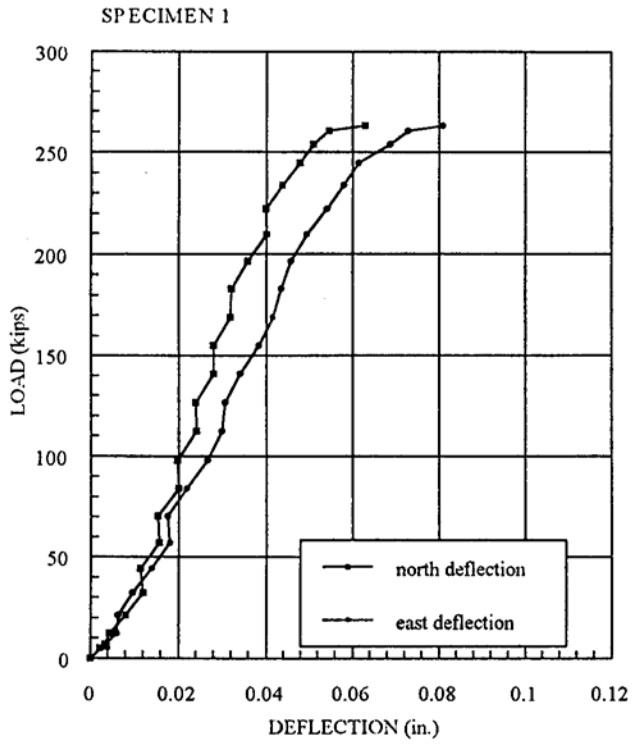

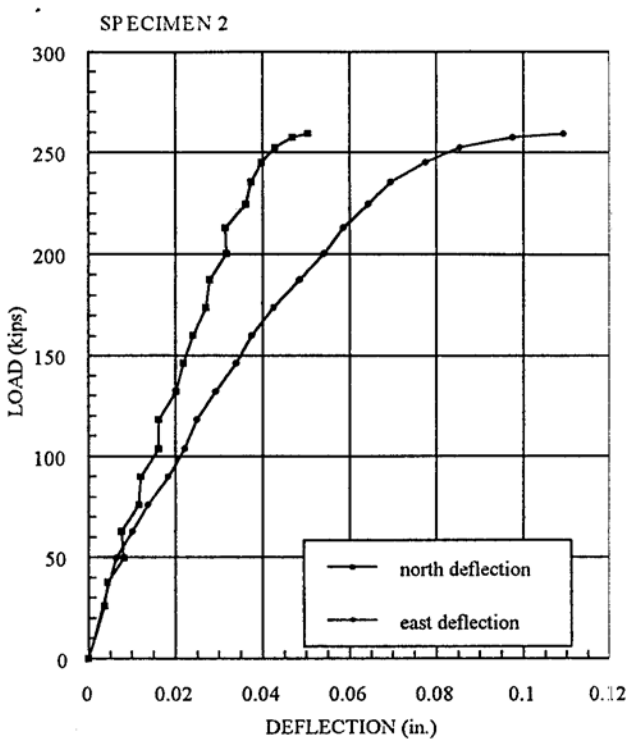

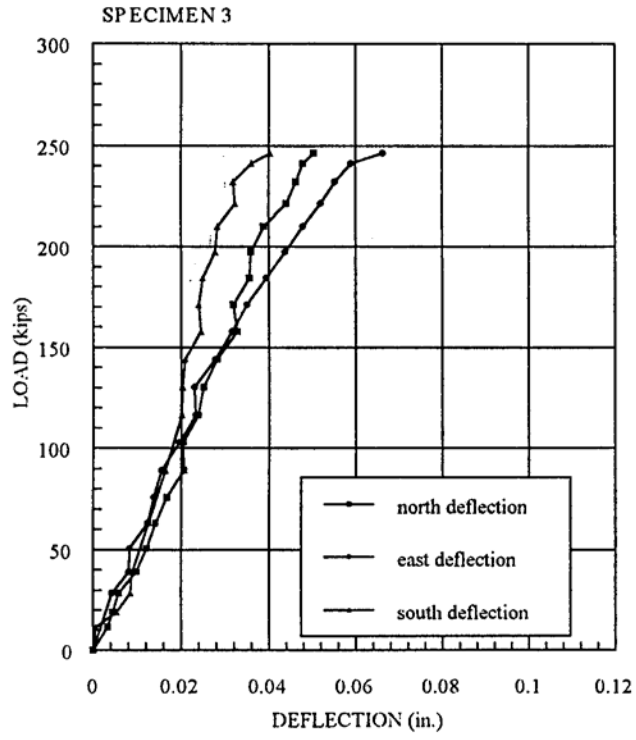

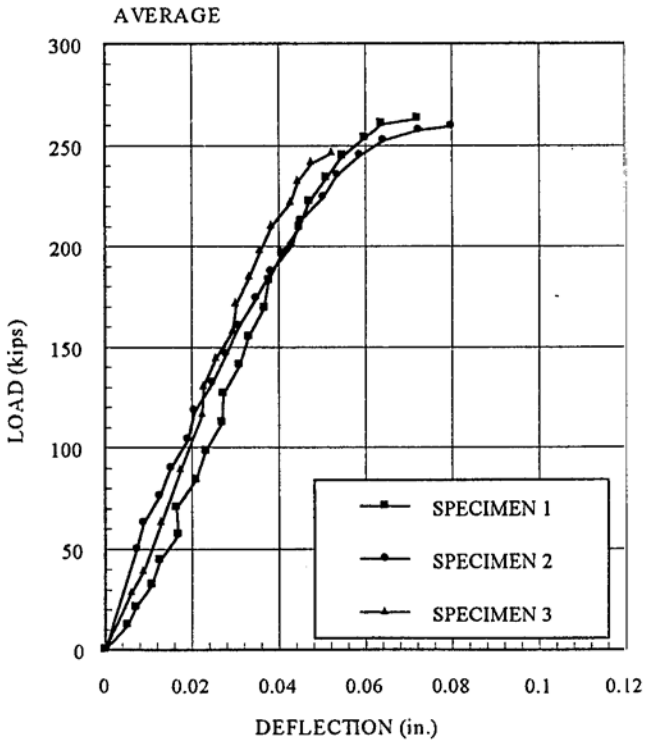

Fig. 4.48 Axial Force vs Axial Deflection Three Layer
(Series 5: 4.25x6.5 , fc'= 6 ksi)

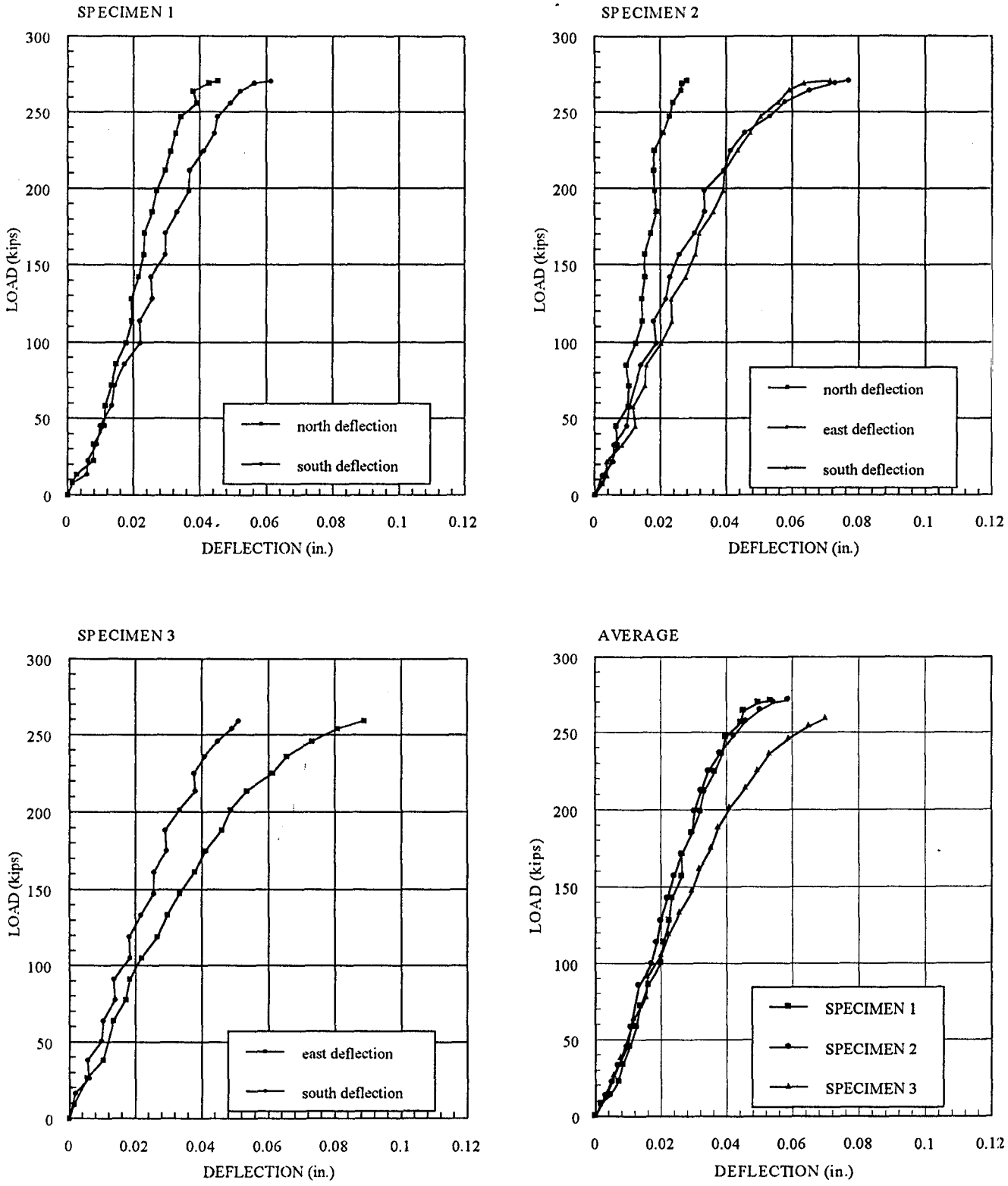

Fig. 4.49 Axial Force vs Axial Deflection Four Layer
(Series 5: 4.25x6.5 , fc'= 6 ksi)

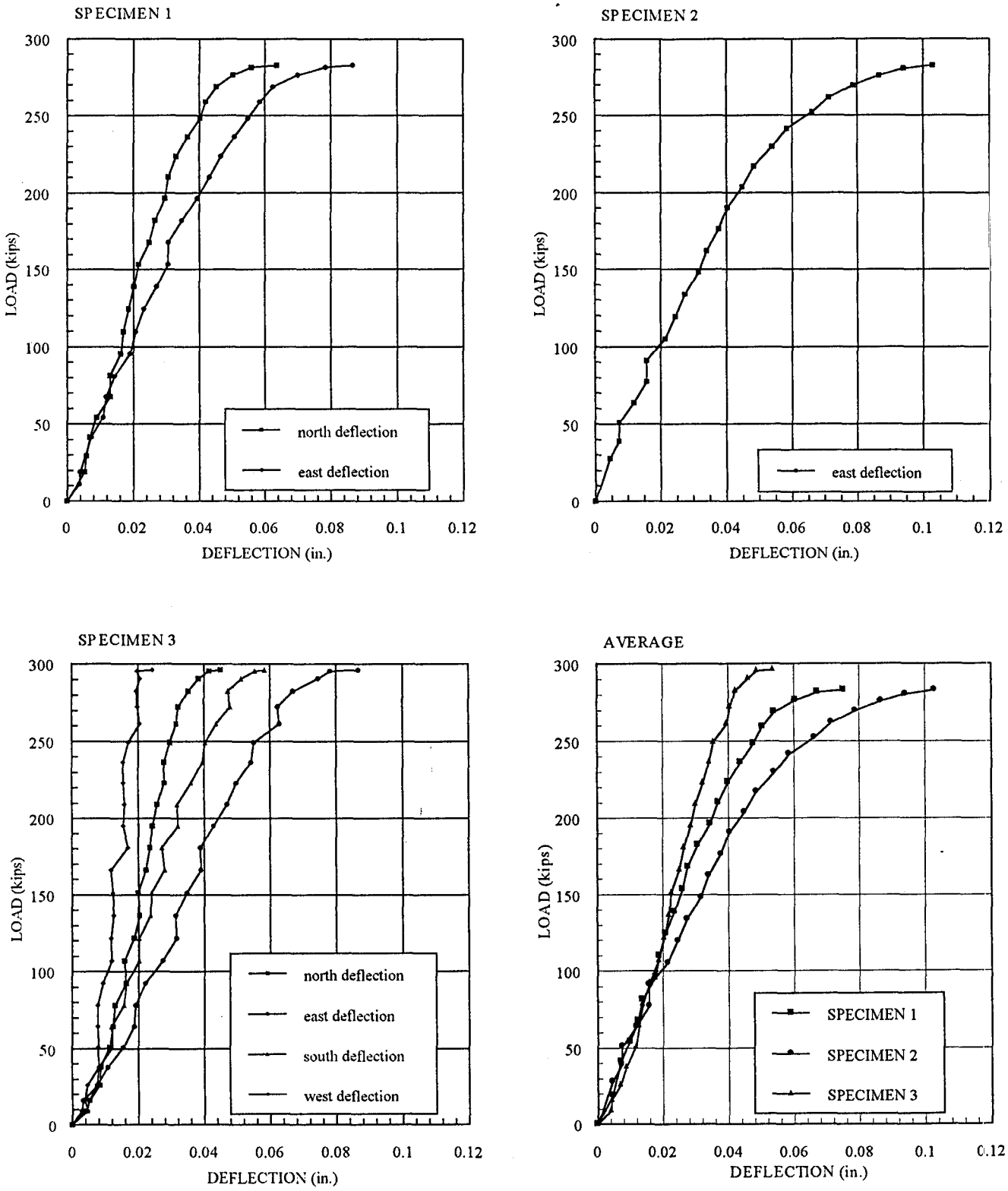

Fig. 4.50 Axial Stress vs Axial and Transverse Strain Control
(Series 5: 4.25x6.5 , fc'= 6 ksi)

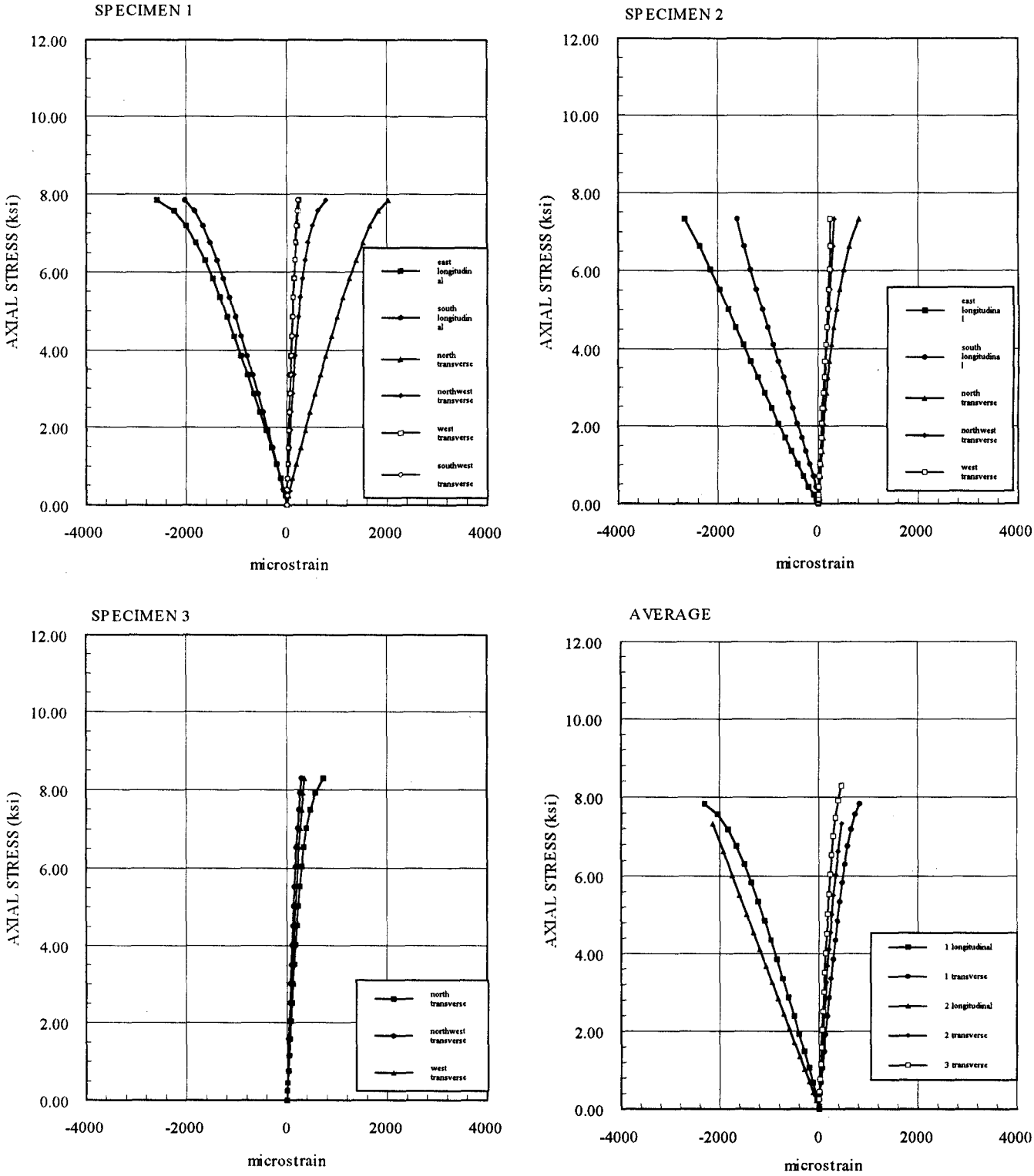

Fig. 4.51 Axial Stress vs Axial and Transverse Strain One Layer

(Series 5: 4.25x6.5 , fc'= 6 ksi)

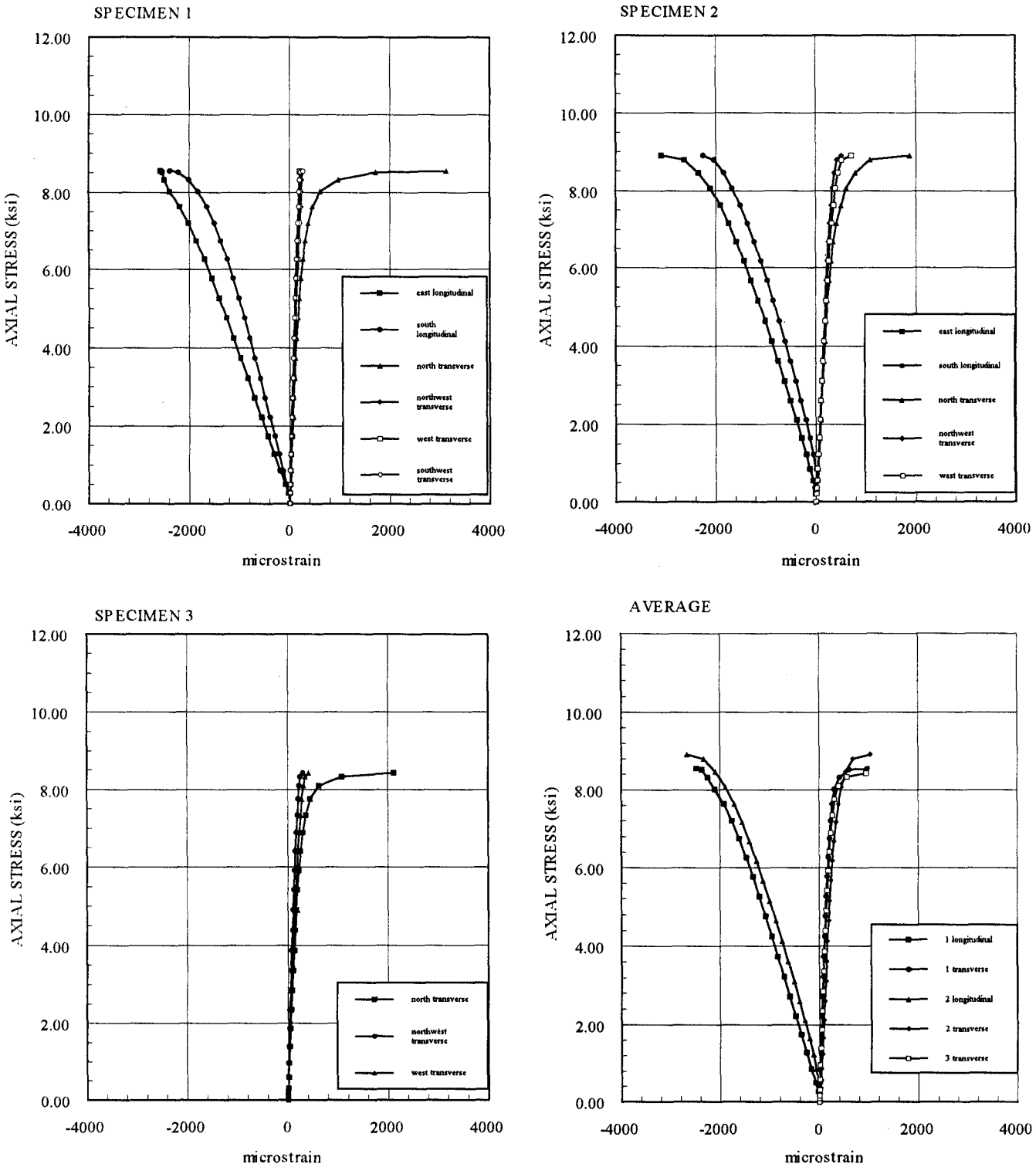

Fig. 4.52 Axial Stress vs Axial and Transverse Strain Two Layers
(Series 5: 4.25x6.5 , fc'= 6 ksi)

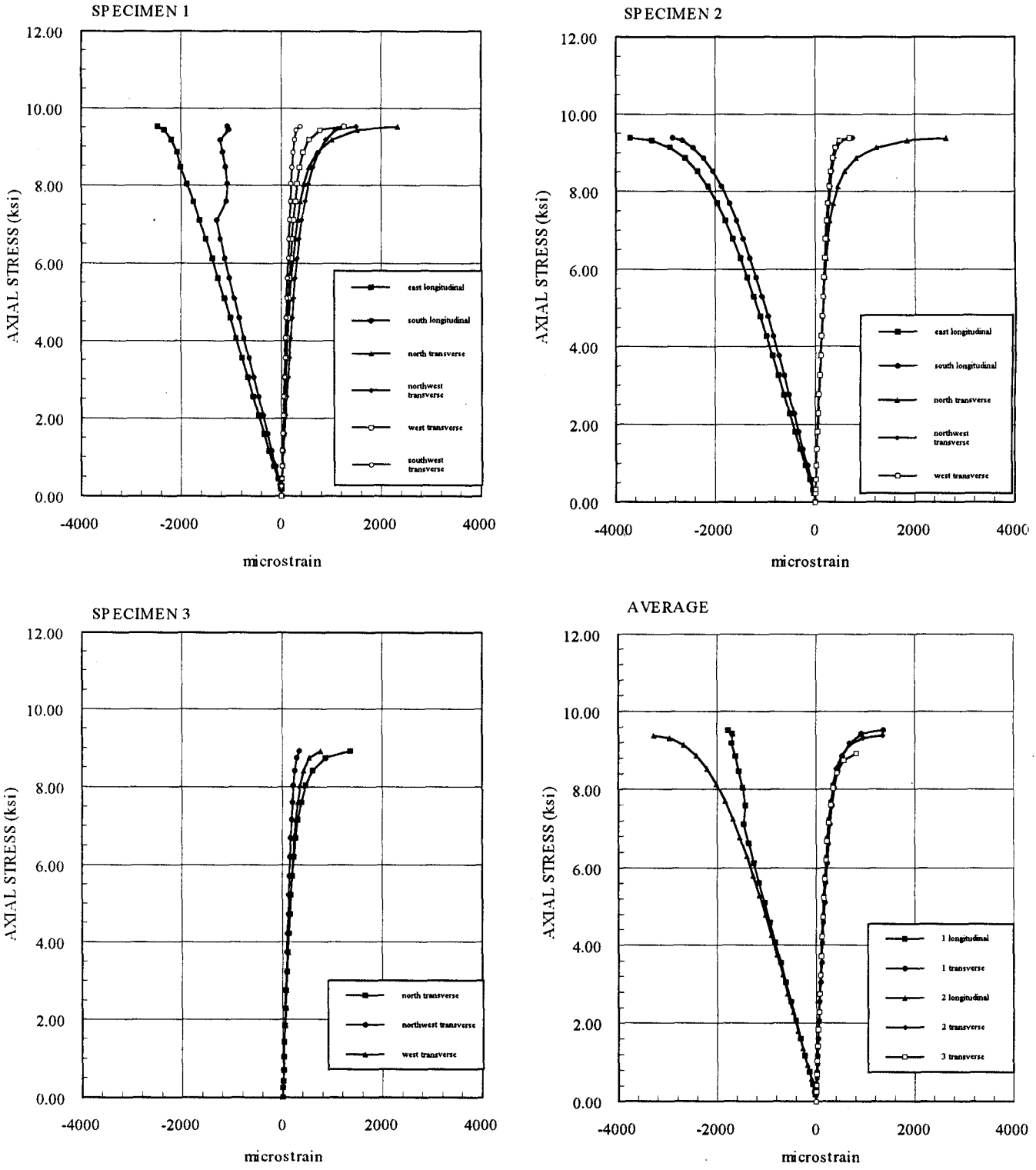

Fig. 4.53 Axial Stress vs Axial and Transverse Strain Three Layers

(Series 5: 4.25x6.5 , fc'= 6 ksi)

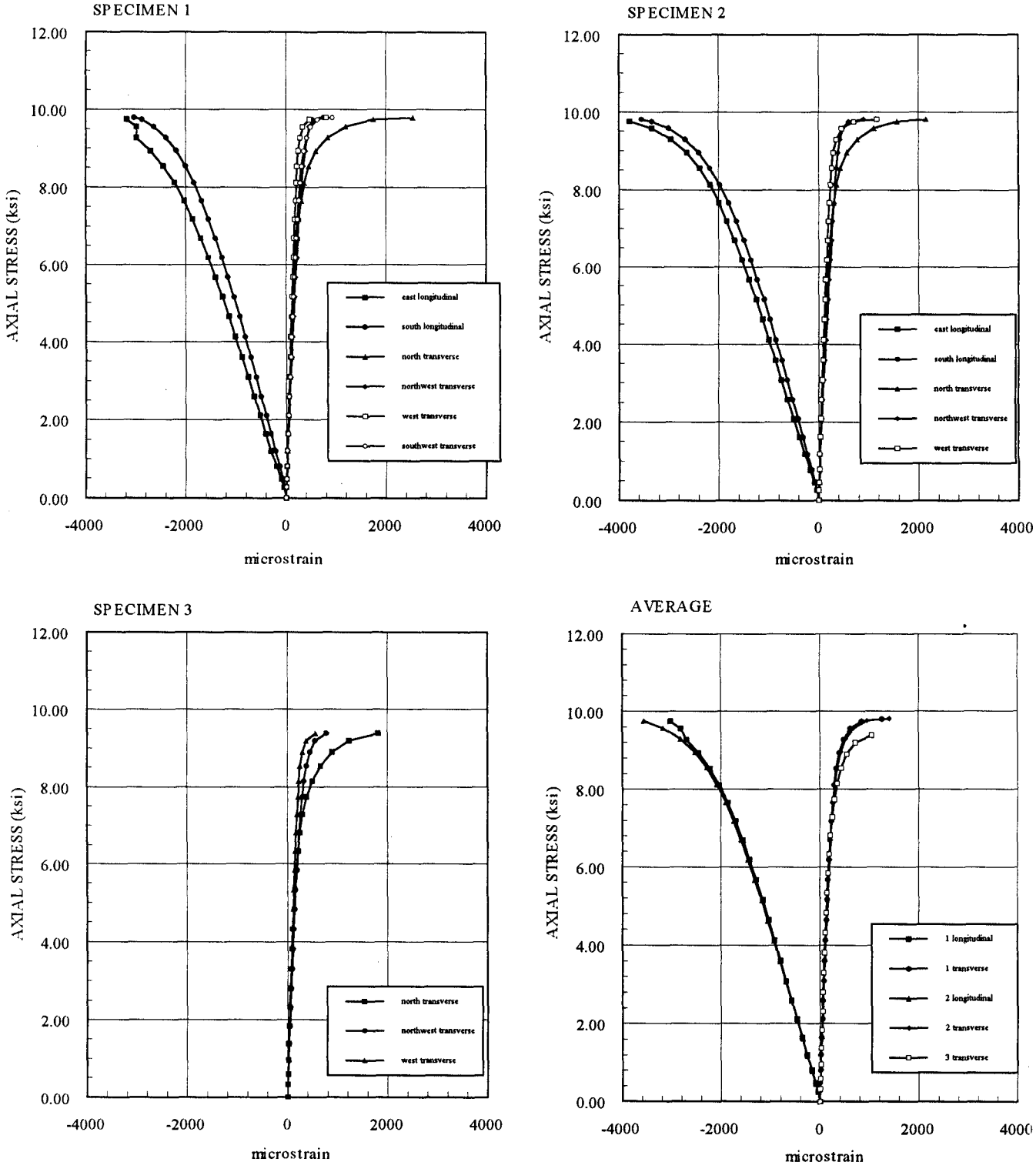

Fig. 4.54 Axial Stress vs Axial and Transverse Strain Four Layers
(Series 5: 4.25x6.5 , fc'= 6 ksi)

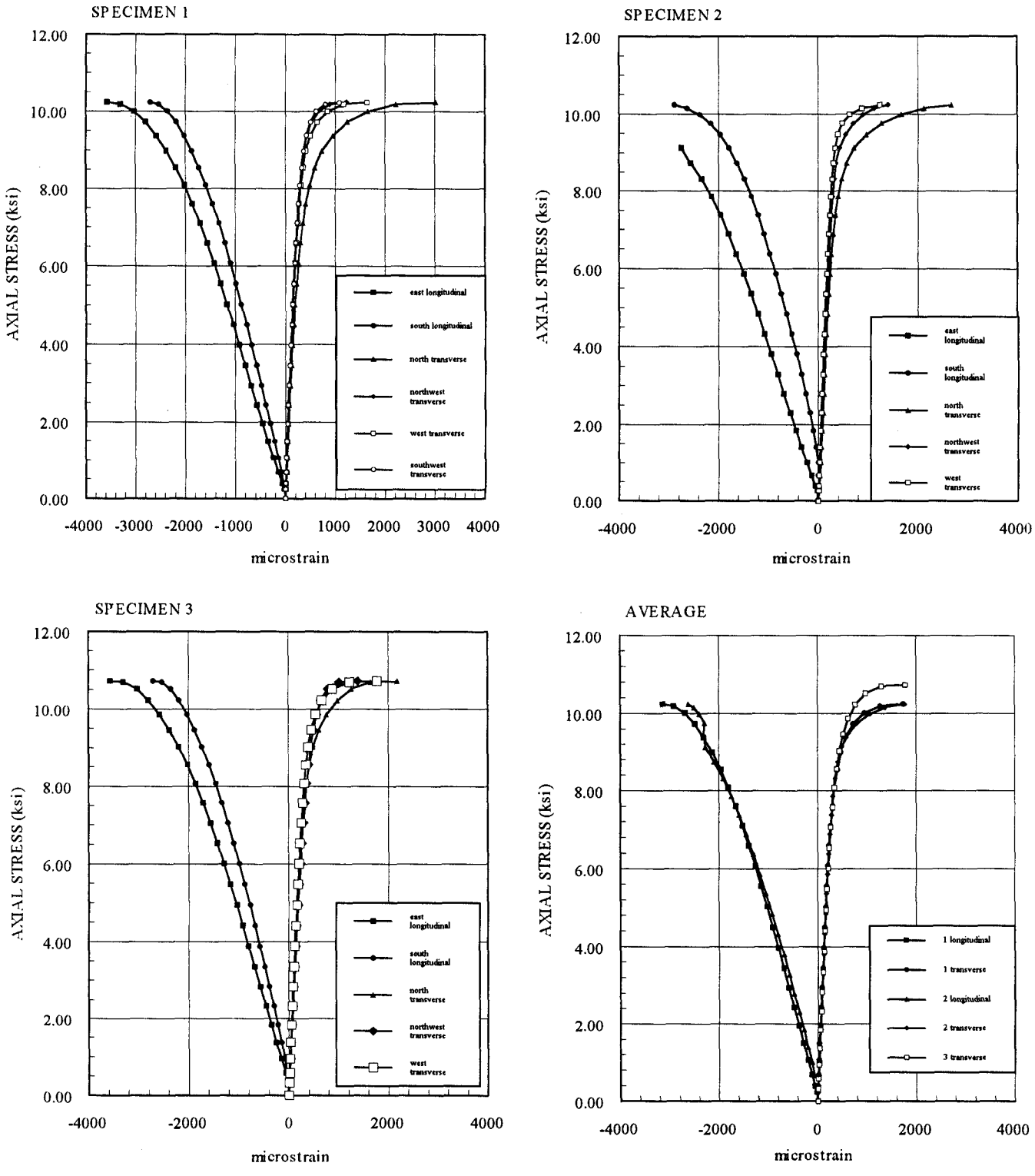

Fig. 4.55 Axial Force vs Axial Deflection Control
(Series 6: 3.75x7.5 , fc'= 6 ksi)

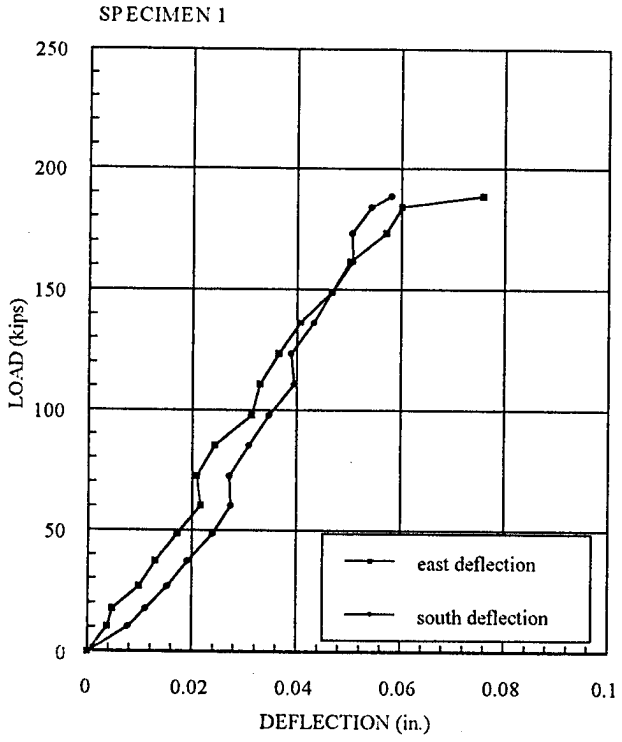

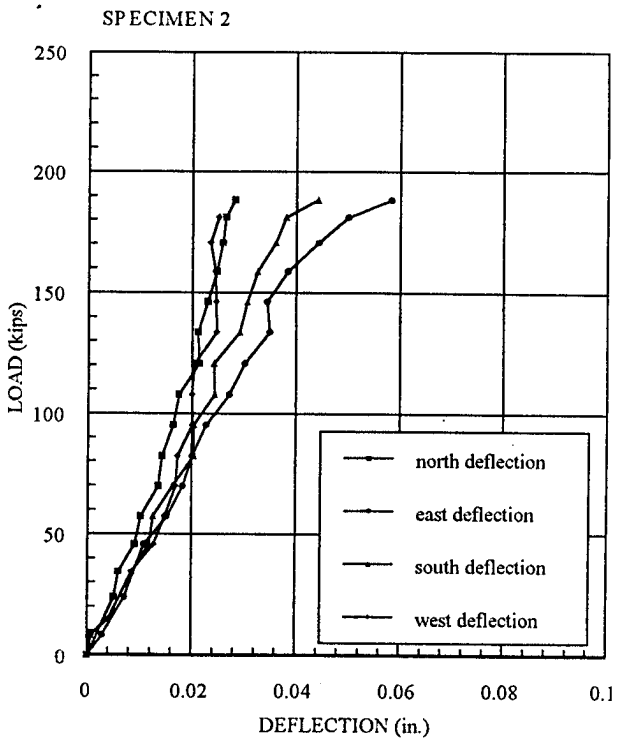

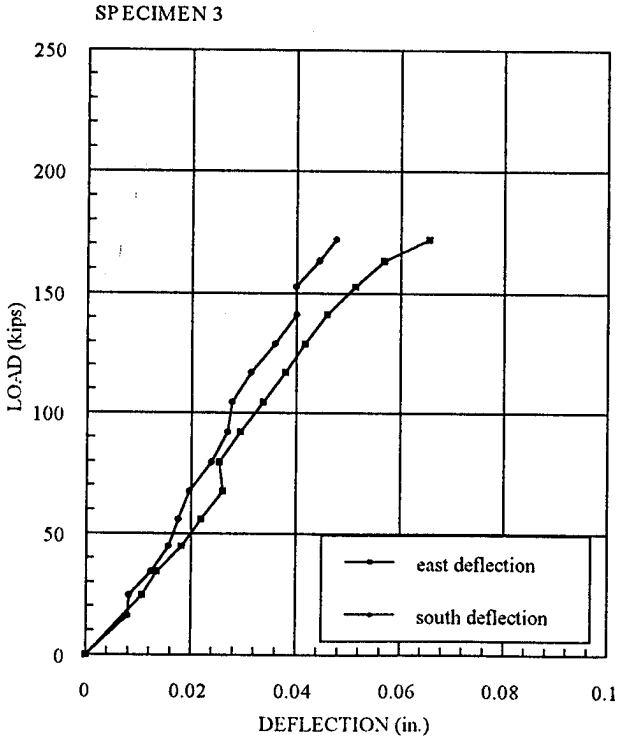

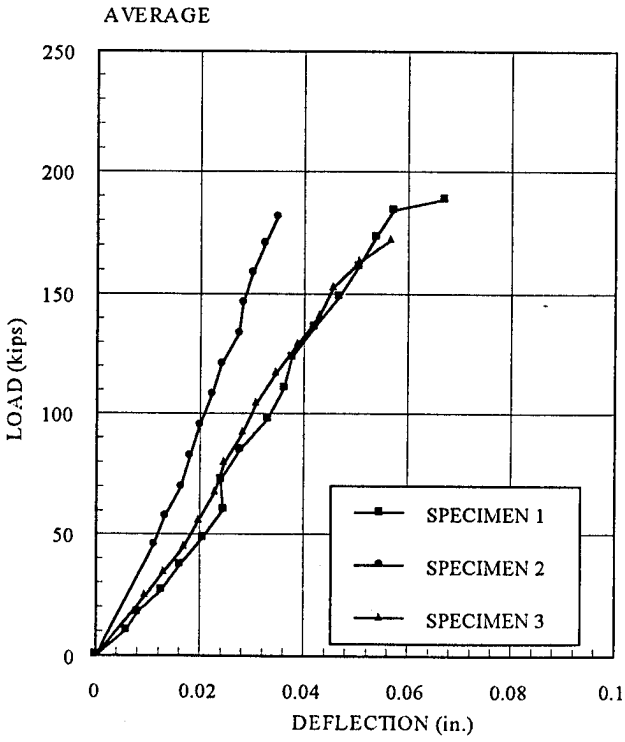

Fig. 4.56 Axial Force vs Axial Deflection One Layer
(Series 6: 3.75x7.5 , fc'= 6 ksi)

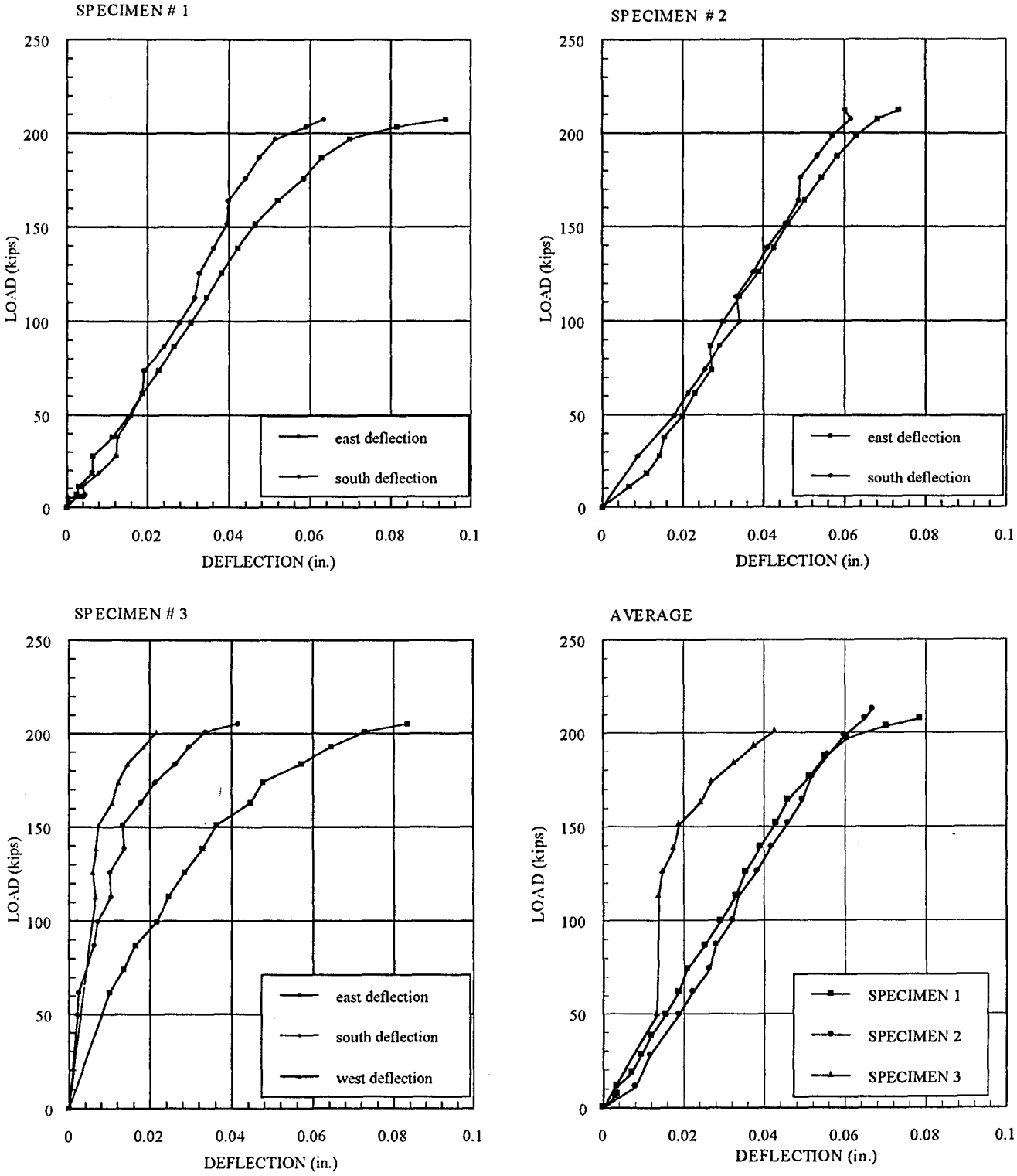

Fig. 4.57 Axial Force vs Axial Deflection Two Layer
(Series 6: 3.75x7.5 , fc'= 6 ksi)

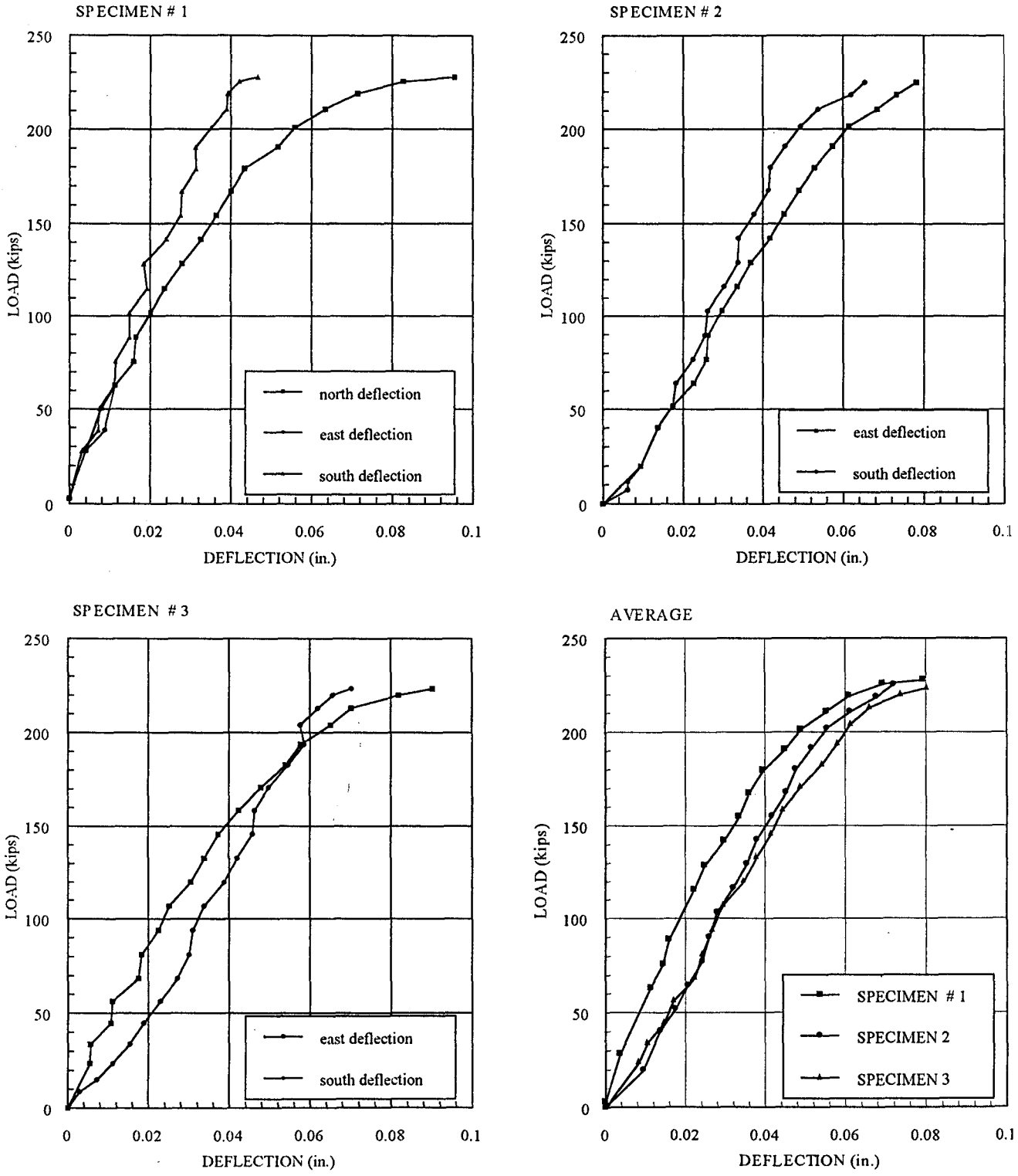

Fig. 4.58 Axial Force vs Axial Deflection Three Layers
(Series 6: 3.75x7.5 , fc'= 6 ksi)

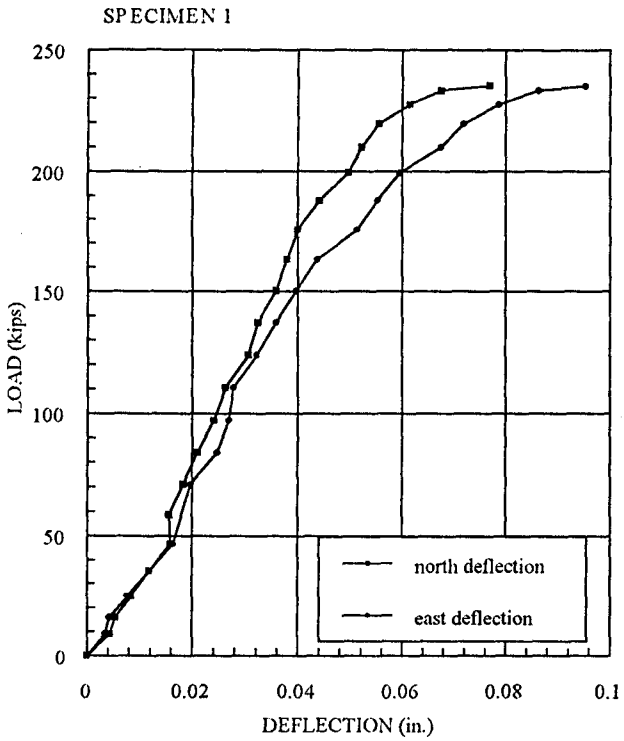

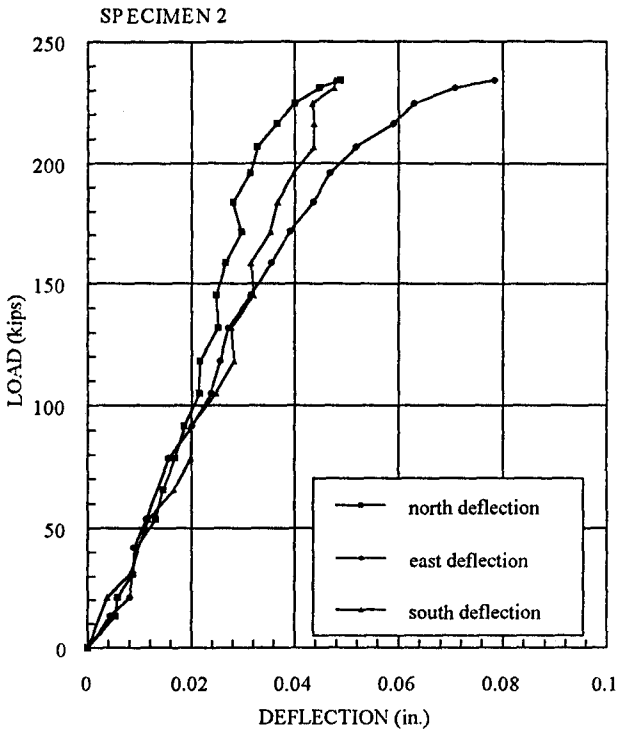

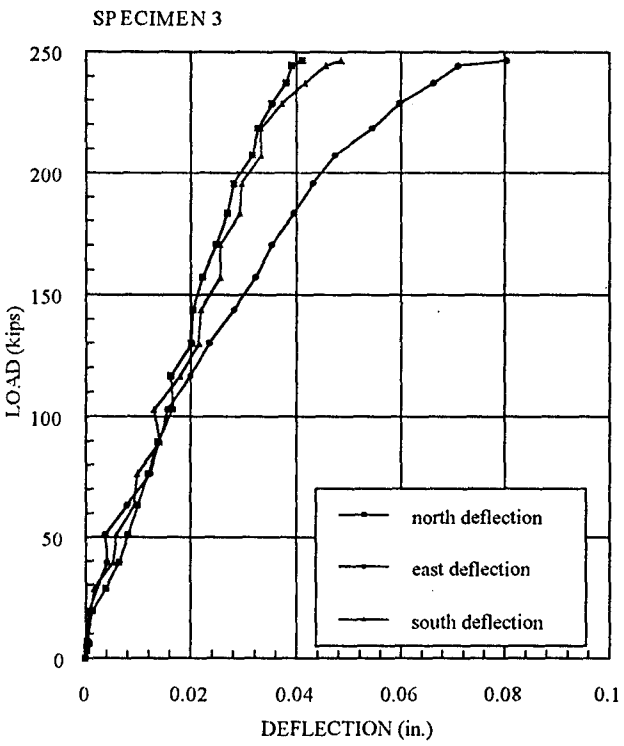

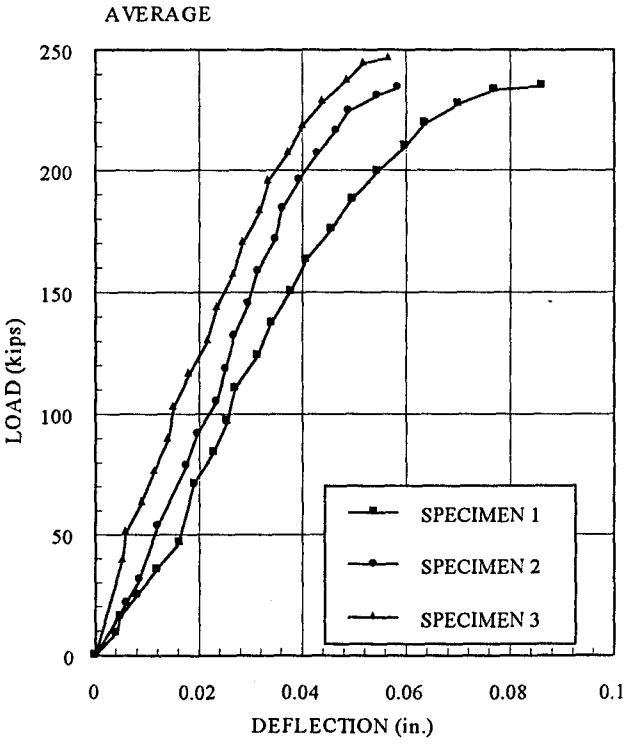

Fig. 4.59 Axial Force vs Axial Deflection Four Layer
(Series 6: 3.75x7.5 , fc'= 6 ksi)

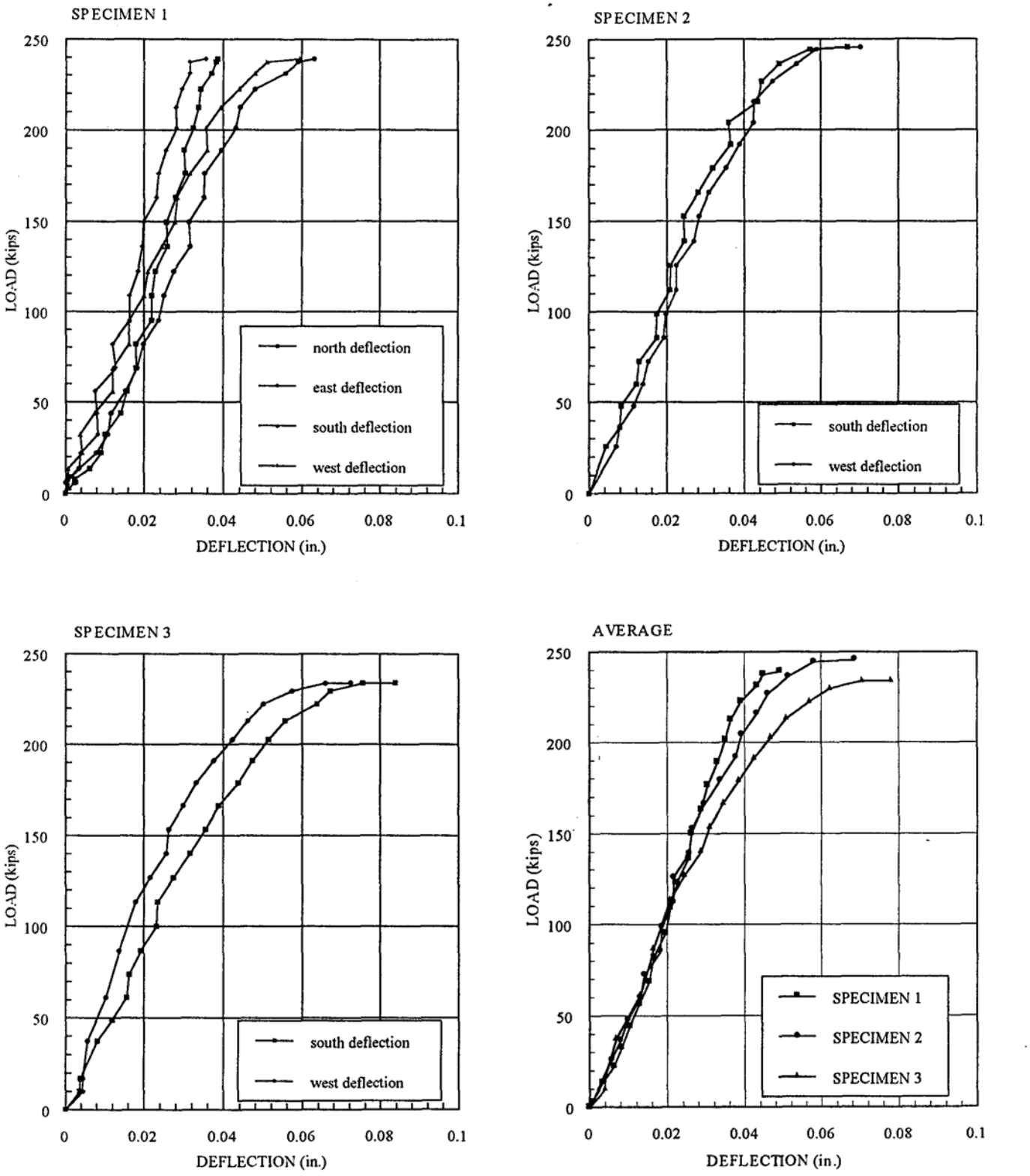

Fig. 4.60 Axial Stress vs Axial and Transverse Strain Control (Series 6: 3.75x7.5 , fc'= 6 ksi)

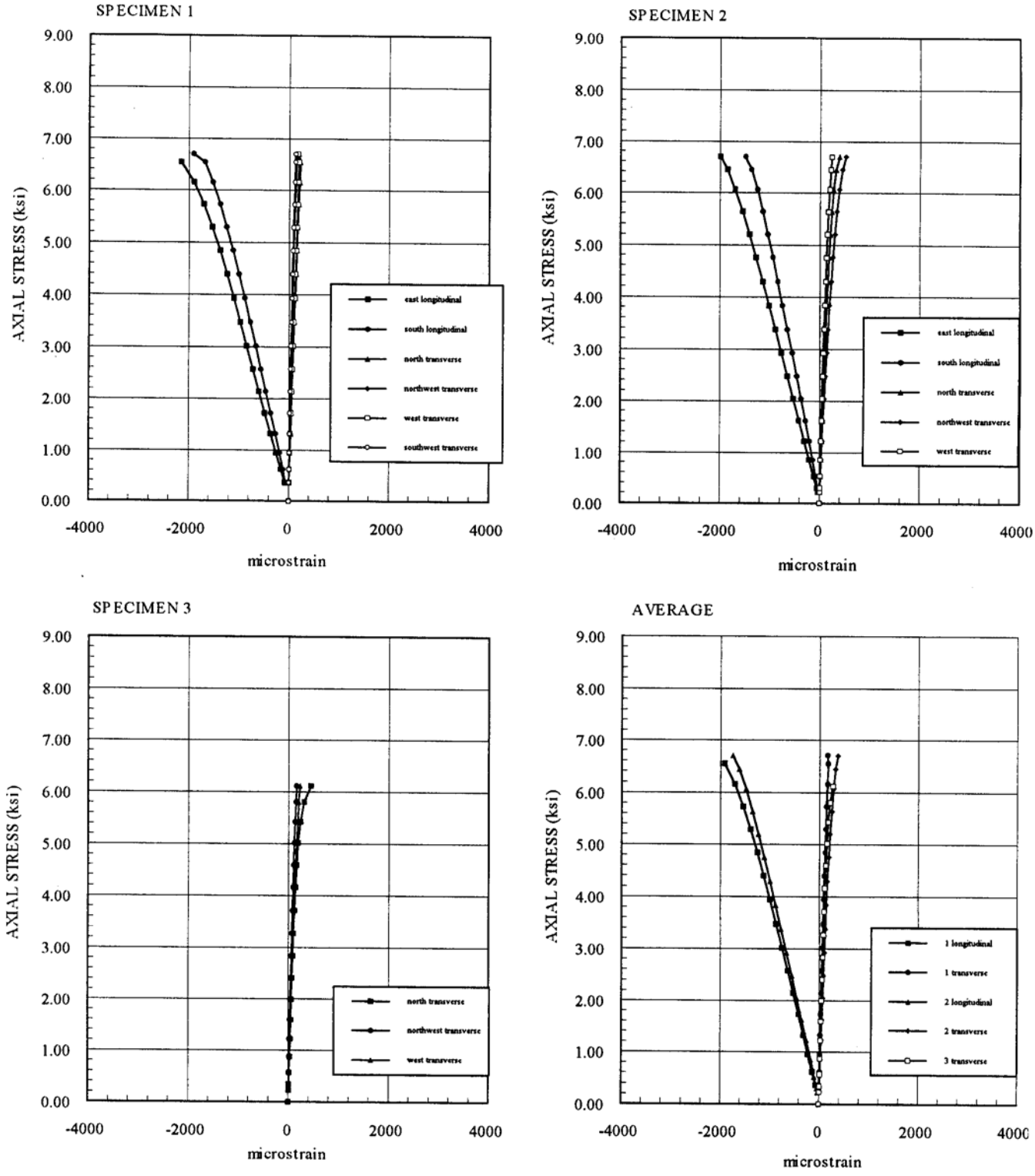

Fig. 4.61 Axial Stress vs Axial and Transverse Strain One Layer
(Series 6: 3.75x7.5 , fc'= 6 ksi)

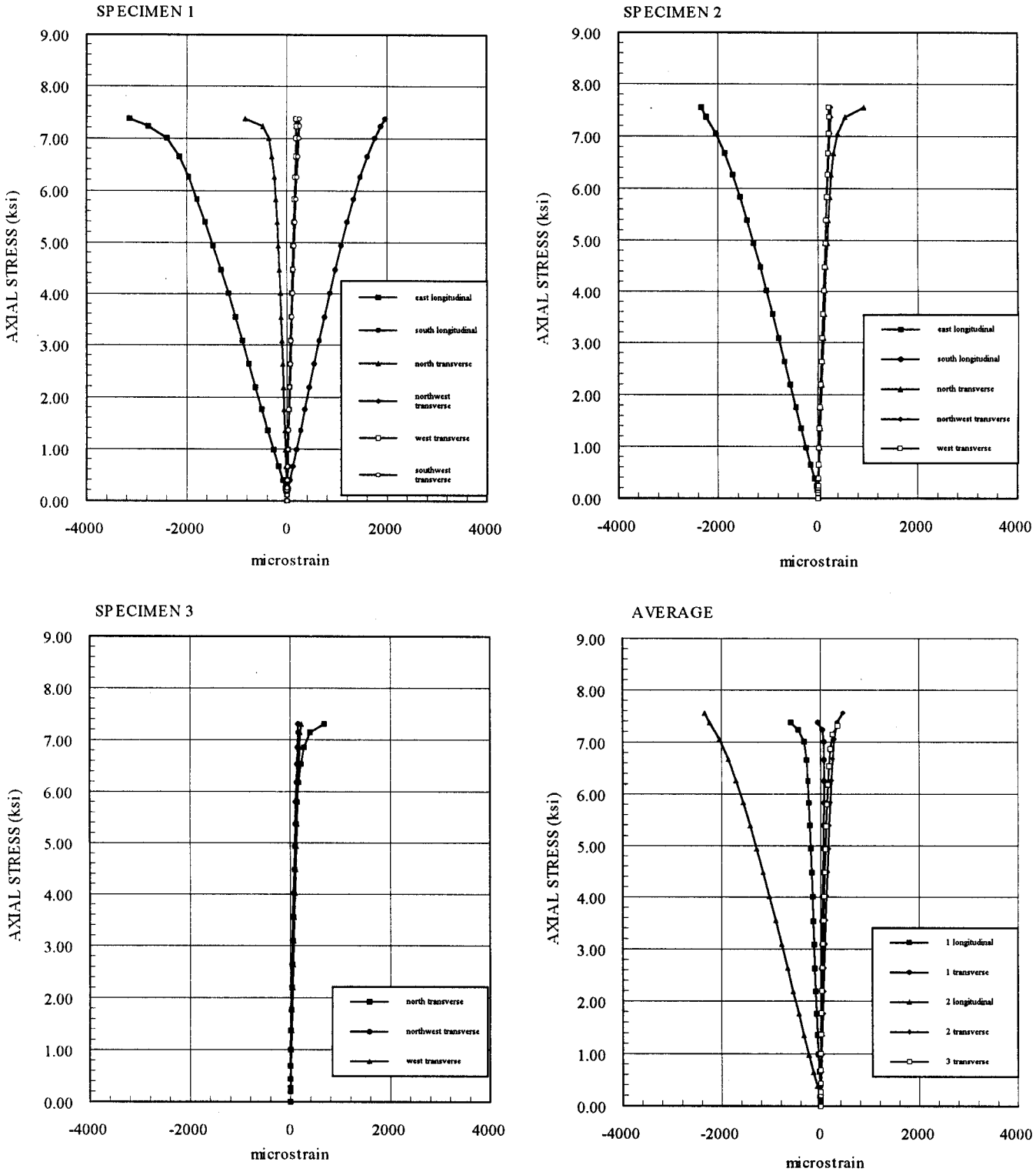

Fig. 4.62 Axial Stress vs Axial and Transverse Strain Two Layers
(Series 6: 3.75x7.5 , fc'= 6 ksi)

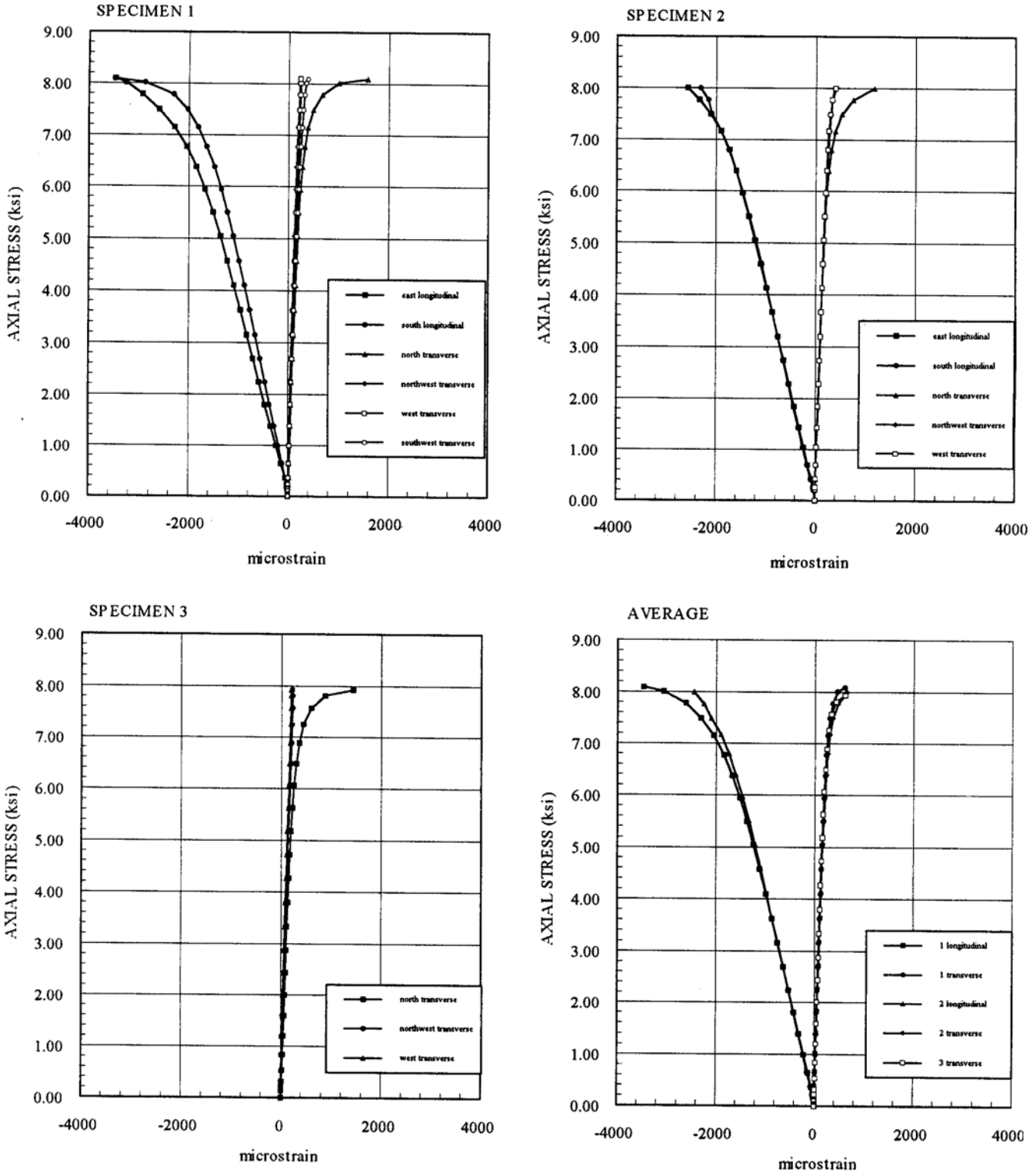

Fig. 4.63 Axial Stress vs Axial and Transverse Strain Three Layers (Series 6: 3.75x7.5 , fc'= 6 ksi)

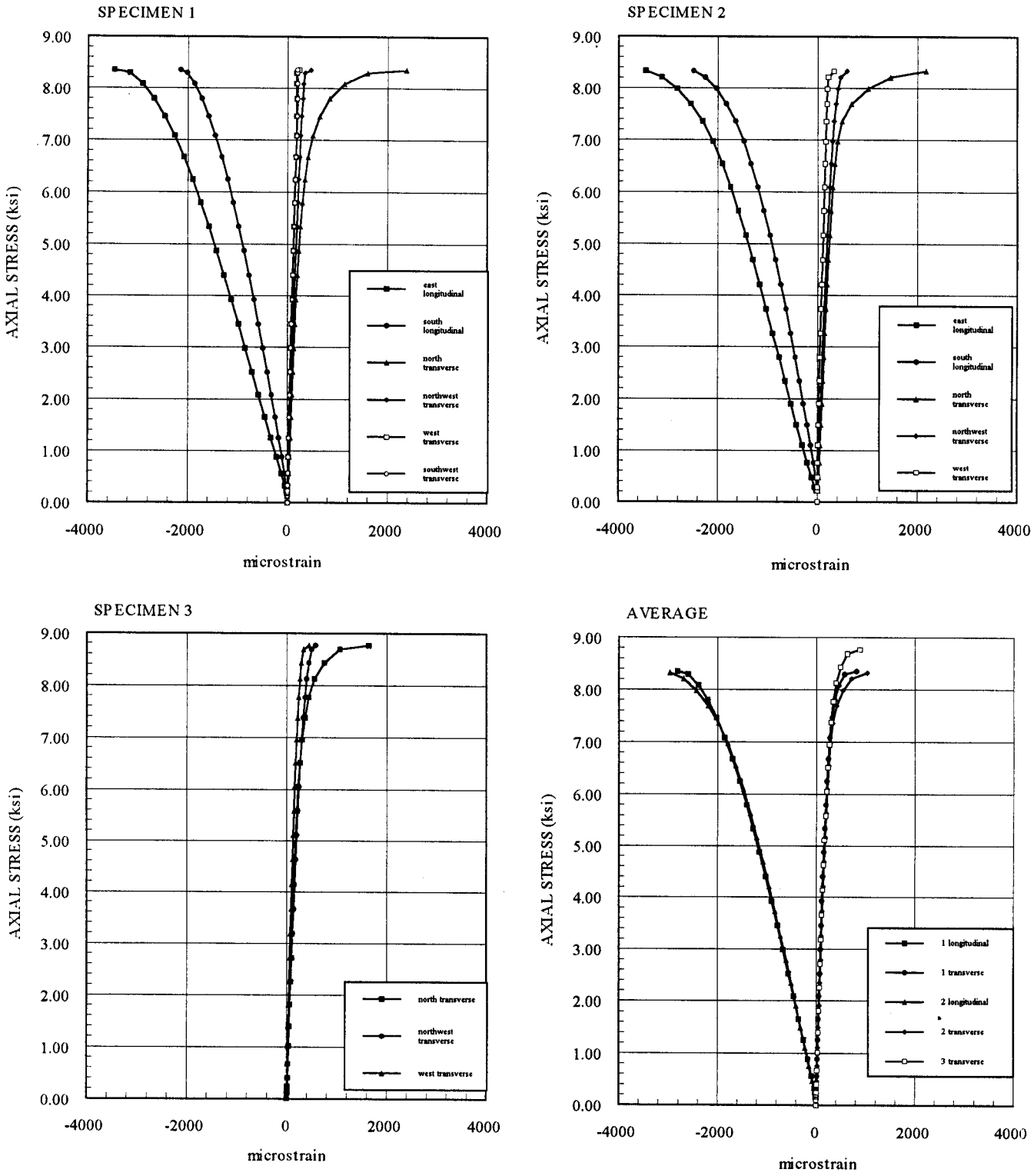

Fig. 4.64 Axial Stress vs Axial and Transverse Strain Four Layers (Series 6: 3.75x7.5 , fc'= 6 ksi)

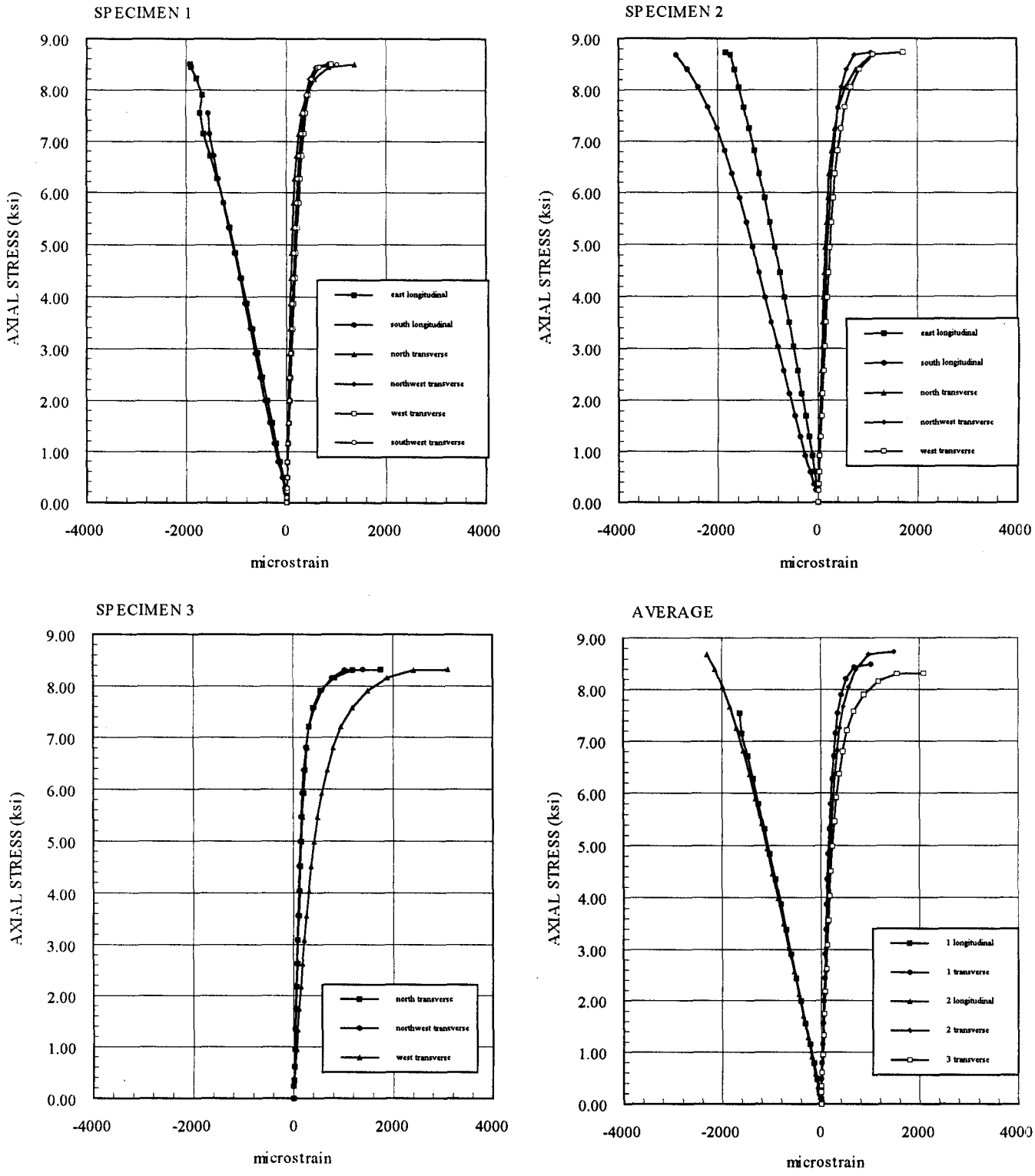

Fig. 5.1 Average Axial Stress vs. Axial and Transverse Strain
(Series 1: 5.25"x5.25", f'c=3ksi)

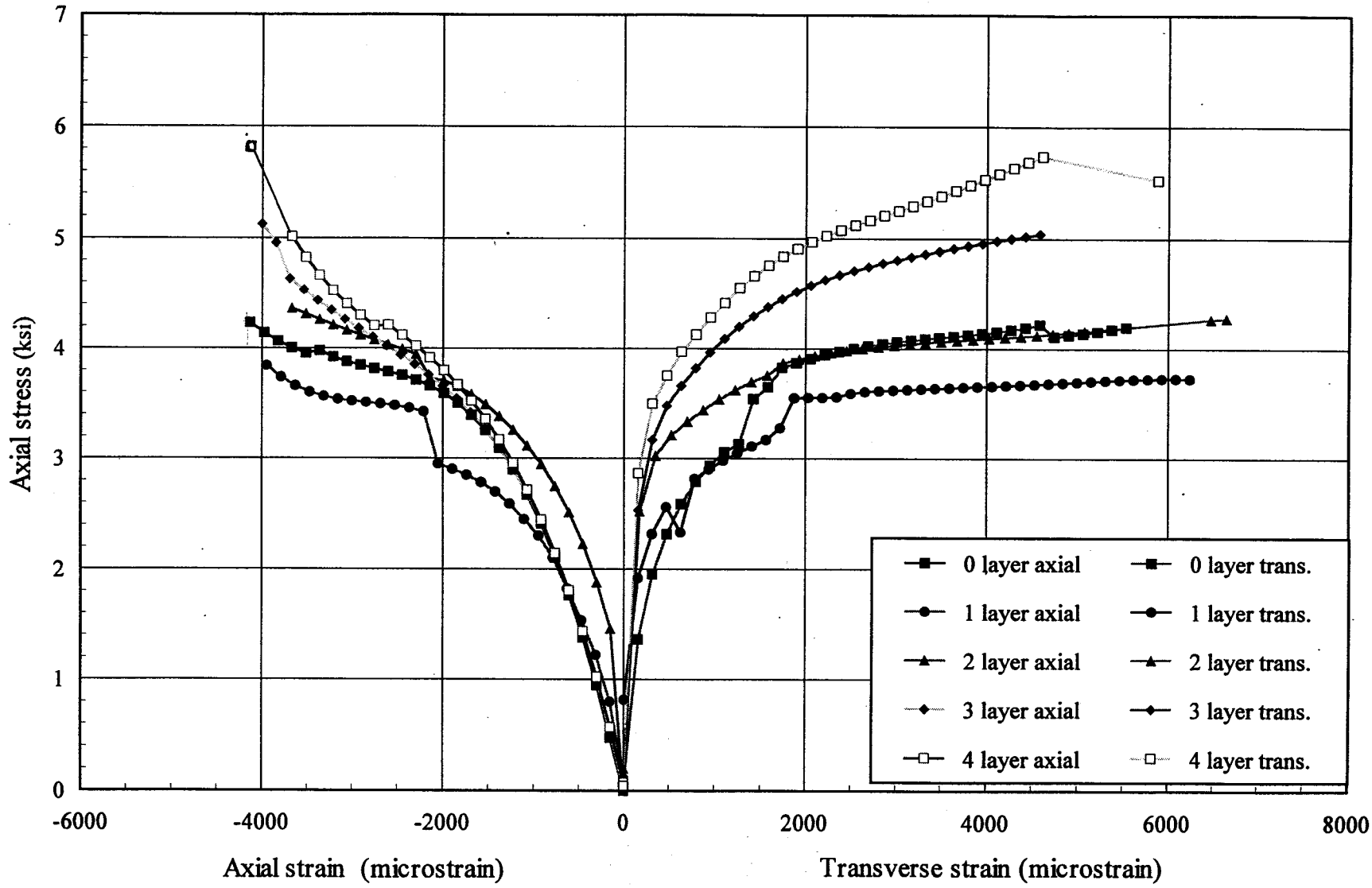

Fig. 5.2 Average Axial Stress vs. Axial and Transverse Strain
(Series 2: 4.25"x6.5", f'c =3ksi)

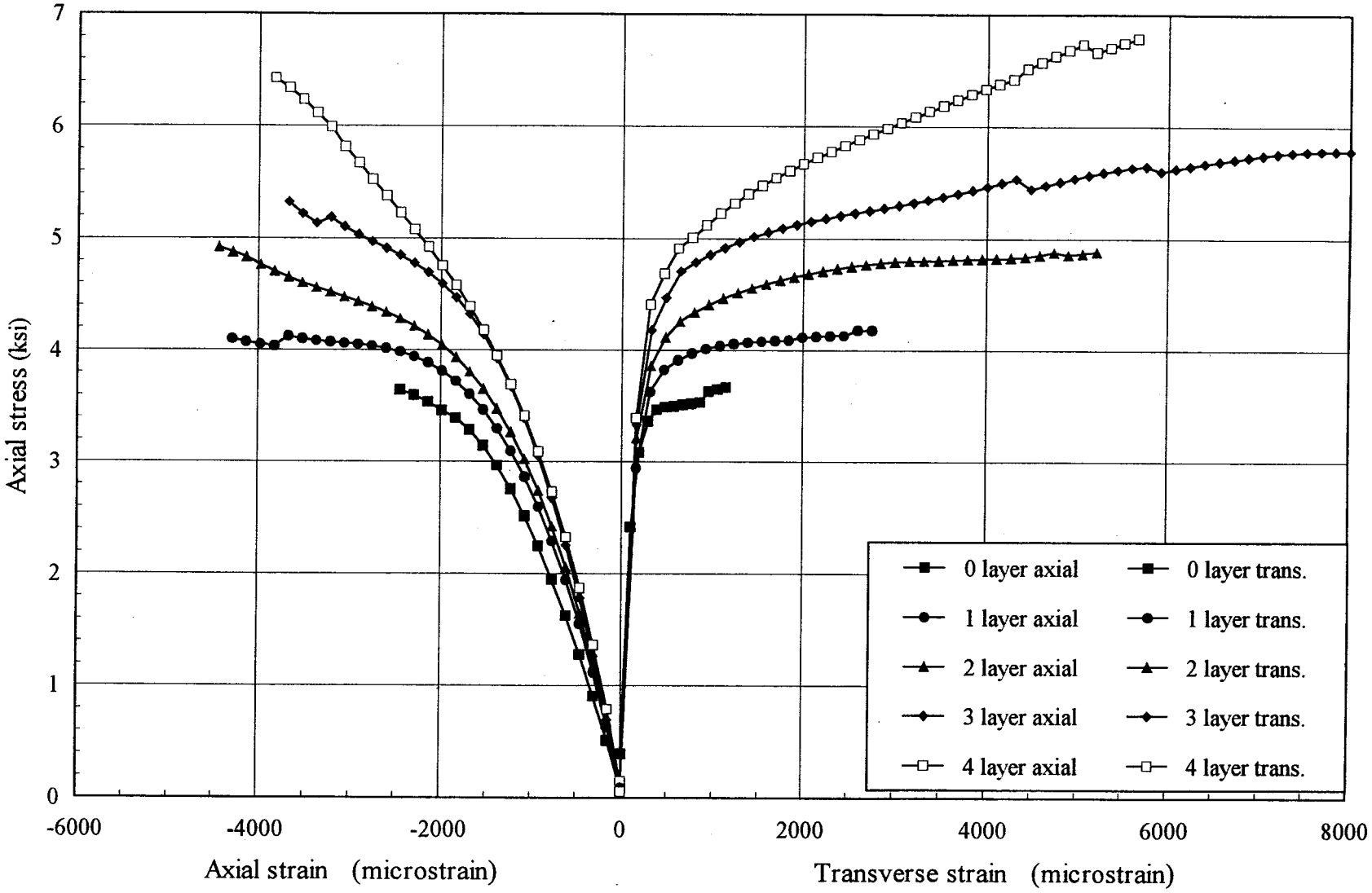

Fig. 5.3 Average Axial Stress vs. Axial and Transverse Strain
(Series 3: 3.75"x7.5", f'c =3ksi)

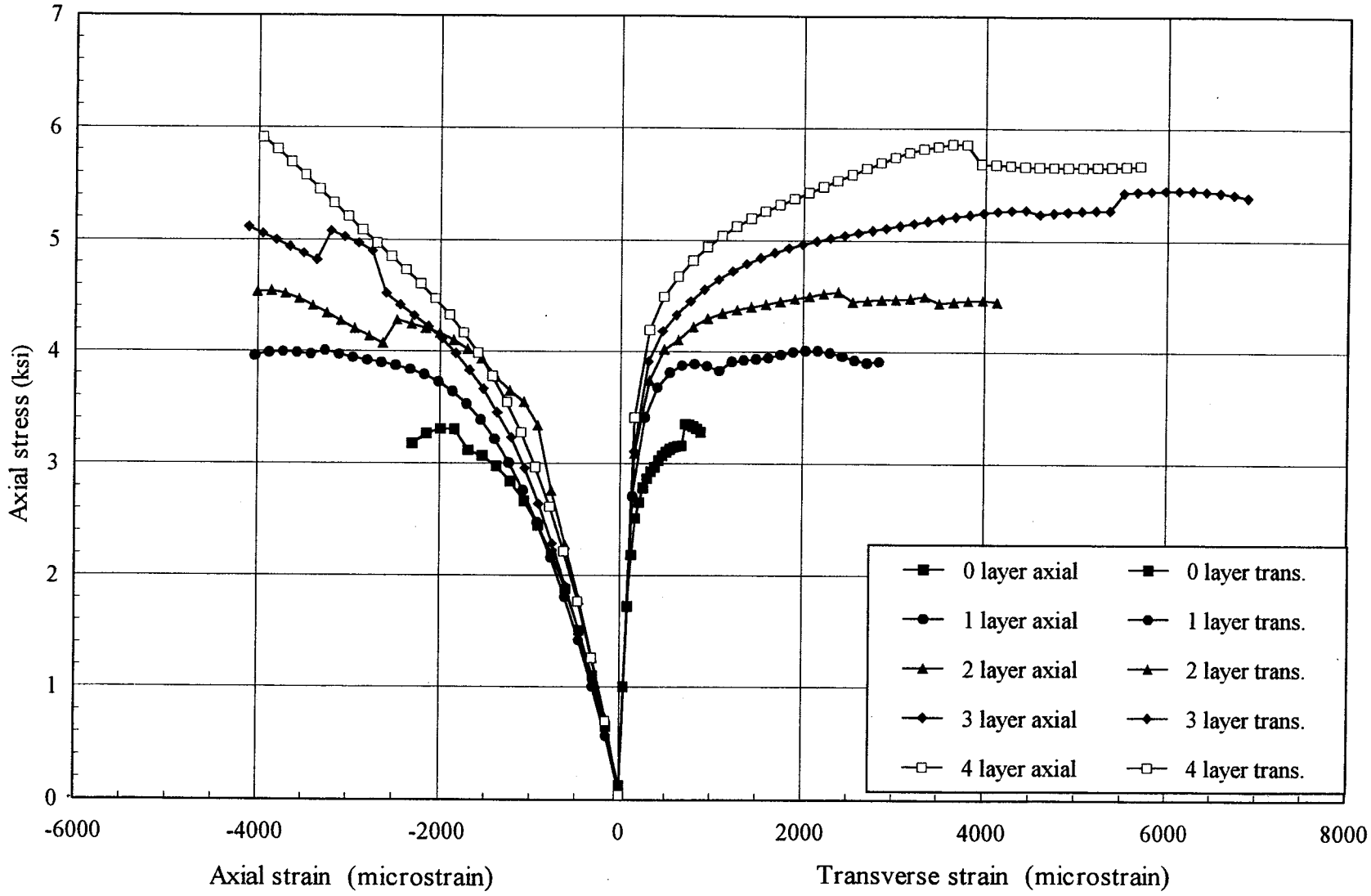

Fig. 5.4 Average Axial Stress vs. Axial and Transverse Strain
(Series 4: 5.25"x5.25", f'c =6ksi)

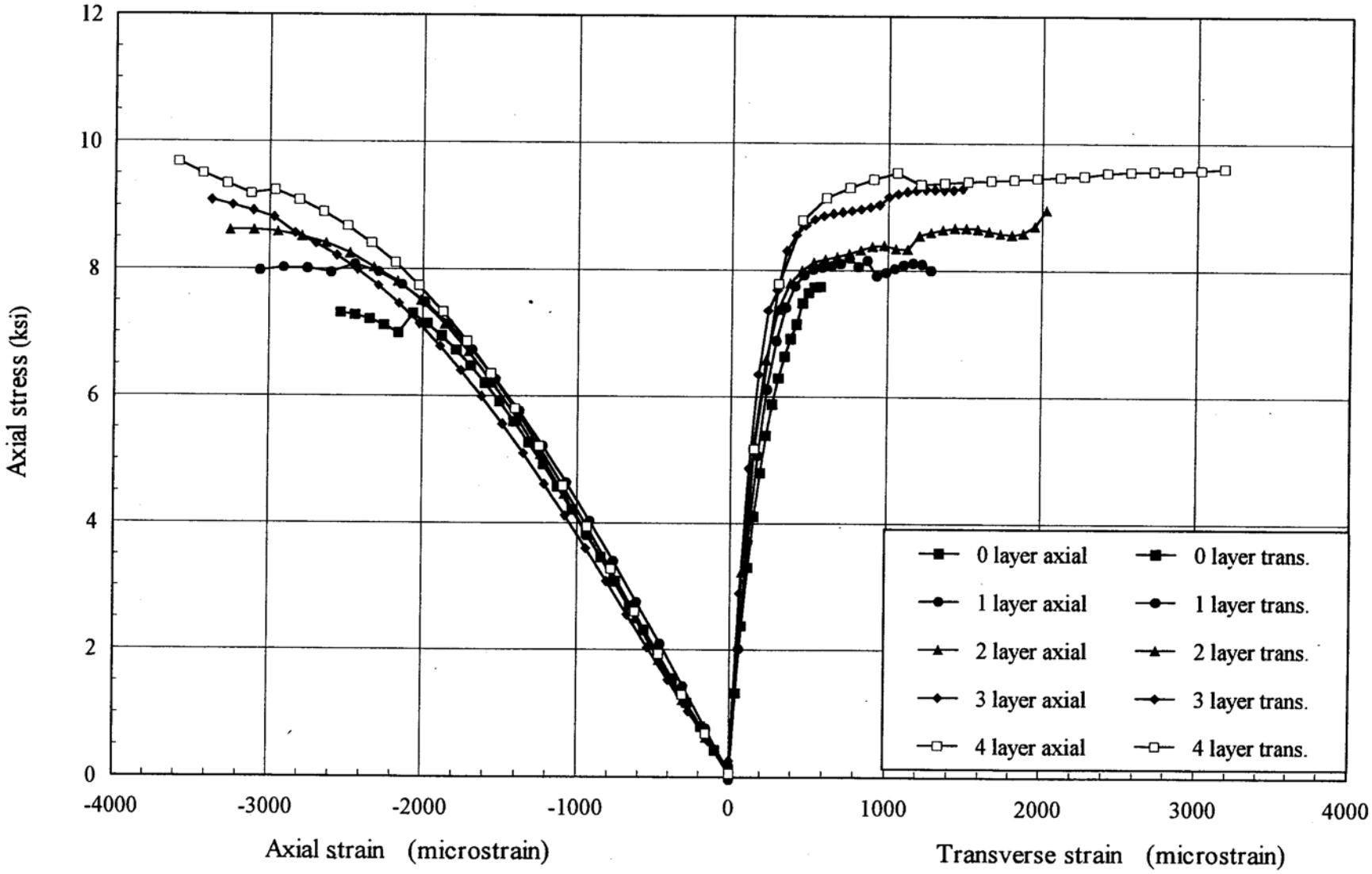

Fig. 5.5 Average Axial Stress vs. Axial and Transverse Strain
(Series 5: 4.25"x6.5", f'c =6ksi)

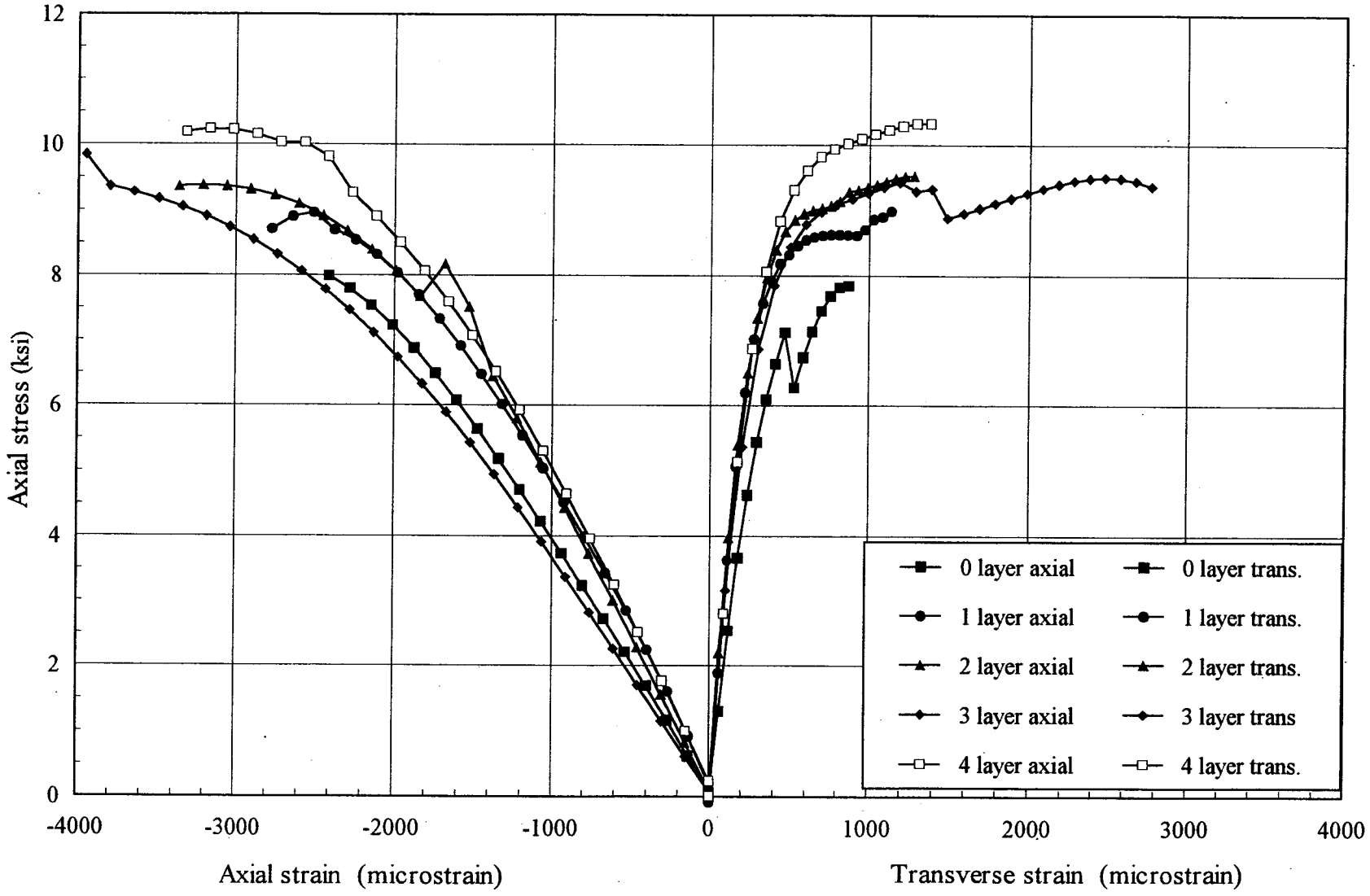

Fig. 5.6 Average Axial Stress vs. Axial and Transverse Strain
(Series 6: 3.75"x7.5", f'c =6 ksi)

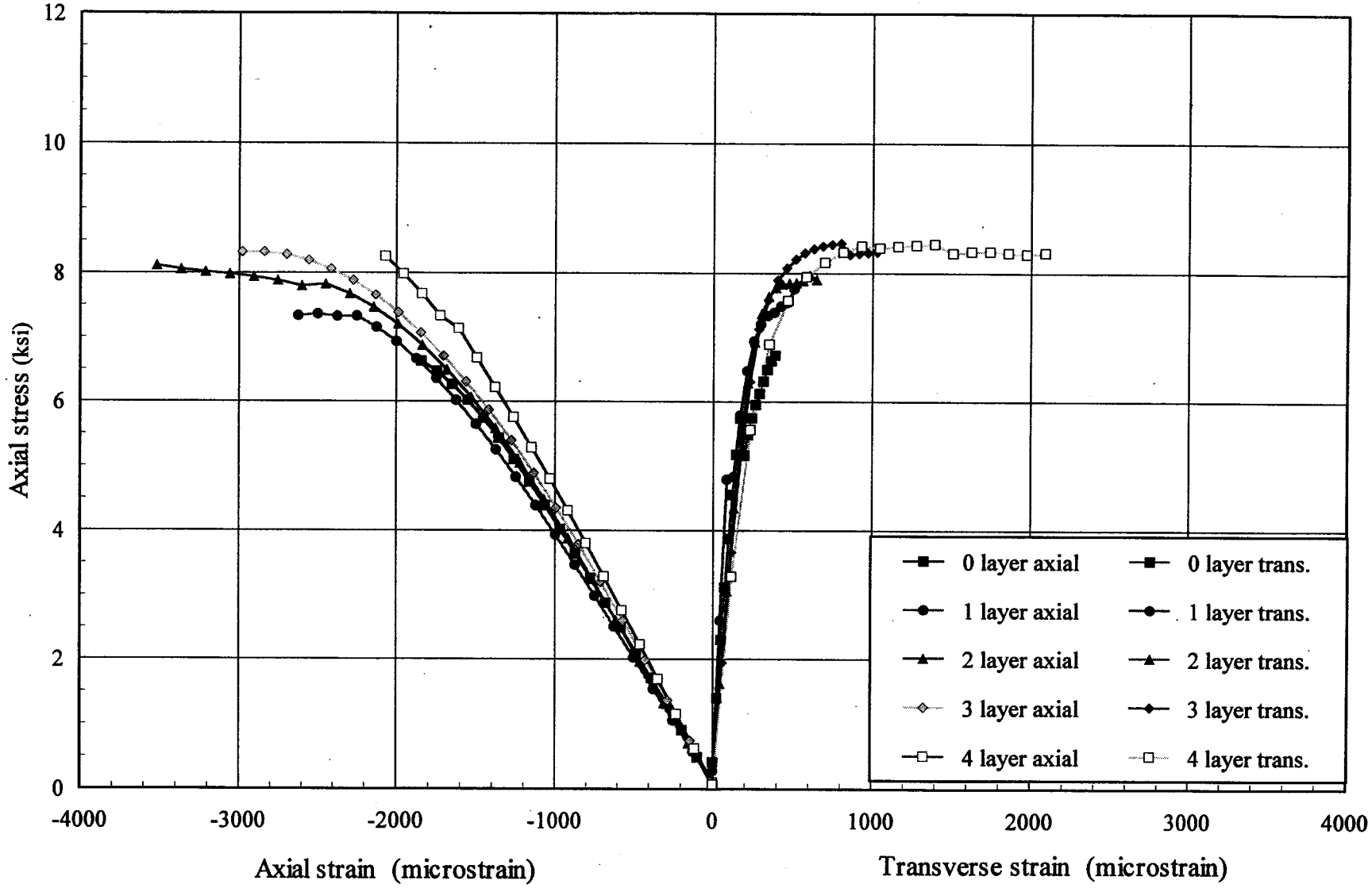

Fig.5-7 Average Normalized Axial Stress vs. Volumetric Strain
(Series1: 5.25x5.25, f'c=3ksi)

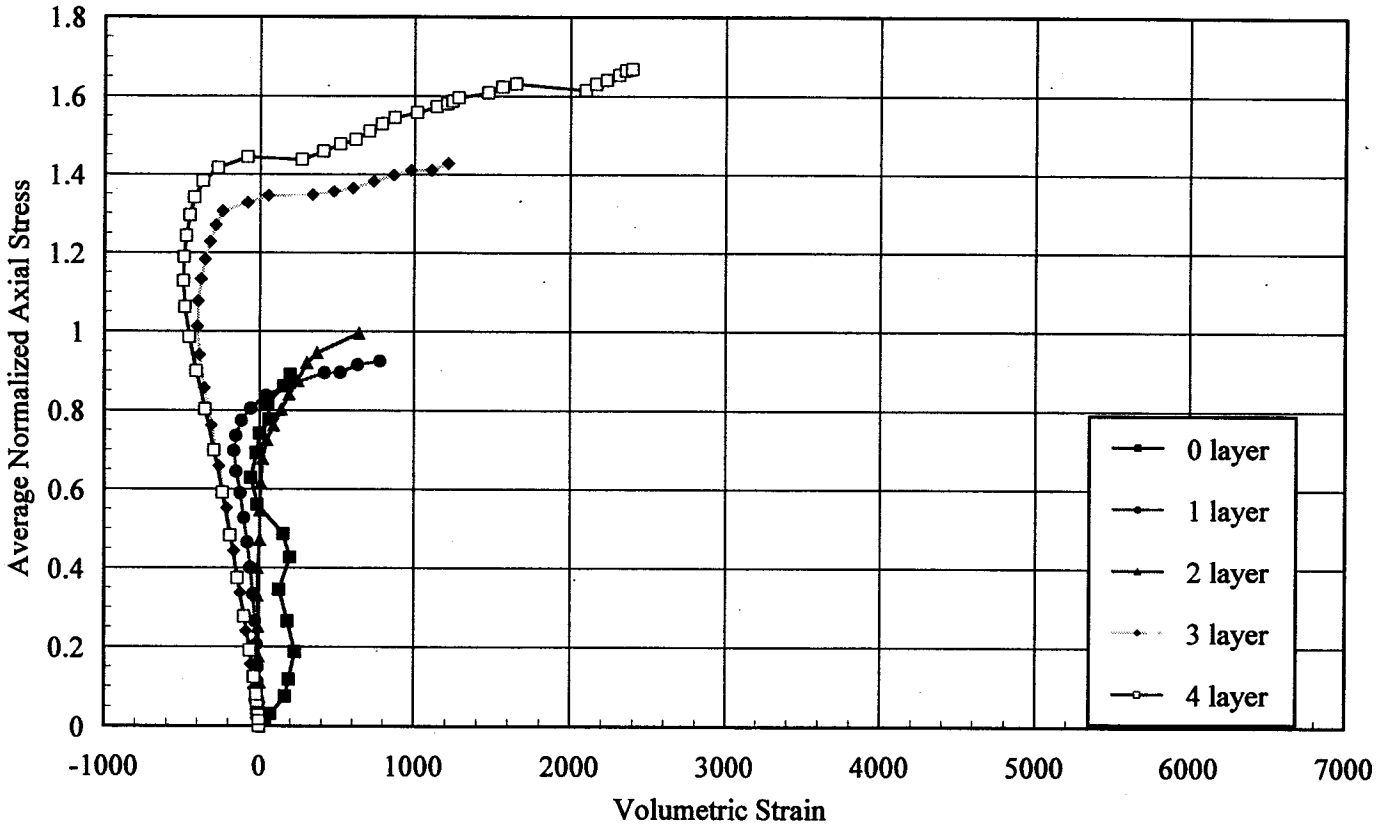

Fig.5-8 Average Normalized Axial Stress vs. Volumetric Strain
(Series2: 4.25x6.5, f'c=3ksi)

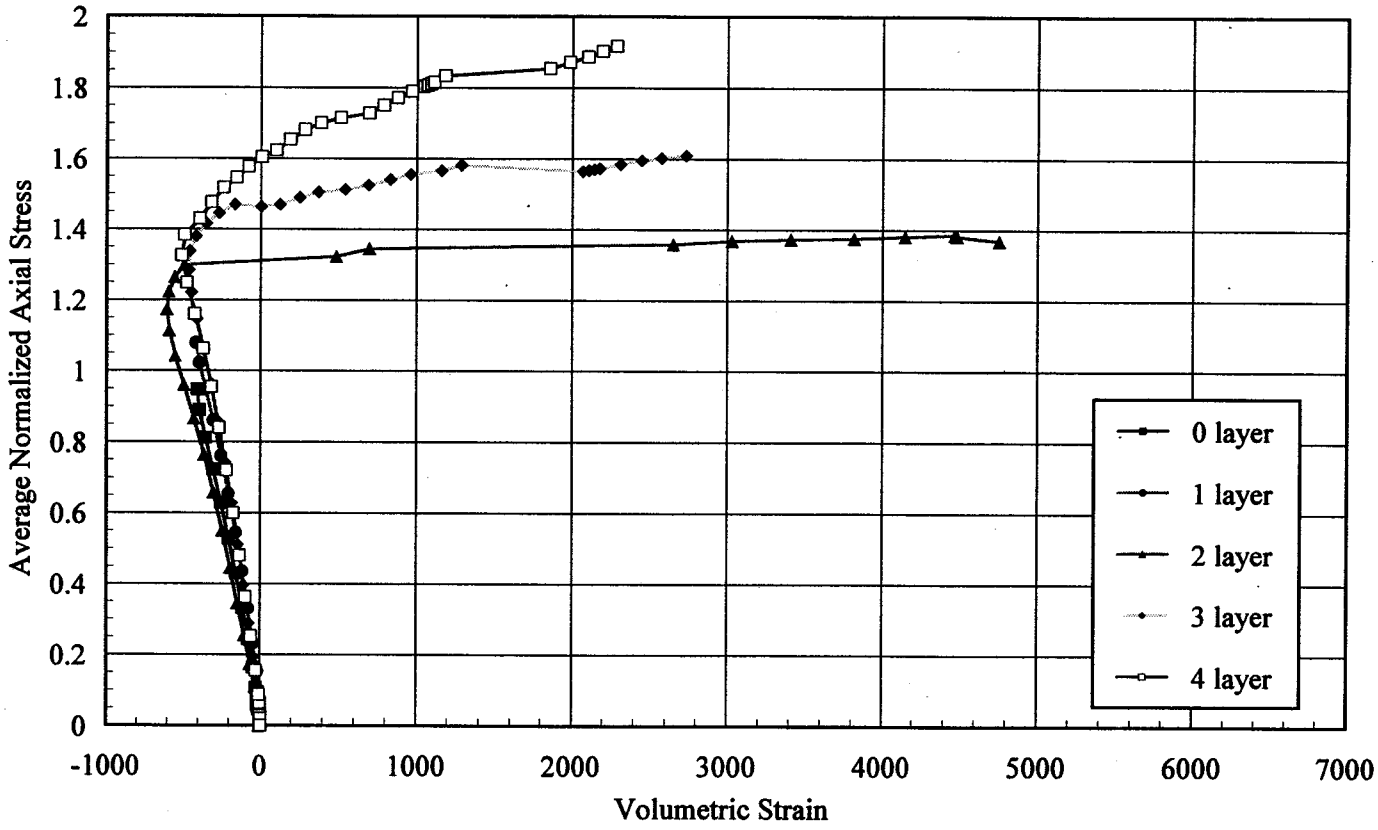

Fig.5-9 Average Normalized Axial Stress vs. Volumetric Strain
(Series3: 3.75x7.5, f'c=3ksi)

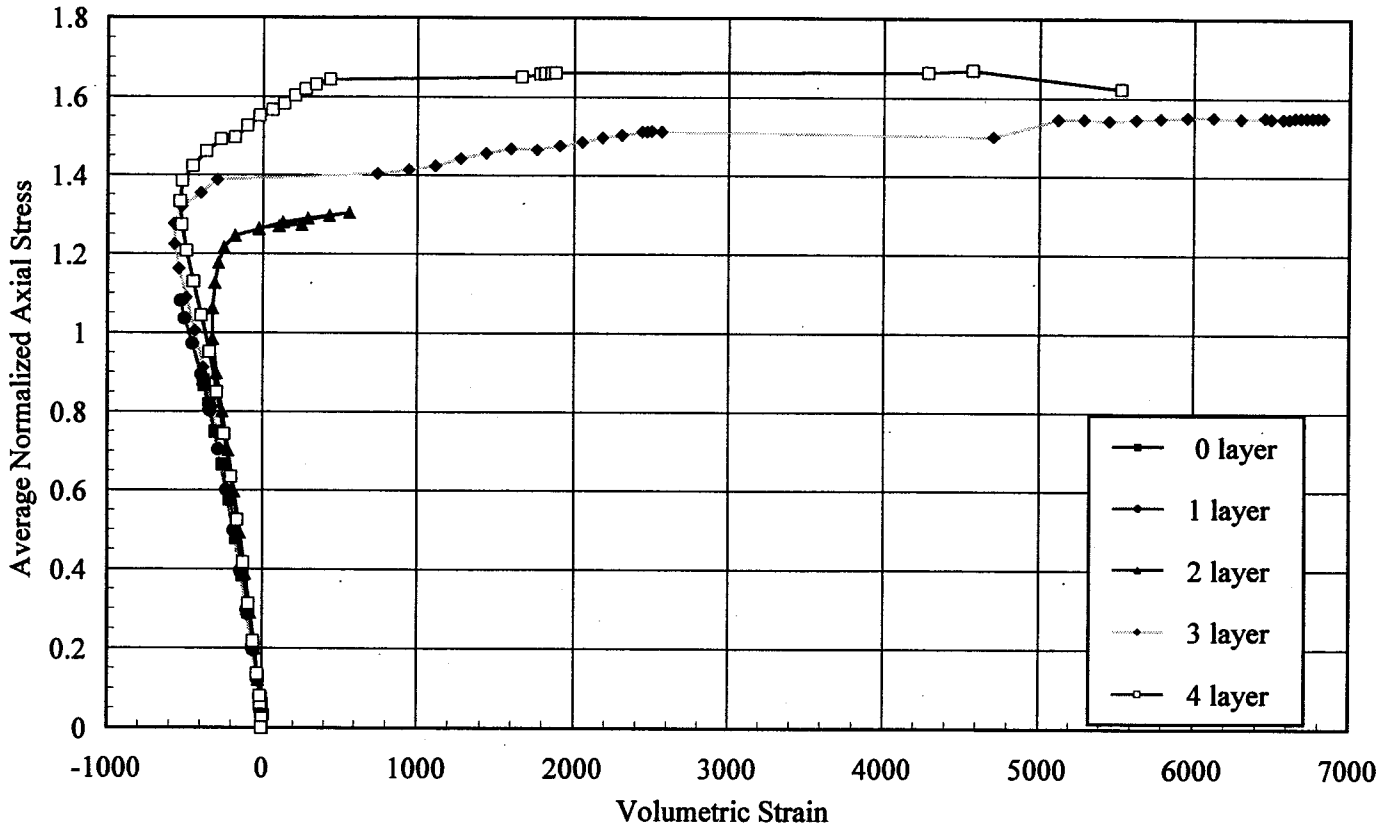

Fig.5-10 Average Normalized Axial Stress vs. Volumetric Strain
(Series4: 5.25x5.25, f'c=6ksi)

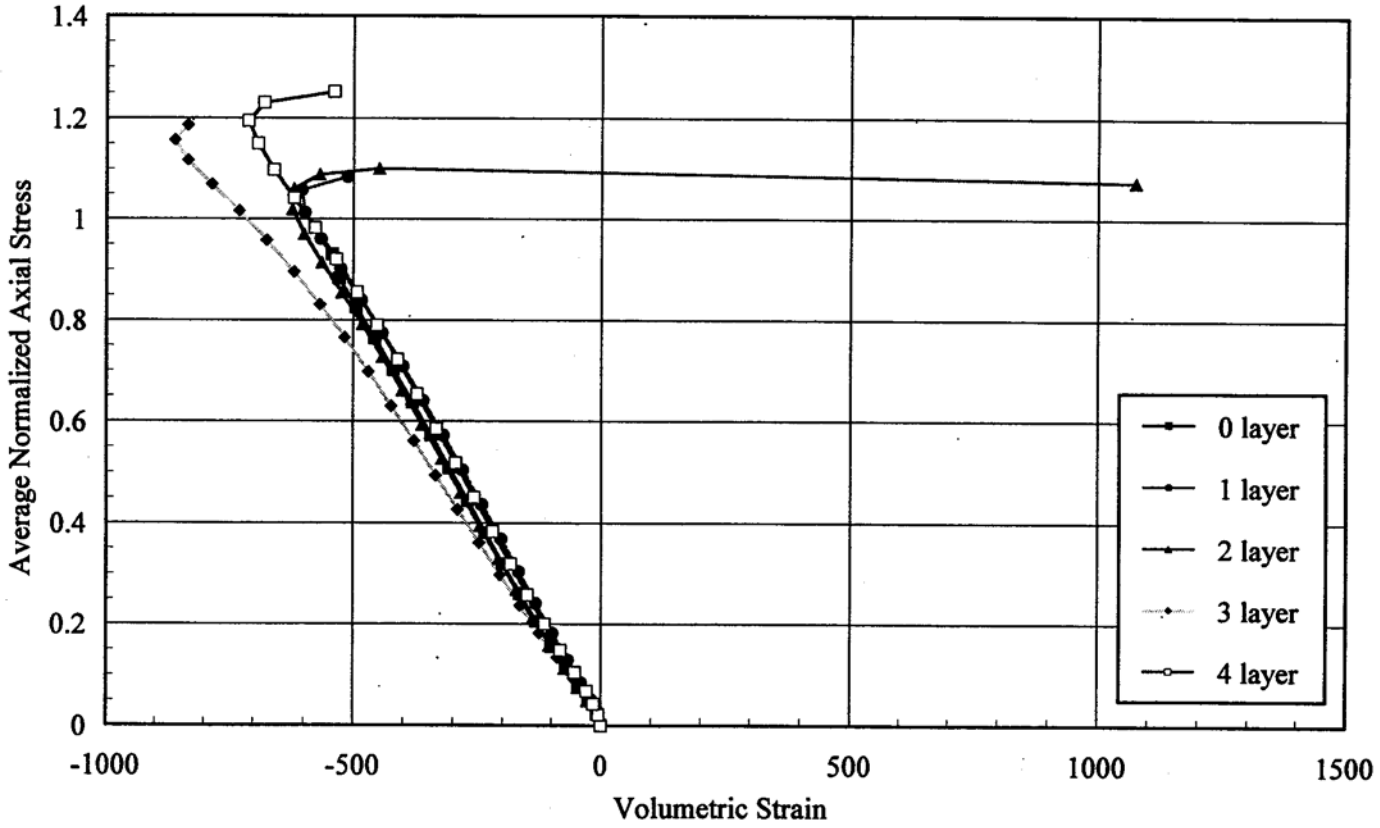

Fig.5-11 Average Normalized Axial Stress vs. Volumetric Strain
(Series5:4.25x6.5, f'c=6ksi)

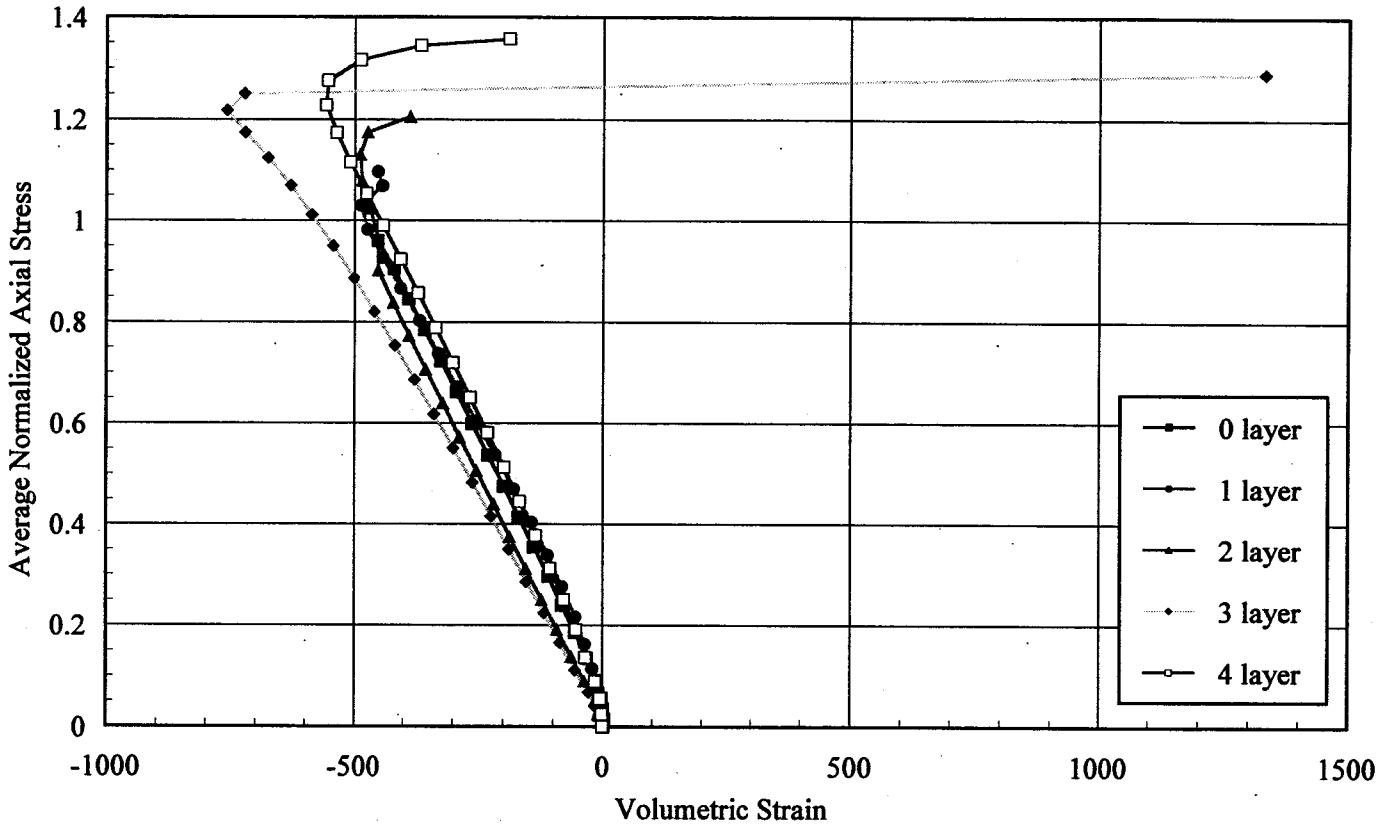

Fig.5-12 Average Normalized Axial Stress vs. Volumetric Strain
(Series 6: 3.75x7.5, f'c=6ksi)

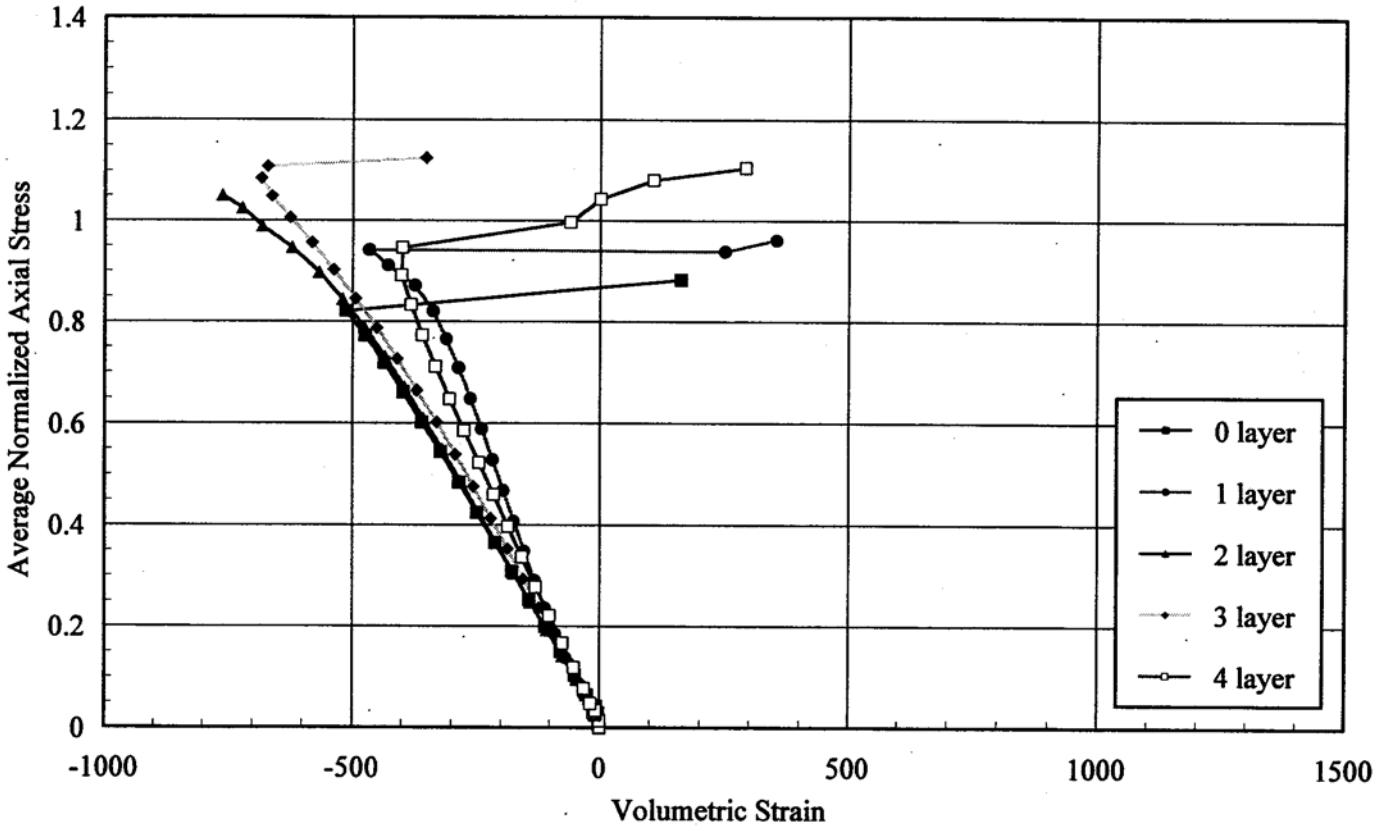

Fig. 5.13 - Typical dilation rate for FRP-encased concrete (Mirmiran and Shahawy, 1997)

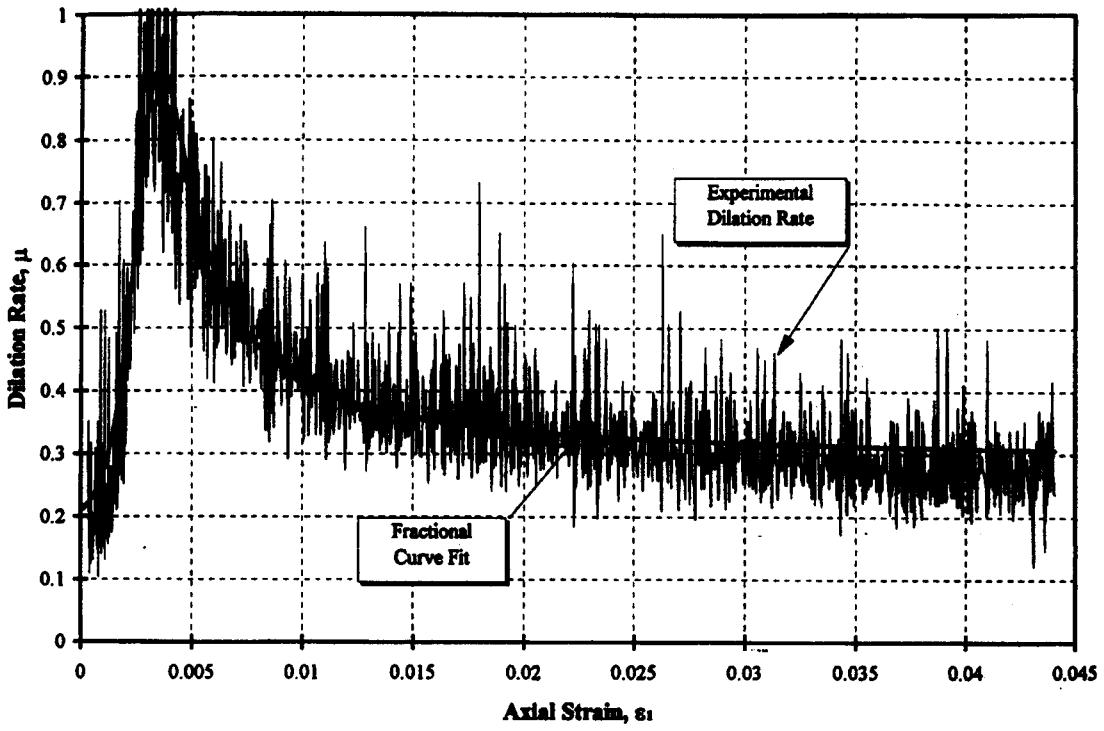

Fig. 5.14- Average Dilation Rate vs. Axial Strain
(Series 1: 5.25 x 5.25, f'c=3ksi)

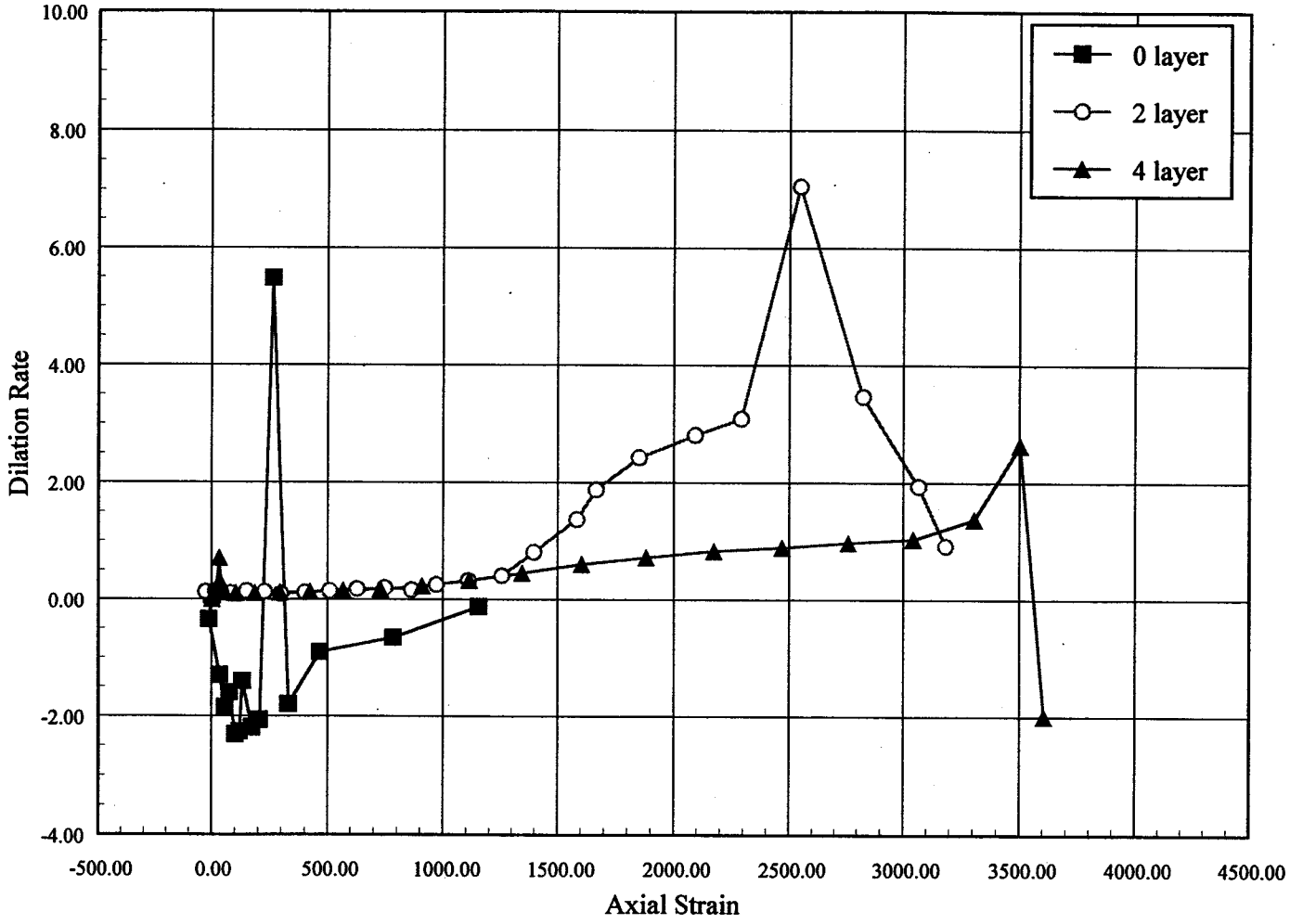

Fig. 5.15- Average Dilation Rate vs. Axial Strain
(Series 2: 4.25 x 6.5, f'c=3ksi)

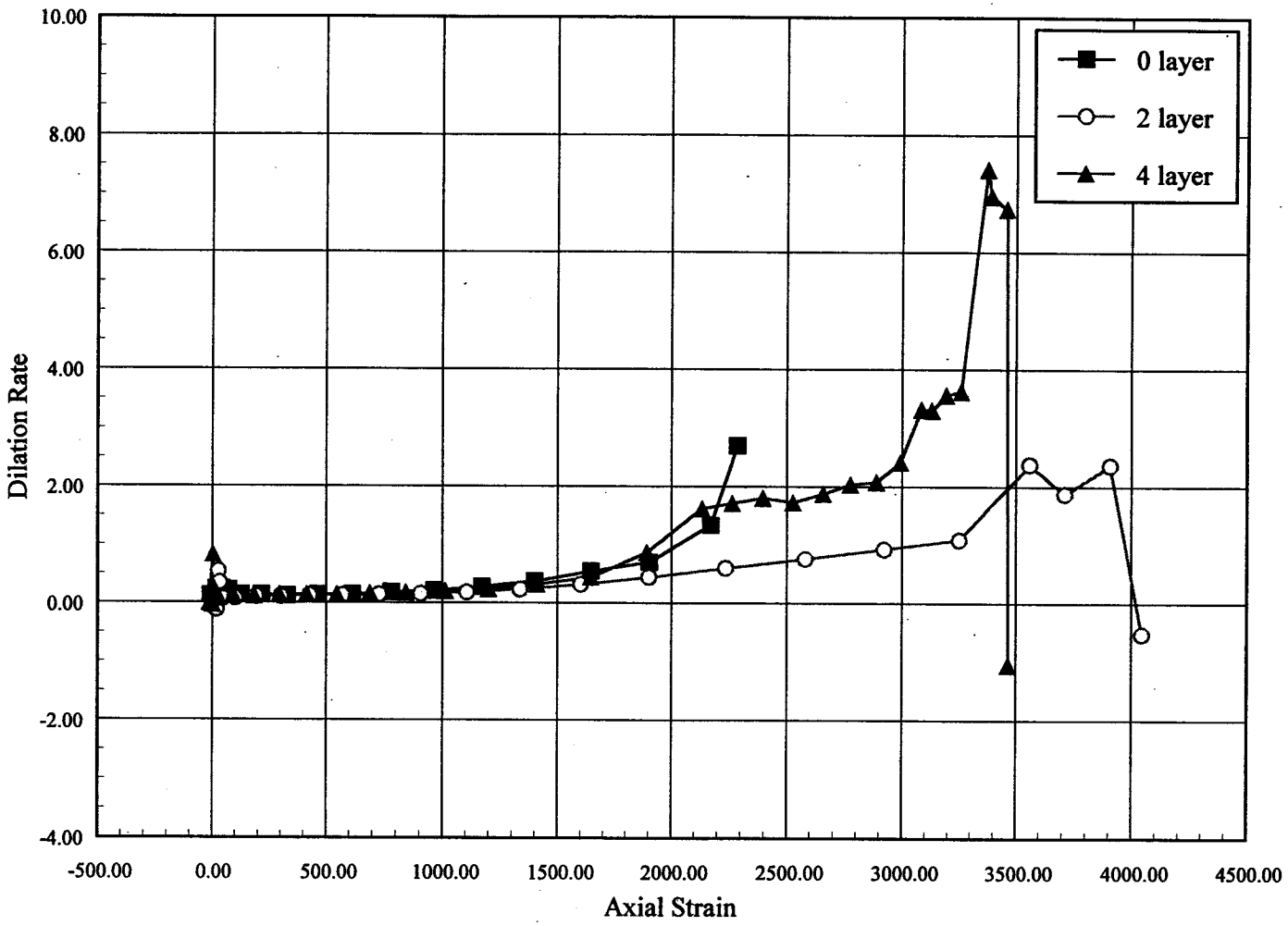

Fig. 5.16 - Average Dilation Rate vs. Axial Strain
(Series 3: 3.75 x 7.5, f'c=3ksi)

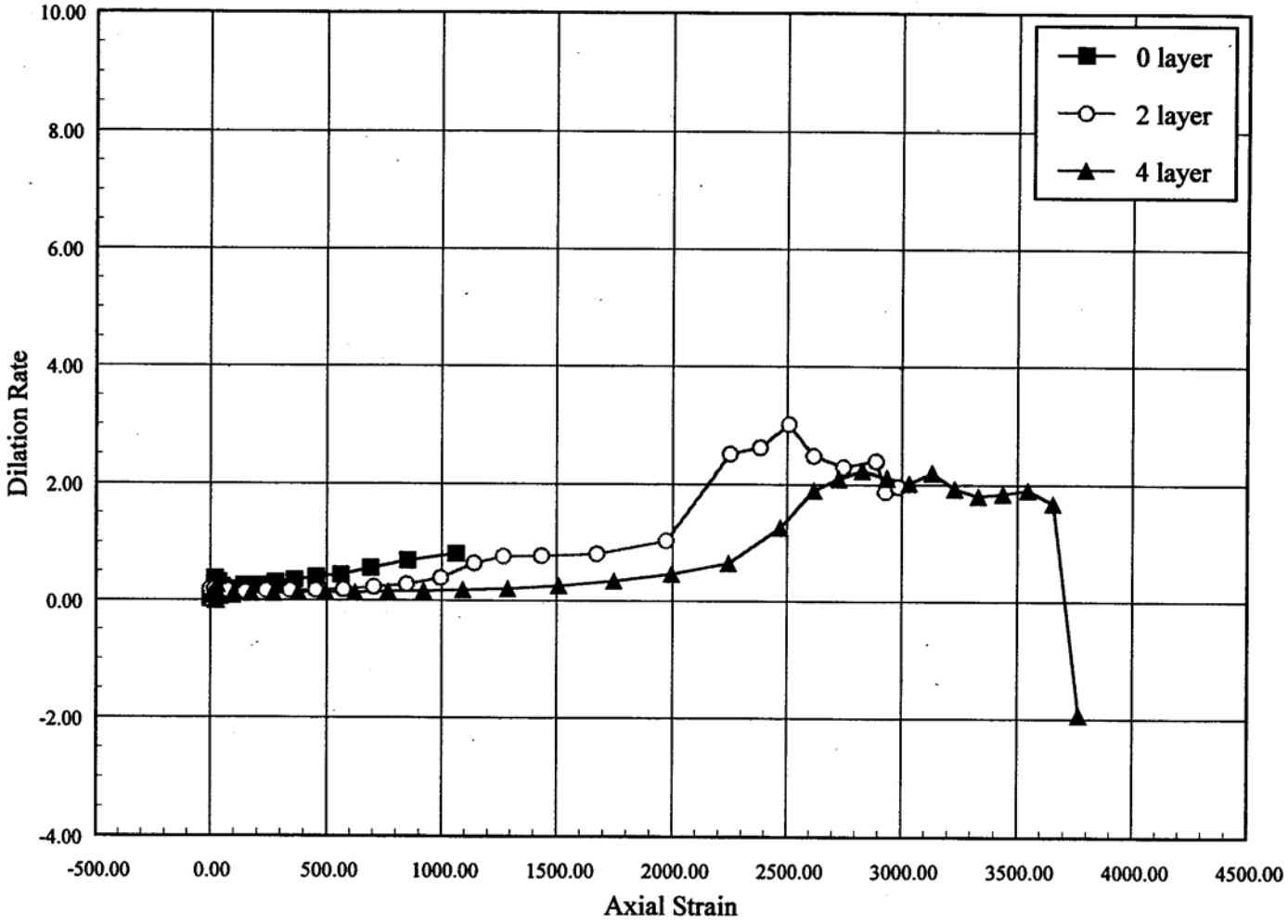

Fig. 5.17- Average Dilation Rate vs. Axial Strain
(Series 4: 5.25 x 5.25, f'c=6ksi)

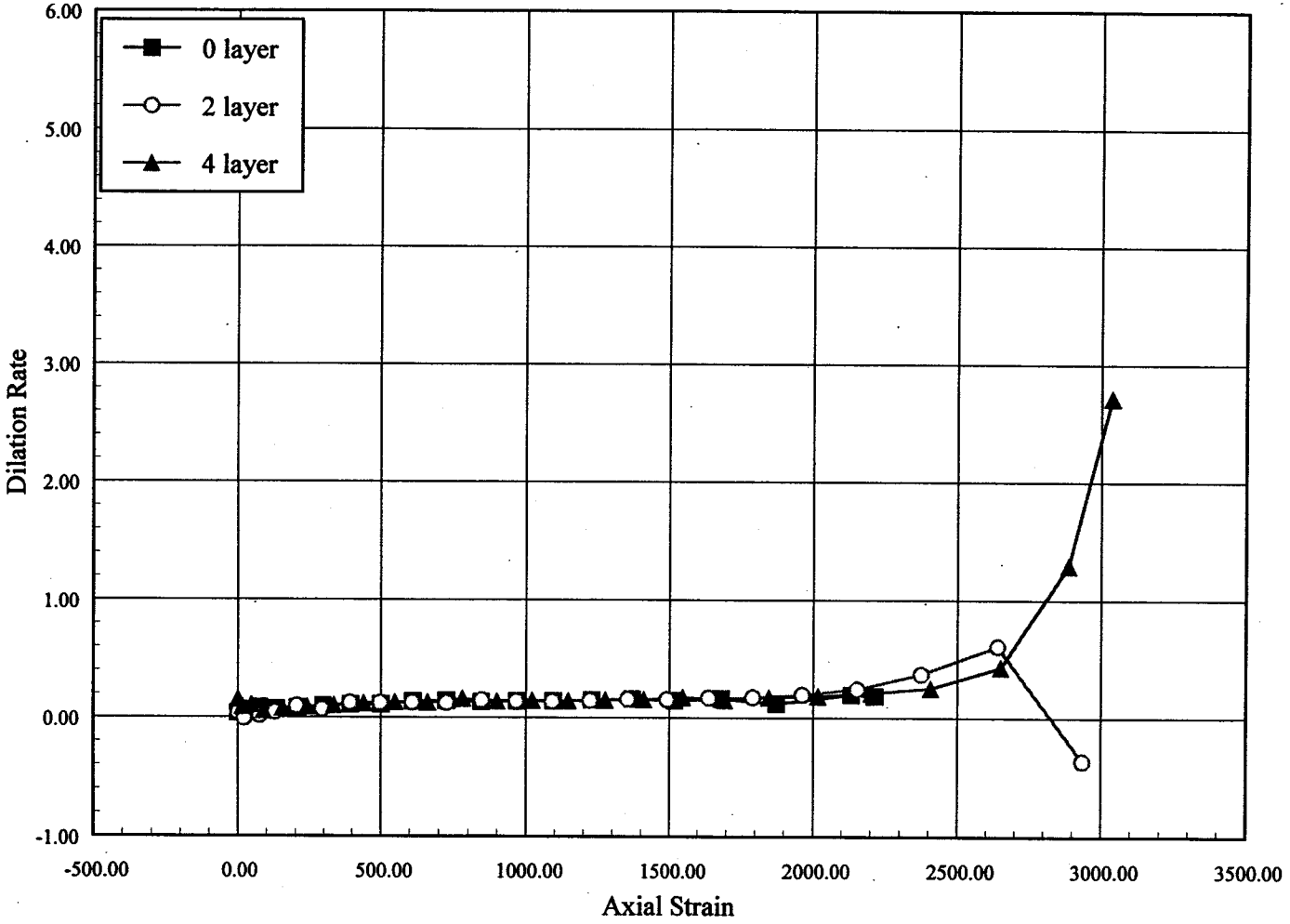

Fig. 5.19 - Average Dilation Rate vs. Axial Strain
(Series 6: 3.75 x 7.5, f'c=6 ksi)

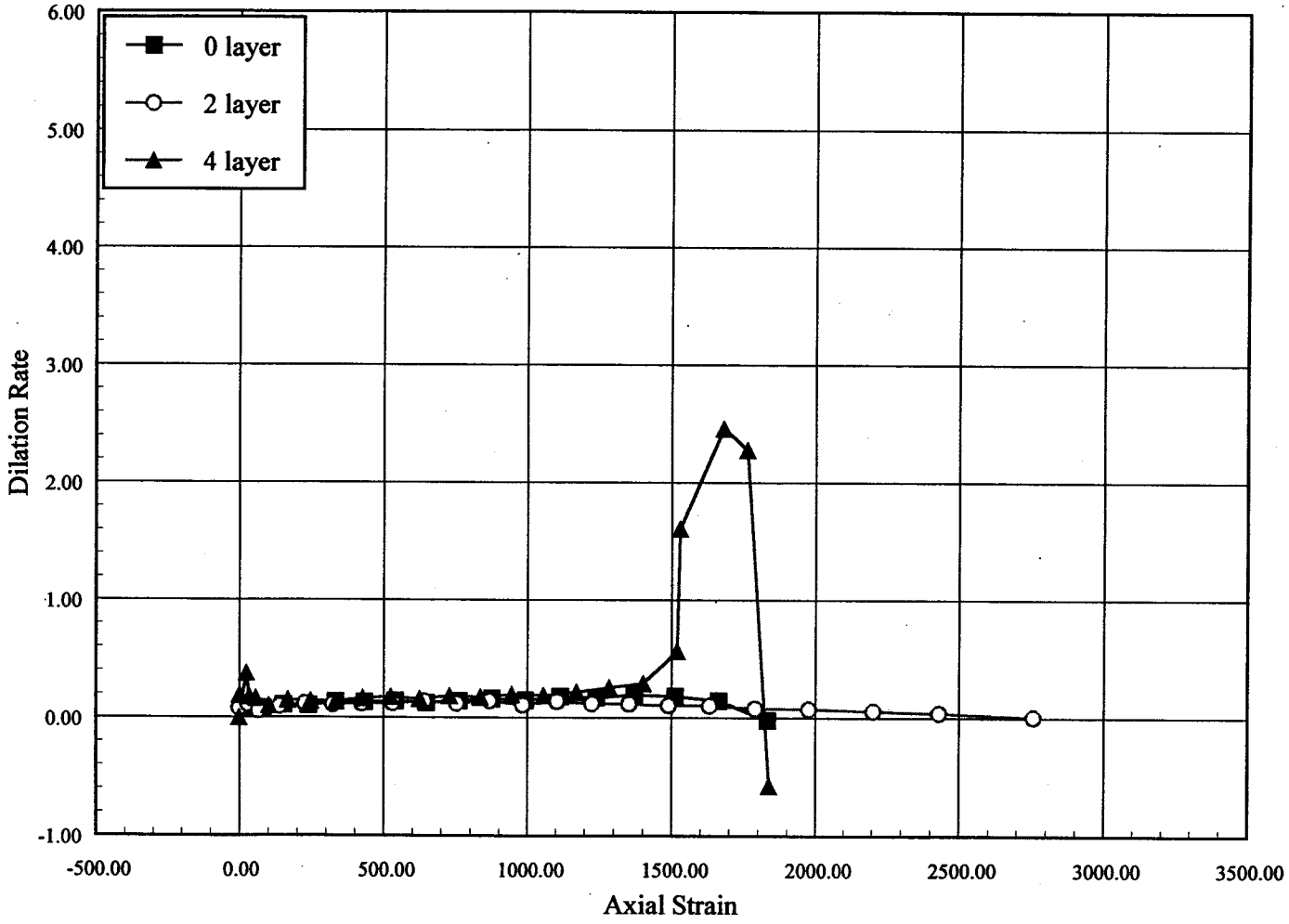

Fig. 5.18- Average Dilation Rate vs. Axial Strain
(Series 5: 4.25 x 6.5, f'c=6ksi)

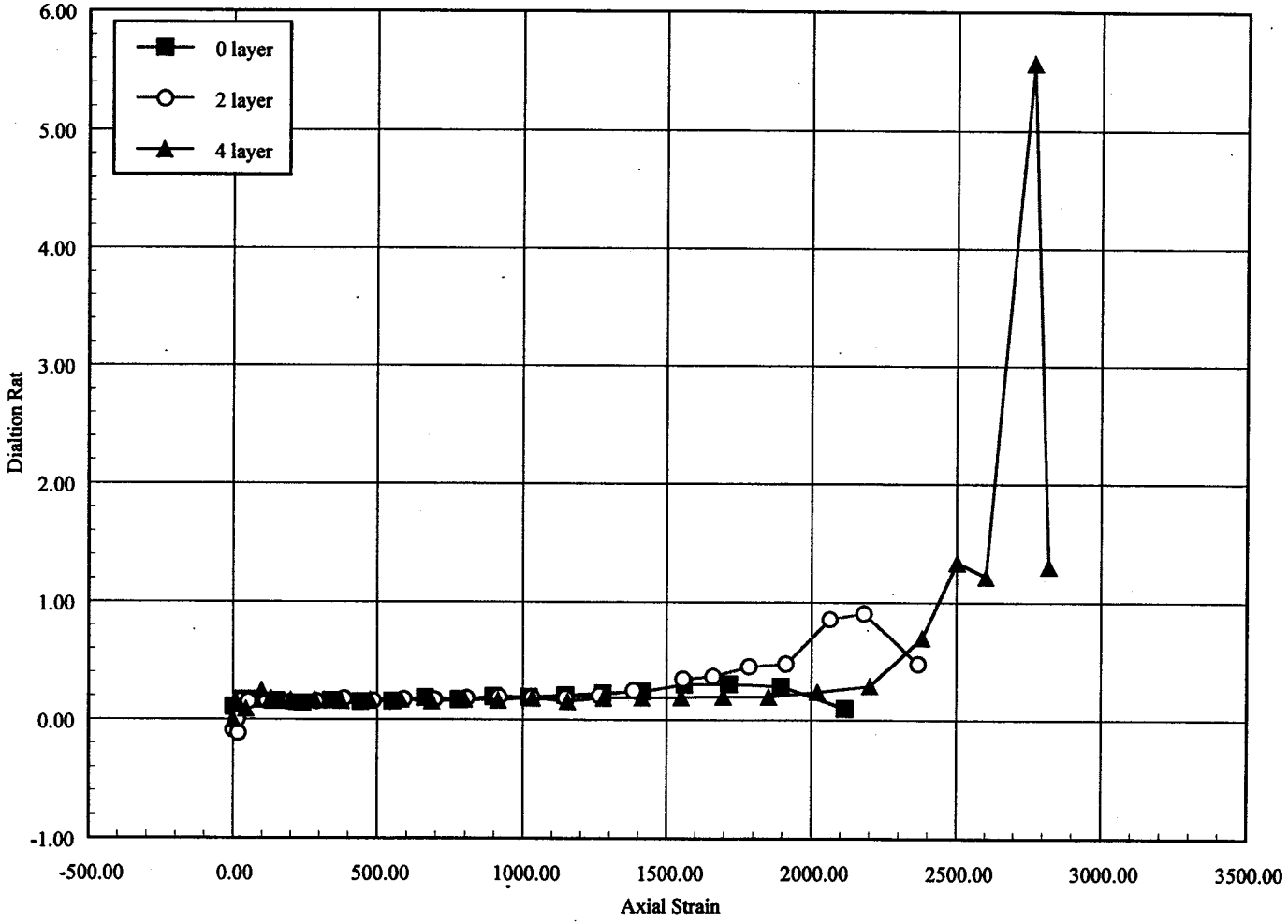

Fig. 5.20 Average Normalized Stress - Strain Curves:
3 ksi vs. 6 ksi Concrete

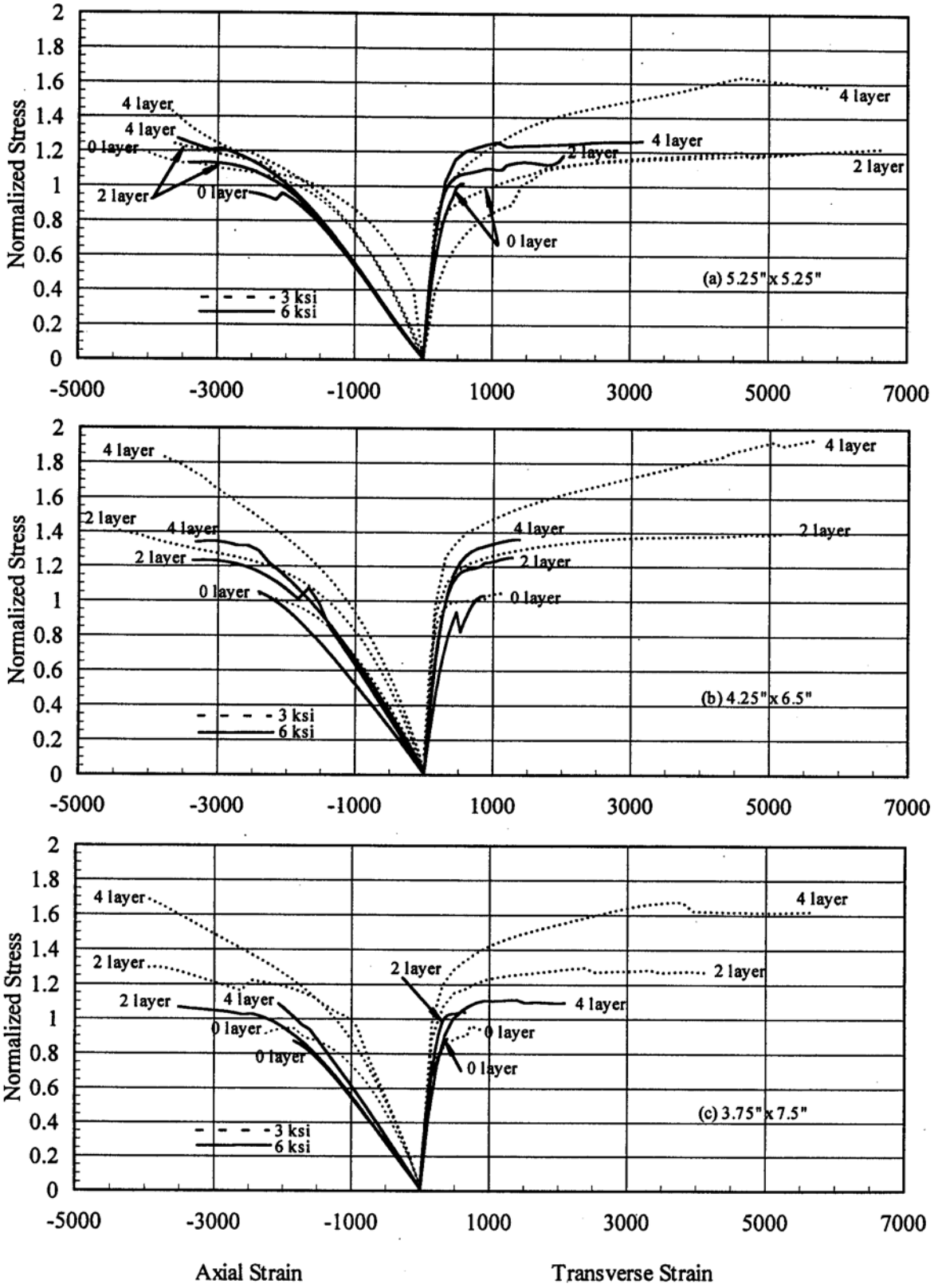

Fig. 5.21-Average Normalized Axial Stress vs. Volumetric Strain:
3 ksi vs. 6 ksi Concrete

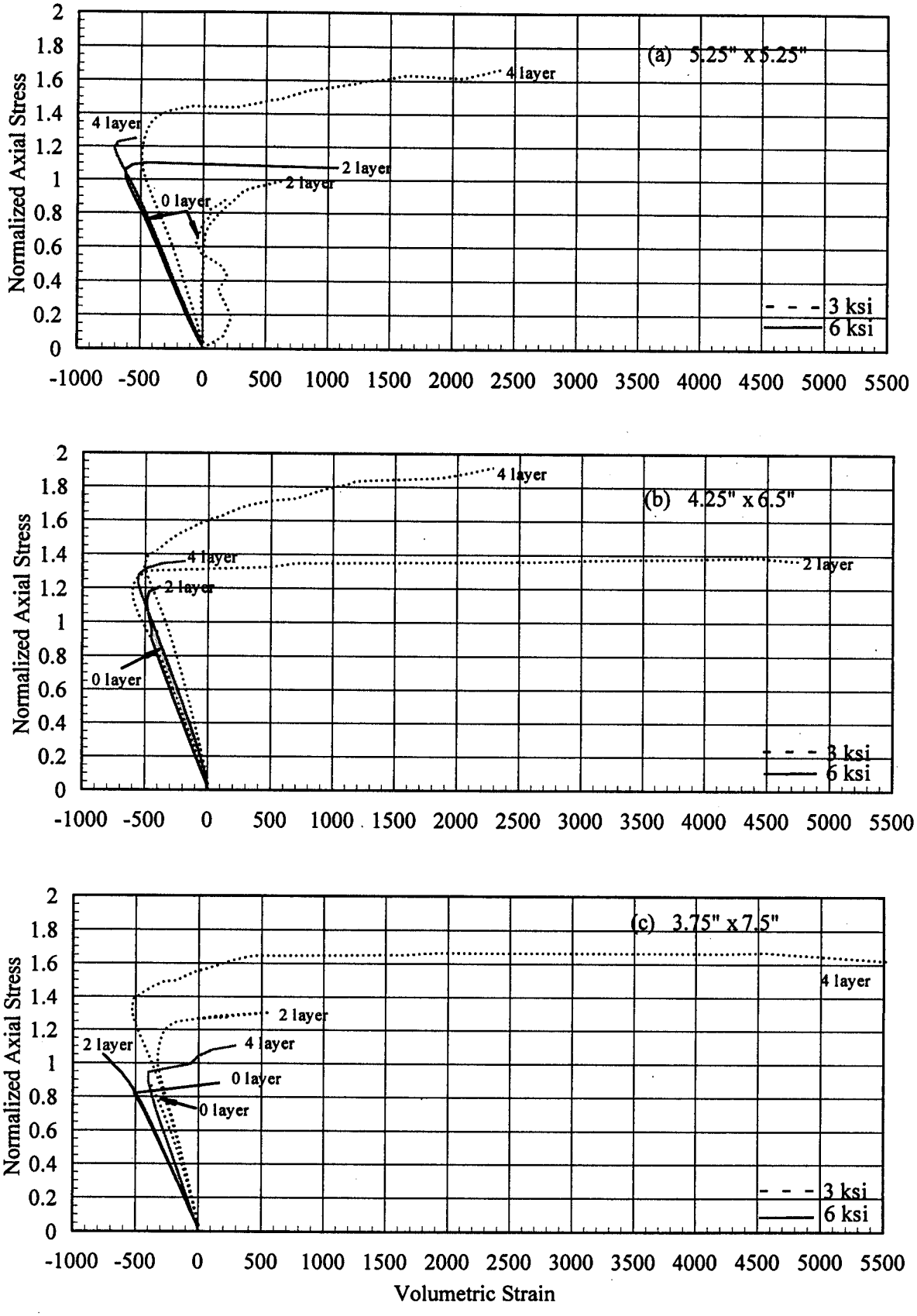

Fig. 5.22 -Average Dilation Rate vs Axial Strain:
3 ksi vs 6 ksi

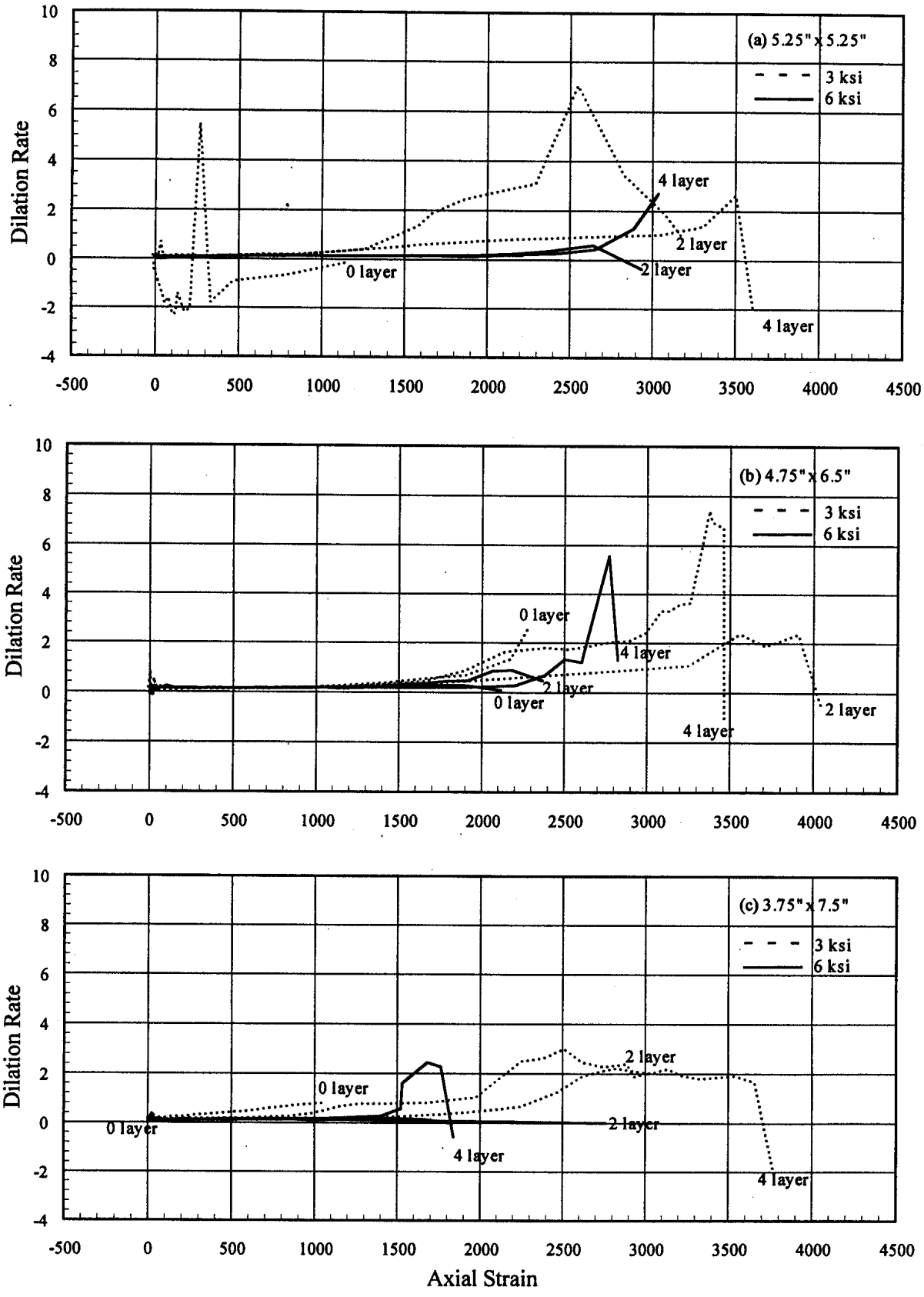

CONFINEMENT MODELING

A.1 Modeling of Axial Stress and Strain

Based on results from tests of concrete-filled glass FRP tubes, a confinement model was developed by Samaan, Mirmiran and Shahawy (1998). The model represents the bilinear response of FRP-confined concrete by a four-parameter relationship (Richard and Abbott 1975) as below:

$$f_c = \frac{(E_1 - E_2)\varepsilon_c}{\left[1 + \left(\frac{(E_1 - E_2)}{f_o}\right)^n\right]^{\frac{1}{n}}} + E_2\varepsilon_c \qquad \text{A.1}$$

where ϵ_c and f_c = axial strain and stress of concrete, E, and E_2= first and second slopes, f_o = reference plastic stress at the intercept of the second slope with the stress axis, and n = a curve-shape parameter which mainly controls the curvature in the transition zone. Figure 4.1 shows the basic parameters of this expression. The confined strength of concrete (f'_{cu}) is calculated as below (ksi):

$$f'_{cu} = f'_c + 3.38 f_r^{0.7} \qquad \text{(A.2)}$$

where f'_c is the unconfined strength, and f_r is the confinement pressure which is calculated as"

$$f_r = \frac{2 f_j t_j}{D} \qquad \text{(A.3)}$$

where f_j is the hoop strength of the jacket, t_j is jacket thickness, and D is the core diameter. The first slope (E_1) is the same as the initial modulus of elasticity of concrete as estimated below (in ksi):

$$E_1 = 47.586\sqrt{1{,}000 f'_c} \quad \text{(A}$$

The second slope (E) is a function of the stiffness of the confining jacket, and to a lesser extent, the unconfined strength of concrete core, as below

$$E_{21} = 52.4111 f_c^{0.2} + 1.3456 \frac{E_j t_j}{D} \quad \text{(A}$$

where E_j = effective modulus of elasticity of the jacket in the hoop direction. The intercept stress f_o is a function of the strength of unconfined concrete and the confining pressure! provided by the jacket, and was estimated as (in ksi)

$f_o = 0.872f'_c+0.371f_r +0.908$
(A.6)

The ultimate strain s_{cu} is determined from the geometry of the bilinear curve as

$$\varepsilon_{cu} = \frac{f'_{cu} - f_o}{E_2} \quad \text{(A}$$

The curve-shape parameter n is set at a constant value of 1.5.

A.2 Modeling of Lateral Strains

Since the axial-lateral strain curve is also bilinear, and the transition zone occurs at the same

$$f_c = \frac{(E_{1r} - E_{2r})\varepsilon_c}{\left[1 + \left(\frac{(E_{1r} - E_{2r})\varepsilon_r}{f_{or}}\right)^n\right]^{\frac{1}{nr}}} + E_{2r}\varepsilon_c \quad \text{(A.8)}$$

where subscript r denotes the lateral (radial) direction. The first slope E_r is given by

$$f_{1r} = \frac{E_1}{V} \quad \text{(A.9)}$$

where v = Poisson's ratio of concrete which usually varies between 0.15 and 0.22. The remaining parameters are found using the dilation rate which is defined as

$$\mu = \frac{d\varepsilon_r}{d\varepsilon_c} \quad \text{(A.10)}$$

The values of μ_u was related to the stiffness of the confining jacket as below:

$$\mu = -0.187 Ln\left(\frac{2E_j t_j}{f'_c D}\right) + 0.881 \quad \text{(A.11)}$$

Then, E_{Zr} is calculated as

$$E_{2r} = \frac{E_2}{\mu_u} \quad \text{(A.12)}$$

and the curve-shape parameter as

$$n_r = \frac{n}{\mu_u} \quad \text{(A.13)}$$

The reference plastic stress, f_{or}, is calibrated in a form similar to f_o as (in ksi)

$$f_{or} = 0.636f_c + 0.223f_r + 0.0661 \quad \text{(A.14)}$$

Finally, the ultimate radial strain is calculated as

$$\varepsilon_{ru} = \frac{f'_{cu} - f_{or}}{E_{2r}} \quad \text{(A.15)}$$